2013

MAPPING AND DECOMPOSING SCALE-DEPENDENT SOIL MOISTURE VARIABILITY WITHIN AN INNER BLUEGRASS LANDSCAPE

Carla Landrum
University of Kentucky, cjla225@g.uky.edu

STUDENT AGREEMENT:

I represent that my thesis or dissertation and abstract are my original work. Proper attribution has been given to all outside sources. I understand that I am solely responsible for obtaining any needed copyright permissions. I have obtained and attached hereto needed written permission statements(s) from the owner(s) of each third-party copyrighted matter to be included in my work, allowing electronic distribution (if such use is not permitted by the fair use doctrine).

I hereby grant to The University of Kentucky and its agents the non-exclusive license to archive and make accessible my work in whole or in part in all forms of media, now or hereafter known. I agree that the document mentioned above may be made available immediately for worldwide access unless a preapproved embargo applies.

I retain all other ownership rights to the copyright of my work. I also retain the right to use in future works (such as articles or books) all or part of my work. I understand that I am free to register the copyright to my work.

REVIEW, APPROVAL AND ACCEPTANCE

The document mentioned above has been reviewed and accepted by the student's advisor, on behalf of the advisory committee, and by the Director of Graduate Studies (DGS), on behalf of the program; we verify that this is the final, approved version of the student's dissertation including all changes required by the advisory committee. The undersigned agree to abide by the statements above.

Carla Landrum, Student

Dr. Junfeng Zhu, Major Professor

Dr. Mark Coyne, Director of Graduate Studies

MAPPING AND DECOMPOSING SCALE-DEPENDENT SOIL MOISTURE VARIABILITY WITHIN AN INNER BLUEGRASS LANDSCAPE

DISSERTATION

A dissertation submitted in partial fulfillment of the requirements for the degree of Doctor of Philosophy in the College of Agriculture at the University of Kentucky

By

Carla Jill Landrum

Lexington, Kentucky

Co-Directors: Dr. Junfeng Zhu, Assistant Professor of Plant and Soil Science
and Dr. Mark Coyne, Professor of Plant and Soil Science

Lexington, Kentucky

2013

ABSTRACT OF DISSERTATION

MAPPING AND DECOMPOSING SCALE-DEPENDENT SOIL MOISTURE VARIABILITY WITHIN AN INNER BLUEGRASS LANDSCAPE

There is a shared desire among public and private sectors to produce more reliable predictions, accurate mapping, and appropriate scaling of soil moisture and associated parameters across landscapes. A discrepancy often exists between the scale at which soil hydrologic properties are measured and the scale at which they are modeled for management purposes. Moreover, little is known about the relative importance of hydrologic modeling parameters as soil moisture fluctuates with time. More research is needed to establish which observation scales in space and time are optimal for managing soil moisture variation over large spatial extents and how these scales are affected by fluctuations in soil moisture content with time. This research fuses high resolution geoelectric and light detection and ranging (LiDAR) as auxiliary measures to support sparse direct soil sampling over a 40 hectare inner BluegrassKentucky (USA) landscape. A Veris 3100 was used to measure shallow and deep apparent electrical conductivity (aEC) in tandem with soil moisture sampling on three separate dates with ascending soil moisture contents ranging from plant wilting point to near field capacity. Terrain attributes were produced from 2010 LiDAR ground returns collected at ≤1 m nominal pulse spacing. Exploratory statistics revealed several variables best associate with soil moisture, including terrain features (slope, profile curvature, and elevation), soil physical and chemical properties (calcium, cation exchange capacity, organic matter, clay and sand) and aEC for each date. Multivariate geostatistics, time stability analyses, and spatial regression were performed to characterize scale-dependent soil moisture patterns in space with time to determine which soil-terrain parameters influence soil moisture distribution. Results showed that soil moisture variation was time stable across the landscape and primarily associated with long-range (~250 m) soil physicochemical properties. When the soils approached field capacity, however, there was a shift in relative importance from long-range soil physicochemical properties to short-range (~70 m) terrain attributes, albeit this shift did not cause time instability. Results obtained suggest soil moisture's interaction with soil-terrain parameters is time dependent and this dependence influences which observation scale is optimal to sample and manage soil moisture variation.

KEYWORDS: Data Fusion, Spatiotemporal Soil Moisture Variation, Scale-Dependent Soil Moisture Variation, Time Stability, Time Instability

Carla Landrum

Student's Signature

12/5/2013

Date

MAPPING AND DECOMPOSING SCALE-DEPENDENT SOIL MOISTURE VARIABILITY WITHIN AN INNER BLUEGRASS LANDSCAPE

By

Carla Jill Landrum

Junfeng Zhu

Co-Director of Dissertation

Mark Coyne

Co-Director of Dissertation

Mark Coyne

Director of Graduate Studies

12/5/2013

Date

ACKNOWLEDGEMENTS

This work is dedicated to my family. I want to thank my brother, Thomas, for lending an ear when times were hard and always providing sound advice. I am forever grateful to my parents, Claudia and Tony, who provided unconditional love and support and had complete confidence that I could make it to the end of this long journey. A loving thanks to my parents and grandparents, Ikey, G. Carl, Phyllis, and Jack, for instilling courage, character, work ethic, and principles in me to finish this work and hopefully make a meaningful contribution to this world, big or small.

I've had an amazing support group at the University of Kentucky. First, I want to thank Dr. Junfeng Zhu for chairing my Committee. Second, I want to thank Dr. Tom Mueller for his altruistic, unwavering support in supplying the resources and help needed to complete this research. And, of course, thank you for introducing me to Dr. Annamaria Castrignanò. I want to thank Dr. Mark Coyne for being an outstanding mentor and editor. This research would not have happened without your support. I also want to thank my Committee members and outside examiner: Dr. Demetrio Zourarakis, Dr. Chris Barton, Dr. Daehyun Kim, Dr. Tasios Karathanasis, and Dr. John Watkins, respectively. I also want to thank Dr. Grove for his wonderful guidance and help in performing laboratory analysis.

The caliber and amount of analyses performed would not have been possible without the endless guidance and teachings of Dr. Annamaria Castrignanò. My education and professional development at the University of Kentucky resonates around you. You are, and always will be, an excellent person, gifted teacher, and dear friend. Thank you.

My gratitude to the Kentucky Department for Environmental Protection (KDEP) for funding me and the College of Agriculture and the Department of Plant and Soil Sciences for funding my research. I want to acknowledge the University of Kentucky Graduate School for funding my travel to Italy to study under Dr. Castrignanò.

I want to send my upmost gratitude to my dear friends and colleagues: Stephanie Pyzola, Alex Williams, Jessi Ghezzi, Kristi Myer, Sleem Kreba and many more. Enduring this experience with you is what got me through. Thank you for your unwavering support and friendship.

Last, but not least, I want to thank Ann Freytag, Tami Smith, Joey Van Noy, Isaraprong Norrueang, Marcos Rodrigues, Rafael Barbieri, Blazan Mijatovic, Steve Blanford, and Heather Turner for their field and technical assistance. Your help was vital to the completion of this research.

Table of Contents

List of Tables

List of Figures

Chapter 1
Introduction

There is a shared desire among public and private sectors to produce more reliable predictions, accurate mapping, and appropriate scaling of soil moisture over large spatial scales (Lin 2003). A discrepancy exists between the scale at which soil moisture is measured and the scale at which it is typically modeled for management decisions and operations (Hopmans et al. 2002, Vereecken et al. 2007). Consequently, the scale of the soil moisture model might not accurately portray the actual hydrologic properties and processes occurring at the scale of interest. Moreover, soil moisture models do not always account for the relative importance of hydrologic variables influencing soil moisture variability through time with concomitant changes in moisture content.

Scale, defined within this research, is the "viewing window," linked directly to the sampling design and observation extent, that best captures spatial variation inherit to different properties and processes composing environmental systems (Wu et al. 2001). Bridging observation scales with prediction scales to better characterize and manage soil moisture variability is a motivating scientific question. Corwin et al. (2006) stated "modeling and monitoring vadose zone processes, such as water flow and solute transport, across spatiotemporal scales can only be achieved by understanding the interrelationship between scale and spatial variability (pg.129)." Hydropedology is an emerging scientific field specifically dedicated to capturing and characterizing soil hydrologic properties and processes within, and across, spatial and temporal scales (Lin 2003, Pachepsky et al. 2006, Lin et al. 2006, Kutilek and Nielson 2007, Pachepsky et al.

2008, Allen et al. 2009, Lin 2012). To do this, hydropedology integrates pedology, soil physics, hydrology, and geomorphology with terminology and symbols rooted in complex systems theory to establish a conceptual framework delineating hydrologic parameters and processes controlling the scale-dependent spatiotemporal variation of soil moisture (Lin 2003, Wilding and Lin 2006, Lin et al. 2006, Kutilek and Nielson 2007, Lin et al. 2008a, Pachepsky et al. 2008, Allen et al. 2009, Lin 2012).

Complex systems theory provides a conceptual understanding of scale dependent variability in complex systems (Wu and David 2002). Over the last two decades literature related to disciplines studying complex systems, such as landscape ecology, socioeconomics, and geomorphology, utilize hierarchy theory, which is a derivative of complex systems theory (Wu 1999, Wu 2004). In the context of hierarchy theory, complex systems are composed of discrete scales of patterned variation that can be decomposed according to the underlying properties and processes exerting influence on the scale-dependent patterned variation (Hay et al. 2002, Wu and David 2002, Hall et al. 2004). Decomposition is the central tenant to hierarchy theory (Wu and David 2000). The idea is to modulate nested (i.e. superimposed) scales of spatiotemporal variation into discrete scales that minimize within-scale variation but maximize between-scale variation (Allen et al. 2009). Decomposition essentially serves two objectives. First, it breaks down, or filters, nested scales of patterned variation within a complex system into individual scales to better determine which properties and processes act at each scale. Second, it delineates scale breaks, or discontinuities, between discrete scales. The scale breaks delineate thresholds where an adjustment in sampling design(s) and model approach(es) might be necessary to optimally capture and characterize patterned variation

in space and time. The structural relationship between discrete scales is organized in a ladder framework (i.e. hierarchy) in which scales exhibiting shorter range patterned variation reside below scales exhibiting longer range patterned variation (Wu and David 2002). Reasoning to this organization, smaller scale patterned behavior serves as building blocks or initiating conditions for larger scale variation; larger scale variation presents constraints (i.e. boundaries) on smaller scale variation (Wu et al. 2000; Wu and David 2002). Ideally, if a hierarchy framework exists, it will depict the spatial and temporal scales at which different soil-terrain parameters and processes operate, but also establish if relations exist between scales to readily upscale or downscale information with practical meaning.

This dissertation research is geared towards making a pragmatic contribution to hydropedology by integrating terrain mapping, environmental geophysics, geostatistics, and spatial regression to capture and characterize scale-dependent spatiotemporal behavior of surface soil moisture across a physiographically diverse landscape. The aim of this research is to shed new light on our current understanding of soil hydrology within complex landscapes and, therefore, introduce a working foundation to make better predictions, accurate mapping, and appropriate scaling of soil moisture.

The scope of this research encompasses terrain attributes (digital elevation model, slope, curvature, and terrain indices) and agriculture-relevant soil properties (apparent electrical conductivity, Mehlich III extractable nutrients, texture, organic matter, cation exchange capacity, etc.) to model and map scale-dependent shallow subsurface soil moisture variation in space with time across a 40 hectare Inner Bluegrass Kentucky landscape. Three observation dates were used to study the time-dependent nature of soil

moisture spatial variation. These three dates followed rainfall events that produced ascending landscape average soil moisture contents through time, ranging from the plant wilting point up to field capacity. It was unanticipated the study period would fall during a drought for Central Kentucky.

Scale-Dependent Soil Moisture Variation and Associated Challenges

Nested, or superimposed, spatial variation is a fundamental component of landscape spatial heterogeneity (Wu et al. 2000). Studying large spatial extents such as landscapes encompasses various soil-terrain parameters that interact with soil moisture. Soil-terrain parameters exhibit uniqueness according to the distance over which they can be considered homogeneous, or self-similar. This distance is called the range of spatial autocorrelation. Soil-terrain parameters inherit different ranges of spatial autocorrelation according to the various external factors influencing their development. Consequently, soil moisture will exhibit self-organized scale-dependent patterned variation according to the dominating soil-terrain parameters molding its spatial distribution at any given scale with time.

In theory, complex hydrologic systems are composed of discrete nested scales of patterned variation that can be decomposed according to inherent "scale breaks" deriving from the underlying spatial autocorrelation of properties and processes that cause soil moisture to self-organize into scale-dependent spatial patterns (Turner et al. 1989, Wiens 1989, Hay et al. 2002, Wu and David 2002, Hall et al. 2004, Wu 2004, Lin et al. 2006). Recognizing scale-dependent patterned variation of soil hydrologic properties and processes is a growing practice in soil science. Lin et al. (2006) asserted the value of recognizing patterned variation to characterize scale-dependent soil hydrologic

phenomena - “Identification and prediction of patterns, or repeated spatiotemporal organization, across scales is becoming a leading area of research in soil science and hydrology. Patterns offer rich and comprehensive insight regarding the variability of structures and functions, as well as the underlying processes controlling hydrologic response” (pg. 5).

In situ studies dedicated to understanding the scale-dependent spatial patterns of soil moisture primarily investigate the field scale and below (less than 100’s m^2) (Hopmans and Schoups 2006, Amidu 2008, Robinson et al. 2008b, Zhu 2009) . Consequently, the scale of data acquisition is typically not commensurate to the scale of real-world problems and applications (Vereecken et al. 2007, Robinson et al. 2008a, Robinson et al. 2008b). Several keystone papers underscore the need for scale-dependent research to better capture and characterize patterned variation of soil moisture in space and through time as a function of observation scale (McBratney 1998, Atkinson and Tate 2000, Hopmans et al. 2002, Western et al. 2002, Corwin et al. 2006, Hopmans and Schoups 2006, Vereecken et al. 2007). Four major questions arise from these review papers:

1. What are the spatial and temporal dependencies of patterned variation in soil moisture?
2. What are the optimal observation scales to capture patterned variation in soil moisture?
3. What soil-terrain attributes define this response?
4. How can we transfer information from one scale to the next with physical meaning?

Answering the aforementioned questions requires studies that encompass observation scales practical for farmers, remediation specialists, and water resource conservationists alike (e.g. 1-100's km^2) to help them effectively sample, monitor, and model soil moisture behavior over large spatial extents.

No single conceptual framework is currently accepted to theorize the scale-dependent heterogeneity of soil hydrologic phenomena (Lin et al. 2006, Wagener et al. 2007, Tetzlaff et al. 2008, Troch et al. 2009). Attempts have been made to establish a conceptual framework including what is coined the "scaleway approach" (Vogel and Roth 2003, Hopmans and Shoups 2006). This approach conceptualizes soil systems as a hierarchical medium with discrete spatial scales of variability, where each scale requires a unique hydrologic model(s) to represent that respective scale, or hierarchy, of variability (Hopmans et al. 2002). To facilitate the construction of a conceptual soil hydrologic model, more research is needed to establish sampling methods capable of capturing nested scales of soil moisture patterned variability over large spatial scales, then applying analytical techniques capable of decomposing and identifying individual scales of variability and the parameters and processes relevant to these scales. Until these two research gaps are filled it will not be possible to organize scale-dependent soil moisture patterned variability into a conceptual, hierarchical framework.

Capturing Scale-Dependent Soil Moisture Variation

The measured variability in soil moisture is often consequential to the sampling coverage or the scale triplet (Atkinson and Tate 2000). The scale triplet consists of three components: sampling support, sample spacing, and sampling extent. Sample spacing is the distance between each observation point. Sample support is the area or volume

represented by each observation point. Sampling extent is the observation domain or area of study. In geostatistics, increasing the sample support is called upscaling and decreasing the sample support is called downscaling (Atkinson and Tate 2000, Stein et al. 2001, Hopmans et al. 2002, Corwin et al. 2006).

Point observations, such as soil coring and *in situ* capacitance monitoring, are commonly employed to capture soil moisture heterogeneity within a landscape. Point observations are limited in providing representative measures of soil moisture variability when studying large areas due to their small sampling support, invasiveness, manual labor, and cost (Park and van de Giesen 2004, Robinson et al. 2009, Besson et al. 2010, Robinson et al. 2012). For these reasons auxiliary methods of capturing soil moisture spatiotemporal variability in support of sparse direct soil moisture measurements are being explored within the soil science community (Rubin and Hubbard 2005). Most prominent of these methods are remote sensing and geophysics.

Remote Sensing and Developing Terrain Attributes

Under saturated or near saturated conditions soil moisture distribution is primarily influenced by gravitational forces and can exhibit an organized spatial pattern mirroring that of the landscape (Grayson et al. 1997, Western et al. 1999, Gòmez-Plaza et al. 2000, Grayson and Western 2001, Grayson et al. 2002, Lin et al. 2008a, Lin and Zhou 2008). Therefore, terrain attributes are attractive proxy tools to quickly and cheaply assess large-scale soil moisture distribution under the appropriate soil moisture conditions. Terrain attributes can include slope (1^{st} derivative of elevation), curvature (2^{nd} derivative of elevation), upland contributing area, aspect, and combinations thereof, producing indices such as the topographic wetness index (TWI) (Western et al. 1999, Grayson and Western

2001, Kienzle 2004, Moller et al. 2008). Remote sensing, specifically light detection and ranging (LiDAR), is becoming an omnipresent technology to model soil-water-terrain interactions due to its ability to capture high resolution data over large areas, increasing availability, and aptness for building terrain attributes in detail.

LiDAR is a well-documented means to capture high resolution 3-D spatial data over large areas and, consequently, has developed into the primary means to generate digital elevation models (DEMs) (Lohr 1998, Wehr and Lohr 1999, Anderson et al. 2007, Meng et al. 2010). The earliest version of LiDAR was introduced during the late 1930's in which pulses of light generated from flash lamps were used to measure cloud height (Weitkamp 2005). This technology was superseded by modern laser sources during the 1960's (Weitkamp 2005). The LiDAR system is mounted on an aircraft, or satellite, georeferenced platform consisting of a transmitter and a detector. The transmitter emits laser pulses with wavelengths ranging from 250 nm to 11 μm that are subsequently intercepted and differentially reflected by underlying atmospheric and earth matter. The returning light pulses are captured by a detector then converted into an electronic code to determine the reflectance (intensity) and location (return time). LiDAR is an alternative approach to photogrammetry and site-specific surveying, both of which can be time consuming, costly, and ineffective in areas densely occupied with vegetation or anthropogenic edifices (Liu 2008). It is desirable to use LiDAR returns to build digital elevation models because of their accuracy and fine resolution. However, it is important to filter unwanted returns (e.g. canopy, power lines, buildings) to reduce noise and inaccuracies in the elevation model. Common techniques used to filter ground returns from other unwanted returns in building a DEM are diverse (e.g. interpolation filters,

slope-based filters, morphological filters, and wavelet filters (Lui 2008). Filters are often insensitive to dense low-lying understory, creating problems for extracting ground returns (Meng et al. 2010, Huang et al. 2011). These filtering methods do not always perform well. This research introduces geostatistical spatial component filtering to reduce unwanted high frequency variation in the raw LiDAR returns to build a DEM.

Constructing a DEM includes two general linear interpolation classes: deterministic and geospatial (Anderson et al. 2007). Deterministic methods include Inverse Distance Weighting (IDW) and splines; an example of a geostatistical method is kriging. Although these techniques are common within remote sensing research, the current research introduces an alternative approach to produce a DEM using nonstationary kriging, specifically, Intrinsic Random Function of Order-k (IRF-k), in tandem with spatial component filtering. Although IRF-k is not used in remote sensing and GIS, it has been employed to model and map various nonstationary datasets including soil moisture (Buttafuoco and Castrignanó 2005), durum wheat (Castrignanò et al. 2004), and anthropic backfill (Ciotoli et al. 2011).

Geophysics

Geophysics was introduced during the mid-20th century for use in oil and gas exploration. In the most basic sense, geophysics documents contrasts in subsurface earth materials by measuring their response to energy fields, whether these fields be it passive (e.g. gravity) or active (e.g. induced electrical current), and imaging this response in space and/or time. Geophysical technologies illustrate contrasts in subsurface properties based on indirect measurements (e.g. geoelectric, electromagnetic, seismic). Within the last two decades, geophysics has been used in the soil science community to study subsurface soil

properties. Geophysical techniques specific to soil systems are diverse and include ground penetrating radar (GPR), electromagnetic induction (EMI), bulk electrical resistivity (ER) and its inverse, electrical conductivity (EC), and near-surface seismic reflection (Allred et al. 2008). These technologies are attractive because they are relatively economic, non-invasive, and perform rapid, reiterative, high resolution data acquisition (Tabbagh et al. 2000, Besson et al. 2004).

Technologies are lacking to map high resolution spatiotemporal variability of soil moisture at the landscape-scale (Robinson et al. 2012). For example, point observations, such as capacitance probes, present sampling supports too small to pragmatically capture large areas with high sampling density. In contrast, remote sensing technologies can encompass a large area with high sample density but are inadequate for capturing soil moisture variation below the top few centimeters of the soil surface (Robinson et al. 2012). Consequently, geophysics is emerging as an "intermediate" technology capable of bridging the sampling gap.

In 2005 several key reviews were published conveying the utility of geophysics for soil science (Corwin and Lesch 2005a, Friedman 2005, Samouelian et al. 2005). These papers focus on the utility, theory, principles, and empirical relationships of geophysical measurements used to map the spatiotemporal variability of static and transient properties within soil environments. For example, in non-saline soils, geophysics has been used as a site reconnaissance tool to map physical and chemical properties such as soil structure and horizonation (Tabbagh et al. 2000, Inman et al. 2001), parent material (Kühn et al. 2009), soil texture (Mertens et al. 2008), depth to confining layers (Mueller et al. 2003, Jung et al. 2005, Saey et al. 2009), soil chemistry (Corwin and Lesch 2003, Johnson et al.

2003, Corwin and Lesch 2005a, Farahani et al. 2005) and bulk density (Besson et al. 2004, Seger et al. 2009). If a spatial correlation exists between sparse primary data (i.e. soil cores) and dense secondary data (i.e. geophysics) then the latter can downscale (via punctual cokriging) the former to map sparsely sampled soil properties across a landscape (Brevik et al. 2006, Amirun et al. 2007). Conversely, block kriging is utilized as the most common form of upscaling high resolution information to model larger sampling supports (Stein et al. 2001).

Geophysical measurements were first applied in agriculture in the 1940's to rapidly and noninvasively map soil moisture using a simple four electrode arrangement (Edlefsen and Anderson 1941, Allred et al. 2008). Soil hydrologists have become increasingly interested in hydrogeophysics (Rubin and Hubbard 2005) to study soil moisture dynamics, particularly ER, GPR, and EMI, due to their rapid data acquisition, non-invasiveness, and sensitivity to target (i.e. water). Studies dedicated to hydrogeophysics (Rubin and Hubbard 2005, Abdu et al. 2008, Robinson et al. 2008b) are numerous and demonstrate the relevance of these techniques to document soil moisture dynamics. Specifically, these studies employ geophysics to assess time-lapse soil moisture variation (Goyal et al. 1996, Michot et al. 2003, Amidu 2008, Besson et al. 2010, Jayawickereme et al. 2010), water content (Schwartz et al. 2008, Cousin et al. 2009, Brunet et al. 2010, Garre et al. 2011), hydraulic conductivity (Garambois et al. 2002) , and soil moisture flow paths and patterned variation (Koch et al. 2009, Robinson et al. 2009, Lin 2010, Robinson et al. 2012).

Hydrogeophysics can characterize soil moisture spatiotemporal variability over a range of spatial scales from the soil profile (Amidu and Dunbar 2007) up to field and landscape-

scales (Robinson et al. 2009, Lin 2010, Robinson et al. 2012). This is highly attractive to soil hydrologists because it allows them to readily address the four questions posed in the previous section. Geophysical technologies are therefore becoming a prominent field inventory method to characterize soil moisture dynamics.

Characterizing Scale-Dependent Patterned Soil Moisture Variation

Soil moisture distribution over a landscape often exhibits an organized patterned variation mirroring that of soil properties and terrain features (Grayson et al. 1997, Western et al. 1999, Gòmez-Plaza et al. 2000, Grayson and Western 2001, Grayson et al. 2002, Lin et al. 2008a). These organized spatial patterns can be time stable, which has been studied most prominently using time stability analysis (Vachaud et al. 1985) . Recent research is trying to incorporate auxiliary sensing, including terrain attributes and geophysics, to better characterize time stable soil moisture distribution patterns over large areas at finer spatial resolutions (Robinson et al. 2009, Besson et al. 2010, Robinson et al. 2012, Minet et al. 2013).

Time Stability

Time stability has been extensively used to characterize the temporal behavior of soil moisture distribution patterns (Mohanty and Skaggs 2001, Martínez-Fernández and Ceballos 2003, Lin 2006, Zhou et al. 2007). Across a given observation domain - such as a plot, field, or watershed - certain regions will exhibit persistent wetness or dryness compared to the observed average moisture content (Lin 2006). The incentive behind time stability analysis is it can identify sample locations with persistently higher or lower soil moisture content relative to an observation domain average through time; these locations require less ambitious sampling with time and thereby save time, labor, and cost

associated with field monitoring efforts specific to soil moisture (Lin 2006, Guber et al. 2008). Studying the patterned behavior of soil moisture variation can minimize soil sampling efforts but also reveal which soil-terrain properties and associated processes govern soil moisture responses (Grayson et al. 1997, Grayson et al. 2002, Lin 2006, Lin et al. 2006).

Vachaud et al.'s (1985) notion was that time stable patterns derive, in part, from a deterministic relationship or interactions with environmental parameters such as texture. Over the last two decades researchers have expanded Vachaud et al.'s (1985) notion to encompass a wide array of measureable parameters that are responsible for soil moisture's time stable patterned behavior including microtopography and vegetation (Gòmez-Plaza et al. 2000), organic matter (Hu et al. 2009) , bulk density (Cosh 2008), landscape position (Lin 2012), and soil depth (Lin 2006). These results seems to propagate more questions than answers, however, because: 1) the aforementioned soil-terrain parameters exhibit inconsistencies within the literature in part due to irregularities in research methods but also due to the diverse soil environments these different studies encompass; 2) it is still unsubstantiated whether soils are more or less time stable in wet or dry conditions; 3) methods to capture and characterize time stable soil moisture patterns according to scale are understudied (Kachanoski 1988, Grayson and Western 1998, Gòmez-Plaza et al. 2000, Western et al. 2002, Lin et al. 2005, Vanderlinden et al. 2011).

Characterizing Time Stable Soil Moisture Patterns Using Geostatistics

Scale-dependency is the notion that unique patterns of spatial autocorrelation are revealed by changes in observation extent and sampling coverage (McBratney 1998, Atkinson and

Tate 2000, Hopmans et al. 2002, Hopmans and Shoups 2006). Observation extent is the size of the observation domain and sampling coverage refers to spacing interval and geometry (Turner et al. 1989, Wiens 1989, Atkinson and Tate 2000, Western et al. 2002). Nested direct sampling schemes together with high resolution georeferenced auxiliary sensing technologies appropriate to remote sensing and geophysics perform data acquisition that inherently capture multiscale pattern variability (Oliver and Webster 1986, Weitz et al. 1993, Van Meirvenne and Goovaerts 2002). To characterize patterned variation in soil moisture it is beneficial to fuse georeferenced hybrid datasets (i.e. direct soil sampling and auxiliary sampling) using a geostatistical interface in which a user can distill unique scales of spatial variability through time using spatial autocorrelation (Taylor et al. 2008, Castrignanò et al. 2012, De Benedetto et al. 2013). For example, De Benedetto et al. (2012) fused EMI and GPR with direct soil measurements to predict clay content using a single geostatistical platform known as kriging with external drift. Castrignanò et al. (2012) used multicollocated factorial cokriging analysis to fuse EMI, gamma-ray emission, and on-site elevation surveys to predict plant available potassium within an agriculture field. Sensor fusion is the future for making predictions specific to large-scale environments in which direct sampling alone will not suffice.

Spatial autocorrelation operates on the principle that "everything is related to everything else, but near things are more related than distant things," which is Tobler's first law of geography. Geostatistics, which was originated in France by Matheron during the 1960's to prospect ore reservoirs, underscores the concept of autocorrelation. Multivariate geostatistics has become a powerful tool providing insight into which measured parameters explain most of the observed spatial variability and the specific scales at

which these parameters operate (Goovaerts 1992). One particularly powerful technique disclosing the sources of variation is factorial cokriging analysis (FCA), which is also employed as multicollocated factorial cokriging analysis (MFCA). Matheron introduced FCA in 1982 and Goovaerts has explored its value specific to soil science investigations (Goovaerts 1992, Goovaerts 1994, Goovaerts and Webster 1994, Goovaerts 1998). Specifically, FCA has been used to establish homogeneous zones of crop management (Castrignanò et al. 2009, Morari et al. 2009, De Benedetto et al. 2012, Diacono et al. 2012) and identify sources of soil heavy metal and salt contamination (Lin et al. 2002, Yang et al. 2009, Sollitto et al. 2010, Zhu 2010).

The benefit of MFCA is it can model multiple soil moisture dates and corollary hydrologic parameters simultaneously to reveal if there is a time stable, scale-dependent relevance to the soil moisture regimes observed and, if so, which soil-terrain parameters best relate to the established time stable patterns. MFCA integrates multiple variables with different sampling supports and units, using a single geostatistical platform (Goovaerts 1998, Yang et al. 2009; Castrignanò et al. 2012). MFCA distills nested spatial structures within a multivariate spatial dataset using a nested semivariogram model called the linear model of coregionalization (LMC) (Castrignanò et al. 2000, Yang et al. 2009). The LMC constitutes a linear combination of basic spatial functions (e.g. direct and cross variograms) in which each spatial function represents an independent range (e.g. scale) of spatial autocorrelation nested within a system (Bourgault and Marcotte 1991, Haining et al. 2009, Yang et al. 2009).

MFCA generates two outputs: 1) maps of individual variables with original units; and 2) maps of regionalized factors that delineate the scale-dependent synergistic interactions

among multiple variables. As applied to soil moisture, the first MFCA output maps soil moisture estimates for each soil moisture date observed. These moisture estimates are conveniently subjected to the supplementary suite of time stability analytical techniques, including the confusion matrix, time stability's MRD in tandem with polygon kriging in addition to principal component analysis (PCA_{MRD}), and the cross-correlogram to ascertain if the observed soil moisture dates exhibit time stable characteristics across the landscape. The confusion matrix is a traditional statistical approach that uses a single metric called the observed accordance to determine whether soil moisture at a given point holds its classification through time. Polygon kriging is a new approach to determine if landscape positions affect time stable soil moisture patterns. Finally, the cross-correlogram measures the cross-correlation of soil moisture between two time-step increments. The second MFCA output is used to better understand which spatial scale(s) soil-terrain parameters most influence soil moisture variation.

Relative Importance of Scale-Dependent Hydrologic Parameters

Soil moisture's spatial heterogeneity derives from its interaction with ambient soil-landform parameters such as soil texture and elevation. This interaction is dynamic due to fluctuations in soil moisture content through time (Coleman and Niemann 2013). Deciphering the temporal relative importance of soil-landform parameters in explaining soil moisture heterogeneity is therefore complex, and this complexity is further compounded when studied over large areas such as landscapes (Wagener et al. 2007, Tetzlaff et al. 2010). Understanding the temporal relative importance and scale of influence among soil-terrain parameters is of interest to the soil hydrologic modeling community to increase the precision and accuracy of predicting soil moisture distribution

and balance with time (Williams et al. 2009, Zhao et al. 2011). Recent research efforts have attempted to understand the temporal relative importance of soil-terrain parameters specific to observation scales ranging from the local (plot) to regional (watershed) (Zhao et al. 2011, Yao et al. 2012). Coleman and Niemann (2013) emphasizes that more research is needed beyond plot and field scales to better understand the physical origin behind time dependent soil moisture patterns.

Bridging Approaches: Theory and Applied Science

The current research attempts to identify the scale-dependent relative importance of soil-landform parameters that mold patterned variation in soil moisture during relatively dry soil moisture conditions.

There are two opposite approaches to identify the spatial scales at which soil-terrain parameters potentially exhibit a relative importance in affecting soil moisture variation through time. The first approach attempts to decompose the landscape system into its respective hydrologic "parts," in terms of significant soil-terrain parameters (environmental variables) and spatial frequencies (spatial variables) that explain soil moisture variation. Because this approach decomposes the studied system into its respective "parts", it is identified as a reductionist approach. A technique called spatial eigenvector mapping (SEVM) used in tandem with multiple regression analysis constitutes this approach. These two techniques will be henceforth collectively identified as spatial regression. Specifically, SEVM is used to extract different spatial frequencies (e.g. scales of variation) nested within a sampling grid. These filters are created strictly from a geographic space, meaning filter genesis has no regard for the spatial autocorrelation of measured environmental properties. Spatial filters serve as proxy

spatial variables (Ali et al. 2010) that are incorporated into a regression model as explanatory variables to determine which spatial scale(s) (e.g. filters) best explain soil moisture variation (Dormann et al. 2007, Legendre and Legendre 2012). This multivariate spatial technique has only recently been applied in soil science to characterize scale-dependent soil moisture variation, first by Ali et al. (2010) and later by Kim (in press). Integrating spatial filters into the regression model alongside measured soil-terrain parameters reduces the potential for overestimating regression coefficients for soil-terrain parameters and underestimating model error (Kim, in press). Consequently, the advantage to this technique is its potential to reduce the bias of traditional regression techniques, but also reveal the variety of spatial scales in which the response variable (e.g. soil moisture) is significant (Dray et al. 2006, Griffith and Peres-Neto 2006).

Within the scope of this research, spatial filters are constructed in a series of steps. The first step is building a pairwise Euclidean distance connectivity matrix that is unique to the sampling design and chosen truncation distance. The second step is performing principal coordinate analysis (PCoA) on the distance matrix to create the spatial filters (eigenfunctions). This approach compliments traditional geostatistics and helps service the common objective of identifying scale-dependent relative importance of soil moisture at the landscape-scale.

In contrast, the second approach uses a multivariate geostatistical model to decompose a system of variables into individual units (or modules) of variation. This approach entails the aforementioned LMC. In comparison to the reductionist approach, the LMC is a holistic approach because soil moisture is modeled as part of an integrated system of spatial variables that are modulated according to their shared spatial autocorrelation. In

reality this is pragmatic, because soil properties and processes do not act independently of one another, but interact in synergistic, complex ways within the environment. The purpose of LMC is to decompose the landscape into different spatial scales at which different soil-terrain parameters exhibit shared spatial autocorrelation, but also disclose which scale-dependent soil-terrain parameters best correlate with soil moisture through time (Goovaerts 1998, Yang et al. 2009).

Coupling the reductionist and holistic approaches is a more thorough method to distill optimal scales of soil moisture variation in space as a function of time across the landscape studied. It is not within the scope of this study to test the performance between the LMC and spatial regression techniques, rather, this study discusses and employs these two techniques as accompanying tools to identify the scale-dependent relative importance of selected soil-terrain parameters influencing soil moisture variation within the landscape observed.

Research Motivation

Soil hydrologic properties and interactions are scale-dependent. For this reason many soil hydrologists must decide *a priori* which observation scale will best serve their objective. Because soil moisture can exhibit scale-dependent heterogeneity in both space and time, it is challenging for soil hydrologists to determine which observation scales are optimal to investigate certain hydrologic properties or processes. It is important to establish these scales because the sampling support is most representative when the scale of observation equals or exceeds the scale of variability (Haws et al. 2004). From this perspective, the prominent questions facing soil hydrologists are how to:

1) fuse multiple datasets with different sampling supports and units to reveal scale-dependent soil moisture patterned variation;

2) associate soil moisture's interaction with soil-landform parameters to the spatiotemporal scales of interest.

This research is geared toward addressing the aforementioned questions by adapting an approach that integrates high resolution secondary sampling, including geophysics and LiDAR, multivariate geostatistical, spatial regression, and time stability analyses to reveal and map the scale-dependent spatiotemporal tendencies of soil moisture nested within a landscape.

Dissertation Overview

Chapter 2 describes the area of investigation (AOI), field sampling design and techniques, and laboratory analyses.

Chapter 3 introduces the utility of IRF-k in tandem with spatial component filtering to create a DEM from nonstationary LiDAR data. Chapter 3 also provides a comprehensive background for calculating terrain attributes relevant to this research and their utility in subsequent chapters as proxy variables for characterizing spatiotemporal soil moisture variation over large areas.

Chapter 4 entails studying time stability and downscaling direct soil moisture measurements using geoelectric measurements and MFCA. Downscaled soil moisture estimates are subsequently subjected to a suite of time stability analyses, including the confusion matrix, Vachaud et al.'s (1985) mean relative difference in tandem with

polygon kriging and principal component analysis, and cross-correlograms, to determine if soil moisture patterns are persistent among the three soil moisture dates.

Chapter 5 addresses the scale-dependent relative importance of soil-terrain parameters that best explain soil moisture variability for the soil moisture regimes. Chapter 5 attempts to use holistic and reductionist approaches to study and characterize the scale-dependent relevance and interactions between soil-terrain parameters and soil moisture in space and through time.

Chapter 6 summarizes the findings of this research and discusses the future direction and challenges of capturing and characterizing the regionalized spatiotemporal variation of soil moisture in complex landscapes.

Chapter 2

Field Site and Data Collection

This chapter will cover the materials and methods used in the research with the exclusion of the numerical and statistical methods which will be addressed in Chapters 3, 4 and 5.

Area of Investigation

The site investigated is at Spindletop Farm in Kentucky's inner bluegrass region, Fayette County, Lexington, KY (38.116030 N, -84.491093 W), a part of the University of Kentucky Agricultural Experiment Station (Figure 2.1). The site spans approximately 40 hectares and is dominated by forage grasses that are periodically mowed. The site is segmented by agricultural crops, predominantly corn and tobacco, which are excluded from analysis. Several locations within the site have histories of agricultural activity, but the exact nature and extent is unknown. The inner bluegrass region is dominated by a karst landscape underlain by Ordovician phosphatic limestone, calcareous shales, and interbedded limestone shales (USDA-NRCS 2013). The site encompasses various soil series illustrated in Figure 2.1 (USDA-NRCS 2013). Soil depths range from 40 – 200 cm, depending on landscape position. Preliminary soil core analysis indicates argillic and fragic confining layers exist approximately 55-70 cm below the surface in some locations.

Site topography exhibits undulating swells (convex features) and swales (concave features). The topographic high and low are approximately 288 m and 269 m above mean sea level, respectively (Figure 2.2). Cane Run Creek meanders N/NW of the area. A drainageway, suspected to be a relic of subsidence from the underlying karst geology, is situated diagonally (SW/NE trajectory) across the area and exhibits considerable

wetness after rainfall events. Several small ($\leq$1 m^2) karst swallets reside within the drainageway. The area is exposed to a seasonal, temperate climate with a mean temperature of 8-18^o C and mean annual precipitation of 100-135 cm (USDA-NRCS 2013).

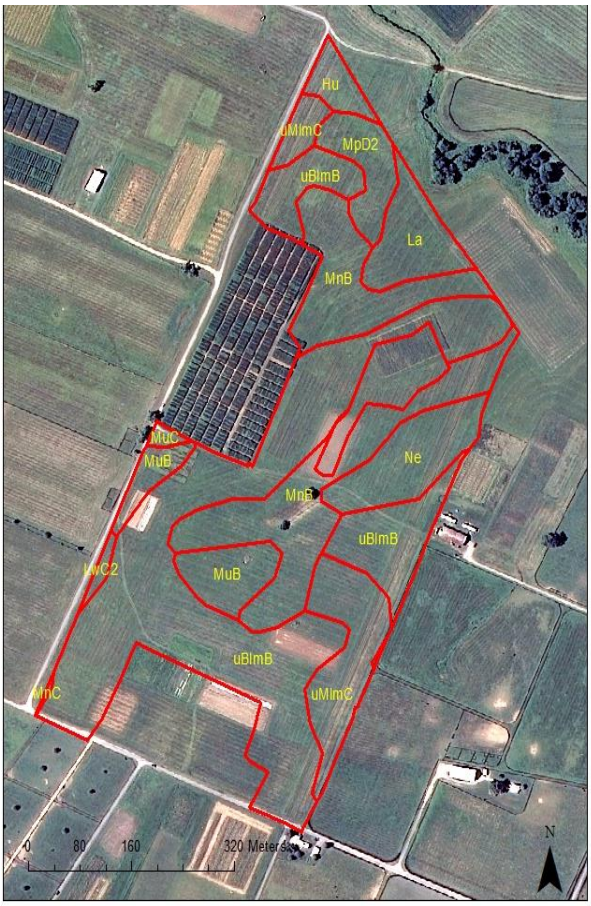

Figure 2.1. Site map and soil map units. NAIP aerial photography is from 07/20/10.

Map Unit	Soil Name	Taxonomic Description
Hu	Huntington silt loam	Fine-silty, mixed, active, mesic Fluventic Hapludolls
La	Lanton silty clay loam	Fine-silty, mixed, superactive, thermic Cumulic Epiaquolls
MnB	McAfee silt loam 2-6% slope	Fine, mixed, active, mesic Mollic Hapludalfs
MnC	McAfee silt loam 6-12% slope	Fine, mixed, active, mesic Mollic Hapludalfs
MpD2	McAfee silty clay loam12-20% slope	Fine, mixed, active, mesic Mollic Hapludalfs
MuB	Mercer silt loam, 2-6% slope	Fine-silty, mixed, semiactive, mesic Oxyaquic Fragiudalfs
MuC	Mercer silt loam, 6-12% slope	Fine-silty, mixed, semiactive, mesic Oxyaquic Fragiudalfs
Ne	Newark silt loam	Fine-silty, mixed, active, nonacid, mesic Fluventic Endoaquepts
uBlmB	Bluegrass-Maury silt loams 2-6% slope	Fine-silty, mixed, active, mesic Typic Paleudalfs
uMlmC	Maury-Bluegrass silt loams, 6-12% slope	Fine, mixed, active, mesic Typic Paleudalfs

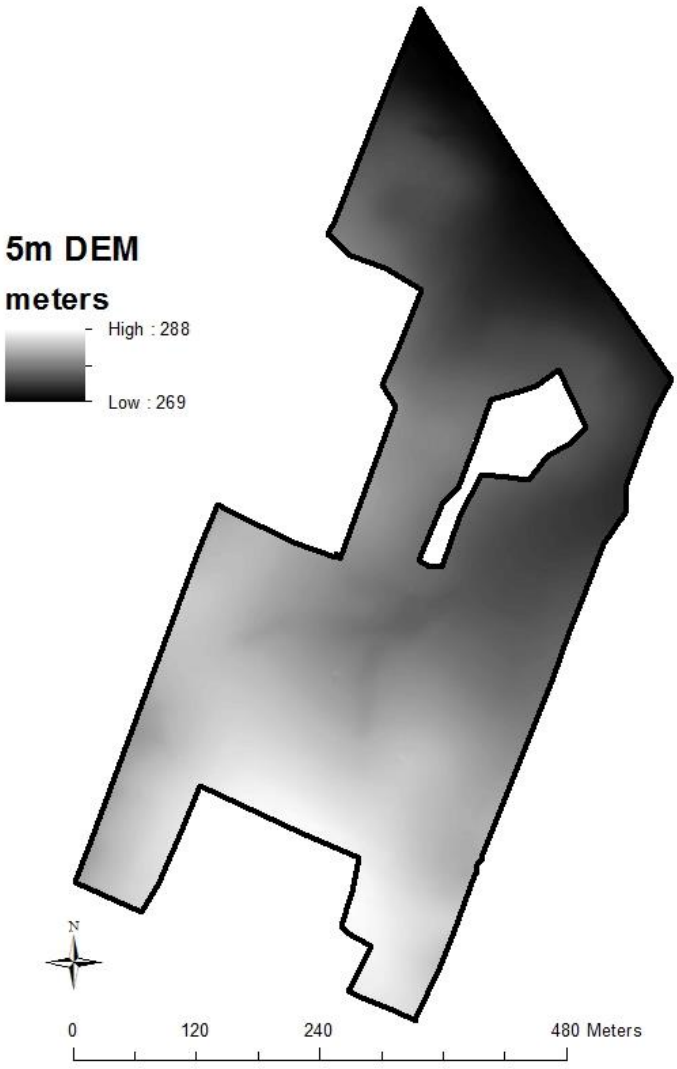

Figure 2.2. 5-m resolution digital elevation model derived from LiDAR data.

Soil Sampling Design

A total of 127 direct soil samples were collected in the study field (Figure 2.3). One hundred of these samples were delegated for model calibration and the other 27 for model validation. Model calibration samples were used for statistical analyses and modeling. Model validation samples were used to validate model estimates. Spatial simulated annealing (SSA) was performed using freeware (SANOS 0.1 for Windows) on 64 of the 100 calibration samples to establish an equal distribution of samples over the field. Spatial simulated annealing is a numerical optimization method that uses a random perturbation of an initial set of parameters, in this case spatial coordinates, to optimize an equal sampling distribution for the site (Oliver 2010).

The optimization method attempts to mimic a thermodynamic system, specifically, a Boltzmann's distribution of atoms cooling in molten metal in which the atoms approach their most stable energy state as the temperature decreases (Oliver 2010). The system is said to be in equilibrium (e.g. optimized) when the lowest energy state is attained, also called entropy. Conceptually, entropy translates into an optimal solution for attaining an equal distribution of sampling points over the site.

To optimize the sampling design the spatial coordinates were randomly perturbed in stepwise fashion according to a cooling schedule. Within SANOS, perturbations are accepted or rejected according to the Metropolis-Criterion (Oliver 2010). The Metropolis-Criterion states that the system has a certain probability of changing its current energy state to one of higher energy (opposite of entropy) as expressed below

$$e^{-(E2-E1)/kT}$$

where E1 is the current energy state or sampling configuration; E2 is the cost of energy change for changing the sampling configuration, k is a constant and T is the temperature for that perturbation step. The Metropolis-Criterion essentially measures the "energy" difference between each random perturbation and selects those that fit within a pre-selected probability threshold. If a random perturbation results in a sampling configuration that reduces the energy state of the system, the new sampling configuration is accepted automatically. Perturbations that decrease the fitness of the objective function (e.g. increase the energy state) are accepted or rejected at random in an attempt to avoid local minimization of the fitness function (van Groenigen et al. 1999, Oliver 2010). A cooling schedule of 45 minutes was chosen for the 64 sampling locations at 0.95 probability threshold. The MMSD (Minimization of the Means of the Shortest Distances) criterion was used to minimize the distance between an arbitrary point and its nearest neighbor (van Groenigen et al. 1999). One advantage to SSA is it can readily handle obstructions such as the exclusions defined within the area of investigation due to crops (Figure 2.1).

Four nests were randomly placed in the field using a randomization algorithm in ArcMap 10.0 (ESRI® ArcMap™ 2010). Each nest consisted of 9 sampling locations that were split in two transects transverse to one another, making the nests appear like a cross. The distance between each sample in the nest was 6m. The objective of the nests was to capture directional, small scale variation and thus, increase the precision of modeling spatial uncertainty (e.g. decrease the nugget effect). The remaining 27 validation points were selected using the randomization algorithm in ArcMap 10.0.

Sampling locations were digitized in the field using a hand-held Trimble GeoXH global positioning system. The GeoXH provides sub-meter accuracy and was used to relocate sampling sites when physical markers were relocated or destroyed by mowing or other field operations. The GeoXH system and post data processing was provided by Ms. Heather Turner of MapSync, Inc. (Lexington, KY).

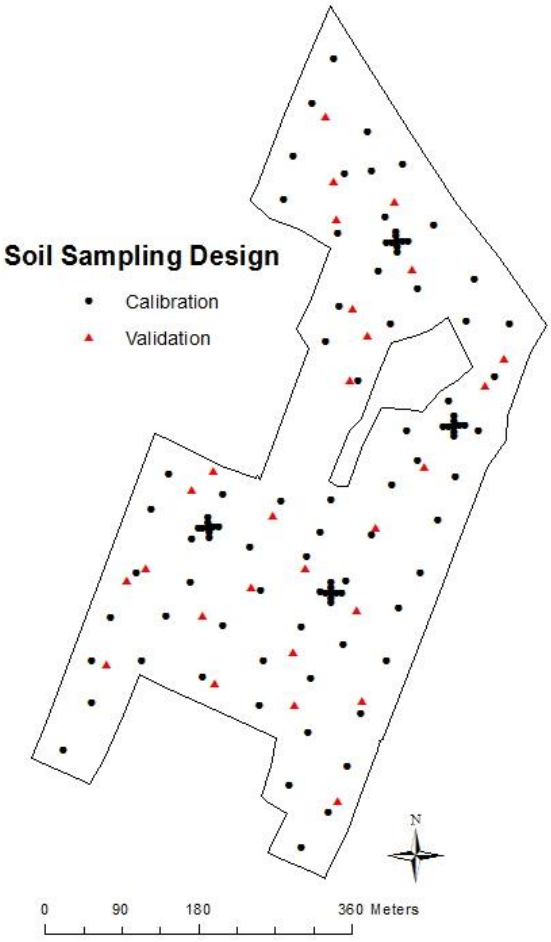

Figure 2.3. Direct soil sampling design.

Field Sampling

Five sampling campaigns were implemented between June 2012 and October 2012. The first sampling campaign assessed background soil properties including soil chemistry and texture. The subsequent three sampling campaigns were implemented to assess the spatiotemporal distribution of soil moisture patterns. The last sampling campaign was implemented to sample bulk density. The top 30 cm of the soil were sampled in triplicate within a 30 cm diameter of the field sample marker resulting in a surface sample support of about 0.09 m^2. Triplicates were bulked to produce one composite sample for each sampling location.

Soil moisture sampling campaigns were scheduled by rainfall events and concomitant changes in soil moisture content through time. The three soil moisture sampling dates were July 7, 2012, September 11, 2012, and October 5, 2012 (Table 2.1). Five plastic cylinder rain gauges were installed in the center and peripheral four corners of the study area to record rainfall on a weekly basis (Figure 2.4). The rainfall record for the study duration is exhibited in Figure 2.5. Rain gauges were mounted on a stand approximately 1 meter above the soil surface. Oil was poured into each gauge to deter evaporation. Rain gauges were too sparse to estimate rainfall distribution across the field using geostatistics (e.g. kriging). Consequently, a simple spline function (Spatial Analyst, ArcMap 10.0) was applied to generalize rainfall input across the site (Figure 2.4). A mesonet station, which records rainfall input on an hourly basis, was located at Spindletop Farm several kilometers from the area of investigation. This data is illustrated in Figure 2.6. The discrepancy in rainfall amounts between the rain gauges and mesonet station is due to

differences in location but also timing of the readings (mesonet produces real-time readings versus weekly rain gauge readings).

The soil moisture range amid the three dates were estimated to encompass the plant wilting point (July) up to field capacity (October) for the silt loam soils studied (Saxton and Rawls 2006) (Table 2.1). The U.S. Drought Monitor declared a Level 1 (moderate) drought for Central Kentucky during June and July 2012 and the remainder of the sampling season was classified as abnormally dry.

Table 2.1. Soil moisture sampling dates.

	July	September	October
Date	7/17/12	9/11/12	10/5/12
Mean*	0.18	0.26	0.31
Range*	0.12 - 0.26	0.18 - 0.33	0.25 - 0.40
Standard Deviation*	0.030	0.030	0.030

*Units are vol./vol.

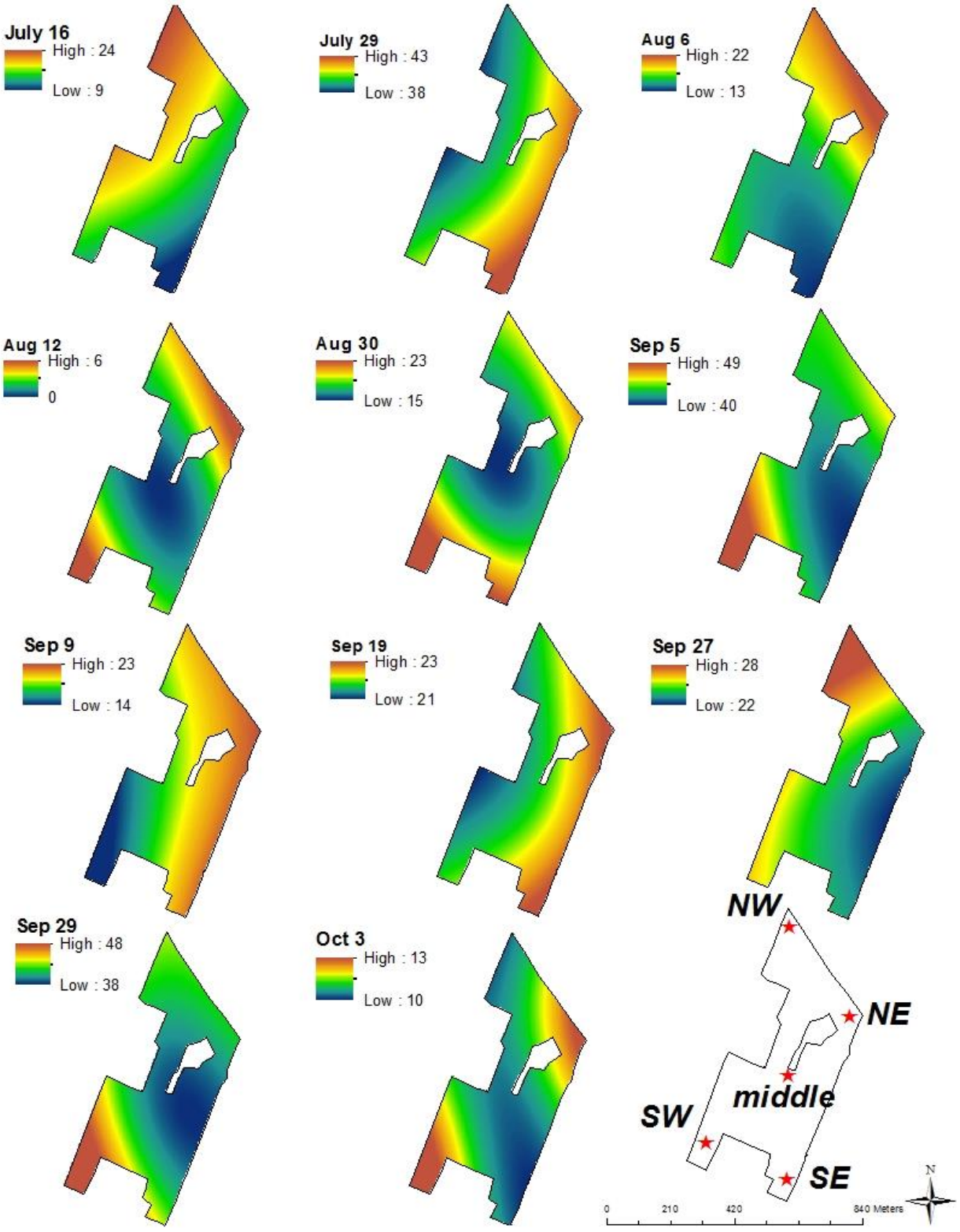

Figure 2.4. Interpolated rainfall input.

Rain gauge positions are illustrated. Units are in millimeters.

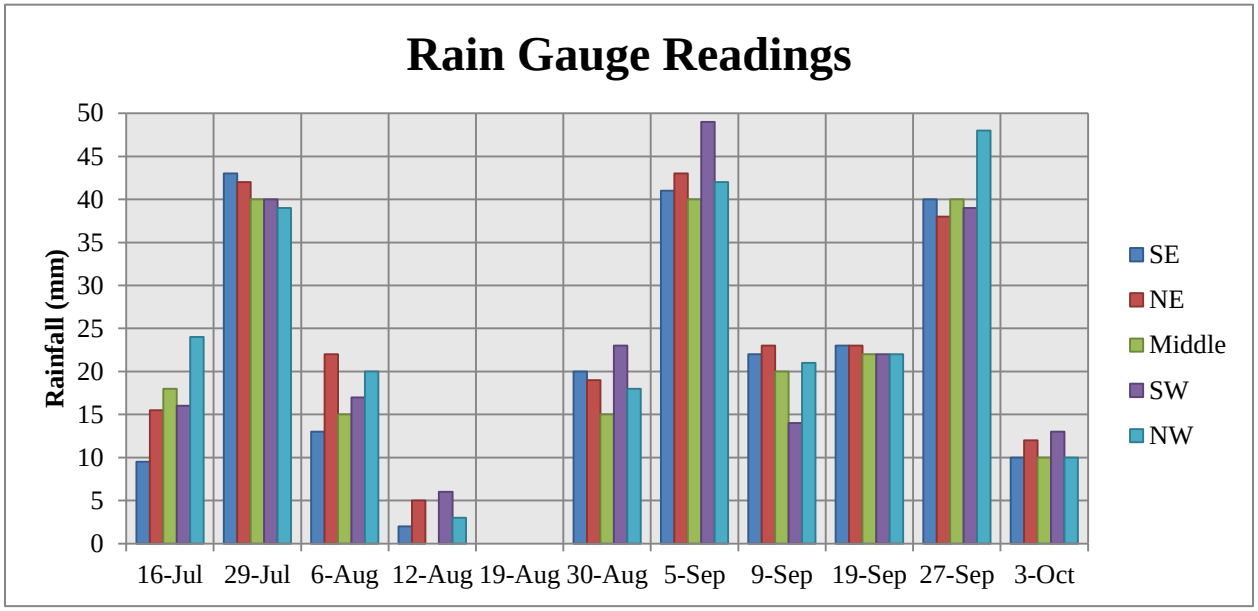

Figure 2.5. Rainfall measurements.

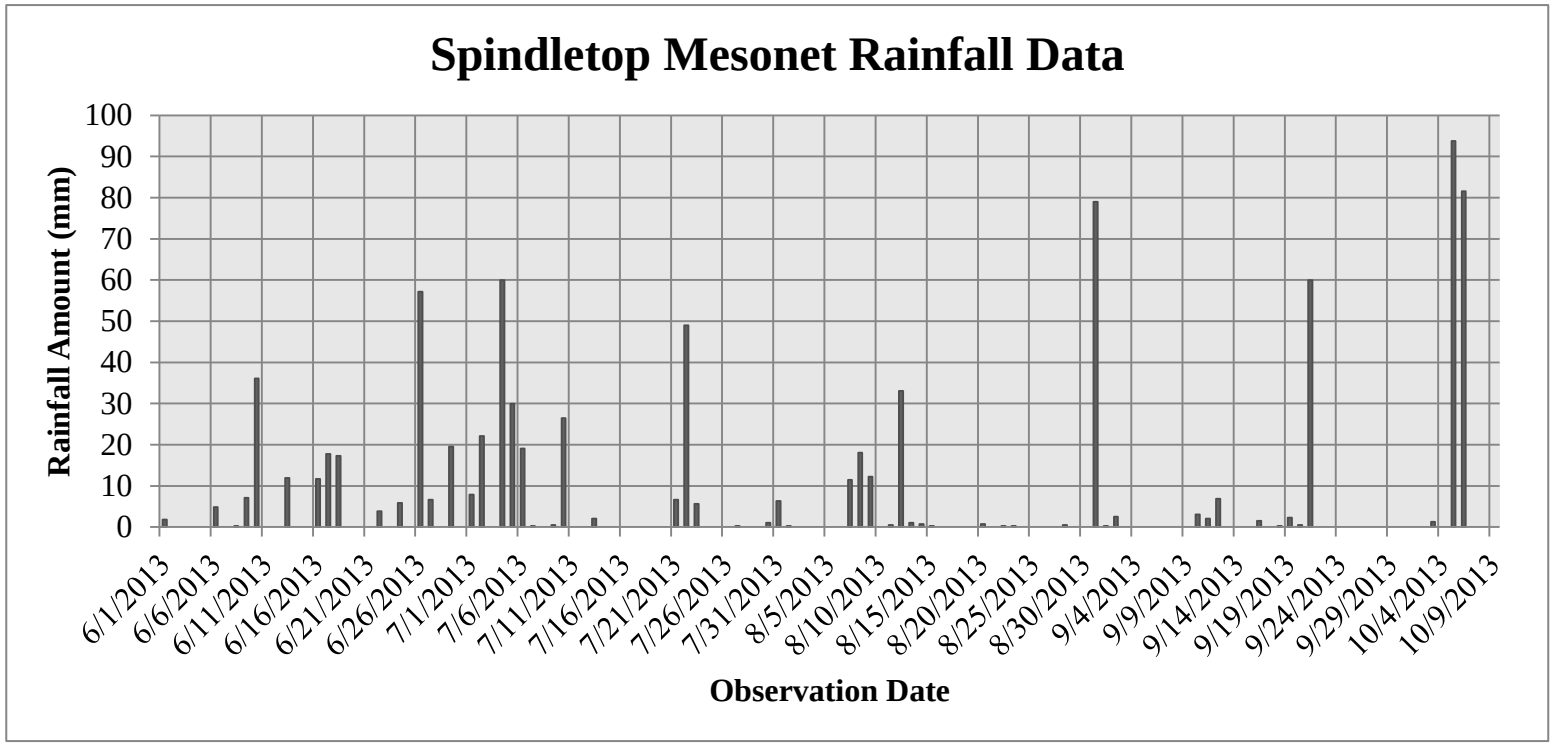

Figure 2.6. Spindletop Mesonet rainfall data.

Background Soil Parameters

Soil Regulatory Services Analyses: Soil pH, Organic Matter and Mehlich III-Extractable Elements

Ground soil samples (n=127) were submitted to the University of Kentucky's Regulatory Services for routine soil tests and organic matter analysis. Routine soil tests include pH, buffer pH, and Mehlich III-extractable P, K, Ca, Mg, and Zn (Anonymous, 2000). Prior to analysis, ground soils were passed through a 2mm screen. A brief description of the analysis procedures follows. To measure pH a soil paste was produced by adding 10 ml of water and a KCl buffer solution to 10 cm^3 of soil and left to stand at least 15 minutes but no longer than 2 hours. A glass electrode was used to measure KCl pH, then 10 ml of Sikora Buffer (a mixture of triethanolamine, imidazole, MES, acetic acid, and KCl) was added and the slurry agitated for 10 minutes. Another measure of pH (buffer pH) was obtained within 2 hours post agitation. Because pH was measured using a KCl solution, to attain soil-water pH [Eqn.2-1], established by the Regulatory Services, was applied to the KCl pH values.

$$\text{soil water pH} = (0.91 \times \text{KCl pH}) + 1.34 \quad \text{[Eqn. 2-1]}$$

Organic Matter

To measure organic matter, 1.5 grams of 2 mm sieved soil was placed in a porcelain boat and injected into a dry combustion instrument (LECO or Elemental) to determine the percent carbon in the soil sample. The percentage of organic matter was calculated by multiplying % carbon by 1.72 and reported as percent weight of air-dried soil. Soil

texture analysis was completed on all 127 soil observations collected in June 2012 using a modified pipette method (Gee and Bauder 1986).

Soil Texture

Sample preparation included removing large debris (e.g. plant roots, bugs, etc.) and subsequently drying the soil samples at ambient temperature for one week. Air dried samples were ground and homogenized. Texture analysis was performed in 20 sample increments resulting in a total of seven procedural runs. Forty grams of soil were pre-weighed and placed in stainless steel cups. Organic matter digestion was performed to oxidize organic matter present within the soil samples. Approximately 10 mL of deionized (DI) water was added to the soil producing a soil slurry. Predetermined levels, per suggested by UK's Regulatory Services, of hydrogen peroxide (30%, Sigma Aldrich) were added to the soil slurry in 20 mL increments every 15 minutes based on soil organic matter content. The digestion slurries were in place for five hours with periodic agitation by swirling the slurry to ensure equal digestion. Fifty milliliters of sodium hexametaphosphate (50 mg/L, Fisher Scientific) and approximately 30 mL of DI water was added to the digestion slurry and subsequently mixed for 5 minutes using an industrial mixer to aid soil particle dispersion. Stainless steel cups filled with mixed soil slurry were rinsed with DI water into 1,000 mL graduated cylinders. Each graduated cylinder was filled with DI to 1,000 mL. A blank graduated cylinder was prepared with 950 mL of DI water and 50 mL of sodium hexametaphosphate. A glass thermometer was placed in the blank to measure the water temperature. Each graduated cylinder (except the blank) was stirred for 1 minute successively until all cylinders were complete. The

settling time for the cylinders was determined by the temperature of the blank solution and Stokes' Law (Eqn. 2-2):

$$\text{settling velocity (cm/s)} = \frac{(\rho_s - \rho_l) * D^2 g}{18\eta} \qquad \text{[Eqn. 2-2]}$$

where ρ_s is the density of a spherical soil particle (2.7 g/cm^3), ρ_l is the density of the liquid (1 g/cm^3); D is the particle diameter (cm); g is the gravimetric constant (cm/s^2); and η is the liquid viscosity (g/cm.s). Soil particles suspended in solution will settle at varying rates depending on the size of the mineral particle; sand particles (diameter 2.00 - 0.05 mm) settle faster than silt (diameter 0.05 - 0.002 mm) or clay (diameter <0.002 mm) particles. Room temperature of the blank was 22° C resulting in a 3 hour 42 minute sampling time for the clay fraction. The clay fraction was sampled at a 5 cm depth beneath the slurry meniscus using a 25 mL glass pipette and bulb. The 25 mL sample was then expulsed into a 50 mL pre-weighed plastic beaker. The remainder of the soil solution in the graduated cylinder was poured and rinsed using a # 270 sieve and DI water to collect the sand fraction. The rinsed sand fraction was poured into a 50 mL beaker. The solution in the blank cylinder was also sampled by extracting 25 mL of blank solution and expulsing the solution in a 50 mL beaker. The 50 ml beakers were placed in the oven and dried over night at 100° C.

To calculate soil texture on a percent basis the weight of the empty 50 mL beakers were subtracted from the weights of the beakers containing dried clay and sand fractions. The weight of the dried sodium hexametaphosphate was subtracted from the clay sample. The clay fraction was calculated by subtracting the weight of the dried sodium

hexametaphosphate from the dried clay and subsequently multiplying the dried clay (g) by 40 (because 25 mL goes into 1,000 mL 40 times). The sand fraction was calculated by subtracting the beaker weight from the dried sand sample. The silt fraction was calculated by subtracting the clay and sand fractions from total weight of pre-weighed soil (40 g).

Cation Exchange Capacity and Exchangeable Acidity

A 20 mL Mehlich III solution containing 0.2 N acetic acid, 0.25 N NH_4NO_3, 0.015 N NH_4F, 0.013 N HNO_3, and 0.001 N EDTA was added to 2 cm^3 soil and subsequently shaken for 5 minutes. The Mehlich III solution was the immediately filtered through Whatman #2 filter paper. The filtered solution was analyzed using inductively coupled plasma spectrometry (ICP). The air dried soils were assumed to have a bulk density of 1 g/cm^3. Soil cation exchange capacity (CEC) was estimated using Regulatory Services' soil test data (Ca, Mg and K) and measured potassium chloride (KCl) exchangeable soil acidity. Units for Regulatory Services' soil test data (Ca, Mg and K) were converted from lbs/acre to molar equivalents (cmol/kg). The conversion was calculated by dividing the Regulatory Services lab value (lbs/acre) by the equivalent weight (molecular weight/valence) of the cation and multiplying by 20.

A potassium chloride method proposed by Thomas (1982) was used to measure exchangeable acidity. Ten grams of ground soil was added to 25 mL of 1N KCl solution and mixed with a stirring rod. After 30 minutes, the KCl soil slurry was transferred to a Büchner funnel fitted with Whatman #2 filter paper and mounted on a 250 mL vacuum flask. The soil slurry was filtered and rinsed with an additional 125 mL of KCl in 25 mL increments culminating a 150 mL filtrate solution. Four to five drops of phenolphthalein

was added to the filtrate solution and titrated with 0.1N NaOH until reaching the first permanent pink endpoint. A blank of 0.1N NaOH was titrated on a daily basis and/or when a new solution was prepared. The blank was subtracted from each sample titration to correct for the NaOH solution. Equation 2-3 was used to calculate KCl exchangeable acidity (meq/100 g).

$$\text{meq KCl} = \frac{(\text{mL NaOH sample - mL NaOH blank}) \times \text{N} \times 100}{100 \text{ g soil}} \qquad \text{[Eqn. 2-3]}$$

where N is the normality of the solution. The estimated CEC was calculated by summing the Ca, Mg, K and KCl exchangeable acidity (cmol/kg).

Bulk Density and Volumetric Water Content

Samples for gravimetric soil moisture for each date were cored using a simple hand augur with a coring shaft 30 cm long and diameter of ~5 cm. Due to unannounced farm management procedures, some sampling locations were unavailable for sampling. The total number of sites sampled in July was 125; in September, 121; and in October, 124. The top 30 cm of the soil were sampled in triplicate within a 30 cm diameter of the field sample marker resulting in a surface sample support of about 0.09 m^2. Soil samples were oven dried 105°C overnight (12 hours) to calculate gravimetric water content (θ_g) [Eqn. 2-4].

$$\theta_g = \frac{Wet\ (g) - Dry\ (g)}{Dry\ (g)} \qquad \text{[Eqn. 2-4]}$$

Bulk density was sampled in a single 4-week sampling campaign using an Arts Machine Shop (AMS) soil corer with a core cylinder length of 10 cm and diameter of 5 cm. Soil cores were collected in 10 cm increments to a depth of 30 cm at each location. Dry bulk

density (cm^3) for the top 30 cm of soil was calculated by averaging the three oven dried depths. Volumetric water content (θ_v) for the top 30 cm of soil was calculated by [Eqn. 2-5] where ρ_b is the bulk density of the soil and ρ_w is the density of water.

$$\theta_v = \frac{\rho_b \theta_g}{\rho_w} \quad \text{[Eqn. 2-5]}$$

Basic statistics for soil attributes are located in Appendix A.

LiDAR Altimetry

Light detection and ranging (LiDAR) uses laser light pulse returns to measure surface characteristics of the Earth. There are four main components that construct a laser scanning platform: a laser emitter-receiver scanning unit, an inertial measurement unit (IMU), a differential global positioning system (GPS), and a computer control system to store data (Reutebuch et al. 2005). The laser scanning systems rapidly emits laser pulses with wavelengths ranging from 250 nm to 11μm. The laser pulse generated travels at a constant and known speed so it is possible to calculate the distance over which the laser returns travel. The simple relationship between light speed, wavelength and frequency is illustrated by [Eqn. 2-6].

$$c = \lambda f \quad \text{[Eqn. 2-6]}$$

where c is the speed of light (299,792, 458 m/s); λ is the light wavelength, and f is the frequency at which wavelengths pass per time. Equation 2-7 exhibits how to calculate the distance of a reflected photon.

$$\text{distance traveled} = \frac{\text{c} \times \text{time of flight}}{2} \quad \text{[Eqn. 2-7]}$$

To ensure accuracy the moving height and orientation of the laser system platform is measured by the IMU. The IMU measures the rotation and acceleration of the airborne platform using gyroscopes and accelerometers.

The laser pulses interact with various objects residing beneath the airborne platform including vegetation, buildings, and power lines. These objects affect the return time of the laser pulses depending on their height. Consequently, the georeferenced laser point returns are collected in different layers and these layers as a collective are commonly referenced as a point cloud. The LiDAR point cloud (LAS version 1.2 file format) was obtained for the research site. LiDAR was flown and post-processed by a private vendor (Photo Science, Inc., Lexington, KY) in spring of 2010 with a nominal pulse spacing of ≤1 meter and vertical accuracy of 18 cm $RMSE_z$ (Photo Science, Inc.). The LiDAR point cloud was imported into ArcGIS 10.0 as a multipoint shapefile using the 3D ArcToolbox (ESRI® ArcMap™ 2010). The multipoint file was converted to raster with a nominal grid cell size to assure each grid cell represented only one LiDAR point value. The ground class LiDAR returns (class 2) was selected from the point cloud to complete terrain analyses (Chapter 3). Just over 490,000 LiDAR pulse returns were included for analysis. The LiDAR returns were re-projected using a horizontal data of NAD 1983, and Universal Transverse Mercator map projection (Zone 16 North) and a vertical datum of NADV88.

Soil Apparent Electrical Resistivity (aER)

According to Ohm's Law, the measured resistance (R) is directly proportional to the voltage (V) and inversely proportional to the electrical current (i) (Rhoades et al. 1999) [Eqn. 2-8].

$$R = \frac{V}{i} \qquad \text{[Eqn. 2-8]}$$

The resistance (R) of a homogeneous conductive medium is inversely proportional to its cross-sectional area (A) and proportional to its length (ℓ) [Eqn. 2-9] (Rhoades et al. 1999).

$$R = \rho \frac{\ell}{A} \qquad \text{[Eqn. 2-9]}$$

Resistivity (ρ; ohm m) is defined as one ohm (ω) of resistance that allows a current of one ampere to flow when a single volt of electricity is applied (Allred et al. 2008) [Eqn. 2-10].

$$\rho = R \frac{A}{\ell} \qquad \text{[Eqn. 2-10]}$$

Electrical conductivity (C, ω^{-1} Siemens, S) is the inverse of electrical resistivity and is commonly measured as millisiemens per meter (mS m^{-1}) (Allred et al. 2008) [Eqn. 2-11].

$$C = \frac{1}{\rho} \qquad \text{[Eqn. 2-11]}$$

When electrical current is passed through a heterogeneous medium, such as soil, electrical resistivity (ER) is commonly notated as aER for bulk *apparent* resistivity. Bulk soil aER was measured using a Veris 3100 (Veris Technologies, Salina, KS). The instrument has six coulter electrodes mounted on a tractor-pulled metal frame chassis. The electrodes are inserted approximately 2.54 cm (one inch) into the soil surface. The instrument injects a 150-Hz 4.5 volt RMS electrical current into the soil between potential electrodes (Hartsock 2001). The measured difference in voltage between potential electrodes is used to calculate apparent electrical conductivity via the Wenner array [Eqn. 2-12]:

$$aEC = \frac{i}{2\pi dV} \qquad \text{[Eqn. 2-12]}$$

where d is the distance between two adjacent electrodes. The observation depth can be estimated by the electrode spacing and configuration. A shallow (~ 31 cm) observation depth and a deep (~91cm) observation depth are obtained using the Veris by alternating the current between electrodes spaced 21 cm and 100 cm apart, respectively (Hartsock 2001). The Veris uses a DGPS (Trimble AgGPS 132, Sunnyvale, CA) to geo-reference aEC observations (Hartsock 2001).

As the electrical current passes through the subsurface it will encounter resistance. The difference in voltage between the potential electrodes measures the resistance of soil electrical properties encountered by the current flow path. Differences in measured voltage provide information about the spatial heterogeneity, or contrasts, of subsurface soil properties. A greater difference in measured potential, or measured resistivity, between observations illustrates a stronger image contrast between subsurface soil

properties (Samouelian et al. 2005). Image contrasts measured using electrical resistivity techniques can therefore serve as a proxy to study subsurface heterogeneity in both space and time (Samouelian et al. 2005, Amidu and Dunbar 2007, Amidu 2008).

In theory, there are three pathways by which an electrical current can pass through a soil medium: the soil pore fluid, the soil-liquid interface and indurated soil minerals (Rhoades et al. 1999, Lesch and Corwin 2003). Because soil minerals are non-conducting, the latter pathway is commonly neglected (Corwin and Lesch 2005a). Soil properties directly influencing apparent EC are texture, porosity, salinity, temperature, and degree of soil saturation (Corwin and Lesch 2003, Corwin and Lesch 2005a, Corwin and Lesch 2005b). Apparent EC measurements are temperature dependent. Therefore, apparent EC measurements are commonly standardized to a reference temperature using empirical models; thereby reducing time dependency to soil moisture (Besson et al. 2008, Ma et al. 2011). This research utilized the ratio model to standardize apparent EC prior to data analysis (Ma et al. 2011) [Eqn. 2-13]:

$$EC_{25} = \frac{EC_T}{1+\delta(T-25)} \qquad \text{[Eqn. 2-13]}$$

where EC_{25} is the standardized electrical conductivity at 25°C, EC_T is the EC at the measured temperature T, and δ is the temperature slope compensation ($0.0191°C^{-1}$). The slope compensation term was derived in a laboratory setting using a 0.01 M KCl solution (Ma et al. 2011).

Five nested soil thermocouples (Campbell Scientific) that were installed in late October 2011 at 10, 20, 40, 70, and 150 cm depth intervals were used to monitor soil temperature. Soil temperature varies in space according to landscape and soil properties, however,

budget constraints limited soil temperature measurements to a single location in the field. This study assumes that the measured soil temperature is representative of the field. Sudduth et al. (2003) shows that most of current flow resides in the 30 cm depth using a modified Wenner array configuration. To standardize apparent EC readings an average soil temperature value was calculated at 30 cm between the 20 and 40 cm depths. The average temperature reading was then utilized in [Eqn. 2-13] to standardize apparent EC readings for temperature. Average soil temperatures for the three dates observed by the Veris were 23.9°C for July 17th, 21.1°C for September 11th, and 17.8°C for October 5th.

High resolution apparent EC (Veris Tech 3100) measurements were captured in tandem with soil moisture sampling. The Veris 3100 sampling grid produced over 9,500 georeferenced apparent EC points for each sampling date: July 17, September 11, and October 5, 2012 (Figure 2.7). Point spacing within a given transect is ~2.3 meters with north/south swaths spanning ~10m. Each georeferenced sampling location consists of a shallow (30cm) and deep (90cm) reading.

Data pre-conditioning consisted of removing negative apparent EC values, sampling duplicates, and outliers. Negative values were prominent for the deeper readings and are thought to arise from poor electrode contact with the soil. The four soil sample nests were sampled counter-clockwise within the field, starting from the SW nest, prior to implementing the larger transect grid. For July, apparent EC for the two nests located on the south side of the field were at least one order of magnitude higher than the rest of the field; including swaths that transverse the nest when completing the transect grid. These values are anticipated to arise from a mechanical source (i.e. leaking water from the tank). Consequently, these values were removed in preparation for analyses. Other dates

did not exhibit the same characteristics. Sampling duplicates arise from superimposed GPS readings and were removed for geostatistical analyses.

Basic statistics for apparent EC are located in Appendix A.

Figure 2.7. Veris 3100 apparent EC sampling grid.

Chapter 3

Using Nonstationary Geostatistics and Spatial Component Filtering to Build a Digital Elevation Model for Modeling Terrain Attributes

Introduction

In saturated or near saturated conditions soil moisture distribution is influenced by gravitational forces and can self-organize into spatial patterns mirroring that of the landscape (Grayson et al. 1997, Western et al. 1999, Gòmez-Plaza et al. 2000, Grayson and Western 2001, Grayson et al. 2002, Lin et al. 2008b). Therefore, terrain attributes and wetness indices are attractive proxy tools to quickly and cheaply assess soil moisture distribution over large observation extents (Zhu and Lin 2009). Terrain attributes can include slope (1^{st} derivative of elevation), curvature (2^{nd} derivative of elevation), upland contributing area, aspect, and combinations thereof producing indices such as the topographic wetness index (TWI) (Grayson et al. 1997, Western et al. 1999, Gòmez-Plaza et al. 2000, Grayson and Western 2001, Kienzle 2004, Lin et al. 2006, Moller et al. 2008, Robinson et al. 2009, Zhu and Lin 2009, Robinson et al. 2012).

The TWI proves most relevant when lateral soil moisture distribution (i.e. surface runoff and subsurface throughflow) dominates (Grayson et al. 1997, Western et al. 1999). In general, the TWI represents convergent gullies as wet and divergent hillslopes as dry (Wilson et al. 2004). The applicability of the TWI depends on antecedent soil moisture conditions, soil horizonation, rainfall input (intensity and duration), and rainfall infiltration rates (Gòmez-Plaza et al. 2000, Manfreda et al. 2007). Because slope has shown to be poorly correlated with soil moisture under dry conditions, Gòmez-Plaza et al. (2001) modified the TWI to produce a ‘Second New Index’ [sic] by removing slope in

the denominator. Western et al. (1999) also made suggestions to improve the TWI by incorporating plan curvature into the calculation.

Curvature is produced by taking the second derivative of elevation and is calculated in two distinct directions oriented perpendicular or parallel to the slope. Plan (i.e. horizontal) curvature is measured perpendicular to the slope and is favored for studying lateral flow. Plan curvature helps identify the tendency for flow to accelerate or decelerate based on topographic convergence (positive curvature) or divergence (negative curvature) (Zevenbergen 1987, Gallant 1996, Florinsky 2012). Profile (i.e. vertical) curvature is measured parallel to the slope and is helpful for measuring flow velocities and differentiating slope positions such as upper and lower slopes (Zevenbergen 1987, Gallant 1996). Profile curvatures with a positive value indicate a convex profile in which the slope increases downhill (indicative of upper slopes) and a negative value that indicates a concave profile in which the slope decreases downhill (indicative of lower slopes) (Gallant 1996).

Modeling soil-water-terrain interactions is readily facilitated using a DEM and a geographic information system (GIS) platform. Building a DEM is a precursor to calculating terrain attributes and can be constructed using various techniques such as binning and interpolation. Binning is arguably the simplest method and can be readily applied to high sample density datasets, such as light detection and ranging (LiDAR). Binning selects different LiDAR class return values using the minimum, maximum, or average criterion to create a raster cell (Wechsler et al. 2009). The minimum binning criteria has been suggested to reduce vertical errors in the DEM (Rosso et al. 2006, Schmid et al. 2011). Interpolation techniques consist of two general classes: 1)

geostatistical (kriging); 2) deterministic (inverse distance weighted, spline, nearest neighbor) (Anderson et al. 2007, Liu 2008, Guo et al. 2010). These techniques are subjective and inherently vary with respect to DEM quality. For example, binning does not take into account the spatial association between adjacent cells that can lead to problems when calculating the derivatives of the DEM and can underestimate elevation in low lying areas (Rosso et al. 2006). Anderson et al. (2007) found that IDW is comparable to ordinary kriging with high resolution datasets; this outcome is supported by other studies (Rosso et al. 2003). However, it has been argued IDW produces interpolation artifacts, or unrealistically shaped terrain features, from irregularly sampled elevation points (Kienzle 2004). Guo et al. (2010) argued kriging is the superior method because it accounts for spatial autocorrelation and models elevation using the best linear unbiased estimates.

These techniques are common, but an alternative approach is to produce a DEM utilizing nonstationary modeling, specifically, Intrinsic Random Function of Order-k, in tandem with spatial component filtering. This geostatistical technique decomposes the total variation into two components: 1) the trend, or deterministic mean component; 2) the stochastic component constituting a spatially correlated random component with mean zero that is associated with a generalized covariance (GC) function. Spatial component filtering operates akin to Fourier analysis in that the total spatial variation can be filtered according to the frequency, or scale, of variation. The impetus behind spatial component filtering is to suppress unwanted high frequency variation to estimate elevation via kriging.

The objective of the research reported in this chapter is to implement nonstationary geostatistics in tandem with spatial component filtering to estimate a high resolution DEM that will be used to derive terrain attributes including slope, plan curvature, profile curvature and the TWI. The motivation of this study is to filter the high frequency component and use only the low frequency spatial component to produce the DEM. The results from spatial component filtering are compared to the more traditional binning technique to illustrate the strengths and weaknesses between the two techniques in terms of surface hydrologic modeling.

Materials and Methods

LiDAR

LiDAR was flown and post-processed by a private vendor (Photo Science, Inc., Lexington, KY) in spring 2010 with a nominal pulse spacing of ≤1 meter and vertical accuracy of 18 cm RMSE (Photo Science, Inc.). Just over 490,000 LiDAR pulse returns were subjected to the subsequent analyses. Ground class LiDAR returns were selected from the LAS (version 1.2) file to build the DEM. The LiDAR were re-projected using horizontal data of North American Datum (NAD) 1983, vertical data of North American Vertical Datum (NAVD) 1988, and Universal Transverse Mercator map projection (Zone 16 North) with linear and vertical units in meters.

Constructing a Digital Elevation Model

In this study two methods were implemented to calculate a DEM using the LiDAR point cloud: 1) binning; 2) nonstationary geostatistics and spatial component filtering.

Binning can be implemented in ArcMap™ 10.1 (ESRI®) in which LiDAR values falling within a given raster grid cell (e.g. pixel) are subjected to an objective function (e.g. averaging, interpolation) or classification (e.g. minimum value, maximum value, etc.) to produce a discrete pixel value. Binning was implemented using the "minimum value" criterion to calculate a 1 m DEM from the LiDAR point cloud. The minimum value criterion was selected because it is desirable to select the lowest return to represent elevation. The average nominal pulse spacing was ≤ 1 m, therefore, at least one point was expected to fall within each grid cell.

Ostensibly, nonstationary geostatistics is a more robust technique because it accounts for the spatial correlation between LiDAR points to estimate elevation at a target location. Nonstationary geostatistics becomes important when elevation exhibits a spatial behavior that neglects the assumptions of second-order or intrinsic stationarity. To model nonstationary spatial processes, techniques such as Universal Kriging, regression kriging, and Intrinsic Random Function of Order-k are applied. Universal kriging (UK) is a stochastic modeling approach commonly implemented to make spatial estimates when the mean is not constant. In such a case, the expected value of the mean is expressed by a linear combination of functions ($f^{l}_{(x)}$) that are, generally, polynomial (e.g. trend function). The universal kriging method is cumbersome because it needs to simultaneously solve two unknowns for the kriging system: 1.) the coefficients of the trend function; 2.) the spatial covariance function of the stationary residuals of the mean. The trend coefficients are not required to solve the kriging system due to the conditions that the estimates are unbiased (i.e. the sum of kriging weights equals 1 and the variance of error is minimized). Because the trend function is unknown, however, it is impossible to filter the mean to

establish the stationary residuals to fit a covariance model, thereby, complicating the second kriging condition. Therefore, solving the universal kriging system requires a computationally cumbersome iterative sequence of calculating the trend coefficients; establishing the stationary residuals of the trend; and fitting the semivariogram to the stationary residuals. This iterative sequence is complete when the variation of coefficients is below a certain threshold.

Intrinsic random function of order-*k* (IRF-*k*) is an approach developed by Matheron in 1973. The attractiveness of IRF-k is it avoids bias in coefficient estimates typical to regression kriging (Lark and Webster 2006) and circumvents the time-consuming, computationally demanding universal kriging iterative approach (Buttafuoco and Castrignanò 2005). In the IRF-*k* model the total variance is split into a trend (deterministic) component and a stochastic component [Eqn. 3-1] (Bleines et al. 2012). Much like the universal kriging system, the IRF-*k* represents the deterministic trend as a low order polynomial function that depends on position (Webster and Oliver 2001) [Eqn. 3-2]. The residuals of the trend component represent a rapidly fluctuating, spatially structured stochastic component $\left(Z_p(\boldsymbol{x})\right)$ [Eqn. 3-1] with zero mean (Buttafuoco and Castrignanò 2005, Cafarelli and Castrignanò 2011). The stochastic component commonly represents several spatial structures of independent, random variation that can be described by a linear nested covariance structure. Each model component references an individual spatial component (p) in [Eqn. 3-1]. Because the trend function is of a higher order (e.g. polynomial assumed to be of a positive order ≤ 2) the covariance calculated by the linear spatial increments established by the semivariogram are not strong enough to filter the trend. Instead, a more robust covariance function, called the

generalized increments of higher order-*k* is used to calculate the correlation structure of the trend's stochastic residuals.

$$Z(\boldsymbol{x}) = \sum_{p=0}^{P} Z_p(\boldsymbol{x}) + m(\boldsymbol{x}) \qquad \text{[Eqn. 3-1]}$$

$$m(\boldsymbol{x}) = \sum_{l=0}^{k} a_l f_{(x)}^{l} \qquad \text{[Eqn. 3-2]}$$

In Eqn.'s 3-1 and 3-2, $f_{(x)}^{l}$ are basic monomials in which l represents the degree of the monomial, K is the number of monomials, and a_l are the unknown coefficients that vary with the search neighborhood (Chilés and Delfiner 1999, Buttafuoco and Castrignanò 2005, Bleines et al. 2012). The coefficients of the trend need not be known *a priori* to estimate the covariance of the residuals, only the degree of the polynomial is necessary (Buttafuoco and Castrignanò 2005).

The 'order k' describes a polynomial function of a given order as illustrated in [Eqn. 3-2]. When k=0 the system resorts to the stationary case where the linear spatial increments (e.g. semivariogram) are sufficient in modeling the covariance function. To establish generalized stationary increments of order *k*, a condition is imposed on the IRF-k ($f_{(x)}^{l}$) functions so the estimates of the trend are unbiased (Bleines et al. 2012). This condition is applied to the weights (λ_α) that define the search neighborhood used to establish the set of monomials of order $\leq k$ in [Eqn.3-3]. The IRF-*k* model establishes an allowable linear combination of these weights if they meet the condition of [Eqn. 3-4] (Chilés and Delfiner 1999).

$$Z(\lambda) = \sum_{\alpha=1}^{N} \lambda_\alpha Z(\boldsymbol{x}_\alpha) \qquad \text{[Eqn. 3-3]}$$

$$\sum_{\alpha=1}^{N} \lambda_\alpha f^l(x_\alpha) - f^l(x_0) = 0 \quad \text{[Eqn. 3-4]}$$

In Eqn.'s 3-3 and 3-4, α represents a sampled location; λ_α are the search neighborhood weights; $Z(\boldsymbol{x}_\alpha)$ are random variables at locations $\boldsymbol{x}_\alpha$; and N is the total sampled population. If $(\lambda_\alpha Z(\boldsymbol{x}_\alpha))$ produces stationary residuals with respect to spatial increments $(\boldsymbol{x}_\alpha - \boldsymbol{x}_\beta)$, then it is considered an intrinsic random function of order-*k*, or allowable linear combination of order-*k* (ALC-*k*), of the polynomial to be filtered.

The spatial covariance $K(x_\alpha - x_\beta)$ of the stationary stochastic residuals can be analyzed as a function of distance (h) between observations (x_α, x_β) using the generalized covariance (GC) $K(\boldsymbol{h})$ structure. For any ALC-k the generalized covariance $K(\boldsymbol{h})$ is (Bleines et al. 2012):

$$Cov\left[\sum_{\alpha=1}^{N} \lambda_\alpha Z(x_\alpha), \sum_{\beta=1}^{N} \lambda_\beta Z(x_\beta)\right] = \sum_{\alpha=1}^{N}\sum_{\beta=1}^{N} \lambda_\alpha \lambda_\beta K(\boldsymbol{x}_\alpha - \boldsymbol{x}_\beta) \qquad \text{[Eqn. 3-5]}$$

where K represents the generalized covariance function. The generalized covariance consists of a linear combination of a given set of generic polynomial structures $K^p(\boldsymbol{h})$ of which the sill (b_p) must be determined [Eqns. 3-6 and 3-7]:

$$K(h) = \sum_{p} b_p K^p(\boldsymbol{h}) \qquad \text{[Eqn. 3-6]}$$

via minimizing the estimation error. Each polynomial structure is scripted as (p). The covariances constituting the GC functions are sensitive only to the modulus of vector $|\boldsymbol{h}|$ and not direction, thereby making the GC model strictly isotropic. The relative importance of each GC component is determined by its preceding coefficient:

$$K(h) = C_0\delta|h| - b_0|h| + b_s|h|^2 log|h| + b_1|h|^3 \quad \text{[Eqn. 3-7]}$$

where $\delta|h| = 0$ for $h > 0$, else $\delta|h| = 1$. For $K(h)$ to be a valid generalized covariance the coefficients must satisfy the following conditions (Chilés and Delfiner 1999):

$$C_0 \geq 0, \qquad b_0 \geq 0, \qquad b_1 \geq 0, \qquad b_s \geq -\frac{3}{2}\sqrt{b_0 b_1}$$

Ensuring the estimation error is an ALC-k [Eqn. 4] and its variance is minimized when fitting the GC [Eqns. 3-6 and 3-7] it is possible to derive the intrinsic kriging system [Eqns. 3-8a and 3-8b] (Buttafuoco and Castrignanò 2005):

$$\begin{cases} \sum_{\beta=1}^{N} \lambda_\beta K(\boldsymbol{x}_\alpha - \boldsymbol{x}_\beta) - \sum_{l=0}^{K} \mu_l f^l(\boldsymbol{x}_\alpha) = K(\boldsymbol{x}_0 - \boldsymbol{x}_\beta) \quad \alpha = 1, \dots, N & \text{[Eqn. 3-8a]} \\ \sum_{\alpha=1}^{N} \lambda_\alpha f^l(\boldsymbol{x}_\alpha) = f^l(\boldsymbol{x}_0) \quad l = 0, \dots, k & \text{[Eqn. 3-8b]} \end{cases}$$

with an intrinsic kriging variance of order-*k* [Eqn. 3-9] (Buttafuoco and Castrignanò 2005):

$$\sigma_K^2 = K(0) - \sum_{\alpha=1}^{N} \lambda_\alpha K\left(\boldsymbol{x}_0 - \boldsymbol{x}_\beta\right) + \sum_{l=0}^{K} \mu_l f^l(\boldsymbol{x}_0) \quad \text{[Eqn. 3-9]}$$

where μ_l is the Lagrange multiplier, $K\left(\boldsymbol{x}_\alpha - \boldsymbol{x}_\beta\right)$ is the generalized covariance, $\boldsymbol{x}_0$ is the estimation point and $\boldsymbol{x}_\alpha$ is the sampling point.

Fitting an IRF-k Model and Kriging

An IRF-k model was fit to the LiDAR point cloud using ISATIS® software (Geovariances 2012). The data exhibited slight departures from normality and were consequently transformed to unit variance and mean zero using Gaussian Anamorphosis in ISATIS®. The modeling approach determines the order of the trend by splitting the entire data set into two rings, one for calibration and one for validation. Ring 1 represents a calibration set and encompasses sampling points in close proximity to the seed, or target point, in which the elevation is to be estimated. Ring 2 is used for validation and encompasses samples in distant proximity from the seed point. The procedure is subsequently repeated by inverting the rings, so ring 1 serves as the validation sample set and ring 2 the calibration sample set. Each polynomial order, $k = 0, 1$ or 2, is subjected to this process. For each model fitted, the experimental errors (predicted – measured) are calculated and ranked according other the error values (smallest to largest). The mean value of the rank, mean value of the experimental error, and the variance of the experimental error are calculated to help determine the best model. The model with the lowest mean rank is preferred (Chilés and Delfiner 1999, Buttafuoco and Castrignanò 2005, Bleines et al. 2012). If the order of the trend is known, it is then possible to determine a compatible generalized covariance. Coefficients of the

generalized covariance structure that do not meet the conditions for [Eqn. 3-7] are discarded. A cross-validation jackknife procedure is implemented on the aforementioned ring components to determine the optimal generalized covariance structure by choosing the GC model with the standardized error closest to one. Ordinary block kriging was performed on the Gaussian data to build a 1 m DEM. Kriged Gaussian estimates were back transformed to represent the DEM in its original units prior to calculating terrain attributes.

Calculating Terrain Attributes

Terrain attributes were calculated by taking the first and second derivative of each DEM to produce values for slope and curvature, respectively. Slope was calculated in ISATIS® using the following simple formula:

$$slope = \sqrt{[Gradient\ x]^2 + [Gradient\ y]^2} \qquad \text{[Eqn. 3-10]}$$

The gradients are the partial derivatives of elevation along each x and y axis. The Gradient y (w_y) corresponds to the partial derivative of elevation ($w(ix, iy)$) along the y axis and is obtained by comparing pixels immediately adjacent to the target cell of coordinates (ix, iy):

$$w_y(ix, iy) = \frac{w(ix, iy+1) - w(ix, iy)}{dy} \qquad \text{[Eqn. 3-11]}$$

and gradient x (w_x) is the partial derivative of elevation along x axis as follows:

$$w_x(ix, iy) = \frac{w(ix+1, iy) - w(ix, iy)}{dx} \qquad \text{[Eqn. 3-12]}$$

Curvature is the second derivative of elevation, or simply taking the slope of the first derivative (i.e. the "slope of the slope"). Plan and profile curvatures were calculated in

ArcMap 10.0 (ESRI®) on a cell by cell basis where a 4th order polynomial is fitted to each grid cell (Z_i) within a 3x3 moving window where θ denotes the angle :

Z_1	Z_2	Z_3
Z_4	Z_4	Z_5
Z_7	Z_8	Z_9

$$Plan\ Curvature = -2(D\ sin^2\theta + E\ cos^2\ \theta + F\ sin\theta\ cos\theta)$$

$$= -\frac{2(DH^2 + EG^2 - FGH)}{G^2 + H^2}$$

$$Profile\ Curvature = -2(D\ cos^2\theta + E\ sin^2\ \theta + F\ cos\theta\ sin\theta)$$

$$= -\frac{2(DG^2 + EH^2 - FGH)}{G^2 + H^2}$$

where

$$D = \left(\frac{Z_4 + Z_6}{2} - Z_5\right)/L^2$$

$$E = \left(\frac{Z_2 + Z_8}{2} - Z_5\right)/L^2$$

$$F = (-Z_1 + Z_3 + Z_7 - Z_9)/4L^3$$

$$G = (-Z_4 + Z_6)/2L$$

$$H = (Z_2 - Z_8)/2L$$

The TWI was calculated using the Terrain Analysis using Digital Elevation Models, TauDEM©,extension (David Tarboton, Utah State University) in ArcMap 10.0 as the natural logarithm of the upland contributing area (CSA) divided by the slope:

$$TWI = ln\left(\frac{CSA}{Slope}\right) \qquad \text{[Eqn. 3-13]}$$

Contributing area (i.e. drainage area or catchment area) is the accumulated flow contributed from up-gradient pixels and was calculated subsequent to establishing a flow field (i.e. surface connectivity) using slope and flow direction (Gallant 1996; Tarboton 2009). The D∞ algorithm used by TauDEM calculates the specific catchment area by dividing the contributing area by the contour length perpendicular to a multi-directional gridded flow direction (Tarboton 2009; Florinsky 2012). Flow contribution from up-gradient cells is whole if the contributing cell falls in a cardinal direction (N, S, E, or W) but is multi-directional, or fractionated, between adjacent cells if the flow direction falls on an angle (Tarboton 2009). Contributions from each grid cell are additive.

Results

The fitted IRF-*k* model consisted of a linear trend component and a generalized covariance function represented by a nugget, 1st order GC function and a 3rd order GC function with the following coefficients, b_0=0.00044, b_1=0.00213, b_3=0.877, respectively. Cross validation resulted in a mean error (0.00003), variance error (0.00049), and mean standardized error (0.00076), all close to zero and variance of the standardized error of 1.0197, which is close to 1.

With spatial component filtering it was possible to decompose and krig each spatial component separately (Figure 3.1). The kriged DEM's for each spatial component were

produced using ordinary block kriging on a 1-m mesh grid. The kriged GC (mean zero) map consists of the 1st and 3rd order spatial functions (Figure 3.1). The third order spatial function weighs the most on the GC inferring undulating microtopography dominates the high frequency spatial variation in the LiDAR data. The DEM produced from the low frequency trend component was used to derive terrain attributes (Figure 3.2). Figures 3.2 through 3.5 illustrates the DEM, first and second derivatives of elevation and the TWIDEMs from the binning and kriging methods.

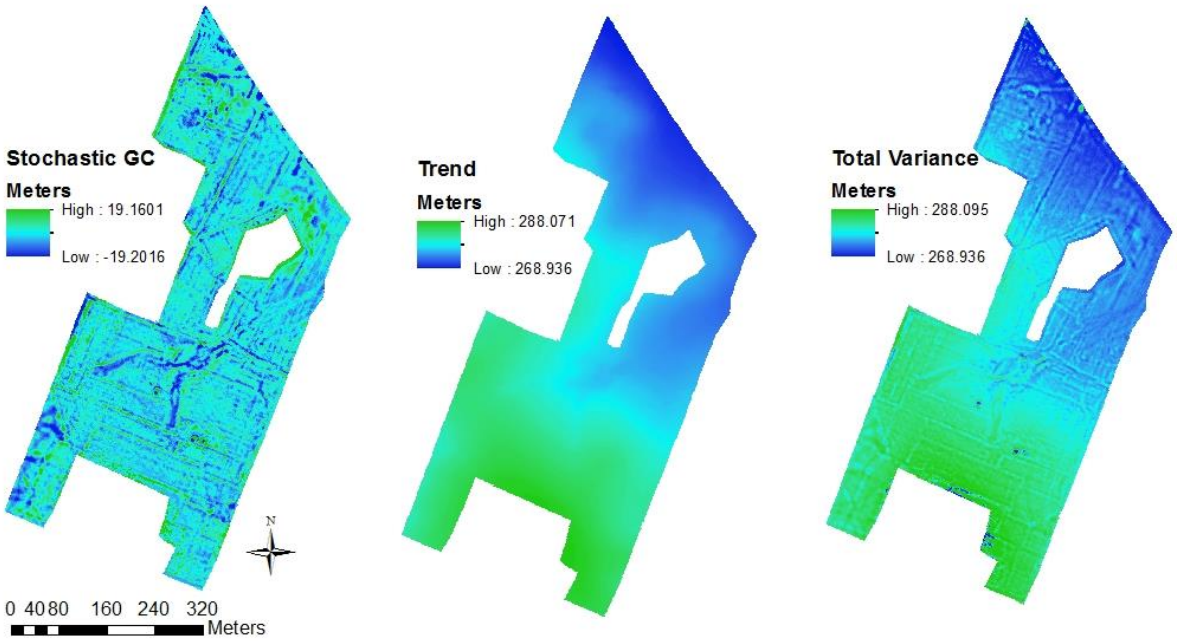

Figure 3.1. Kriged spatial components.

Left - 1st and 3rd generalized covariance spatial components with zero mean; Middle - linear trend; and Right - the two maps added together to create the total variance.

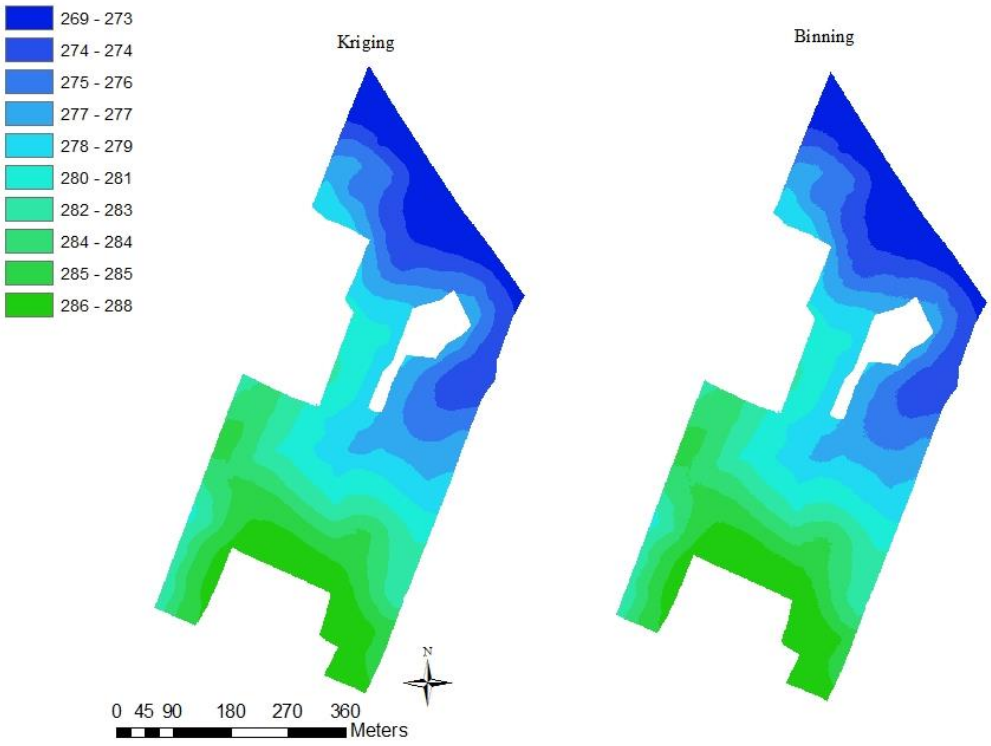

Figure 3.2. 1 m DEM produced using ordinary kriging (left) and binning (right). Elevation units are in meters.

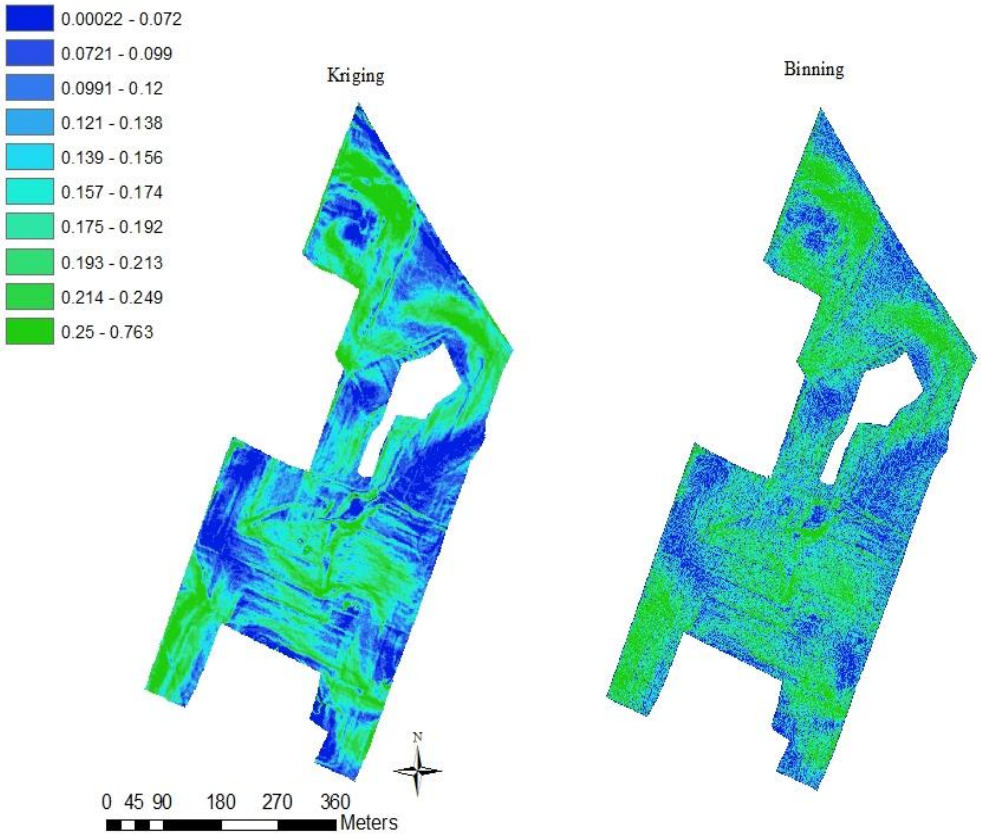

Figure 3.3. Slope calculated from the ordinary kriging DEM (left) and binned DEM (right). Slope is unitless.

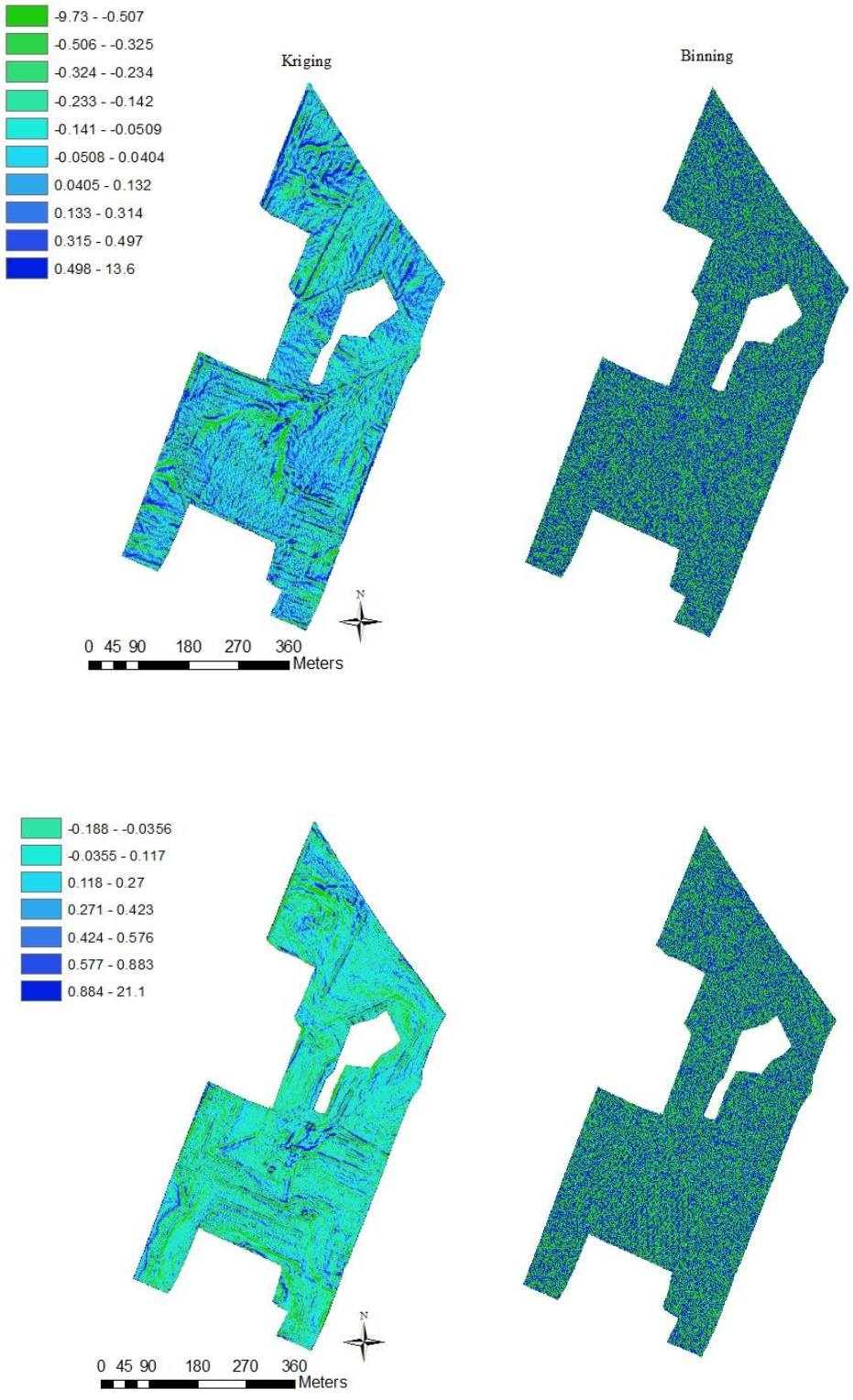

Figure 3.4. Plan (top) and profile (bottom) curvature produced using DEM's from kriging (left) and binning (right) DEM's.

Curvature is unitless.

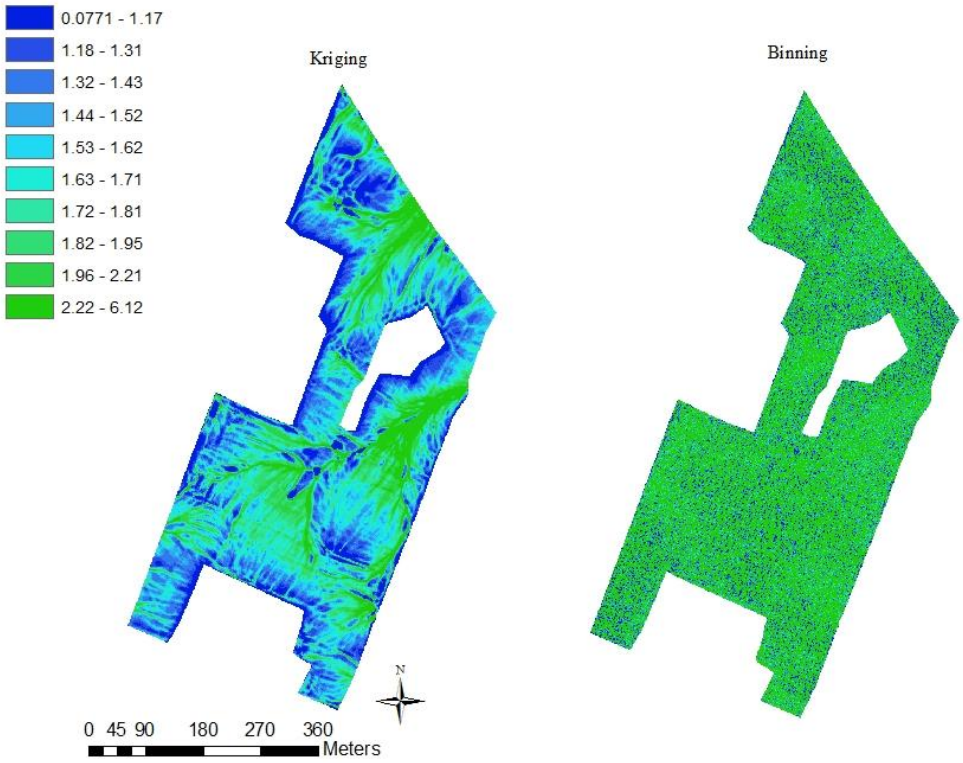

Figure 3.5. Maps of the Topographic Wetness Index produced using DEM's from ordinary kriging (left) and binning (right).

Discussion

Fitting polynomial functions to LiDAR data to build DEMs has been presented in previous studies (Zheng et al. 2007), however, the approach did not take into account the spatial autocorrelation. The purpose of this study was to extract the low frequency trend component to build a 1 m DEM. Extracting the low frequency trend component is an attempt to suppress the high frequency variation introduced by the stochastic GC spatial component. The results obtained from the spatial component filtering were compared with the more traditional binning technique. Kriging assumes an inherent spatial association between each location as a function of distance, or lag, whereas binning does not.

The differneces between binning (spatially independent) and kriging (spatially dependent) were miniscule in the case the 1-m DEMs (Figure 3.2). The relative highs and lows in elevation were slightly lower (within 1 meter) for the kriged DEM, which may be consequential to smoothing during the kriging process. In this case, the smoothing was not considered great given how close the two DEM techniques resemble one another. Calculating the slope, however, produced dissimilarities between the two techniques (Figure 3.3). It is noticeable the kriging approach produced a more continuous map of slope detailing sharp contrasts in steep versus gentle sloping terrain. This is because slope was calculated via a moving window technique where juxtaposed pixels were used to establish the slope gradient at the target pixel. Kriging creates spatial continuity from one pixel to the next so that the boundaries between steep and gentle sloping terrain are distinguishable. By comparison, the binning technique, which did not account for the spatial association between pixels, produced a less refined map due to

greater autonomy between juxtaposed pixels, therefore, making the boundaries between steep versus gentle sloping terrain more inconsistent (Figure 3.3). The range of slope values for the kriged DEM was smaller, which is due to smoothing during kriging. The greater range in slope values for the binning technique was attributed to the lack of spatial continuity between pixels. Calculating the second derivative of elevation created a starker difference between the two techniques (Figure 3.4). The binning technique produced a map depicting no physical impression of curvature. Kriged plan curvature highlighted the drainageway traversing the site in addition to some other drainage lines. Profile curvature is measured in a direction orthogonal to plan curvature and illustrated terrain features such as ridgetop areas and the main drainageway. Linear striations become apparent when calculating the derivatives of elevation. These features are authentic and mimic anthropogenic activity including roadways, ditches and historic cropping rows. In the kriged profile curvature map these features appeared accentuated because they are parallel to the direction orthogonal to the slope.

The TWI represents regions of the field that have higher tendencies to be wet or dry based on flow direction, gradient, and accumulation (Figure 3.5). Regions with higher TWI indicate a higher potential for water accumulation; lower TWI values indicate a lower potential for water accumulation. Depression areas show high TWI values whereas upland areas impart low TWI values. Cropping experiments excluded from analyses are, not coincidently, located on ridgetop or upland positions where the potential for water accumulation is low.

This study underscores the utility of nonstationary geostatistics in tandem with spatial component filtering to build a digital elevation model. Geostatistics mathematically

represents the spatial correlation in sampled elevation that imparts spatial continuity in the kriged estimates. Nonstationary modeling is one approach to map elevation in the presence of a trend. Spatial component filtering made it possible to produce a DEM using the low frequency trend component, thereby reducing the effect of the high frequency component. Striations apparent in the calculated terrain attributes are physically real and result from anthropogenic activity and include roadways, cropping rows and mowing lines. These features could ostensibly interfere with surface soil moisture distribution and arguably should be retained. These features, however, potentially depreciate the applicability of the calculated terrain attributes in making inference toward subsurface soil moisture distribution.

The DEM, slope, profile and plan curvature, and the TWI calculated from the kriging method are incorporated as environmental variables in subsequent Chapters to study the scale-dependent spatiotemporal characteristics of soil moisture variation. Specifically, to test their efficacy as high resolution secondary variables to downscale soil moisture estimates using geostatistics but also how they influence soil moisture variation in space and time.

Conclusion

Because of its ease of use and convenience, binning is often a preferred method for generating DEMs from LiDAR data. This research underscores the utility of geostatistics as an alternative method to build DEMs. Geostatistics mathematically represent the spatial correlation in sampled elevation that imparts spatial continuity in the kriged estimates. The importance of spatial continuity became apparent when calculating the derivative of elevation as shown in the results obtained between the kriging versus

minimal binning techniques. Using spatial component filtering it was possible to produce a DEM using the low frequency trend component, thereby reducing the effects of the high frequency components.

Findings from this Chapter are an antecedent preliminary step to understanding how terrain attributes affect surface soil moisture distribution across the area studied. The DEM, slope, profile and plan curvature, and the TWI from the kriging method are incorporated as environmental variables in subsequent Chapters.

Chapter 4

An Integrated Statistical Approach to Study the Time Stability of Soil Moisture Patterns at the Landscape-Scale

Introduction

Characterizing soil moisture variability using direct sampling at the landscape-scale proves costly, labor intensive, and time consuming. Consequently, direct soil moisture sampling schemes often lack the spatial resolution and temporal frequency to adequately ascertain soil moisture variation (Lin 2003, Zhu et al. 2012). Nuanced statistics together with on-the-go proximal and remote sensing technologies are surmounting these sampling challenges facing agriculturalists, conservationists, and remediation specialists. One quintessential approach for sampling soil moisture over large spatial extents is recognizing its patterned behavior or repeated spatiotemporal organization (Lin 2006, Brocca et al. 2010). If soil moisture patterns maintain their spatial organization across the landscape through time, it is possible to establish a minimalist and parsimonious sampling approach by directing sampling efforts utilizing this patterned organization.

Vachaud et al. (1985) introduced a foundational parametric statistic to soil hydrology called time stability analysis. Time stability, also referenced herein as temporal stability (Chen 2006, Lin 2006, Vanderlinden et al. 2011), has been used extensively to characterize the temporal behavior of soil moisture distribution patterns (Mohanty and Skaggs 2001, Martínez-Fernández and Ceballos 2003, Lin 2006, Zhou et al. 2007). The impetus behind this statistic is it can identify sample locations that maintain their statistical relevance through time. Time stability employs two statistical measures to define the statistical relevance of each sampling location: the mean relative difference (MRD) and the standard deviation of the mean relative difference (SD_{MRD}). Over a given

observation domain - such as a plot, field, or watershed - certain areas will exhibit persistent wetness or dryness compared to the average moisture content (Lin 2006). The MRD generalizes this persistence by characterizing individual sampling locations as being persistently higher, lower, or equal to an observed average. The standard deviation of the MRD (SD_{MRD}) is a measure of a location's temporal precision, or time stability. The MRD and SD_{MRD} measure the ability for each sampling location to maintain its soil moisture characterization through time. Locations that maintain their statistical relevance require less ambitious sampling and can thereby save time, labor, and cost associated with field investigative efforts (Lin 2006, Guber et al. 2008).

Time stability is well integrated within the soil hydrology literature and has shown a diverse array of applications including data extrapolation (Pachepsky et al. 2005, De Lannoy et al. 2006); *in situ* soil moisture sensor calibration (Hu et al. 2009); patterned time stability characterization (Vachaud et al. 1985, Grayson and Western 1998, Martínez-Fernández and Ceballos 2003, De Lannoy et al. 2006); scale-dependent patterned time stability characterization (Kachanoski 1988, Grayson and Western 1998, Gómez-Plaza 2000, Choi et al. 2007); predicting soil moisture variability across spatial extents (Kachanoski 1988, Jacobs et al. 2004, Teuling et al. 2006, Choi et al. 2007, Cosh et al. 2008, Guber et al. 2008); and identifying the soil-terrain parameters controlling patterned soil moisture variation (Vachaud et al. 1985, Brocca et al. 2009, Takagi and Lin 2012, Coleman and Niemann 2013).

Studying soil moisture patterned behavior can reveal clearer relationships between the properties and processes governing soil moisture response (Grayson et al. 1997, Grayson et al. 2002, Lin 2006, Lin et al. 2006, Coleman and Niemann 2013). Vachaud et al.'s

(1985) notion, for example, was that the probability of a location acquiring a particular soil moisture classification derives, in part, from soil moisture's interaction with environmental parameters such as texture (Vachaud et al. 1985). Environmental parameters driving soil moisture variability are integrated, complex, and diverse, thereby compounding the challenges in deciphering parameters that are most relevant at any given soil moisture content. According to Grayson et al. (1997) two general scenarios define the spatial patterns of soil moisture variation: 1) when evapotranspiration exceeds precipitation, or under dry soil moisture condition; 2) when precipitation exceeds evapotranspiration, or under wet soil moisture conditions (Grayson et al. 1997, Gómez-Plaza 2000). Ostensibly, environmental parameters governing the spatial variation of soil moisture exhibit a relative importance based on fluctuations in soil moisture content with time (Takagi and Lin 2012, Coleman and Niemann 2013, Penna et al. 2013). For example, Grayson's first scenario relates to "local controls" such as soil texture, microtopography, and vegetation (Grayson et al. 1997, Gómez-Plaza 2000). Grayson's second scenario is necessary for topographic or landform parameters (e.g. "nonlocal controls") to take effect and promote the occurrence of gravitational flow (e.g. preferential drainage, surface runoff and throughflow) (Grayson et al. 1997, Grayson and Western 2001, Western et al. 2002). Other environmental parameters influencing the patterned variation of soil moisture include organic matter (Hu et al. 2009), bulk density (Cosh et al. 2008), and soil depth (Lin 2006).

Over the last two decades researchers have tried to determine which soil-terrain parameters are responsible for the time stable patterned behavior of soil moisture variation. This has been challenging because the literature abounds with conflicting

results that clearly preface the need for further investigation. A case in point is soil texture. Jacobs et al. (2004) concluded soils with higher clay content exhibit greater time stability while Mohanty and Skaggs (2001) indicated sandy loam soils attain higher time stability in comparison to silt loam soils. Other studies favor time stability in both sandy soils (Comegna and Basile 1994) and clay soils (Vachaud et al. 1985). Moreover, it is inconclusive whether soils are more or less time stable during wet or dry soil conditions. Soils prone to lower soil moisture contents, as found in drier climates or on steep sloping landscapes, exhibit higher time stability under dry conditions (Martínez-Fernández and Ceballos 2003, Penna et al. 2013). Soils prone to higher soil moisture, as found in wetter climates or low-lying topographic positions, favor time stability under wetter conditions (Gómez -Plaza 2000, Zhao et al. 2010). Other findings could not differentiate soil moisture stability between wet or dry periods (Vanderlinden et al. 2011, Penna et al. 2013).

Clearly, various environmental parameters influence the spatiotemporal variation of soil moisture and become important for understanding the scale-dependent temporal persistence of soil moisture distribution patterns. Different observation scales will synthesize different soil moisture patterns according to the underlying spatial autocorrelation of environmental parameters controlling the distribution of soil moisture (Kachanoski 1988, Western et al. 2002). Topographic parameters, such as elevation and the topographic wetness index (TWI), are typically considered long-range parameters whereas soil properties, vegetation and other local controls listed by Grayson (1997) are typified as short-range parameters. Moreover, not every observation scale will exhibit time stability. For example, Gómez-Plaza et al. (2000) studied soil moisture time

stability along transects with different ranges and found distances between 100 – 200 m exhibited strong stability whereas distances below 100 m were time unstable. This highlights the importance of the sampling scale triplet (sample spacing, extent, and support) when studying scale-dependent soil moisture patterned variation because environmental parameters influencing time stable or time unstable soil moisture patterns operate at unique spatial scales according to their characteristic spatial autocorrelation (Gómez-Plaza 2000, Western et al. 2002, Lin et al. 2005, Vanderlinden et al. 2011). Researchers must be more cognizant of the scale triplet because it inevitably predisposes the soil moisture patterns and corollary environmental parameters captured (Grayson et al. 2002, Brocca et al. 2010). More empirical research is necessary to establish at which spatial scale(s) soil moisture exhibits time stable patterned variation across landscapes and the corollary soil-terrain parameters controlling this behavior. Findings could help field investigators make more informed decisions for determining optimal observation scales most appropriate for sampling and managing soil moisture variation specific to their management interest.

Direct soil sampling at the landscape-scale often results in poor spatial resolution and temporal frequency due to cost, labor, and time limitations (Lin 2003, Zhu et al. 2012). Recent literature has tied Vachaud et al.'s (1985) statistical approach with the use of proximal sensing and multivariate geostatistics (Robinson et al. 2009, Besson et al. 2010, Zhu 2010, Buttafuoco et al. 2011, Minet et al. 2013). Characterizing the spatial variability of subsurface soil moisture using geophysical technologies has been used in hydrogeophysics (Rubin and Hubbard 2005, Schwartz et al. 2008, Robinson et al. 2009). Integrating direct sampling with proximal and remote sensing has expanded Vachaud et

al.'s (1985) classic approach to allow field investigators to explore soil moisture patterns with greater resolution and continuity over larger spatial extents (Robinson et al. 2009). Moreover, proximal and remote sensing provides a cost effective, minimally invasive, and rapid sampling approach that can be used to optimize direct sampling efforts. Combining data acquisition techniques (e.g. LiDAR, geoelectric and direct sampling) with unique sampling supports is quenching the demand to better capture spatial information at different scales (Zhu et al. 2012). Multivariate geostatistics is an approach to decompose and analyze multi-scale spatial information. This research explores the use of a multivariate geostatistics technique called multicollocated factorial cokriging analysis (MFCA) to study scale-dependent time stable patterns across a landscape. The benefit of this technique is it can fuse multiple data sources, with different sampling supports and units, within a single geostatistical platform to model soil moisture and associated hydrologic parameters as one synergistic system relative to their shared spatial dependence (Yang et al. 2009, Goovaerts 1992). Specific to time stability, MFCA can model multiple soil moisture dates and corollary hydrologic parameters simultaneously to reveal if there is a time stable, scale-dependent relevance to the soil moisture regimes observed, and if so, which hydrologic parameters best relate to the established time stable patterns. More research and development is needed to adequately capture scale-dependent time stable patterns of soil variation over large spatial extents but also pinpoint environmental parameters controlling the patterned variation of soil moisture (Lin 2003). This research aims to make a contribution to this effort by addressing three of the four questions posed in the Introductory Chapter:

1. What are the spatial and temporal dependencies of patterned variation in soil moisture?
2. What are the optimal observation scales to capture patterned variation in soil moisture?
3. What soil-terrain attributes define this response?

It is anticipated that nested spatial scales of patterned soil moisture variation will emerge according to the characteristic ranges of spatial autocorrelation of the underlying soil-terrain attributes interacting with soil moisture. If the temporal dependency of soil moisture's patterned response is persistent, then its interaction with controlling soil-terrain attributes is expected to be relatively constant regardless of fluctuations in soil moisture content with time. If the temporal dependency of patterned soil moisture response is time instable, then long-range parameters (e.g. terrain attributes) are expected to dominate soil moisture distribution during wetter conditions and, conversely, soil attributes are expected to dominate during drier conditions.

The objective of this study is threefold. First, apply MFCA to simultaneously downscale sparse direct soil moisture measurements using high resolution proximal sensing across the studied landscape and determine if there is a scale-dependent time stable association between soil moisture variation and selected soil-terrain attributes. Second, subject downscaled soil moisture estimates to a suite of analytical techniques, including the confusion matrix, MRD and SD_{MRD}, and the cross correlogram, to study the time stable patterned variation for the soil moisture regimes observed. Additionally, use polygon kriging, specific to landscape position, to determine if the soil-terrain parameters defined within the scope of this study affect the measured MRD. Finally, determine if the soil-

terrain parameters defined within the scope of this study affect the scale-dependent time stable patterned variation of soil moisture.

The temporal scope of this research spans the three soil moisture dates observed, which fell during a drought period for Central Kentucky. The spatial scope of this study encompasses the soil-terrain attributes analyzed across the 40 hectare Central Kentucky landscape investigated.

Materials and Methods

Gaussian Anamorphosis

Geostatistics employs a probabilistic model to assess spatial uncertainty that inherently assumes the sampled population derives from a stochastic or random phenomenon. Because soil and terrain properties can exhibit departures from a Gaussian distribution, it is important to normalize variables prior to multivariate geostatistical analyses. Gaussian anamorphosis (GA) is a modeling technique applied in ISATIS® to transform any variable into a normal variable standardized to mean zero and standard deviation of 1.

GA estimates a function Φ to transform a raw variable (Z), with any distribution, to a standard Gaussian variable (Y) (Buttafuoco et al. 2011) [Eqn. 4-1]:

$$Z = \Phi(Y) \qquad \text{[Eqn. 4-1]}$$

Transforming the raw variable into a Gaussian variable requires inverting the above function [Eqn. 4-2].

$$Y = Z\,\Phi^{-1} \qquad \text{[Eqn. 4-2]}$$

The raw variable's data distribution is fitted to the standard Gaussian distribution using an expansion of the Hermite polynomial $H_i(Y)$, preceded by coefficient being estimated (Ψ_i), that are restricted to a finite number of terms (N) [Eqn. 4- 3]:

$$\Phi(Y) = \sum_{i=1}^{N} \Psi_i H_i(Y) \qquad \text{[Eqn. 4-3]}$$

To test the goodness of the GA transformation, two cross-validation statistics were calculated: mean and standard deviation of the error. The former should be close to zero whereas the latter should be less than one order of magnitude of the standard deviation of the raw variable. Gaussian transformed variables are used for variogram modeling and (co)kriging. (Co)Kriged Gaussian variables are then back transformed into their original units using the function above.

Estimating Apparent Electrical Conductivity (aEC)

The terrain attributes calculated in Chapter 3 and the geoelectric measurements discussed here are the two prospected secondary sampling techniques to downscale soil moisture estimates across the landscape. Elevation, slope, curvature, and the TWI calculated in Chapter 3 were applied to a 5.0 meter mesh grid for this Chapter . The Veris 3100 on-the-go sampling grid produced over 9,500 georeferenced apparent electrical conductivity (EC) points for three soil moisture sampling dates: July 17, September 11, and October 5, 2012. It was necessary to downscale apparent EC measurements to match the 5 m mesh grid produced for terrain attributes.

Data pre-conditioning consisted of removing negative apparent EC values, sampling duplicates, and outliers. Negative values were prominent for the deeper readings and are

thought to arise from poor electrode contact with the soil but also low soil moisture content deeper within the soil profile. Duplicate readings were present and arise from superimposed GPS readings. Both negative values and duplicates were removed prior to variogram modeling. Apparent EC readings exhibited non-normal distributions for each observation date. Consequently, variography and cokriging was performed on Gaussian transformed apparent EC readings.

Several variogram models, including spherical, exponential, and K-Bessel, were fitted using a linear model of coregionalization (LMC) to establish the best fit variogram model. The best fit model was chosen using cross validation statistics and the Akaike Information Criterion. The LMC, cross validation statistics, and AIC criterion are discussed in detail in forthcoming sections. Joint variation between the 30 cm and 90 cm depths were characterized for July, September, and October, respectively, using the isotropic exponential variogram model [Eqn. 4-4] in ISATIS® with lag distance of 10 meters for a total of 20 lags:

$$\gamma_{ij}(\mathbf{h}) = C_0 + C\left[1 - exp\left(\frac{-\boldsymbol{h}}{a}\right)\right] \qquad \text{[Eqn. 4-4]}$$

where $\gamma_{ij}(\mathbf{h})$ is the crossvariogram, h is the lag distance, C is the sill and a is the distance parameter (Webster and Oliver 2001). The model approaches the sill asymptotically, therefore, the effective range is considered when the semivariance reaches 95% of the sill variance, which is ~3a (Webster and Oliver 2001).

Full punctual cokriging was performed in ISATIS® to downscale apparent EC measures on the aforementioned 5 m mesh grid . Full cokriging exhausts all information in the cokriging neighborhood to estimate a value at the targeted grid node. Full punctual

cokriging was used to downscale shallow apparent electrical resistivity on a 5m mesh grid. The cokriging estimate $z^*_{CK}(u)$ constitutes a linear combination of both neighboring shallow (Z) and deep (Z') measures (Oliver 2010) [Eqn. 4-5]:

$$z^*_{\mathrm{CK(ECshallow)}}(u) = \sum_{a=1}^{n} \lambda_a(u) Z(u_a) + \sum_{a=1}^{m} \lambda_{a'}(u) Z'(u_{a'}) \qquad \text{[Eqn. 4-5]}$$

Cokriged Gaussian estimates for the shallow depth were then back transformed to their original units. Georeferenced direct sampling points (n=127) were superimposed on the 5 m mesh grid to sample apparent EC to the nearest (< 2m) raster grid value using the Migrate Grid to Point tool in ISATIS®.

Exploratory Analyses

Data reduction was necessary to manage the computation effort for multivariate analyses. The sampled attributes delineated in Chapter 2, in addition to the terrain attributes produced in Chapter 3, were subjected to exploratory analyses. Georeferenced direct sampling points (n=127) were superimposed on the 5 m mesh grid to "sample" terrain attributes (Chapter 3) and apparent EC estimates to the nearest (< 2m) raster grid value using the Migrate Grid to Point tool in ISATIS®. These estimates were then subjected to the forthcoming exploratory analyses. Due to missing field markers, not all direct sample locations were sampled for soil moisture, therefore, exploratory analyses were only employed on 94 of the 100 georeferenced calibration sampling points to distill attributes exhibiting prominent influence on soil moisture variation.

An integration of data reduction methods were performed including the Pearson's correlation coefficient, stepwise regression, variogram analyses, and principal component

analysis (PCA). Soil-terrain attributes exhibiting a Pearson's correlation coefficient of ~0.3 or greater with the wettest observed date (October) were noted. The wettest observation date (October) was favored with the motivation of selecting soil-terrain attributes that best relate to soil moisture. Stepwise regression, which is an automatic fitting regression technique, was also performed to select an optimal subset of predictor variables from the entire set of sampled attributes. Stepwise regression was performed in R version 2.12.2 (R Development Core Team 2008) using October soil moisture as the dependent variable and the best fit model was selected using the Akaike Information Criterion (AIC), which is described in a later section. Variogram analysis was employed to ensure spatially structured variation was present in the direct and cross variograms. Principal component analysis (PCA) was also performed to distill which variables dominated in explaining the total variation captured. Variogram analysis, PCA, and Pearson's correlation coefficients were performed in ISATIS® (Geovariances, release 2012).

Exploratory statistics, including the four statistical moments and correlation coefficients were performed on selected attributes using Quick Statistics in ISATIS®. Quick Statistics automatically tests for outliers falling below Q25-1.5*(Q75-Q25) or above Q75+1.5*(Q75-Q25); where Q stands for quartiles. Histogram plots were also studied to establish if tested outliers were singular to a specific attribute or shared among attributes. Normal distributions were tested by performing a Chi-squared significance test (0.5% significance) on the Q-Q plots between the experimental distribution and Gaussian distribution for each attribute. Selected attributes exhibiting potential outliers and non-

normal distributions were submitted to Gaussian anamorphosis. Exploratory analyses were performed on raw variables.

Cross Validation

Cross-validation is performed by the leave-one-out approach, in which a measurement is temporarily removed and replaced with an estimated (e.g. predicted) value using a surrounding neighborhood of values. The predicted value is compared to the measured value using the following four criteria:

Mean Error (ME):

$$\frac{1}{N}\sum_{N}(Z^{*}-Z)$$

Variance of Error (VE):

$$\frac{1}{N}\sum_{N}(Z^{*}-Z)^{2}$$

Mean Standardized Error (MSE):

$$\frac{1}{N}\sum_{N}\left(\frac{Z^{*}-Z}{\sigma}\right)$$

Variance of the Standardized Error (VSE):

$$\frac{1}{N}\sum_{N}\left(\frac{Z^{*}-Z}{\sigma}\right)^{2}$$

where Z^{*} is the estimated value, Z is the true value, σ is the standard deviation of the estimates and N is the number of observations. The mean error (ME) and mean standardized error (MSE) measure the degree of unbiasedness and should be close to zero. The variance of error (VE) measures precision of estimates and should be as small as possible; taking the square root of the VE results in the standard deviation. The mean

standardized error (MSE) allows one to compare the performance of different modeled variables. The variance of the standardized error (VSE) compares experimental (numerator) and kriging (denominator) variances. The numerator of the variance of the standardized error represents all model parameters except the sill, while the denominator is directly proportional to the sill. The VSE should be close to unity. The tolerance interval for the variance of the standardized error is defined as (Chilés and Delfiner 1999) [Eqn. 4-6], where N is the number of observations:

$$\text{tolerance} = 1 \pm 3\sqrt{\frac{2}{N}} \qquad \text{[Eqn. 4-6]}$$

The Aikaike information criterion (AIC) [Eqn. 4-7]:

$$\text{AIC} = -nlog\left(\frac{RSS}{n}\right) + 2K \qquad \text{[Eqn. 4-7]}$$

was also used to select the best fit model where K is the number of parameters in the model, RSS is the residual sum of squares and n is the number of sampled locations. The model with the lowest AIC infers the best fit model.

Cross validation statistics were performed on apparent EC cokriged estimates and the 12 soil-terrain attributes estimated via the forthcoming MFCA.

Principal Component Analysis

Principal component analysis (PCA) is a multidimensional (e.g. multivariate), nonparametric ordination method. PCA is a robust technique because it accounts for the covariance between variables and also their underlying structures; both of which are important for interpreting large, complex datasets. Multidimensional analytical

techniques exploit a data matrix $(\boldsymbol{X})$ with (i) sampled locations that are realizations of (p) random variables ("descriptors"). Each random variable (p) contributes a dimension to the data matrix $(\boldsymbol{X})$, or by translation, each sampled location constitutes one realization of the p^{th} dimension. It is possible to plot sampled locations in a p^{th} dimensional Euclidean space that inherits a number of axes equivalent to the number of variables, or descriptors, studied. Visualizing a multi-dimension Euclidean space is feasible using 2 or 3 variables (e.g. 2 or 3 dimensions) but then becomes convolutedly complex when trying to visualize higher ordered (3+) dimensions. Sample locations are plotted as a p^{th}-dimensional vector with Euclidean coordinates that constitute either the calculated covariance or correlation coefficients of the random variables.

Prior to performing PCA the dataset must undergo preconditioning, which consists of centering the column variables to mean zero and standardizing to a unit variance. After centering and standardizing the data the centroid of the entire dataset lies at zero but the relative dispersion, or position, of each vector does not change. Transposing the normalized matrix results in a dispersion correlation matrix $\boldsymbol{S} = (\boldsymbol{X}^T\boldsymbol{X})$. Correlation PCA is subsequently performed on the symmetric dispersion matrix $\boldsymbol{S}$. Within the dispersion matrix there exists gradients of variance according to the intercorrelations among variables. The objective of PCA is to extract the gradients of variation in descending order (largest first). Each gradient is represented as a principal axis that entails a linear combination of the original variables that is fitted using a least squares approximation. The first principal axis is oriented in the direction of maximum variance and the second orthogonal (rotated 90^o) to the former. In return, each axis is independent of the other. The projection of a variable on each principal axis represents the magnitude

of influence, or loading value, describing how important the axis is in explaining a variable (Syms 2008). The total number of orthogonal principal axes extracted equals the total number of variables studied (p). Normalizing these weights give rise to the coordinates (e.g. position) of attributes with respect to the principal axis, now identified as a principal component.

The $\boldsymbol{S}$ dispersion matrix can be decomposed using eigenanalysis into eigenvalues (λ_k) and eigenvectors ($\boldsymbol{u}_k$). The eigenvalues represent the proportion of variation explained by each principal axis, often represented as a percentage of the total variation observed (e.g. sum of all eigenvalues). Each (λ_k) therefore accounts for a certain percentage of the total variation and are listed in descending order so those that represent the greatest variability are first identified.

$$|\boldsymbol{S} - \lambda_k \boldsymbol{I}| = \boldsymbol{0} \quad \text{[Eqn. 4-8]}$$

By solving Equation [4-8] for the eigenvalues λ_k it is then possible to plug these values into [Eqn. 4-9] to solve for the eigenvectors $\boldsymbol{u}_k$.

$$(\boldsymbol{S} - \lambda_k \boldsymbol{I})\boldsymbol{u}_k = \boldsymbol{0} \quad \text{[Eqn. 4-9]}$$

Eigenvalues greater than 1 are considered significant because they are standardized to a standard deviation equal to 1. Multiplying the variance/covariance matrices by the matrix of normalized eigenvectors produces a matrix of principal components.

PCA was applied at multiple stages in this study. First, PCA was applied as part of exploratory statistics to select an optimal subset of soil-terrain parameters. Second, PCA_{LMC} was applied to the coregionalized matrices derived by fitting the linear model of coregionalization (LMC) to map homogeneous zones of shared spatial variation between

multiple attributes. Finally, PCA_{MRD} was applied to selected soil-terrain parameters to identify which of these parameters were significant to interpreting the patterned behavior of the measured MRD.

Geostatistical Approach

Geostatitsics assumes each realization, or measurement, originates from a randomly distributed population that exhibits autocorrelation at some scale(s) (Goovaerts 1994). For the univariate case, it is possible to model an autocorrelated random variable using [Eqn. 4-10]:

$$Z(\boldsymbol{x}) = \mu + \varepsilon(\boldsymbol{x}) \qquad \text{[Eqn. 4-10]}$$

where μ is the mean value and $\varepsilon(\boldsymbol{x})$ is a random process with mean zero and spatial structured variance represented by the variogram. The semivariogram $\gamma(\boldsymbol{h})$ is defined as [Eqn. 4-11]:

$$\gamma(\boldsymbol{h}) = \frac{1}{2N(\boldsymbol{h})} \sum_{i=1}^{N(\boldsymbol{h})} [A_i(\boldsymbol{x}_i) - A_i(\boldsymbol{x}_i + \boldsymbol{h})]^2 \qquad \text{[Eqn. 4-11]}$$

where $(\boldsymbol{h})$ is the lag or separation distance, $A_i$is an observation at georeferenced location i, and $N(\boldsymbol{h})$ is the number of pair of data points separated by a particular lag vector. The intrinsic hypothesis assumes that the expected value of difference in $A_i(\boldsymbol{x}_i)$ and $A_i(\boldsymbol{x}_i + \boldsymbol{h})$, called a linear spatial increment, is constant (mean equal to zero) and the variance of these increments depends only on $\boldsymbol{h}$, thereby reducing [Eqn. 4-10] to $\gamma(\boldsymbol{h})$ (Goovaerts 1994). The cross variogram [Eqn. 4-12] is the fundamental component to cokriging and expresses the spatial behavior between two properties. The cross variogram is similar in

stature to the semivariogram except it measures the covariance between two different variables A_i and B_j based on the absolute value of the lag distance ($\boldsymbol{h}$).

$$\gamma_{ij}(\mathbf{h}) = \frac{1}{2N(\boldsymbol{h})} \sum_{a=1}^{N(h)} \left[A_i(\boldsymbol{x}_i) - A_i(\boldsymbol{x}_i + \boldsymbol{h})\right]\left[B_j(\boldsymbol{x}_j) - B_j(\boldsymbol{x}_j + \boldsymbol{h})\right] \quad \text{[Eqn. 4-12]}$$

Where $\gamma_{ij}(\mathbf{h})$ is the cross variogram, $N(h)$ is the number of data pairs within a class distance (and direction) for a given lag vector **h** (Oliver 2010)**.**

The experimental variogram may be modeled by one simple spatial function or a linear summation of several nested simple spatial functions acting at unique spatial scales [Eqn. 4-13]:

$$\gamma(\boldsymbol{h}) = \gamma^1(\boldsymbol{h}) + \gamma^2(\boldsymbol{h}) + \cdots \quad \text{[Eqn. 4-13]}$$

where each superscript is an independent spatial function. In theory, linear summation of independent spatial functions represents the superimposition of different physical properties and processes acting at different spatial scales that define the overall behavior of the experimental variogram (Castrignanò et al. 2000). It is possible to represent [Eqn. 4.13] as a linear combination of basic variograms, also identified as the linear model of regionalization (LMR) [Eqn. 4-15]:

$$\gamma(\boldsymbol{h}) = \sum_{l=0}^{L} b^l g^l(\boldsymbol{h}) \qquad \text{[Eqn. 4-15]}$$

where b^l represents the relative contribution, or importance, of each simple spatial function $g^l(\boldsymbol{h})$.

Time stability analyses applied herein employs a multivariate geostatistical technique called multicollocated factorial cokriging analysis (MFCA). The MFCA produces several outputs, some of which set the working foundation for forthcoming time stability analyses.

Multicollocated factorial cokriging analysis (MFCA) is a multivariate geostatistical technique extended from factorial kriging analysis developed by Matheron in 1982 (Buttafuoco et al. 2011).There are four general steps to multicollocated factorial cokriging analysis (Castrignanó et al. 2009):

1. Model the coregionalization (scale-dependency) of measured variables using the Linear Model of Coregionalization (LMC);
2. Apply multicollocated cokriging to map the set of selected attributes in their original units;
3. Analyze the regionalized correlations among variables by applying PCA_{LMC} to the variance-covariance spatial matrices produced using the LMC;
4. Cokrig regionalized factors (e.g. scale-dependent principal components) using a modified cokriging system called multicollcoated factorial cokriging.

Soil moisture interacts with multiple scale-dependent properties across a landscape that influence its spatial variability, therefore, field investigations rarely result in a single attribute but multiple attributes (e.g. three or more) under study. Conceivably, these properties can be regionalized, or decomposed into homogeneous units, according to the scales in which they synergistically exert influence on soil moisture distribution. In the multivariate case the LMC is applied in comparison to the univariate case where the

LMR is used. The LMC assumes all studied variables derive from independent physical processes that act at different spatial scales L (Wackernagel 2003). The LMC models multiple variables (n) using a symmetric $n(n+1)/2$ coregionalized matrix of direct variograms, $\gamma_{uu}(\boldsymbol{h})$ and $\gamma_{vv}(\boldsymbol{h})$, and cross variograms $\gamma_{uv}(\boldsymbol{h})$, that are standardized to a unit sill $g^{l}(\boldsymbol{h})$ [Eqn. 4-16] (Castrignanò et al. 2000).

$$\gamma_{uv}(\boldsymbol{h}) = \sum_{l=0}^{L} b_{uv}^{l} g_{uv}^{l}(\boldsymbol{h}) \qquad \text{[Eqn. 4-16]}$$

The symmetric coregionalization matrix $[b_{uv}^{l}]$ must meet the criterion that all principal minors are nonnegative [Eqns. 4-17 and 4-18]:

$$b_{uu}^{l} \geq 0, b_{vv}^{l} \geq 0 \qquad \text{[Eqn. 4-17]}$$

$$|b_{uv}^{l}| = |b_{uv}^{l}| \leq \sqrt{b_{uu}^{l} b_{vv}^{l}} \qquad \text{[Eqn. 4-18]}$$

Under the constraint of positive semi-definiteness an LMC is automatically fitted in ISATIS® using the weighted least-squares approximation through an iterative approach. Variogram model selection is ultimately chosen by the user based on automatic fitting criterion (e.g. AIC) but also cross validation statistics. Small discrepancies in the shape of the fitted variograms among variables are ignored because the confidence intervals of estimated semivariances are often wide (Goovaerts 1992). If, however, all simple variograms have unique shapes, it is not possible to fit an LMC. Often, three basic variogram functions (e.g. a nugget and two additional spatial functions) are sufficient for fitting an LMC to a multivariate data set. The sill values for each regionalized matrix represent the variance-covariance matrix at each spatial scale. Therefore, each coregionalizion matrix $\boldsymbol{B}_{uv}^{l}$ produces a scale-dependent variance-covariance matrix that

is used to calculate the structural correlation coefficients specific to each scale [Eqn. 4-219]:

$$r_{uv}^{l} = \frac{b_{uv}^{l}}{\sqrt{b_{uu}^{l} b_{vv}^{l}}} \qquad \text{[Eqn. 4-19]}$$

The scale-dependent correlation coefficients differ from the quintessential Pearson's correlation coefficients because they 1) focus on specific spatial scales thereby distilling interactions between attributes according to specific spatial scales (Yang et al. 2009); 2) utilize the sill values fitted to the matrix of direct and cross variograms using the LMC.

It is possible to apply PCA_{LMC} to each scale-dependent coreginalized matrix to extract independent factors that synthesize interrelationships between the studied attributes (Guagliardi et al. 2012). Applying PCA_{LMC} decomposes the set of second-order random variables $\{Z_i(X); i = 1, \ldots\ldots, n\}$ into a set of reciprocally orthogonal regionalized factors, also identified here as principal components, $\{Y_v^u(X); v = 1, \ldots\ldots, n; u = 1, \ldots. N_s\}$ with transformation coefficients a_{iv}^{u} [Eqn. 4-20]

$$Z_i(x) = \sum_{u=1}^{N_s} \sum_{v=1}^{n} a_{iv}^{u} Y_v^u(x) \qquad \text{[Eqn. 4-20]}$$

Regionalized factors Y_v^u are characterized by the standardized variogram specific to scale u. A linear combination of (n), which is equal to the number of variables, regionalized factors corresponding to the same spatial scale u represent the spatial components of variable Z specific to scale u [Eqn. 4-21]:

$$Z_i^u(x) = \sum_{v=1}^{n} a_{iv}^u Y_v^u(x) \qquad \text{[Eqn. 4-21]}$$

By using a modified cokriging system (Wackernagel 2003) it is possible to estimate regionalized factors at each scale u. Maps of the spatial component $Z_i^u(x)$serve the practical utility of illustrating the scale-dependent relative importance of each variable.

Multicollocated Cokriging

After fitting the LMC it is possible to cokrig the 12 individual soil-terrain attributes in addition to their coregionalized principal components, or coregionalized factors. October apparent EC was the secondary variable selected to downscale the 12 attributes and associated coregionalized principal components via cokriging.

Integrating densely sampled secondary measurements can lead to more consistent descriptions of sparsely sampled direct measurements (Castrignanò et al. 2009). However, when the secondary variable is sampled much more densely than the primary variable it can cause instability because the correlation between close secondary data is greater than that of sparse primary data (Goovaerts 1997). Multicollocated cokriging is an efficient method to integrate exhaustive secondary measurements with sparse primary measurements to estimate the primary variable at point locations not directly sampled (Morari et al. 2009). Multicollocated cokriging is similar to ordinary cokriging except the neighborhood search specifically utilizes the secondary variable information collocated with the measured primary variable and the target location to be estimated.

MFCA creates two cokriging outputs. First is a set of multicollocated cokriged maps of the 12 attribute in their original units. Second is a set of multicollocated regionalized

factor maps that represent the synergistic interrelationships among attributes at each spatial scale, called coregionalized factor maps. Coregionalized factor maps were classified into three isofrequency classes to illustrate synthetic "homogeneous zones" delineating a high, medium, and low presence of variables weighing positively on the coregionalized factor. The zones represent the joint variation of several attributes interacting synergistically to define the observed spatial patterns. Cokriging and factor cokriging used the aforementioned October apparent EC estimates (n=8,734) as the auxiliary variable to downscale point measured soil-terrain attributes (n=94) along a 5 m mesh grid. Geoelectric measurements were the chosen auxiliary variable because they correlated better with soil moisture for all three dates and exhibited stronger spatial autocorrelation in comparison to the terrain attributes.

Time Stability Analyses of Cokriged Soil Moisture Estimates

The multicollocated cokriged soil moisture estimates downscaled to a 5 m grid were subjected to a suite of time stability analytical techniques including, the confusion matrix, Vachaud et al.'s (1985) time stability analysis in tandem with polygon kriging in addition to principal component analysis (PCA_{MRD}), and the cross correlogram, to ascertain if the observed soil moisture dates exhibited time stable characteristics across the landscape.

Confusion Matrix

Within the scope of this study, the traditional approach consists of applying a confusion matrix and the Kappa Index to study the classification accordance, or agreement, of a soil moisture estimate to itself through time. If a soil moisture estimate holds its classification through time it is considered time stable. Each soil moisture estimate is ranked from lowest to highest and classified into 4 iso-quantile classes (1 being the

lowest soil moisture content and 4 being the highest) for each observation date prior to calculating the confusion matrix. The confusion matrix produces a single value, identified here as the observed accordance, indicating the overall agreement between soil moisture classes for two observation dates. Ostensibly, the stronger the observed accordance the more convincing the system is time stable. It is possible in some cases that the observed accordance arises from mere chance. The Kappa Index is a measure of the accordance corrected for chance occurrence. If the Kappa Index is significant it is sufficient to say that the observed association occurs outside of mere chance.

This study employed R (version 2.15.2) to calculate the confusion matrix and Kappa statistics for time steps: July vs. September; September vs. October; for July vs. October. The method requires a "predictor" and "response" dataset to compare classifications; it does not matter which soil moisture date serves which role. The diagonal of the confusion matrix is the observed accordance, or the number of pixels that hold their classification through time. The off-diagonal represents the number of pixels that do not hold their classification through time. The confusion matrix output provides three measures: the observed accordance, expected accordance, and the Kappa statistic. The observed accordance is simply the proportion of matching pixels (sum of diagonal cells in the matrix produced) out of the total pixels measured. The expected accordance is the sum of marginal class products divided by the squared total number of pixels for each class, where the marginal class product is the sum of pixels in the row and sum of pixels in the column for each class multiplied together. The Kappa Index is then calculated as the difference between the observed and expected accordance divided by one minus the expected accordance. To visualize the observed accordance, identified here as the spatial

accordance, with time, soil moisture classes were imported into ArcMap 10.0 and depicted in raster format. Calculating the difference between rasters according to date depict the pixels that maintain their classification through time; raster pixels with a value of zero exhibit spatial accordance through time in comparison to those attaining a positive or negative value that did not retain their spatial accordance.

Vachaud et al.'s Time Stability Analysis

Over a given observation domain, certain areas will exhibit persistent patterns of wetness or dryness compared to the average moisture content across the observation domain (Lin 2006). This persistence can be assessed using time stability (Vachaud et al. 1985). Vachaud et al.'s (1985) time stability analysis is applied to soil moisture cokriged estimates derived from the aforementioned multicollocated cokriging analysis.

The first step of the Vachaud et al.'s (1985) time stability analysis is to calculate the relative difference for each sampled value respective to each sampling date [Eqn. 4-22] (Vachaud et al. 1985):

$$\delta_{ij} = \frac{\Delta_{ij}}{\overline{S}_j} \qquad \text{[Eqn. 4-22]}$$

where Δ_{ij} is the difference between an individual measurement (S_{ij}) at location *i* and time *j* and the field mean for time *j* ($\overline{S}_j$) [Eqn. 4-23 and Eqn. 4-24] (Vachaud et al. 1985):

$$\Delta_{ij} = S_{ij} - \overline{S}_j \qquad \text{[Eqn. 4-23]}$$

and

$$\overline{S}_j = \frac{1}{n}\sum_{i=1}^{n} S_{ij} \qquad \text{[Eqn. 4-24]}$$

where n is the number of sampling locations.

Equation 4-23 centers soil moisture because soil moisture will inherit a unique $\overline{S_j}$ across a sampling domain as soil moisture content fluctuates through time. The MRD specific to sampling location *i* is defined by [Eqn. 4-25]:

$$\overline{\delta_i} = \frac{1}{m}\sum_{j=1}^{m} \delta_{ij} \qquad \text{[Eqn. 4-25]}$$

where m is the number of days sampled. Positive MRD values, negative MRD values and values equal to zero indicate sampling locations that are persistently higher than, less than, or equal to the field average, respectively. The second step is calculating the standard deviation of the MRD. Calculating the standard deviation $\sigma(\delta_{ij})$ is used to assess the time stability for each location (i) [Eqn. 4-26] (Vachaud et al. 1985).

$$\sigma(\delta_i) = \sqrt{\frac{1}{m-1}\sum_{j=1}^{m}(\delta_{ij} - \bar{\delta_j})^2} \qquad \text{[Eqn. 4-26]}$$

Locations exhibiting a small SD_{MRD} $(\sigma(\delta_i))$ are considered time stable. The MRD is an indicator of the location's bias and the SD_{MRD} characterizes the locations precision (Jacobs et al. 2004, Teuling et al. 2006). Jacobs et al. (2004) used the root means squared error ($RMSE_i$) to simultaneously assess the bias and precision of a location [Eqn. 4-27] (Vanderlinden et al. 2011). It is suggested that the most representative and time stable locations of the field are those with the lowest RMSE.

$$RMSE_i = \sqrt{\overline{\delta_i}^2 + \sigma(\delta_i)^2} \qquad \text{[Eqn. 4-27]}$$

The MRD and $RMSE_i$ assess how soil moisture varies over time relative to the field average.

Certain management practices, such as precision agriculture, are more interested in assessing how soil moisture varies at each location in a more direct and localized manner. One approach is simply calculating the difference between consecutive time steps and dividing by the total observed dates to obtain an average difference (AD) [Eqn. 4-28] at each observation point.

$$\overline{w}_i = \frac{1}{m}\sum_{j=1}^{m}\left(w_{i,j+1} - w_{i,j}\right) \qquad \text{[Eqn. 4-28]}$$

where $\overline{w}_i$ is the average difference of location *i*; m is the number of observation dates; and *j* is a specific observation date. It is possible to calculate the standard deviation of the time step differences (SD_{AD}). Unlike the MRD, the AD is not calculated relative to a mean value.

The intent here is not to impress superiority of the Vachaud et al.'s (1985) MRD over the AD, or vice versa, because the two approaches are not comparable by stature. The purpose here is to underscore their individual utility to characterize soil moisture spatial variability as a function of time. If the objective is to study time stable soil moisture patterns across the landscape then Vachaud et al.'s (1985) technique is suggested because it characterizes soil moisture variation with respect to soil-landscape properties and processes. If the objective is to optimize management operations for soil moisture, such as irrigation, then the average difference approach is suggested because it represents soil moisture variation with respect to localized soil moisture fluctuations across the

landscape. Outcomes for the MRD and AD techniques were then imported into ArcMap 10.0 and displayed in raster format for visual assessment.

PCA_{MRD} was used to establish which selected soil-terrain attributes best intercorrelate with the MRD across the landscape studied. PCA_{MRD} was performed using the direct measurements of soil properties. Therefore, the MRD raster was sampled at each of the 100 georeferenced calibration locations where direct measurements were obtained using the nearest neighbor function in Spatial Analyst (ArcMap 10.0).

To discover which landscape positions exhibit a significant difference in the calculated MRD polygon kriging was applied using a 2D landscape model (Park et al. 2001). Polygon kriging is akin to block kriging in that both techniques average observations falling within a specified domain. Much like block kriging, polygon kriging upscales MRD values according to landscape position (Guber et al. 2008). Polygon kriging produces a weighted average estimate and kriging variance for a defined area using an irregular shaped polygon. Polygon kriging weights are implemented such that values lying near the boundary edge hold less weight than those lying near the center of the polygon domain. Landscape position polygons were created using a simple process-based landscape unit model adapted from Park et al. (2000). The landscape model was constructed in ArcMap 10.0 Model Builder using a series of conditional statements and calculations prescribed in Park et al. (2001) and applied to terrain attributes (upland contributing area and curvature) produced in Chapter 3.

The landscape model constructed (Park et al. 2001) was ground-referenced in Spring 2012 using a hand-held Trimble GeoXH global position system and field guidance from

Steve Blanford (USDA Natural Resource Conservation Service). Ridgetop positions were added although their initial exclusion from the model was due to the high presence of cropping activity in these locations. Results from the process-based raster model and the ground-reference model were integrated to perform polygon kriging (ISATIS®) for five landscape positions including backslope, drainageway, footslope, ridgetop, and shoulder positions. Polygon kriging results in a kriging estimate and kriging standard deviation for the MRD according to landscape position. Using the kriging standard deviation for each polygon it was possible to calculate the MRD 95% confidence interval (CI) respective to landscape position. If a kriged polygon estimate (e.g. MRD estimate for a given landscape position) fell outside the 95% CI of another polygon estimate the two were considered to have significantly different MRD's. Polygon kriging was performed on the aforementioned sample set selected for PCA.

Cross Correlograms

The cross correlogram is a geostatistical tool that measures the spatial correlation between two variables as a function of spatial increments or lag ($\boldsymbol{h}$) separation [Eqn. 4-29].

$$r_c(\boldsymbol{h}) = \frac{cov[A_i(\boldsymbol{x}_i), B_i(\boldsymbol{x}_i + \boldsymbol{h})]}{\sqrt{var[A_i(\boldsymbol{x}_i)]}\sqrt{var[B_i(\boldsymbol{x}_i + \boldsymbol{h})]}} \qquad \text{[Eqn. 4-29]}$$

Observations closer together will exhibit a stronger spatial correlation than observations farther apart. Calculating [Eqn. 4-29] at lag zero resorts to the linear correlation coefficient. The cross correlogram is applied here to measure the spatial autocorrelation of soil moisture between two consecutive time steps (De Lannoy et al. 2006). By

convention, time stability is determined by studying the apex of the cross correlogram between two time steps; if the apex of the cross correlogram centers on lag zero, then there is no apparent spatial shift in the spatial patterned highs and lows between time steps. If the cross correlogram exhibits symmetry about the apex, then it is apparent that the source(s) of variation driving the patterned behavior is consistent between the observed time steps. Unlike the MRD, the cross correlogram is a geostatistical technique meaning it takes into account the spatial autocorrelation of sampling locations between individual time increments. The MRD treats each sampling location discretely relative to a field temporal average. Moreover, the cross correlogram is a good application for studying when the sources of soil moisture spatial variation change, particularly transitioning between states of soil wetting and drying. The cross correlograms for July versus September and September versus October were calculated using the 8,734 MFCA derived soil moisture point estimates in ISATIS® (Geovariances 2012).

Results

Estimating Apparent Electrical Conductivity (aEC)

Positive skewness and kurtosis are present for each sampling date, albeit greater for the shallower readings (Table 4.1). Consequently, cokriging was performed on Gaussian transformed apparent EC measurements. The cross variogram parameters for Gaussian transformed apparent EC are in Table 4.2. The fitted range increases while the sill of the cross variogram decreases for each successive date indicating apparent EC spatial continuity increases with increasing soil moisture content. The correlation coefficient between measured (Z) apparent EC and estimated (Z*) apparent EC was > 0.9. The model estimates are unbiased as demonstrated by the nominal ME (Table 4.3). The VSE

decreases through time with increasing soil moisture content (Table 4.3). The decrease in VSE is credited to the increased spatial autocorrelation and lower experimental sill values with time with increasing soil moisture contents. Cokriging estimates for shallow apparent EC are illustrated in Figure 4.1. It is noticeable apparent EC increases with time. The cokriged estimates for October apparent EC served as the secondary variable to downscale direct soil measurements subjected to LMC modeling.

Table 4.1. Basic statistics for deep and shallow raw apparent EC (aEC) readings.

	Min.	Max.	Mean	Std. Dev.	Skewness	Kurtosis	Count	Correlation
July aEC (S)	0.20	3.6	1.2	0.36	1.5	6.8	9860	0.79
July aEC (D)	0.51	14	4.9	1.6	1.2	5.7	9860	
September aEC (S)	0.11	7.8	1.9	0.65	1.8	8.8	10290	0.83
September aEC (D)	0.65	17	5.8	0.65	1.2	5.6	10290	
October aEC (S)	0.35	8.3	2.3	0.89	1.7	7.2	9915	0.48
October aEC (D)	4.2	199	75	20	0.21	4.0	9915	

Shallow (~30 cm) depths are annotated as (S) and deeper (~90 cm) depths as (D). Units are in mS/m.

Table 4.2. Variogram parameters for Gaussian transformed apparent EC fitted by the LMC.

Date	Nugget Shallow Variogram	Nugget Deep Variogram	Nugget Cross Variogram	Range (m)	Sill Shallow Variogram	Sill Deep Variogram	Sill Cross Variogram
July	8.9×10^{-2}	9.2×10^{-2}	8.1×10^{-3}	69	0.82	0.89	0.72
September	7.0×10^{-2}	8.0×10^{-2}	2.7×10^{-2}	72	0.83	0.82	0.71
October	1.0×10^{-1}	5.7×10^{-1}	-5.8×10^{-3}	88	0.84	0.43	0.49

Table 4.3. Cross validation statistics for cokriged shallow apparent EC.

Date	ME	VE	MSE	VSE
July (n=9,857)	1.7×10^{-3}	0.18	2.1×10^{-3}	0.95
September (n=10,290)	4.5×10^{-3}	0.14	6.0×10^{-4}	0.84
October (n=9,915)	1.0×10^{-4}	0.12	1.0×10^{-4}	0.65

(ME) Mean error
(VE) Variance of error
(MSE) Mean standardized error
(VSE) Variance of the standardized error

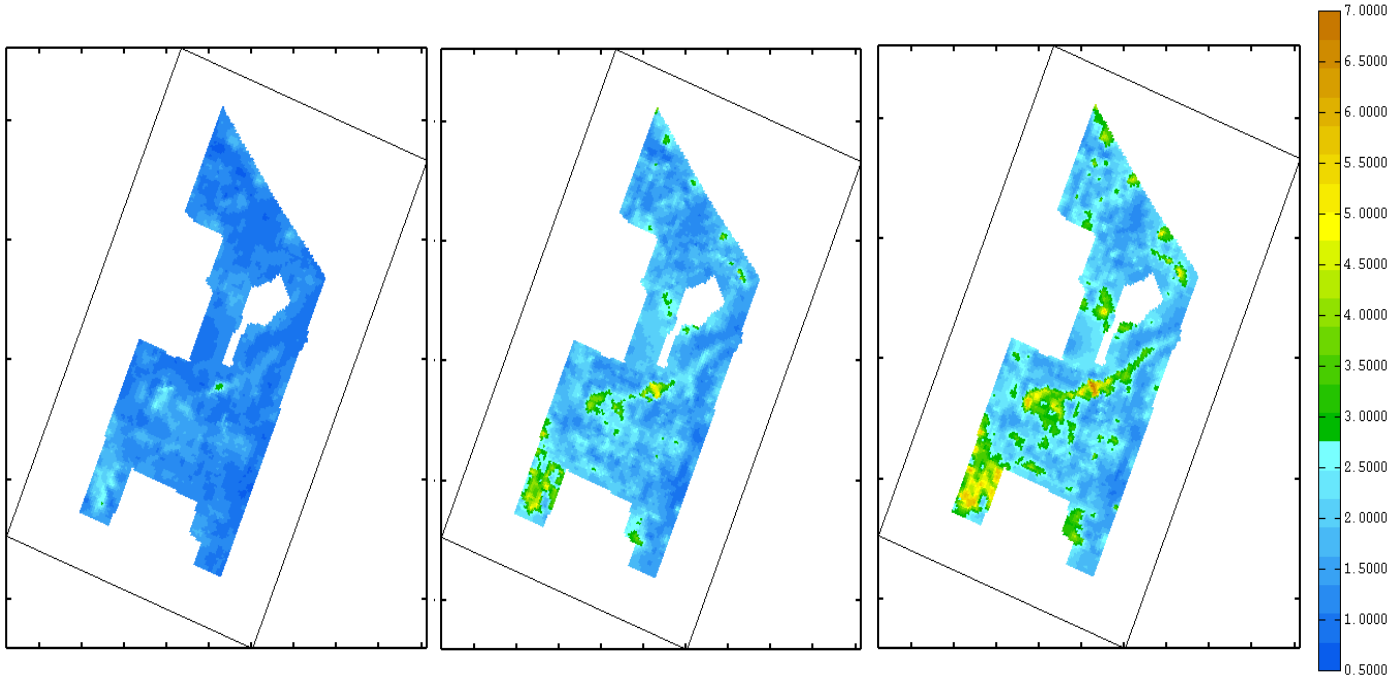

Figure 4.1. Cokriged estimates for shallow apparent electrical conductivity.

July (left), September (middle), and October (right). Units are in mS/m. Scale marks on the horizontal axis are in 100 meter increments. Scale marks on the vertical axis are in 250 meter increments. Estimates were produced on a 5 m mesh grid. October apparent electrical conductivity served as the secondary variable for cokriging attributes for MFCA.

Exploratory Analysis and Gaussian Anamorphosis

Exploratory statistics performed on the initial raw 27 variates revealed 11 best associated with October volumetric soil moisture and included terrain features identified in Chapter 3 (slope and elevation), soil physical and chemical properties (calcium [Ca^{2+}], organic matter, clay, and sand), geoelectric measurements (apparent electrical conductivity for July, September and October) and volumetric soil moisture for July and September. Table 4.4 includes the Pearson correlation coefficients between all 27 variables considered for this study and October volumetric water content. Variables showing a correlation > ±0.30 with October volumetric water content included clay, sand, silt, July and September volumetric water content, and apparent electrical conductivity for all three observation dates. The best fit model from the stepwise regression showed elevation, slope, Ca^{2+}, magnesium (Mg^{2+}), organic matter, bulk density, and October apparent EC best associated with October volumetric water content. The first significant principal component from PCA is shown in Table 4.5. The first principal component explained 25% of the total observed variation. Attention was focused on absolute values of variable loading values differing within 10% of the maximum loading value. For the first significant PC, Ca^{2+}, clay, pH, apparent EC for all three dates, sand, nitrogen, zinc (Zn), and silt were considered. Notably, pH, nitrogen and Zn are the only variables not identified in the aforementioned exploratory selections. Due to multicollinearity, pH and silt were automatically excluded because these variables were derived from calculations using direct measurements. Bulk density was automatically excluded because it was used to derive volumetric water content. Overall, terrain attributes calculated in Chapter 3 do not show a strong association with October volumetric water content. Nonetheless, stepwise regression and PCA indicate elevation is a good candidate for further

investigation. Slope was selected because it exhibited a higher correlation coefficient than other studied terrain attributes and was selected by stepwise regression. Clay, Ca^{2+}, sand, organic matter, volumetric water content for all three dates, and apparent electrical conductivity for all three dates were selected because they were identified by at least two of the three exploratory analyses performed. Finally, preliminary variogram analyses indicated the 11 pre-selected variables, plus October volumetric water content, exhibit structured variation, indicating they were good candidates for MFCA.

Table 4.4. Pearson's correlation for exploratory analysis.

Variable	Pearson's Correlation Coefficient
Oct Volumetric H_2O	1.0
Jul Volumetric H_2O	0.69
Sept Volumetric H_2O	0.68
Oct Apparent EC	0.47
Sept Apparent EC	0.42
Sand	0.34
Clay	0.32
Jul Apparent EC	0.31
Bulk Density	0.23
Slope	0.22
Phosphorus	0.18
Calcium	0.17
Nitrogen	0.17
Aspect	0.16
Cation Exchange Capacity	0.14
pH	0.14
Magnesium	0.11
Zinc	0.11
Plan Curvature	<0.10
Organic Matter	<0.10
Elevation	<0.10
Potassium	<0.10
Profile Curvature	<0.10
Upland Contributing Area	<0.10
Exchangeable Acidity	0.00
Topographic Wetness Index	-0.13
Silt	-0.41

The correlation coefficients in this table are related specifically to October volumetric water content.

Table 4.5. Loading values for the first significant principal component generated from PCA..

Variable	PC1
October Apparent EC	0.30
Calcium	0.29
September Apparent EC	0.27
Clay	0.25
pH	0.25
July Apparent EC	0.25
Sand	0.25
July Volumetric H_2O	0.24
Organic Matter	0.24
Zinc	0.24
Nitrogen	0.21
October Volumetric H_2O	0.20
September Volumetric H_2O	0.20
Phosphorus	0.18
Aspect	0.10
Potassium	0.10
Slope	0.10
Magnesium	0.08
Plan Curvature	0.06
Cation Exchange Capacity	<0.10
Elevation	<0.10
Profile Curvature	<0.10
Upland Contributing Area	<0.10
Exchangeable Acidity	<0.10
Topographic Wetness Index	-0.10
Bulk Density	-0.10
Silt	-0.31

The first PC explained 25% of the total observed variation.

The four statistical moments for the 12 selected variables are expressed in Table 4.6. Clay and elevation were the only variables exhibiting skewness below or equal to 0.20 and were considered symmetric about their means. All other variables were considered asymmetric exhibiting slight to extreme positive skewness. Peaked distribution curves were observed among most variables that attained kurtosis values above 3.0. Elevation exhibited a bi-modal distribution and singularly exhibited a kurtosis value below 3.0. The Q-Q plots are exhibited in Figures 4.2 and 4.3. The Chi-squared significance test performed on the Q-Q plots indicated most variables were non-normally distributed. Consequently, all 12 soil-terrain attributes were subjected to Gaussian anamorphosis, which transforms the raw data set into a normally distributed Gaussian data set with mean zero and unit variance prior to performing MFCA.

Table 4.6. Basic statistics (n=94) for the 12 selected soil-terrain attributes.

Variable	Minimum	Maximum	Mean	Variance	Kurtosis	Skewness
Calcium (mg/kg)	2.7×10^3	2.1×10^3	4.6×10^3	4.9×10^6	37	5.0
Clay (%)	17	34	25	8.8	3.0	0.20
Elevation (m)	2.9×10^2	3.1×10^2	3.0×10^2	72	1.9	0.17
July aEC(mS/m)	0.71	3.2	1.2	0.15	12	2.5
July H_2O (vol./vol.)	0.13	0.26	0.18	0.00	3.0	0.62
Organic Matter (%)	2.3	11	3.6	1.1	29	4.2
Oct aEC (mS/m)	1.3	5.3	2.1	0.69	6.8	1.9
Oct H_2O (vol./vol.)	0.25	0.44	0.32	0.00	4.3	0.92
Sand (%)	6.3	18	1.1×10^1	5.8	3.3	0.89
Sep aEC (mS/m)	1.1	4.2	1.8	0.40	6.9	1.8
Sep H_2O (vol./vol.)	0.20	0.39	0.27	0.00	4.7	1.1
Slope (unitless)	0.00	4.0×10^{-2}	1.0×10^{-2}	0.00	6.2	1.7

(aEC) Apparent EC
(H_2O) Volumetric water content

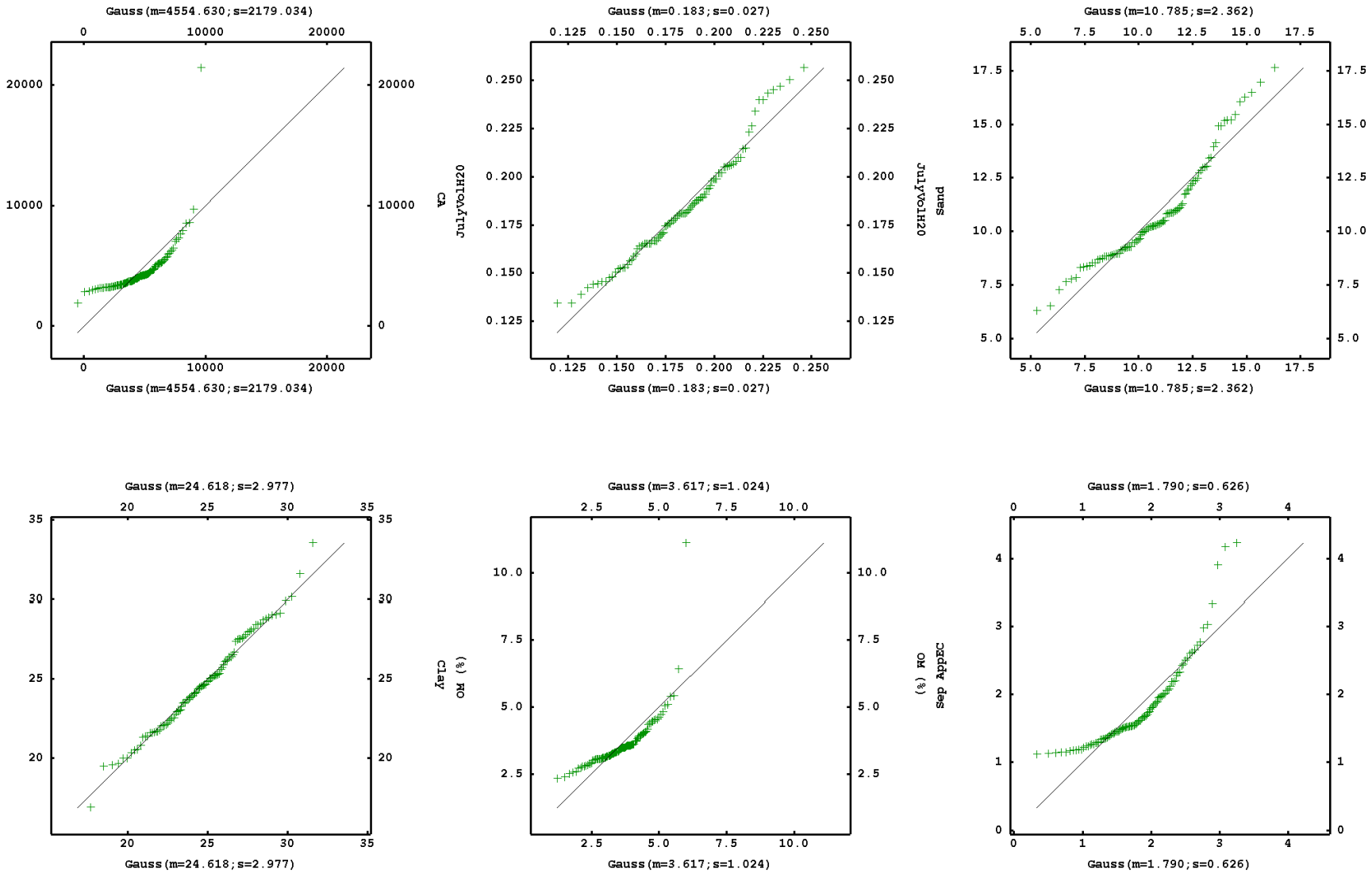

Figure 4.2. Q-Q plots for the 6 of the 12 selected soil-terrain attributes.

Viewing from top left to bottom right: Ca^{2+}, July volumetric water content, sand, clay, organic matter, and September apparent electrical conductivity.

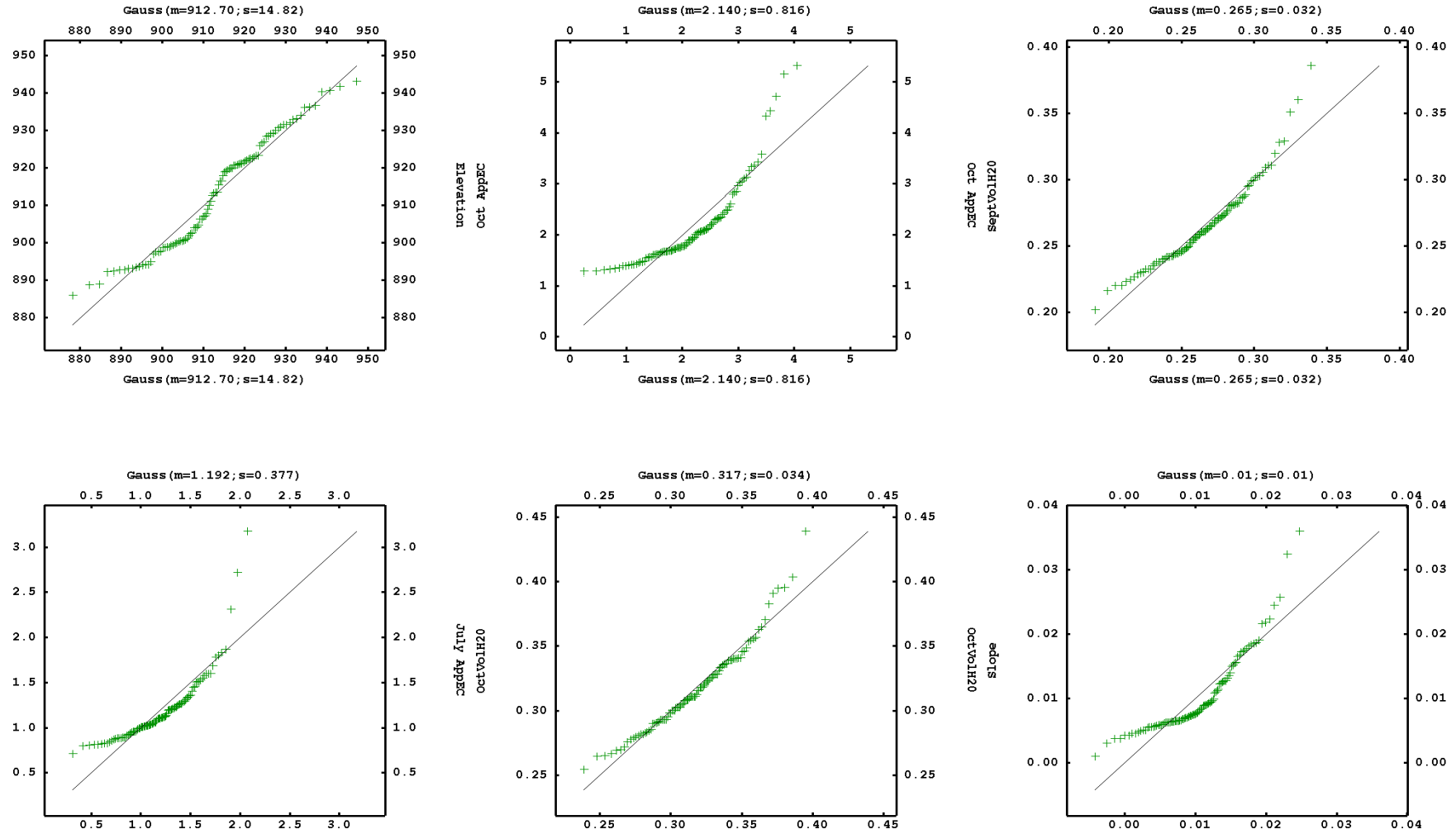

is **Figure 4.3. Q-Q plots for the 6 of the 12 selected soil-terrain attributes.**

Viewing from top left to bottom right: elevation, October apparent electrical conductivity, September volumetric water content, July apparent electrical conductivity, October volumetric water content, and slope.

MFCA

A linear combination of basic variogram functions was simultaneously fitted to all 12 soil-terrain Gaussian transformed attributes using a matrix of direct and cross experimental variograms. The LMC consisted of 78 direct and cross variograms modeled by 3 basic functions: nugget, spherical (short-range scale = 40m), and exponential (long-range scale=250m; with an effective range of 750m [Eqn. 4-4]). The LMC cross-validation statistics for each Gaussian variable are illustrated in Table 4.7. Overall, the ME is close to zero (≤ 0.05) for all 12 attributes. The variance of the standardized error for all variables fall within the tolerance threshold established by Chilés and Delfiner (1999) except for elevation. Attributes with high spatial continuity will exhibit lower experimental variance causing the variance of the standardized error to be obviously lower than 1. This appeared to be the case for elevation, geoelectric measurements, and soil moisture content for wetter observation dates. Moreover, these statistics are performed on Gaussian transformed attributes, which, to a degree, smooth some of the natural variation in the raw attribute causing a lower experimental variance.

Volumetric soil moisture for the three observation dates (Figure 4.4) were of most interest for time stability analyses. Plotting kriged soil moisture estimates versus validation soil moisture measurements (n=27) for all three dates indicate a robust correlation (rho = 0.83) (Figure 4.5). The mean error for each observation date is close to zero, indicating the estimates are unbiased (Table 4.8). The VSE is slightly above 1 for all three observation dates but are within the tolerance threshold (Chilés and Delfiner 1999) (Table 4.8). The slightly high VSE is attributed to the small number of validation samples.

Table 4.7. Cross validation statistics for the LMC.

Variable	ME	VE	MSE	VSE	R^2
Ca^{2+} (mg/kg)	3.2×10^{-2}	0.43	-3.1×10^{-2}	0.69	0.75
Clay (%)	1.2×10^{-3}	0.55	-3.7×10^{-3}	0.91	0.67
Elevation (m)	2.7×10^{-3}	7.5×10^{-2}	2.8×10^{-3}	0.32	0.96
July H_2O (vol./vol.)	1.2×10^{-2}	0.67	8.9×10^{-3}	1.0	0.57
July aEC (mS/m)	-5.1×10^{-2}	0.51	-4.9×10^{-2}	0.83	0.69
Oct H_2O (vol./vol.)	1.1×10^{-2}	0.62	7.4×10^{-4}	0.86	0.61
Oct aEC (mS/m)	1.2×10^{-2}	0.52	-2.5×10^{-3}	0.01	0.68
Organic Matter (%)	5.6×10^{-3}	0.53	5.7×10^{-3}	0.81	0.68
Sand (%)	3.0×10^{-2}	0.65	2.8×10^{-2}	0.98	0.58
Sept aEC (mS/m)	-4.7×10^{-2}	0.47	-4.7×10^{-2}	0.68	0.72
Sept H_2O (vol./vol.)	-3.3×10^{-2}	0.84	3.6×10^{-2}	0.99	0.43
Slope (unitless)	2.2×10^{-3}	0.60	8.6×10^{-2}	1.1	0.62

Plotting estimates versus true values generated the R^2 value. (aEC) Apparent EC(H_2O) Volumetric water content
ME) Mean Error
(VE) Variance of error
(MSE) Mean standardized error
(VSE) Variance of the standardized error

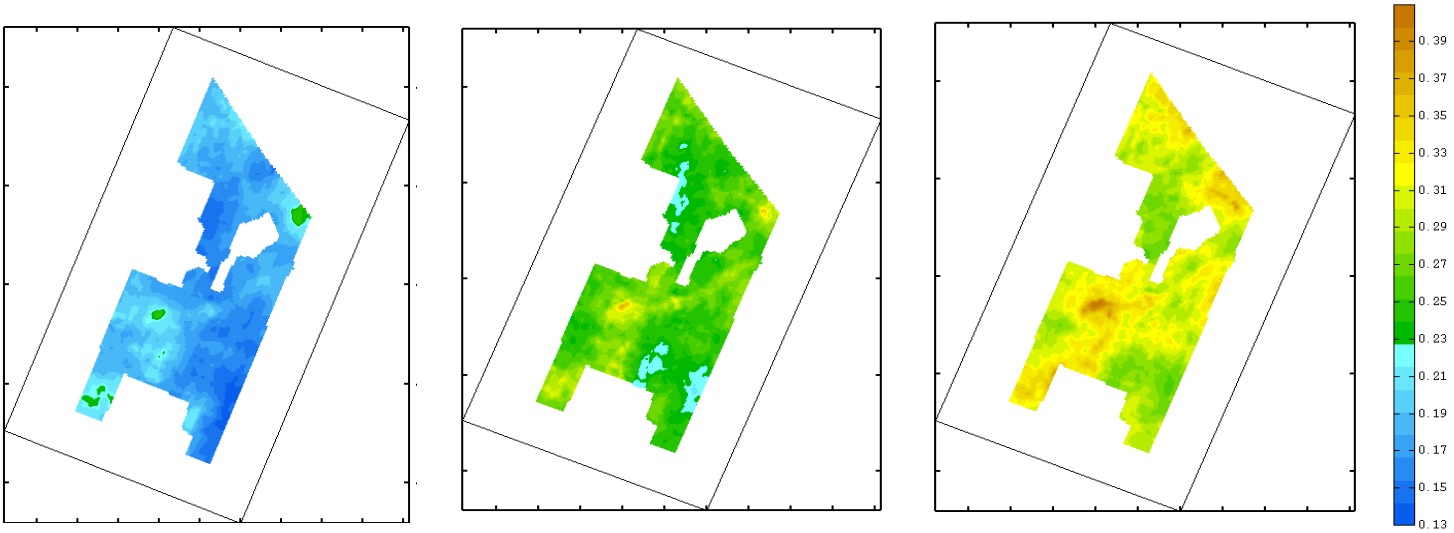

Figure 4.4. Multicollocated cokriged volumetric soil water content.
July (left), September (middle), and October (right). Volumetric water content is expressed as (vol/vol). Scale marks on the horizontal axis are in 100 meter increments. Scale marks on the vertical axis are in 250 meter increments.

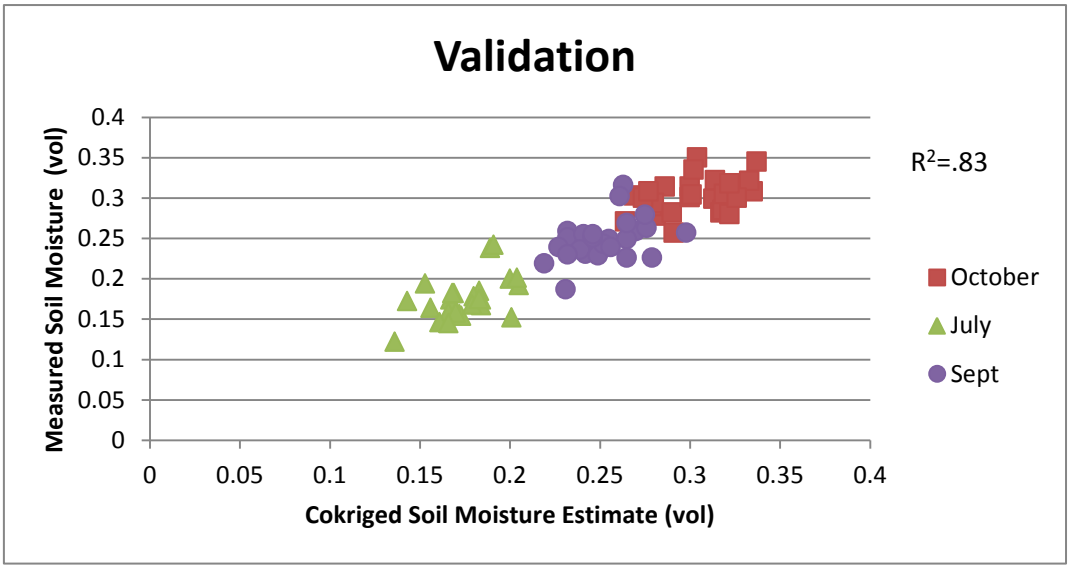

Figure 4.5. Scatterplot of measured soil moisture content versus cokriged soil moisture estimates.
July, September, and October are shown. The measured soil moisture values collected at the 27 validation sampling locations (Chapter 2).

Table 4.8. Cross validation statistics for volumetric water content (n=27).

Date	ME	MSE	VSE
July	1.6×10^{-4}	9.1×10^{-3}	1.7
September	3.9×10^{-3}	0.21	1.8
October	-3.5×10^{-3}	-0.17	1.7

(ME) Mean Error(MSE) Mean standardized error
(VSE) Variance of the standardized error

The coregionalized variance-covariance matrix for the short-range (40 m) and long-range (250 m) scales are illustrated in Tables 4.9 and 4.10, respectively. Applying PCA_{LMC} to the coregionalized variance-covariance matrices generated a set of scale-dependent structural correlation coefficients in addition to a set of regionalized factors. The structural correlation matrices are exhibited by Tables 4.11 and 4.12, respectively.

At the short-range scale (40 m), July volumetric water content correlated with sand, July apparent EC, and volumetric water content for September and October; October volumetric water content correlated with October apparent EC, slope, and July volumetric water content; and September volumetric water content inversely correlated with September apparent EC and positively correlated with July volumetric water content. The correlation between elevation and other measured soil-terrain attributes was significant at this scale except for clay, suggesting elevation is influential at smaller scales. The inverse relationship between September volumetric water content and September apparent electrical conductivity is attributed to the relatively high nugget effect for September volumetric water content. The low correlation coefficients between September and October volumetric water contents do not support the notion of time stability at the short-range scale.

At the long-range scale (250 m), however, there was a moderate to strong correlation between the three soil moisture dates, Ca^{2+}, clay, sand, and organic matter. The significant correlation between the three soil moisture dates suggests time stability is specific to this scale. The studied terrain attributes are not significant in relation to soil moisture at this scale (250 m). The scale-dependent structural correlation coefficients differ from the Pearson's correlation coefficients (Table 4.13) because they focus

specifically on the scales distilled by the LMC, therefore, avoiding a dilution effect from processes occurring at different spatial scales (Castrignanò et al. 2000).

Table 4.9. Coregionalized matrix for the short-range scale (40 m).

Variable	Ca^{2+}	Clay	Elev	Jul aEC	Jul H_2O	OM	Oct aEC	Oct H_2O	Sand	Sept aEC	Sept H_2O	Slope
Ca^{2+}	0.32	-0.037	-0.042	0.19	0.00	0.21	0.24	0.050	-0.040	0.21	-0.028	-0.10
Clay	-0.037	0.14	0.010	0.078	-0.017	-0.052	0.069	0.010	-0.097	0.089	-0.042	0.11
Elevation	-0.042	0.010	0.010	-0.025	0.00	-0.021	-0.027	-0.012	0.014	-0.017	-0.010	0.013
Jul aEC	0.19	0.078	-0.025	0.44	0.067	0.11	0.30	0.10	0.014	0.29	-0.011	-0.015
Jul H_2O	0.00	-0.017	0.00	0.067	0.036	-0.011	0.033	0.044	0.056	0.010	0.029	-0.010
OM	0.21	-0.052	-0.021	0.11	-0.011	0.19	0.12	-0.027	0.00	0.13	-0.040	-0.13
Oct aEC	0.24	0.069	-0.027	0.30	0.033	0.12	0.41	0.17	0.099	0.36	-0.066	0.091
Oct H_2O	0.050	0.010	-0.012	0.10	0.044	-0.027	0.17	0.16	0.11	0.11	0.017	0.12
Sand	-0.040	-0.097	0.014	0.014	0.056	0.00	0.099	0.11	0.35	0.068	-0.010	0.034
Sept aEC	0.21	0.089	-0.017	0.29	0.010	0.13	0.36	0.11	0.068	0.35	-0.093	0.079
Sept H_2O	-0.028	-0.042	-0.010	-0.011	0.029	-0.040	-0.066	0.017	-0.010	-0.093	0.062	-0.032
Slope	-0.10	0.11	0.013	-0.015	-0.010	-0.13	0.091	0.12	0.034	0.079	-0.032	0.25

Values represent the direct and cross variogram sill values fitted by the LMC.(aEC) Apparent EC(Elev) Elevation
(H_2O) Volumetric water content
(OM) Organic matter

Table 4.10. Coregionalized matrix for the long-range scale (250 m).

Variable	Ca^{2+}	Clay	Elev	Jul aEC	Jul H_2O	OM	Oct aEC	Oct H_2O	Sand	Sept aEC	Sept H_2O	Slope
Ca^{2+}	0.79	0.77	0.028	0.14	0.60	0.76	0.25	0.29	0.50	0.12	0.49	0.22
Clay	0.77	0.94	0.11	0.23	0.74	0.69	0.35	0.35	0.62	0.19	0.59	0.081
Elevation	0.028	0.11	0.38	0.24	0.048	-0.12	0.23	-0.064	-0.049	0.23	-0.019	0.15
Jul aEC	0.14	0.23	0.24	0.26	0.21	0.041	0.25	0.013	-0.032	0.23	0.11	-0.021
Jul H_2O	0.60	0.74	0.048	0.21	0.80	0.58	0.31	0.50	0.58	0.16	0.63	0.14
OM	0.76	0.69	-0.12	0.041	0.58	1.0	0.089	0.46	0.52	0.010	0.55	0.13
Oct aEC	0.25	0.35	0.23	0.25	0.31	0.089	0.29	0.041	0.12	0.22	0.18	0.090
Oct H_2O	0.29	0.35	-0.064	0.013	0.50	0.46	0.041	0.60	0.35	-0.010	0.49	0.029
Sand	0.50	0.62	-0.049	-0.032	0.56	0.52	0.12	0.353	0.78	-0.033	0.47	0.31
Sept aEC	0.12	0.19	0.23	0.23	0.16	0.010	0.22	-0.010	-0.033	0.20	0.074	0.023
Sept H_2O	0.49	0.59	-0.019	0.11	0.63	0.55	0.18	0.49	0.47	0.074	0.54	0.073
Slope	0.22	0.081	0.15	-0.021	0.14	0.13	0.09	0.029	0.31	0.023	0.073	0.72

Values represent the direct and cross variogram sill values fitted by the LMC.(aEC) Apparent EC(Elev) Elevation
(H_2O) Volumetric water content
(OM) Organic matter

Table 4.11. Structural correlation coefficients for short-range (40 m) Gaussian transformed variables.

Variable	Ca^{2+}	Clay	Elev	Jul aEC	Jul H_2O	OM	Oct aEC	Oct H_2O	Sand	Sept aEC	Sept H_2O	Slope
Ca^{2+}	1.0											
Clay	-0.17	1.0										
Elevation	-0.87*	0.19	1.0									
Jul aEC	0.51*	0.31*	-0.44*	1.0								
Jul H_2O	0.00	-0.23*	-0.20	0.53*	1.0							
OM	0.86*	-0.31*	-0.56*	0.39*	-0.13	1.0						
Oct aEC	0.66*	0.28*	-0.49*	0.70*	0.27*	0.44*	1.0					
Oct H_2O	0.22*	0.00	-0.35*	0.37*	0.58*	-0.15	0.66*	1.0				
Sand	-0.12	-0.43*	0.28*	0.00	0.50*	0.00	0.26*	0.44*	1.0			
Sept aEC	0.61*	0.39*	-0.33*	0.73*	0.10	0.51*	0.94*	0.45*	0.19	1.0		
Sept H_2O	-0.19	-0.44*	-0.23*	-0.06	0.61*	-0.36*	-0.42*	0.16	-0.03	-0.62*	1.0	
Slope	-0.35*	0.60*	0.29*	-0.10	-0.10	-0.61*	0.28*	0.57*	0.11	0.26*	-0.25*	1.0

(aEC) Apparent EC(Elev) Elevation
(H_2O) Volumetric water content
(OM) Organic matter(*) Significant ($p < 0.05$)

Table 4.12. Structural correlation coefficients for long-range (250 m) Gaussian transformed variables.

Variable	Ca^{2+}	Clay	Elev	Jul aEC	Jul H_2O	OM	Oct aEC	Oct H_2O	Sand	Sept aEC	Sept H_2O	Slope
Ca^{2+}	1.0											
Clay	0.91*	1.0										
Elevation	0.10	0.18	1.0									
Jul aEC	0.32*	0.47*	0.76*	1.0								
Jul H_2O	0.76*	0.85*	0.10	0.45*	1.0							
OM	0.84*	0.69*	-0.18	0.10	0.64*	1.0						
Oct aEC	0.52*	0.67*	0.70*	0.92*	0.65*	0.16	1.0					
Oct H_2O	0.42*	0.46*	-0.14	0.00	0.72*	0.58*	0.10	1.0				
Sand	0.65*	0.72*	-0.10	-0.10	0.71*	0.58*	0.26*	0.52*	1.0			
Sep aEC	0.30*	0.44*	0.83*	0.99*	0.41*	0.00	0.93*	0.00	-0.10	1.0		
Sep H_2O	0.76*	0.83*	0.00	0.28*	0.96*	0.73*	0.45*	0.86*	0.73*	0.23*	1.0	
Slope	0.30*	0.10	0.28*	-0.10	0.18	0.15	0.20	0.00	0.41*	0.10	0.12	1.0

(aEC) Apparent EC(Elev) Elevation
(H_2O) Volumetric water content
(OM) Organic matter
(*) Significant ($p < 0.05$)

Table 4.13. Pearson's correlation coefficients for Gaussian transformed variables.

Variable	Ca^{2+}	Clay	Elev	Jul aEC	Jul H_2O	OM	Oct aEC	Oct H_2O	Sand	Sep aEC	Sep H_2O	Slope
Ca^{2+}	1.0											
Clay	0.57*	1.0										
Elevation	0.10	0.18	1.0									
Jul aEC	0.45*	0.42*	0.52*	1.0								
Jul H_2O	0.48*	0.54*	0.00	0.34*	1.0							
OM[3]	0.75*	0.41*	0.00	0.18	0.34*	1.0						
Oct aEC	0.62*	0.51*	0.41*	0.82*	0.46*	0.23*	1.0					
Oct H_2O	0.37*	0.34*	0.11	0.30*	0.64*	0.32*	0.49*	1.0				
Sand	0.48*	0.35*	0.00	0.00	0.44*	0.38*	0.28*	0.38*	1.0			
Sep aEC	0.51*	0.43*	0.46*	0.86*	0.38*	0.15	0.94*	0.41*	0.13	1.0		
Sep H_2O	0.37*	0.46*	0.06	0.36*	0.69*	0.31*	0.46*	0.71*	0.36*	0.37*	1.0	
Slope	0.18	0.20	0.00	-0.10	0.16	0.00	0.12	0.00	0.31*	0.00	-0.10	1.0

(aEC) Apparent EC(Elev) Elevation
(H_2O) Volumetric water content
(OM) Organic matter
(*) Significant ($p < 0.05$)

There is visual redundancy, or correlation, in the patterned variation between apparent electrical conductivity (see Figure 4.1), soil moisture, and soil physicochemical attributes including Ca^{2+}, organic matter, sand, and clay (Figure 4.6) in terms of relative highs and lows. The drainageway transecting the site is evident in the cokriged maps of apparent EC, soil moisture, clay, organic matter, Ca^{2+}, and sand. With the exception of the drainageway, slope exhibitedsimilarities with these soil attributes as well. Elevation exhibited a linear trend (Chapter 3) from southwest to northeast. Applying PCA to the coregionalized matrices (Tables 4.9 and 4.10) collapsed spatially redundant variables into a set of regionalized factors that describe how the total observed variation is partitioned among spatial functions fitted by the LMC. The nugget explained 17%, short range scale explained 22%, and long range scale explained 60% of the total measured variation, indicating most of the observed variation resides in the long-range scale. The regionalized factors (e.g. spatial principal components) for the short- and long-range scales are exhibited in Tables 4.14 and 4.15, respectively. The first regionalized factors in Tables 4.14 and 4.15, respectively, were mapped and classified into three inter-quantile classes, or homogeneous units, that signify the high, medium, and low presence of variables loading on the principal component (Figures 4.7 and 4.8).

The first factor for the short-range scale was significant (eigenvalue > 1.0) whereas the first and second factors for the long-range scale were significant (Tables 4.14 and 4.15). Attention is focused on absolute values of loading values differing within 10% of the maximum loading value. The percentage of total variation explained by the short range-scale (22%) is close to the percentage of total variation explained by the nugget (17%), indicating the landscape is affected mostly by variation at the long-range. The factor

loading values for the short-range scale indicate July, September, and October apparent EC explain most of the short-range variation; albeit this scale explained only 11% of the total measured variation.

The first two regionalized factors at the long-range were significant and explained 60 % of the total measured variation. The first regionalized factor overshadowed the second regionalized factor by explaining 59% of the variation at this spatial scale. Variables loading on the first long-range factor include clay, organic matter, July volumetric water content, Ca^{2+}, and September volumetric water content. These findings suggest soil physicochemical properties impact soil moisture patterns during drier conditions (July and September) but to a lesser degree as the soil approaches field capacity (October). The mapped homogeneous zones for the long-range first factor detail regions characterized by a high, medium, and low presence of the variables weighing on this factor (Figure 4.8). These properties improve the water retention capability of the soil; therefore, the zones exhibiting a higher presence of these variables are expected to be wetter, especially under dry conditions. July apparent EC, October apparent EC, and elevation weighed on the second long-range factor, which explained 15% of the variation at this scale. The second regionalized factor is not mapped because it explained only ~10% of the total observed variation. The importance of the second long-range factor is it underscores the relevance of apparent EC and elevation at this scale. This confirms apparent EC is a good proximal measure of the cumulative variability at both spatial scales nested within the landscape.

The long-range factor loadings exhibited by October volumetric water content do not fall within the 10% loading value threshold criterion. Notably, however, October volumetric

water content exhibits comparable inverse factor loadings between the first and second significant factors at this scale, possibly indicating a transition period where terrain attributes achieve a stronger interaction with soil moisture.

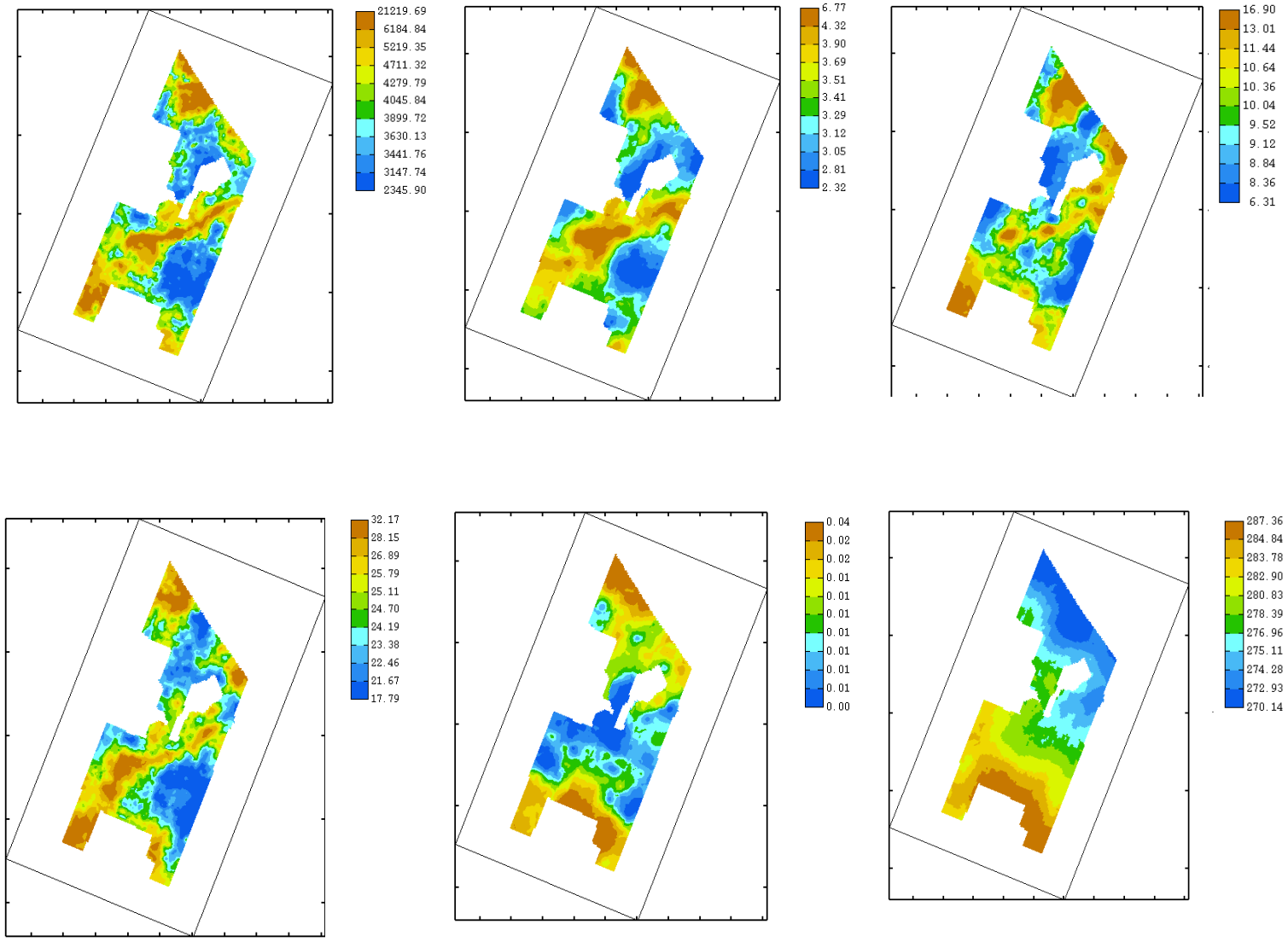

Figure 4.6. Multicollocated cokriged soil-terrain attributes.

From top left to bottom right: Ca^{2+} (ppm); organic matter (%); sand (%); clay (%); slope (unitless); and elevation (meters). Scale marks on the horizontal axis are in 100 meter increments. Scale marks on the vertical axis are in 250 meter increments. Moisture is excluded.

Table 4.14. Regionalized factors (e.g. principal components) for the short-range scale (40 m).

	Ca^{2+}	Clay	Elev	Jul aEC	Jul H_2O	OM	Oct aEC	Oct H_2O	Sand	Sept aEC	Sept H_2O	Slope	Eig.	%
F1	0.36	0.08	-0.04	0.48	0.05	0.22	0.53	0.19	0.10	0.49	-0.08	0.05	1.3	49
F2	-0.42	0.21	0.06	-0.05	0.06	-0.42	0.15	0.31	0.32	0.10	-0.03	0.60	0.58	21
F3	-0.03	0.48	-0.01	0.14	-0.14	-0.13	-0.02	-0.15	-0.79	0.09	-0.09	0.23	0.42	15
F4	-0.23	0.01	-0.01	0.72	0.31	-0.23	-0.17	0.09	-0.01	-0.23	0.36	-0.23	0.22	8.2
F5	0.42	-0.24	-0.15	-0.20	0.09	-0.15	0.13	0.55	-0.32	-0.28	0.37	0.18	0.15	5.6
F6	-0.08	0.38	-0.02	-0.29	0.19	-0.25	0.62	-0.11	0.03	-0.21	0.08	-0.48	0.02	0.67
F7	-0.57	-0.42	-0.13	-0.16	0.10	0.14	0.18	0.00	-0.33	0.46	0.24	-0.13	0.00	0.00
F8	0.09	0.26	0.19	-0.15	-0.07	-0.24	-0.40	0.50	0.01	0.44	-0.06	-0.46	0.00	0.00
F9	-0.08	-0.07	0.73	-0.03	0.46	0.26	0.07	0.17	-0.18	-0.16	-0.28	0.05	0.00	0.00
F10	0.33	-0.05	0.14	-0.16	0.50	-0.31	-0.14	-0.47	0.05	0.37	0.30	0.17	0.00	0.00
F11	0.01	-0.13	-0.53	0.00	0.49	-0.16	-0.10	0.07	-0.09	-0.02	-0.64	-0.04	0.00	0.00
F12	-0.08	0.50	-0.28	-0.16	0.35	0.60	-0.20	0.13	0.10	0.00	0.28	0.11	0.00	0.00

(aEC) Apparent EC
(Elev) Elevation
(H_2O) Volumetric water content
(OM) Organic matter
(Eig.) Eigenvalue
(%) Percent of total observed variation explained by respective regionalized factor

Table 4.15. Regionalized factors (e.g. principal components) for the long-range scale (250 m).

	Ca^{2+}	Clay	Elev	Jul aEC	Jul H_2O	OM	Oct aEC	Oct H_2O	Sand	Sept aEC	Sept H_2O	Slope	Eig	%
F1	0.39	0.43	0.02	0.08	0.40	0.41	0.14	0.25	0.34	0.06	0.33	0.11	4.3	59
F2	0.04	0.18	0.51	0.42	0.09	-0.30	0.42	-0.24	-0.18	0.39	-0.07	0.09	1.1	16
F3	-0.07	0.13	-0.11	0.16	0.11	0.05	0.03	0.17	-0.32	0.09	0.13	-0.87	0.81	11
F4	-0.43	-0.18	0.07	-0.01	0.33	-0.49	0.04	0.55	0.21	0.00	0.27	0.09	0.52	7.0
F5	0.01	-0.38	0.19	0.14	-0.02	0.45	-0.06	0.42	-0.56	0.12	0.07	0.28	0.35	4.8
F6	0.25	-0.10	-0.63	0.01	0.42	-0.27	0.16	-0.19	-0.40	0.03	0.10	0.22	0.14	1.9
F7	-0.48	-0.34	-0.15	0.28	0.33	0.43	0.17	-0.36	0.28	0.08	-0.07	-0.05	0.1	0.89
F8	0.36	-0.32	-0.22	0.29	-0.19	-0.07	0.37	0.38	0.30	0.01	-0.46	-0.11	0.00	0.00
F9	0.05	-0.07	-0.05	-0.42	0.14	0.01	-0.22	0.05	0.11	0.81	-0.25	-0.06	0.00	0.00
F10	-0.15	0.07	-0.36	0.20	-0.59	0.01	0.12	0.00	0.09	0.38	0.51	0.11	0.00	0.00
F11	-0.13	-0.01	0.06	-0.62	-0.09	0.14	0.74	0.02	-0.10	-0.07	0.05	-0.05	0.00	0.00
F12	0.43	-0.59	0.27	-0.10	0.02	-0.10	-0.04	-0.26	0.17	0.00	0.48	-0.21	0.00	0.00

(aEC) Apparent EC
(Elev) Elevation
(H_2O) Volumetric water content
(OM) Organic matter
(Eig.) Eigenvalue
(%) Percent of total observed variation explained by respective regionalized factor

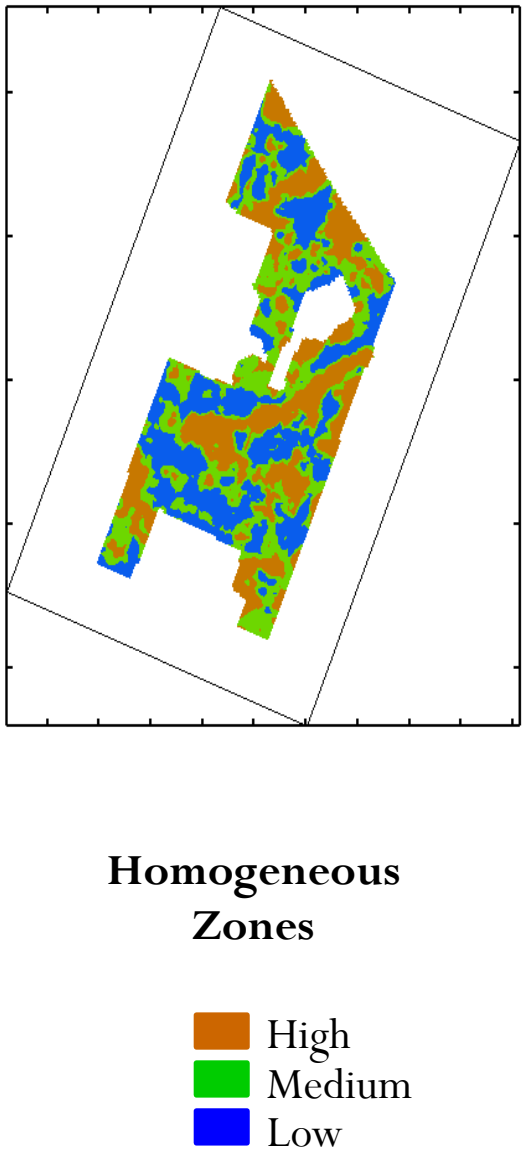

Figure 4.7. Map of the first short-range regionalized factor.

Homogeneous zones represent the joint variation of July, September and October apparent electrical conductivity. Zones demarcate regions where these variables exhibit a high, medium and low presence. Scale marks on the horizontal axis are in 100 meter increments. Scale marks on the vertical axis are in 250 meter increments.

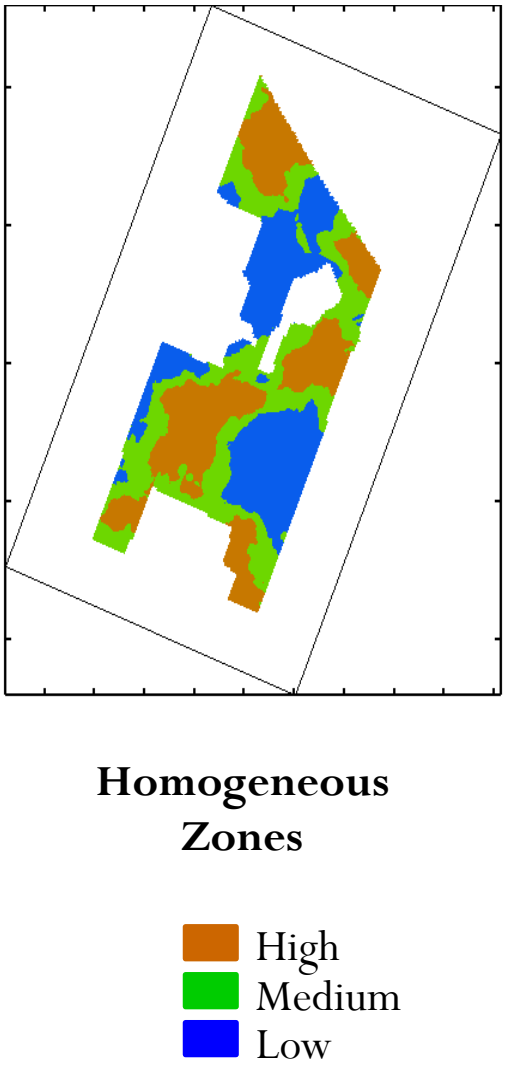

Figure 4.8. Map of the first long-range regionalized factor.

Homogeneous zones represent the joint variation of July and September volumetric water content, clay, organic matter and Ca^{2+}. Zones demarcate regions where these variables exhibit a high, medium and low presence. Scale marks on the horizontal axis are in 100 meter increments. Scale marks on the vertical axis are in 250 meter increments.

Confusion Matrix

Tables 4.16 through 4.18 represent the confusion matrix, observed accordance, expected accordance, and Kappa Index values for respective time steps: July vs. September (Table 4.16); September vs. October (Table 4.17); and July vs. October (Table 4.18). The diagonal of the confusion matrix for consecutive time steps show that Classes 1 and 4 (driest and wettest) hold their classification better with time than intermediate Classes (2 and 3). Regardless where each time step falls along the soil moisture spectrum it is expected that certain locations (e.g. pixels) will hold their classification as the wettest or driest respective to the sampled population. For example, sampling locations in low lying areas are expected to persistently fall within the fourth iso-quantile Class due to their high potential for being wetter than the rest of the landscape. This appears to be the case for the extreme classes (e.g. Classes 1 and 4). The overall observed accordance increases only slightly regardless of the time step. The observed accordance for each time step is considered significantly different than zero, as prescribed by the Kappa statistic. Given this significance, the observed accordance does not occur by chance alone. The Kappa statistic lies between 0.3 and 0.4 for consecutive time steps inferring fair agreement between time steps (Landis and Koch 1977).

Table 4.16. Confusion matrix between July and September moisture estimates.

		September				
	Classification	**1**	**2**	**3**	**4**	**Total**
July	**1**	1597	325	163	61	2146
	2	1286	930	599	722	3537
	3	82	205	433	495	1215
	4	0	49	211	1576	1836
	Total	2965	1509	1406	2854	8734

Observed Accordance	$= (1597 + 930 + 433 + 1576)/8734 = .5194$
Expected Accordance	$= (2965/8734 * 2146/8734) + (1509/8734 * 3537/8734) + (1406/8734 * 1215/8734) + (2854/8734 * 1836/8734) = .2169$
Kappa Index	$= (.5194 - .2169)/(1 - .2169) = .3862$
p-value	<0.0000

Soil moisture estimates for each date were classified into the four iso-quantile classes shown (1 being the lowest soil moisture content and 4 being the highest). The diagonal of the confusion matrix exhibit observed accordance, or the number of pixel that hold their classification through time. The off-diagonal represents the number of pixels that do not hold their classification through time. Example calculations for the observed accordance, expected accordance, and Kappa Index are shown.

Table 4.17. Confusion matrix between September and October.

		September				
	Classification	**1**	**2**	**3**	**4**	**Total**
October	**1**	1963	336	61	5	2365
	2	912	903	855	523	3193
	3	75	187	238	570	1070
	4	15	83	252	1756	2106
	Total	2965	1509	1406	2854	8734

Observed Accordance	**Expected Accordance**	**Kappa Index**	**p value**
.5564	.2708	.3917	<0.0000

Table 4.18. Confusion matrix between July and October.

		October				
	Classification	**1**	**2**	**3**	**4**	**Total**
July	**1**	1320	728	78	20	2146
	2	993	1604	463	477	3537
	3	47	586	264	318	1215
	4	5	275	265	1291	1836
	Total	2365	3193	1070	2106	8734

Observed Accordance	**Expected Accordance**	**Kappa Index**	**p value**
.5128	.2371	.3613	<0.0000

The confusion matrix is a traditional statistical tool used to infer if the landscape studied is time stable using an overall observed accordance value. The current capacity of the confusion matrix is limited because it provides generic knowledge of time stability using a single numeric value, the calculated observed accordance. This does little to help users relate geographic meaning to the results obtained. For this reason, this research generated Figure 4.9 to translate the information in Tables 4.16, 4.17, and 4.18 into a geographic context. Figure 4.19 illustrates how each location maintains its soil moisture classification between time steps. Three shades are represented: light gray, medium gray, and black. The medium gray color in Figure 4.19 illustrates the temporal accordance, or time stability, of a raster pixel between two time steps. These pixels are best represented by the wettest and driest soil moisture classes (1 and 4). The black color illustrates a pixel promoted in class between time steps due an increase in soil moisture content with time. The light gray color represents pixels that are demoted in class due to decrease in soil water content with time. Figure 4.9 illustrates lack of spatial coherency in certain locations, particularly in regions where pixels do not hold their classification well. This is because the confusion matrix treats each pixel discretely, ignoring any spatial association among soil moisture estimates. In Figure 4.9, the medium gray pixels cover approximately 50-60% of the observation extent, which corroborates with the calculated observed accordance in Tables 4.16, 4.17, and 4.18.

Figure 4.9. Confusion matrix maps.

Maps represent the tendency for a pixel to hold its classification over time according to color. Medium gray pixels hold their classification and are considered time stable; black pixels are promoted in class over time due to increased soil moisture content; and light gray pixels are demoted in class due to loss of water. The left represents pixels classification between July and September; the middle image represents pixel classification between October and September; the right image represents pixel classification between October and July.

Vachaud et al.'s MRD and SD_{MRD}

The calculated MRD and SD_{MRD} for the three dates studied are presented in Figure 4.10. Pixels consistently estimated above the field average have a positive MRD, pixels consistently below the field average have a negative MRD, and pixels at the field average have a MRD value equal, or close to, zero. The MRD is a good measure of patterned bias, or persistent patterns of soil moisture highs and lows across the landscape. The MRD in Figure 4.10 shows a clear patterned distribution of relative highs and lows. Most notable is the drainageway transecting the site that exhibits persistently higher soil moisture contents relative to the temporal mean. Moreover, the MRD pattern mimics that of clay, organic matter, sand, and Ca^{2+} (see Figure 4.6), which corroborates with the significant structural correlation established at the longer range between these variables and soil moisture content for all three dates (Table 4.10). Negative MRD values are spatially associated with aged soils that are considered well drained, including the Maury and Mercer silt loam soil series. The SD_{MRD} is a good measure of temporal precision, or time stability. The RMSE in Figure 4.13 is useful because it concurrently illustrates the bias (e.g. MRD) and precision (e.g. SD_{MRD}) using a single metric (Jacobs et al. 2004). The SD_{MRD} and the RMSE in Figure 4.10 do not show immediate spatial associations with the studied soil-terrain attributes. This is likely due to the limited number of observations with time and highlights, one shortcoming to Vachaud et al.'s (1985) approach to studying time stability – it requires a fairly extensive temporal dataset for useful interpretation. Performing a site reconnaissance in real-world scenarios does not always permit generating recurrent temporal measurements. In scenarios such as this, Vachaud et al.'s (1985) approach is not always pragmatic for optimizing or strategizing the placement and timing of future sampling efforts. Nonetheless, the SD_{MRD} and the

RMSE results suggest that depression areas, such as the drainageway and the area north of the drainageway, exhibits relatively high temporal stability, but more repeated measurements over multiple wetting and drying cycles are necessary to make this conclusive.

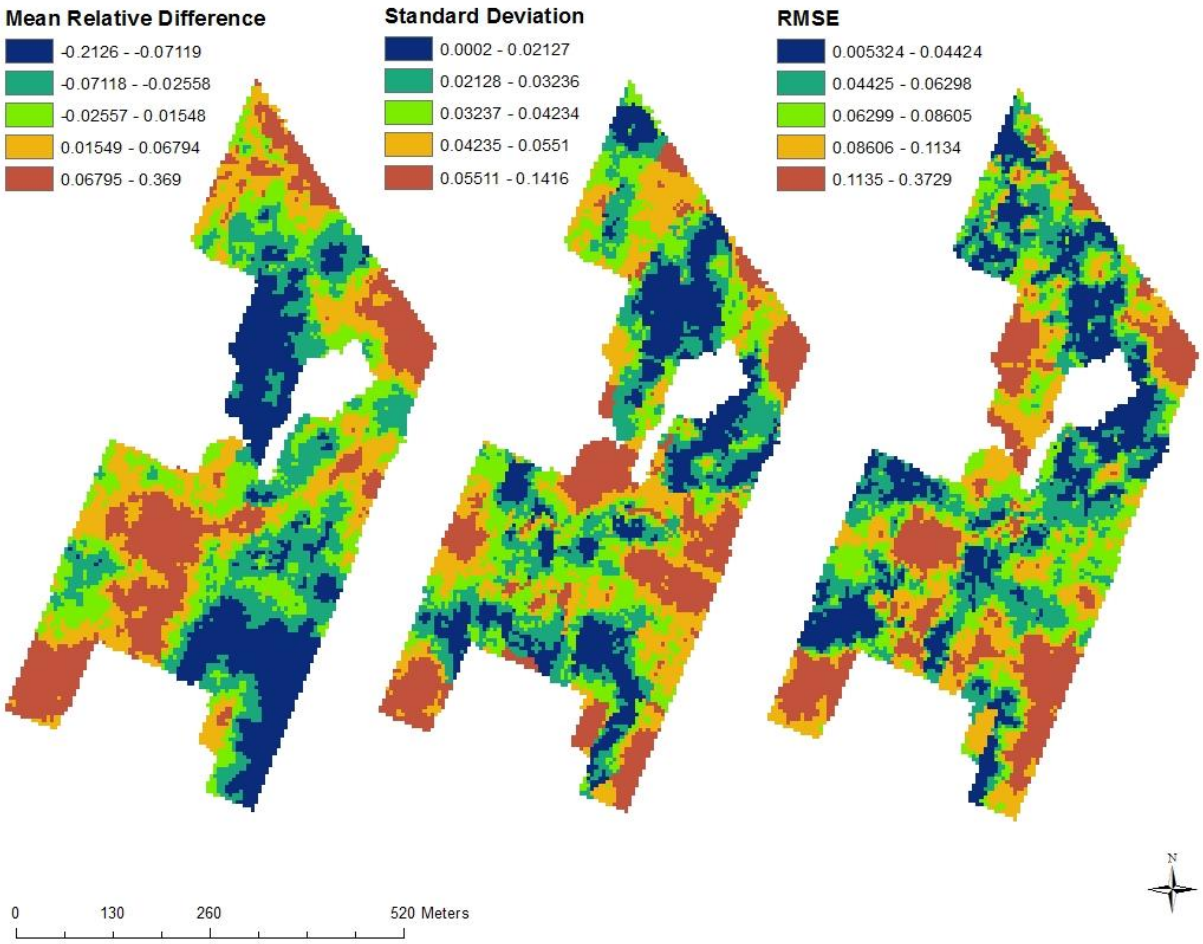

Figure 4.10. Vachaud et al.'s (1985) MRD, SD_{MRD}, RMSE.

The mean relative difference (MRD) (left); Standard Deviation (SD_{MRD}) (middle); and root mean square error (RMSE) of the MRD and SD_{MRD} (right). Calculations are unitless.

Precision agriculture and environmental risk assessment specialists find it necessary to make real-time, or near future, management decisions based on sparse soil moisture temporal datasets. Calculating the average difference (AD) is a fitting approach to assess soil moisture patterned variation in a temporally "localized" manner. Figure 4.11 illustrates the average of the differences (AD), standard deviation of the average differences (SD_{AD}), and RMSE of the AD and SD_{AD}. The patterned distribution of the AD (Figure 4.11) indicates that the drainageway and ambient locations exhibit the greatest average difference. Specific to the results obtained, this is indicative of an increase in soil moisture content with time. The standard deviation of the AD is small, which causes the $RMSE_{AD}$ to mimic the AD map. The AD technique is practical because it represents a more localized interpretation of soil moisture change in space and time and, for applied practices, results are represented in original units of measure.

Comparing the patterned distribution of pixel classification, change between time steps in Figure 4.9 show notable congruencies with the patterned distribution of the AD map in Figure 4.11. Pixels promoted in class (black pixels) between July and September and July and October spatially correspond with pixels exhibiting the greatest average difference with time. Regions that exhibit minimal average difference with time correspond to classes that are demoted in class with time (light gray pixels). These regions can be considered most transient in terms of changes in soil moisture content over the duration studied. The reason for congruencies between the AD technique and confusion matrix technique is they treat each pixel discretely over time. The MRD technique treats each pixel discretely as well, but subsequent to standardizing each pixel to a field average.

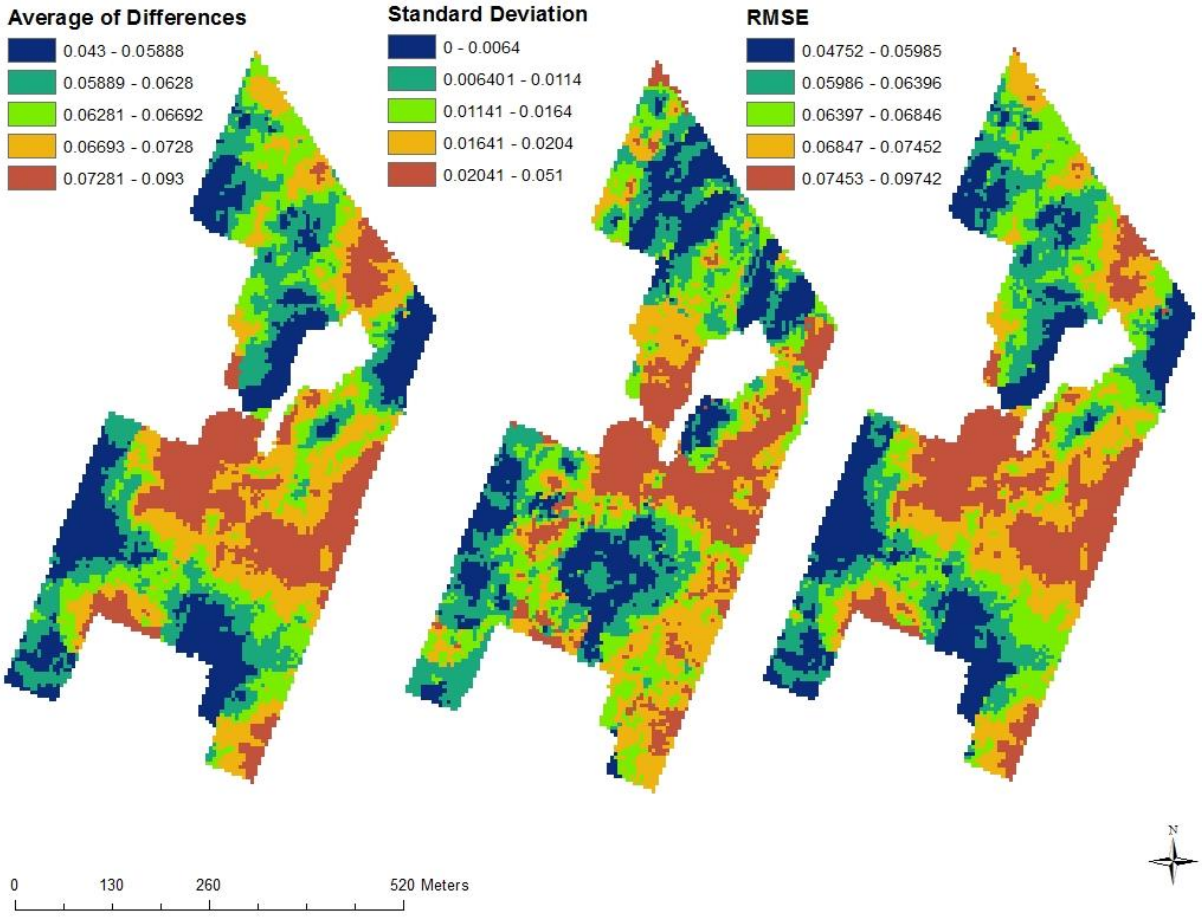

Figure 4.11. Average of the consecutive differences (AD); standard deviation of the AD (SD_{AD}); and $RMSE_{AD}$. Values are in original units.

PCA_{MRD} was performed on the 94 sampled locations to determine how the soil-terrain attributes best associate with the measured MRD. The PCA_{MRD} correlation circle for the soil-terrain and the MRD are illustrated in Figure 4.12. The first and second principal components were significant (eigenvalue > 1.0) and explained 47% and 19% of the total variation, respectively. Clay and MRD strongly intercorrelate, to the degree that they appear superimposed in Figure 4.12. Clay's inferred control in the patterned MRD across the landscape is supported by the MFCA findings, however, the other soil physicochemical properties identified by MFCA are overlooked here. This is because PCA_{MRD} is applied to the variance-covariance matrix of the collective observation extent rather than the coregionalized covariance-variance matrices. The MFCA revealed more meaningful relationships between measured attributes by synthesizing information specific to the spatial scale(s) attributes interact.

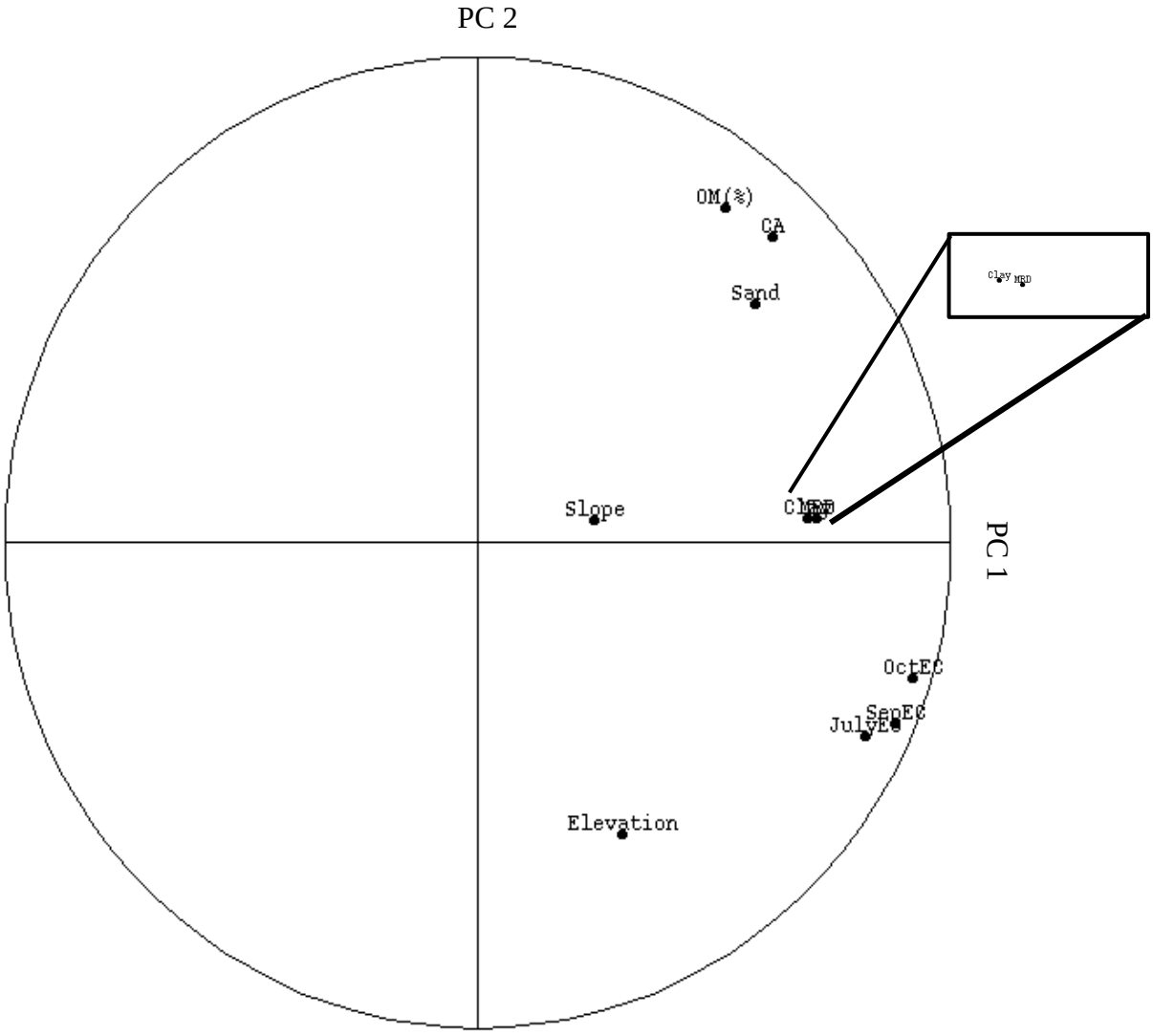

Figure 4.12. PCA_{MRD} correlation circle for the first two significant (eigenvalue > 1) principal components.

In theory, Park et al.'s landscape model reflects the influence of soil-water-gravity interrelationships governed by surface forms and therefore lends insight toward soil moisture variation governed by different landscape positions. Figures 4.13 and 4.14 illustrate the constructed landscape model and the ground referenced landscape model, respectively. This research introduced Park et al.'s (2001) landscape model, in tandem with polygon kriging, to service the objective of understanding how the MRD behaves relative to landscape position. For the three soil moisture regimes observed, the drainageway exhibited a significantly higher estimated MRD in comparison to other landscape positions (Figure 4.15). This is expected because low lying areas and depressions are prone to higher soil moisture contents than other landscape positions. There was no clear difference between ridgetop, shoulder, and footslope positions, but they show a MRD close to zero, meaning these estimates are representative of the field mean. The average MRD for backslope positions is visibly lower than the other four landscape positions. Ideally, backslope positions will exhibit a lower MRD because soil moisture infiltration should be lower on higher sloping regions (Famiglietti et al. 1998, Gómez-Plaza 2001).

Park et al.'s landscape model is underutilized within the soil science community. It is a pragmatic and prospective technique to help hydrologists, pedologists, geomorphologists, and terrain modelers alike understand the soil-gravity-water dynamics driving surface and subsurface soil variability. High resolution, accurate elevation datasets are more readily available now than ever and, as such, their use has increased to understand how terrain attributes affect soil moisture variation. This study shows that landscape position is more

relevant than calculated terrain attributes, albeit the same terrain attributes (upland contributing area and curvature) were used to derive the landscape model. The landscape model proved more relevant because it goes one step further by establishing conceptual and empirical relationships, rooted in soil morphology, pedology, and geomorphology, between the calculated terrain attributes to better explain the observed spatiotemporal soil moisture variability.

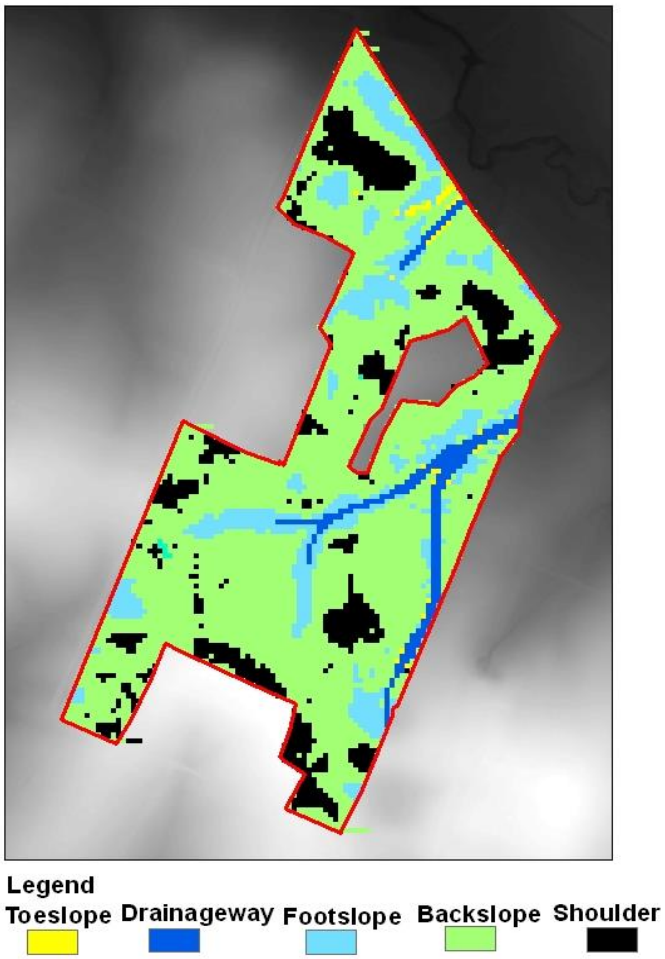

Figure 4.13. Two dimensional process-based landscape model.

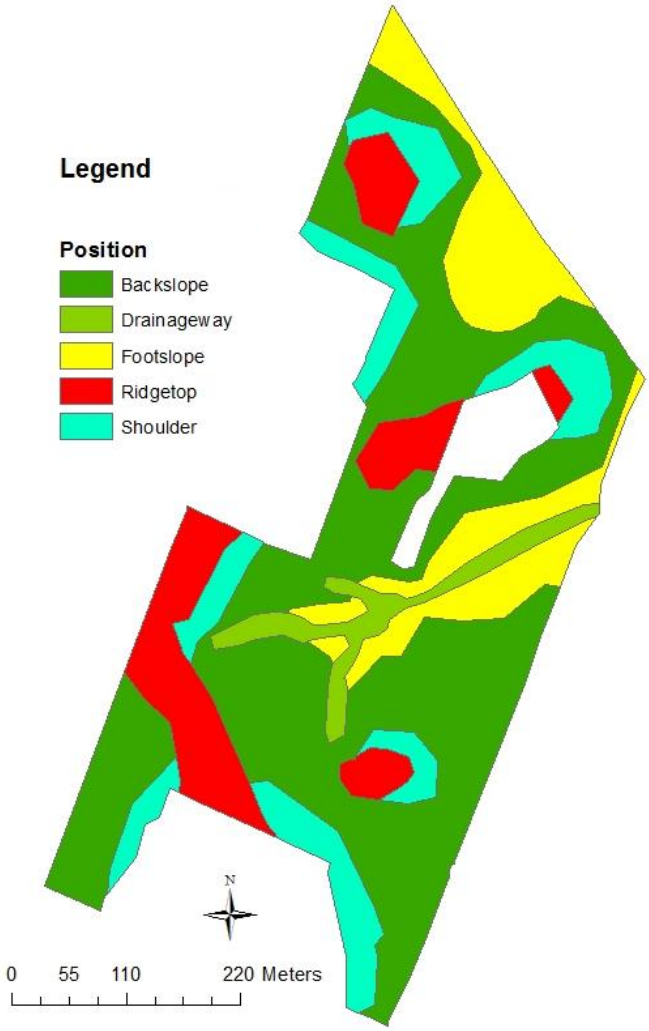

Figure 4.14. Ground-referenced landscape model used for polygon kriging.

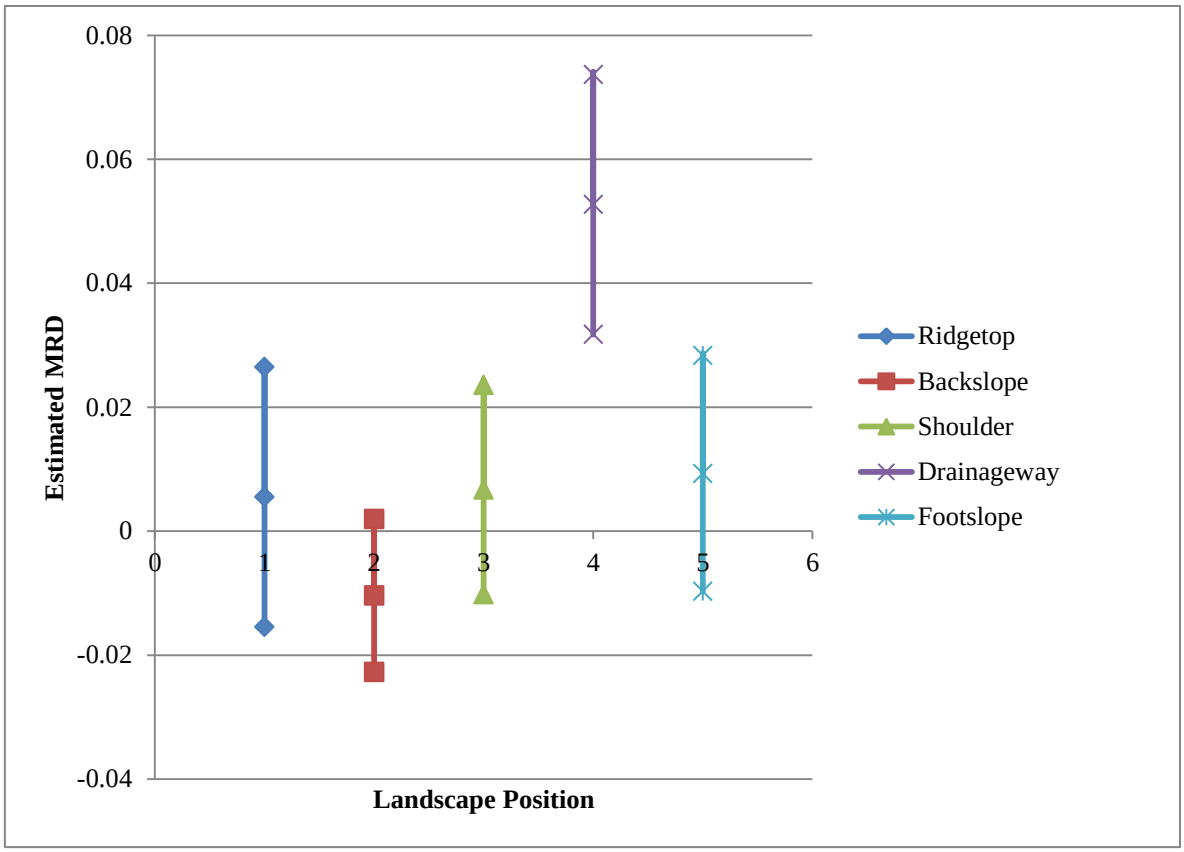

Figure 4.15. Estimated MRD according to landscape position.

The average MRD for each landscape position is enveloped by the upper and lower bounds for the 95% confidence interval. If the average MRD for a given landscape position falls within the CI for another landscape position the difference is insignificant.

Cross Correlogram Analysis

The cross correlograms indicate time stability for the three observed soil moisture dates. Figure 4.16 shows the cross correlograms calculated on the 8,734 soil moisture point estimates between July and September and September and October. Overall, the correlation coefficients (correlation at lag zero) between consecutive time steps are high, indicating time stability. The apex of the correlogram is centered on lag zero for both time increments. The centering of the apex on lag zero indicates the patterned distribution of soil moisture highs and lows across the landscape are stationary between two dates. In other words, the locations of the sources of variation for soil moisture remain stationary with one wetting rainfall event. The correlogram for July and September is symmetric about lag zero. A slight asymmetry is present for the September and October correlogram. This is probably due to the transitory interaction between texture and topography influencing soil moisture variation, as highlighted earlier by October's comparable inverse loading values between the significant long-range regionalized factors. The working advantage of the cross correlogram is it can lend insight to whether the sources of soil moisture variation are consistent between time steps along with their position across the landscape. These advantages are not necessarily evident through the MRD or the SD_{MRD}.

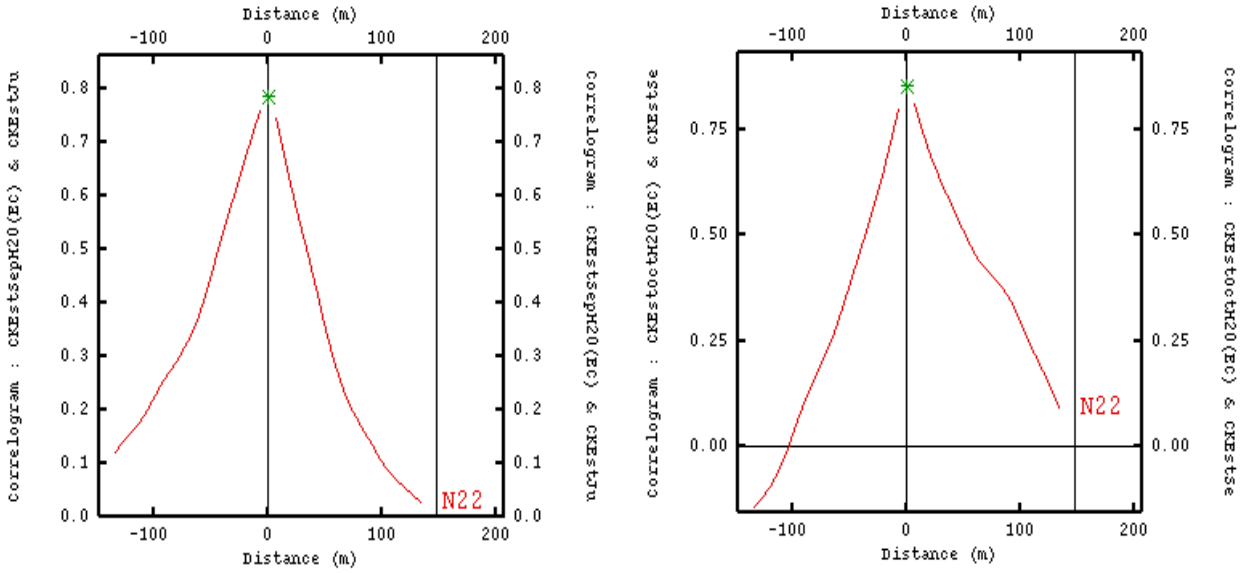

Figure 4.16. The cross correlogram between July and September (left) and September and October (right).

Discussion

Several empirical adaptations have evolved to study time stable soil moisture patterns first pioneered by Vachaud et al. (1985). Examples include Jacobs et al. (2004) studying locations representative of the field mean using an exponential fit between the mean soil moisture content and the coefficients of variations. This approach was later implemented by Choi et al. (2007) to study time stable soil moisture patterns across three different spatial extents (including the field, watershed, and basin). Kachanoski et al. (1988) introduced spatial coherency analysis, which employs a spatial power spectrum, to study scale-dependent time stable soil moisture patterns. For the purpose of making more informed decisions toward sampling and managing soil moisture variation, it has been recommended to combine alternative approaches to study the temporal consistency of soil moisture patterns (Guber et al. 2008).

This research integrated a suite of statistical approaches including MFCA, the confusion matrix, Vachaud et al.'s (1985) MRD and SD_{MRD}, polygon kriging, $PCA_{MRD,}$ and cross correlogram analysis, to characterize the persistence in soil moisture patterns across a landscape with time. MFCA served dual purposes for this research. First, it fused multiple data sets, with different sampling supports and units, within a single geostatistical platform to downscale sparse direct soil moisture measurements, and other related hydrologic soil-terrain parameters, across the topographically diverse landscape investigated. Second, applying MFCA revealed the scale-dependent interaction between soil moisture and soil physicochemical properties (clay, sand, organic matter and Ca^{2+}) with time. By comparison to the approaches demonstrated by Choi et al. (2007) and Kachanoski et al. (1988), MFCA is an efficient approach to simultaneously study nested

scales of spatial variation and the corollary scale relevant physical parameters influencing this variation with time.

At the beginning of this study two high resolution secondary measures were prospected for downscaling soil moisture estimates: LiDAR terrain attributes and apparent EC. Exploratory analyses showed terrain attributes interacted weaker with soil moisture than apparent EC, which is primarily attributed to the drought conditions observed. Results indicated October apparent EC was a preferable proximal variable to downscale (via cokriging) sparse direct soil moisture measurements in the three observed soil moisture regimes. These findings suggest that if soil moisture spatial variation is time stable then temperature standardized apparent EC collected periodically (e.g. seasonally or annually), in comparison to each sampling event, might suffice. Within the scope of this research, it is evident a single Veris 3100 assay could help farmers extrapolate sparse multivariate data, such as Ca^{2+}, texture, soil moisture, and organic matter, to make more informed management decisions (Mueller et al. 2003) .

The intercorrelation between soil physicochemical attributes and soil moisture for the three dates was scale-dependent and predominately operated at a spatial range of 250 meters. This spatial range is similar to the range established by Gómez-Plaza et al. (2000). This spatial range indicates soil moisture variation can exhibit long-range structured variation under relatively dry soil moisture conditions, which debunks the notion that soil moisture inherits a more random appearance during dry conditions per hypothesized as a preferred state by Grayson et al. (1997). The first long-range regionalized factor was mapped to represent synthetic homogeneous zones that delineate regions high, medium, or low presence of soil moisture and the associated soil

physicochemical parameters interacting with soil moisture. It is conceivable direct soil moisture measurements could be upscaled (Guber et al. 2008) using these homogeneous zones to help manage irrigation input, estimate groundwater recharge, and model soil contaminant fate and transport.

Sand and clay exhibited a positive significant correlation with soil moisture for all three dates. The literature reviewed has not shown a cooperative interaction between these fractions in explaining time stable soil moisture patterns. Portable X-ray fluorescence spectroscopy (PXRF) results (data not reported) performed on the bulk soil samples and the sand fraction isolated from these same samples indicated the iron (Fe) content (13% w/w) and manganese (Mn) content (12.0 ppt, or parts per thousand, w/w) in the sand fraction was at least one order of magnitude higher than the Fe content (2.8 %) and Mn content (1.8 ppt) in the bulk soil. Moreover, plotting sand vs. Fe and clay versus Fe revealed correlation values equal to 0.60 and 0.47, respectively. Plotting sand vs. Mn and clay vs. Mn revealed correlation values of 0.22 and -0.11, respectively. Correlation plots between sand and clay exhibited a correlation value of 0.37. The Fe and Mn content in the sand fraction, which will exhibit a physicochemical attraction to soil moisture, might explain the positive correlation between sand and soil moisture.

Terrain attributes have shown to influence the persistence in soil moisture patterns (Jacobs et al. 2004, Grayson and Western 1998). Time stability and null MRD values (close to zero) have been associated with steep sloping and upslope drainage areas, respectively (Brocca et al. 2009). Moreover, the TWI and slope have been shown to control time stable subsurface soil moisture distribution at the catchment scale (Takagi and Lin 2012). However, results here show that terrain attributes are inferior to soil

physicochemical attributes in influencing the soil moisture patterns attained and these results agree with other findings within the literature (Da Silva et al. 2001). It is known that soil moisture variability under relatively dry soil conditions are not dominated by gravitational forces thereby limiting the effects of soil moisture lateral redistribution guided by terrain attributes (Grayson et al. 1997, Gómez-Plaza 2000). Considering the observed soil moisture contents never reached field capacity, and rainfall events encompassed by this study were not excessive to cause substantial runoff or lateral flow, underscores why terrain attributes (nonlocal controls) were inferior to soil physicochemical attributes. Similar findings relating soil moisture variation to terrain attributes under relatively dry conditions are supported elsewhere (Kachanoski 1988, Teuling et al. 2006, Cosh et al. 2008). These results infer that terrain attributes become more influential as the soil becomes wet and underscore their time-relative utility as high resolution secondary variables to effectively downscale and study soil moisture variation. Chapter 5 will investigate the relative importance of soil and terrain attributes in influencing scale-dependent soil moisture distribution in space with time according to scale.

Polygon kriging results suggest landscape position is important for describing the MRD patterned behavior. The drainageway exhibited a significantly higher MRD than other landscape positions and backslope positions showed a visibly lower MRD than other landscape positions. Jacobs et al. (2004) found similar results showing depressional areas overestimated the MRD and hilltop regions, along with steep sloping regions, underestimated the MRD over a range of soil moisture contents. Lin (2006) also found that valley floors and swales consistently stored higher water contents in comparison to

hillslope and hilltop regions. The similarities in these findings suggests Park et al.'s model could readily be adapted to a range of geographic settings and climates to provide a pragmatic and fundamental utility in helping field investigators understand the spatiotemporal characteristics of soil moisture variation relative to landscape position. Spatial component filtering was performed in Chapter 3 to exclude high frequency spatial variation in the digital elevation model, calculated terrain attributes, and Park et al.'s model. Future work could be dedicated to testing the detection limits of Park et al.'s model by including the high frequency spatial component to identify micro-scale (e.g. $\leq$ 1.0 – 5.0 m^2) karst features and different landscape positions.

The three soil moisture dates for this study fell during a drought for Central Kentucky and ranged from the plant wilting point to near field capacity (Saxton and Rawls 2006). Dry soil conditions have been found to favor time stability (Martínez-Fernández and Ceballos 2003), especially in semi-arid climates (Gómez-Plaza 2000, Cosh et al. 2008), and correspond with the findings established herein, albeit Central Kentucky ordinarily exhibits wetter summers. October was the wettest date observed and displayed results, through the loading values on the long-range coregionalized principal component and the apparent asymmetry in the cross correlogram between September and October, suggesting different sources of soil moisture variation are present. It is interpreted here that October might represent the beginning of a "transition period" alluding to an apparent shift in the sources of soil moisture variation, from soil physicochemical properties to terrain attributes, as the landscape approached field capacity. This also became more evident with the increase significant structural correlation between elevation and soil moisture for September and October at the short-range scale.

Kachanoski et al. (1988) found that transition periods from wet to dry preserve time stable soil moisture characteristics whereas the same cannot be said for transition periods from dry to wet. This provides one possible explanation for the insignificant structural correlation coefficient between October and September soil moisture, inferring time instability, at the short-range scale. Other findings support time instability during transition periods of both wetting and drying (Zhou et al. 2007) and suggest the effects of these periods are transitory where soil moisture patterns re-emerge as soils reached equilibrium (order of days) (Kornelsen and Coulibaly 2013). More research observing multiple wetting and drying events are needed to determine how rainfall events, and concomitant wetting and drying of the soil, affect the long-term temporal stability of soil moisture patterns over the Kentucky landscape observed.

The next chapter (Chapter 5) examines the scale-dependent relative importance of soil-terrain attributes according to individual time steps (e.g. July, September, and October) and is anticipated to reveal if there is a relative importance among soil-terrain attributes in explaining soil moisture variation with time. Based on findings here, it is anticipated October will show different soil-terrain parameters influencing soil moisture variation. The MFCA methods applied herein do not explain how soil-terrain attributes affect soil moisture variation directly, rather, they explain how soil moisture interacts with an integrated system of hydrologic parameters. Chapter 5 will employ a spatial multivariate regression technique to illustrate the relative contribution different soil-terrain parameters make in explaining soil moisture variation in space with time.

Conclusion

This chapter focused on fusing different data sources and integrating analytical applications that can help optimize sampling efforts dedicated understanding and managing the spatiotemporal variation of soil moisture over large spatial extents. This study showed Veris EC proximal sensing together with geostatistics is effective for downscaling sparse soil moisture estimates collected over a landscape during relatively dry soil conditions. The downscaled soil moisture estimates made it possible to characterize the temporal persistence of soil moisture patterns at higher spatial resolutions and greater continuity not attainable with direct observations alone. These estimates set a working foundation to study time stability using various analytical techniques, including Vachaud et al.'s (1985) MRD, polygon kriging and the cross correlogram. Additionally, MFCA sets a working foundation to study time stable scale-dependent tendencies of soil moisture variation while lending insight into which variables are most active in influencing these scale-dependent tendencies. Although only three dates were observed, the soil moisture patterns attained could assist in strategizing the placement of future sampling and monitoring sites to study the hydrodynamics of the landscape or manage resources, such as irrigation input, especially during drought conditions. To fully understand the time stable characteristics of the studied landscape more observations are needed over multiple seasons of wetting and drying.

Chapter 5

Scale-Dependent Spatiotemporal Relevance of Soil Moisture and Associated Soil-Terrain Parameters

Introduction

Soil-terrain parameters operate uniquely according to their spatial autocorrelation, or characteristic scale of variation (Ali et al. 2010). Consequently, scale becomes important when identifying controlling parameters influencing soil moisture variation over a given observation domain, which can span a plot, field, landscape, or watershed, depending on the research or management objective. Modeling soil moisture variation is germane to fields such as environmental remediation, watershed management, resource conservation, and precision agriculture. Hydrologic parameters used to model soil moisture variation, such as the topographic wetness index (TWI) and soil texture, are often applied universally among observation scales and soil moisture contents with little regard for their potential relative importance in space and with time.

The relative importance between soil-terrain parameters describing soil moisture variation is underdeveloped and poorly understood. For example, Bogena et al. (2010) showed that soil moisture status regulates the strength of correlation between topography and soil moisture in which the highest correlations were observed during drier periods. This finding contradicts the general assumption that terrain attributes become most important during wet soil conditions. Terrain attributes, such as slope, curvature, and topographic indices (e.g. the TWI), are heavily utilized to study the spatial distribution of soil moisture over landscapes in part due to the growing availability of elevation data and the general ease of deriving terrain attributes from these data .

There are three general assumptions prefacing terrain attributes as a dominant control in soil moisture distribution (Grayson et al. 1997, Grayson and Western 2001, Western et al. 2002):

1. Soil water content is near or at saturation;

2. Restrictive layers are present to promote lateral redistribution, such as bedrock or confining soil horizons;

3. Effects from other controlling factors, such as soil and vegetation, are minor.

Research has shown that terrain attributes are not guaranteed to be dominant factors controlling soil moisture patterned behavior and if they do this dominance is time relevant. For instance, Western et al. (1999) found terrain indices explained 61% of soil moisture variation during wet periods but explained only 22% of soil moisture variation during dry periods. Famigletti et al. (1998) suggested that in situations such as this no single predictive indices is applicable for all soil moisture contents.

This relative importance has gained empirical footing within the hydrologic modeling communities. Wilson et al. (2004) found a weighted combination of indices based on changes in average wetness was an effective approach to model soil moisture variation with time. To improve the predictive capacity of terrain indices in dry environments, Gómez-Plaza (2001) suggested two modifications to the existing TWI (demonstrated in Chapter 3 [Eqn. 3-13]). Because evapotranspiration is a driving factor of soil moisture spatial variation in dry environments Gómez-Plaza (2001) created a new index (NI) by multiplying contributing area and aspect with the reasoning that the latter is a good surrogate for potential insolation. They further reasoned that slope was of little predictive

value in vegetated semiarid regions resulting in the second new index (NI2) where slope is removed from the denominator in [Eqn. 3-13]. These modifications seem promising but their universal application has yet to be tested and validated.

At any point in time it is rare for terrain indices to explain more than half of the variation in soil moisture, meaning there are other influential physical parameters (Wilson et al. 2004). Famiglietti et al. (1998) recognized the combined influences of soil-terrain attributes affecting soil moisture distribution. Their results show that during wet conditions soil porosity and hydraulic conductivity were the dominating parameters controlling soil moisture variation whereas during dry conditions elevation, aspect, and texture were more important. In some cases soil properties have shown to dominate over terrain attributes in explaining soil moisture variation, primarily during dry soil conditions and areas with low topographic relief (Western et al. 1999, Florinsky et al. 2002, Zhu and Lin 2011, Zhu et al. 2012). Specific rainfall events have also regulated the dominant control between soil and terrain attributes in explaining soil moisture variation (Gao et al. 2011). It is generally excepted that integrating multiple parameters, such as terrain, vegetation, texture, and land use, can improve soil moisture predictions (Jawson and Niemann 2007, Korres et al. 2010, Zhu et al. 2012) but more research is needed to understand their relative importance with time.

Studying the time stable patterned behavior of soil moisture variation has brought attention to the relative importance of hydrologic parameters in space with time. Hu et al. (2009) found organic matter, clay, aspect, elevation, and bulk density explained time stable soil moisture distribution patterns under relatively wet conditions. Hydraulic conductivity, evapotranspiration, and pore connectivity have been associated with

causing time instability in soil moisture distribution patterns (Coleman and Niemann 2013). The physical origins of soil moisture's time stable, or time instable, patterned behavior are not yet fully understood (Coleman and Niemann 2013). Chapter 4 showed soil moisture is time stable at the long-range scale for the three observation dates although the soil-terrain parameters interacting with soil moisture, and their corresponding scale of influence, might change with time. These results lead to the following question: even though soil moisture exhibits time stability, does this mean the controlling hydrologic parameters and their scale of operation persist with time?

To this point there has been little consideration of how scale plays a role in understanding the relative importance of soil-terrain parameters for explaining soil moisture variation with time. Within natural systems there is often a shift in relative importance between controlling parameters with changes in scale (Turner et al. 1989). This is important for this chapter because one objective is to determine which controlling factors are relevant with time according to scale. For instance, Yao et al. (2012) found that land use dominated over slope and precipitation in controlling soil moisture heterogeneity but the magnitude of this dominance was relative to observation scale. Zhao et al. (2011) established that grazing management significantly influenced soil moisture variation according to scale, where a short-range (45 m) explained the majority of soil moisture variation in ungrazed areas and a long-range (90m) explained most spatial variation in grazed areas. Jawson and Niemann (2007) found that texture correlated best with soil moisture during drier periods at longer ranges whereas terrain features correlated best during wet periods at shorter ranges. Other studies have shown that the range of spatial autocorrelation shifts with changes in soil moisture content due to different hydrologic

processes operating at different spatial scales (Mohanty and Skaggs 2001). Western et al. (1998) showed that the autocorrelation structure of soil moisture fluctuated seasonally in which larger correlation lengths were observed during the dry season and resulted from the lateral distribution of soil moisture. Manfreda et al. (2007) found soil wetting and drying cycles significantly controlled the spatial behavior of soil moisture patterns and stated further work is needed to understand the correlation structure of parameters influencing the feedback of these patterns with time.

Wagenet (1998) conceptualized very clearly how different environmental parameters can operate at specific spatial scales to influence soil moisture variation, including the soil pore scale in which aggregate size and organic matter coatings are prominent; the field scale in which soil texture, organic matter, and precipitation are effective; the landscape scale in which vegetation and texture are dominant; the regional scale in which geomorphology and land use are influential; and finally, the global scale in which climate and biome type are important (Zhu and Lin 2011, Lin 2012). These scales are cataloged according to each parameter's characteristic spatial autocorrelation and set a fundamental basis for developing stronger explanations for how scale relates to soil moisture variation in space with time.

Conceptual models have been proposed within soil science to illustrate the hierarchical organization of hydrologic parameters relative to scale, space, and time (Wagenet 1998, Roth 1999, Lin 2003a, Vogel and Roth 2003, Hopmans et al. 2002, Lin et al. 2006). To date no single conceptual framework currently exists to conceptualize the scale-dependent heterogeneity of soil hydrologic phenomena (Wagner 2007, Tetzlaff et al. 2008, Troch et al. 2009). The purpose of conceptual models is not to make predictions,

rather, to allow investigators to organize information sampled from complex environments with meaning (Allen et al. 2009). Ideally, conceptual models help researchers develop stronger hypotheses and useful methodologies that lead to more accurate and precise empirical predictions. These conceptual models are adaptations deriving from general systems theory, specifically hierarchical theory, to characterize soil hydrologic systems (Wu 1999, Wu and David 2002, Lin 2003a).

Complex landscapes are thought to have self-organized structural and functional units that can be decomposed and organized in a hierarchical framework (Kotliar 1990, Wu 1999, Wu and David 2002) according to the characteristic spatiotemporal scales hydrologic properties and processes operate. Hierarchy theory is a very helpful tool for conceptualizing the scales at which soil hydrologic properties operate; determining the relative importance of hydrologic properties with changes in scale; and establishing possible scaling relations to transfer information at one scale another with physical meaning.

Specific to hydropedology there are two hierarchical frameworks. The first is the mapping hierarchy that focuses on the spatial heterogeneity of hydrologic parameters, or "forms," at different spatial scales (Lin et al. 2008a, Tetzlaff et al. 2008). The second is a soil modeling hierarchy that focuses on the temporal dynamics, or "functions," that depict hydrologic processes at different temporal scales (Lin et al. 2008a, Tetzlaff et al. 2008). Linking the two hierarchies is challenging because there are often disparities between the structural hierarchy of soil properties and the functional hierarchy of soil processes (Grayson et al. 2002, Hopmans et al. 2002, Corwin et al. 2006). This disparity seeds the challenge of identifying relevant hydrologic parameters in space to model hydrologic

processes with time, but also investigate the validity of upscaling and downscaling soil hydrologic properties and processes across observation domains.

Scaling defines the process of transferring information from one observation domain to the next with physical meaning (Wu et al. 2000). Scaling is germane to model development because the scale of sampling often does not match with the scale of modeling. A good working example of this are pedotransfer functions. The utility of pedotransfer functions rose from the desire to use readily available databases, usually acquired from soil surveys (e.g. bulk density, organic matter content, and particle size distribution), to estimate hydraulic parameters used to model soil moisture at larger scales. The underlying mechanisms validating the universal functionality of pedotransfer functions are still not fully understood (Lin, 2003). This is partly due to the incomplete consideration of relevant parameters, such as soil structure and land use (Lin 2003), but also not understanding at which optimal scales these parameters are most influential (Pachepsky et al. 2006, Zeleke and Si 2006). Moreover, even if a functional relationship is established between scales to readily transfer information with meaning, little is known about how these scaling functions behave with changes in soil moisture content. Understanding the relationship between spatial variability of soil hydrologic properties and scale, both conceptually and empirically, is the working foundation to making better predictions within and across scales (Turner et al. 1989, Veerecken 2007).

This chapter revisits the four main questions posed in Chapter 1:

1. What are the spatial and temporal dependencies of patterned variation in soil moisture?

2. What are the optimal observation scales to capture patterned variation in soil moisture?
3. What soil-terrain attributes define this patterned response?
4. How can we transfer information from one scale to the next with physical meaning?

The first three questions are answered within the scope of this chapter. This chapter does not directly answer question four. Rather, this chapter will attempt to assimilate answers obtained for the first three questions into a conceptual framework for others to develop stronger hypotheses and methodologies to answer this question.

The objective of this chapter is to detect if there is a relative importance between soil-terrain parameters influencing soil moisture variation as a function of time and determine if this relative importance is scale-dependent. It is hypothesized that the relative importance of selected soil-terrain parameters will change with concomitant changes in soil moisture content. It is anticipated soil properties will dominate during drier conditions and terrain attributes will dominate during wetter conditions. Moreover, soil moisture spatial variation is expected to exhibit a scale-relevance according to the spatial autocorrelation of underlying parameters controlling soil moisture variation. Times of higher soil moisture content are anticipated to favor long-range scales whereas times of lower soil moisture content will favor short-range scales.

Materials and Methods

Exploratory Statistics

Each observation date, July 7, September 11, and October 5, 2012 was assessed individually. Because the objective was not to estimate soil moisture, information collected at all 127 sampling locations (calibration and validation) were utilized (Figure 2.3 in Chapter 2). For July all sampling locations (n=127) were sampled but fewer locations were sampled in September (n=121) and October (n=123) due to missing field markers.

The pool of variables subjected to exploratory statistics for this Chapter differs slightly from that used in Chapter 4. Instead of investigating exchangeable acidity and Mehlich III extractants separately, the calculated cation exchange capacity (CEC) was used. Aspect, which is the direction of steepest decent in elevation, was also considered. The normalized difference vegetation index (NDVI) was introduced to infer potential impact of vegetation. Vegetation indices take advantage of the differential absorption/reflection of radiation by plants. Leaves preferentially absorb blue and red radiation for photosynthesis and reflect green and near infrared radiation (Campbell 2007). The plant's ability to differentiate red (R) from infrared (IR) provides a unique spectral fingerprint identified through the use of band ratioing (Campbell 2007) [Eqn. 5-1]:

$$NDVI = \frac{IR - R}{IR + R} \qquad \text{[Eqn. 5-1]}$$

Soil moisture is essential for plant growth response. Thus, vegetation can serve as a biological indicator of soil moisture variation (Haas 2010). The NDVI was calculated using 1 m multispectral orthoimagery collected in 2010 by the National Agriculture

Imagery Program (NAIP). The incorporation of the NDVI was not without hesitation because of the two year discrepancy between direct soil moisture measurements and the multispectral imagery.

Principal component analysis (PCA) guided the selection of soil-terrain parameters along with bias towards the attributes selected in Chapter 4. Attributes weighing the most on the first five significant (eigenvalue > 1) principal components were singled out for selection.

Analytical Approaches

This research couples two complimentary, yet different, analytical approaches to distill the various scales at which soil-terrain parameters operate to best explain soil moisture variation in space with time. The two analytical techniques use opposite approaches to extract nested scales of variation, and therefore, will hopefully provide more thorough insight toward the scales at which relevant soil-terrain parameters influence soil moisture variation.

The first approach uses a spatial regression technique that fully decomposes a hydrologic system into individual studied "parts" that significantly ($p < 0.05$) explain soil moisture variation. Parts are identified as individual soil-terrain attributes and spatial scales (e.g. spatial frequencies). This approach will reveal the spatial frequencies, or scales, at which soil moisture exhibits variation but it will not reveal the underlying soil-terrain parameters operating at these spatial frequencies to drive this variation. Using this technique it is therefore purely speculative, based on the investigator's working

knowledge of the site, to draw conclusions as to which underlying soil-terrain parameters operate at these spatial frequencies to control soil moisture variation.

The second approach employs a multivariate geostatistical technique to decompose a hydrologic system into functional multivariate units, or modules, according to the characteristic scales of shared spatial autocorrelation between soil-terrain parameters and soil moisture. These multivariate units are functional in the sense they are composed of several "parts" that synergistically interact to influence soil moisture's scale-dependent spatial variation. Each scale represents a distinct pattern of spatial variation that is considered to be self-organized according to the underlying shared spatial structures and synergistic interactions between soil-terrain parameters. It possible to decompose a system according natural inflection points, or "scale breaks", identified by the range of spatial autocorrelation distinct to different soil-terrain parameters operating synergistically within the landscape. This approach reveals the scale-dependent interrelationships between soil-terrain parameters and soil moisture but, unlike the spatial regression technique, will not reveal the specific contribution of individual soil-terrain parameters in explaining soil moisture variation.

It becomes clear the two techniques exhibit complementary strengths to the other's weakness. This is because the two techniques are completely different approaches to decomposing a hydrologic system according to its nested scales of soil moisture variation. Because the spatial regression technique decomposes the hydrologic system into individual parts, it is identified here as the reductionist approach. Conversely, because the multivariate geostatistical technique decomposes a hydrologic system into hydrologic functional units, it is identified here as the holistic approach. The motivation

here is to employ the two techniques in an accompanying manner to better understand the scale-dependent relative importance of hydrologic parameters influencing soil moisture variation in space with time.

Multivariate Geostatistics

The linear model of coregionalization (LMC) is a multivariate geostatistical tool that fits several simple spatial functions to a matrix of direct and cross variograms to model the scale-dependent spatial variation shared among multiple variables. The LMC studies soil moisture variation as part of an integrated system of spatial variables. The LMC was used to study the coregionalized spatial variation of study variables respective to date. All soil-terrain variables are held constant between dates with time except volumetric water content and apparent EC. After fitting the LMC, PCA_{LMC} was applied to the coregionalized variance/co-variance matrix to reveal the synergistic interaction between multiple soil-terrain parameters and soil moisture at different scales. The LMC was discussed at length in Chapter 4.

For comparison, each date was fitted using the same model. If discrepancies were present for a best fit model between dates, model selection was based on the best for at least two of the three dates. Model selection was guided by the fitted LMC in Chapter 4 but also cross validation statistics.

Spatial Regression

Spatial eigenvector mapping (SEVM), in tandem with multivariate regression, was implemented to determine which spatial filters and soil-terrain parameters best explain soil moisture variation. These two techniques will be henceforth collectively identified

as spatial regression. Spatial regression is performed in two general phases. First, extract a set of proxy spatial variables using spatial connectivity matrix applied to the sampling grid. These spatial variables are viewed as proxy measures of spatial variation because they are inherit to the sampling grid coordinates and not any specific underlying property (Ali et al. 2010). Second, select the most appropriate soil-terrain and spatial variables to best explain the spatial variation of soil moisture.

Spatial Eigenvector Mapping (SEVM)

SEVM is a nonparametric technique that decomposes a sampling space into a set of spatial frequencies (e.g. spatial filters) that potentially explain soil moisture spatial variation. Ideally, each spatial frequency represents an individual scale of variation. In this sense the SEVM technique has been defined as a design-based approach (Ali et al. 2010) because the spatial filters attained specifically depend on the sampling grid design (irregular or regular). SEVM makes no assumptions regarding the underlying spatial structure of studied soil-terrain properties (Ali et al. 2010).

There are three basic steps to complete SEVM (Dray et al. 2006). First, compute a matrix of geographic distances by calculating the Euclidean distances between all possible pairs of sampling points within a sampling grid. Second, apply a truncation distance to the distance matrix. Third, apply principal coordinate analysis (PCoA) to the truncated distance matrix producing a set of spatial eigenvalues and eigenvectors.

Choosing a truncation distance is subjective to the user and has no real empirical credence. This research used a truncation distance equal to the largest range established via the LMC. Applying the truncation distance transforms the distance matrix into a spatial connectivity matrix where actual values indicate the strength of potential

interaction between two spatial locations (Ali et al. 2010). Any sampling pair distance larger than the truncation distance assumes an arbitrary constant equal to four times the chosen truncation distance (Dray et al. 2006) with the logic that there is no spatial autocorrelation beyond this range established by the LMC. Therefore, after applying the truncation distance to the distance matrix not all sites are connected as previously calculated using the pairwise Euclidean distance.

Spatial eigenvector mapping (SEVM) uses principal coordinate analysis (PCoA) to build spatial filters from the truncated distance matrix (Dray et al. 2006). PCoA is computationally equivalent to PCA (Chapter 4) except with PCoA the objects are not soil-terrain properties but are distances. Prior to performing PCoA the truncated distance matrix is double centered by subtracting the mean from each column and row corresponding to a given distance in the distance matrix and dividing by the average value for all distances within the distance matrix. PCoA produces a set of orthogonal principal coordinates, or spatial eigenfunctions, that collectively represent the multiscale distance relationships nested within the sampling grid (Dray et al. 2006). In essence, spatial eigenfunctions represent different spatial scales of variation. Spatial eigenfunctions, also identified herein as spatial filters, can serve as explanatory variables in regression analysis (or any statistical analyses) to describe soil moisture spatial variation (Ali et al. 2010). Spatial eigenvector mapping (SEVM) was performed in SAM® (version 4.0) (Rangel 2010).

Multiple Linear Stepwise Regression

For each observation date soil volumetric water content served as the response variable. Selected soil-terrain attributes, along with the spatial filters produced from SEVM,

respective to date, were subjected to stepwise linear regression to distill a subset of significant predictor variables. Stepwise regression adds and subtracts predictor variables in a stepwise fashion until a best fit model is attained. For each step the AIC (see Chapter 4) was calculated and the best fit model was chosen based on the lowest AIC. Stepwise regression was performed in R version 2.2.4 (R Development Core Team 2008). Partial regression was then performed on the optimal set of predictor variables selected via Stepwise regression to observe what proportion of total variation the spatial proxy variables and environmental variables explained. Partial regression was performed in SAM® (version 4.0) (Rangel 2010). Significant spatial filters were imported into ISATIS® and kriged on a 5 m mesh grid using Quick Interpolation. Mapping the significant spatial filters depicts the relative highs and lows of soil moisture across the landscape. Linear model kriging was the chosen interpolation method, which is essentially ordinary kriging using a linear variogram (with a chosen range of 300 m).

The specific contribution of the spatial regression technique to this chapter is the ability to simultaneously model soil moisture variation using a set of measured environmental variables and a set of proxy spatial variables (e.g. spatial filters) (Ali et al. 2010, Kim in press). The working benefit to incorporating spatial filters is they inherently reduce the predictive bias of environmental variables (Kim in press). The downside to this technique, however, is it cannot reveal which environmental variables correlate with significant spatial frequencies that define soil moisture spatial variation, which inherently complicates answering the third question posed in the Introduction.

Results

Exploratory Analysis

The first five principal components were significant (eigenvalue > 1) for each date and are illustrated in Tables 5.1 - 5.3. Attributes weighing the most on the first five factors were fairly consistent between dates and resulted in the following selections: CEC, elevation, profile curvature, and slope. The topographic wetness index (TWI) weighed the most on the 5th principal component but was excluded because it includes slope in its calculation, which appears to be more significant. Results from Chapter 4 led to the additional inclusion of organic matter, clay, sand, and apparent EC (respective to observation date).

Table 5.1. Principal component analysis results for July.

	Factor 1	Factor 2	Factor 3	Factor 4	Factor 5
Aspect	0.11	0.29	-0.013	0.037	0.13
Elevation	-0.058	0.53	-0.019	-0.023	0.21
Plan Curvature	-0.031	-0.19	-0.45	-0.34	0.31
Profile Curvature	-0.060	0.15	0.53	0.34	-0.11
Slope	-0.084	0.059	0.24	-0.52	0.33
TWI	-0.11	-0.20	-0.47	0.12	-0.45
Cation exchange capacity	0.47	-0.042	-0.13	0.19	0.12
Clay	0.27	0.16	-0.17	-0.28	-0.28
July aEC	0.23	0.41	-0.10	-0.029	-0.33
July Vol. H_2O	0.21	0.13	0.13	-0.38	-0.43
NDVI	-0.074	0.46	-0.26	0.052	0.22
Organic matter	0.41	-0.016	-0.17	0.31	0.056
Phosphorus	0.30	-0.34	0.18	-0.073	0.10
pH	0.41	-0.046	-0.14	0.22	0.25
Sand	0.38	-0.058	0.087	-0.26	-0.054
Eigenvalue	3.7	2.3	1.8	1.6	1.1
Percent	25%	16%	12%	11%	7.2%
Cumulative percent	25%	41%	53%	64%	71%

(aEC) Apparent EC
(%) Percent variance explained by the eigenvalue

Table 5.2. Principal component analysis results for September.

	Factor 1	Factor 2	Factor 3	Factor 4	Factor 5
Aspect	0.10	0.29	0.069	-0.054	-0.15
Elevation	-0.076	0.53	0.020	-0.067	-0.20
Plan Curvature	-0.058	-0.16	-0.49	-0.15	-0.39
Prof Curvature	0.10	0.12	0.57	0.17	0.27
Slope	0.091	0.049	-0.16	0.53	-0.40
TWI	-0.16	-0.18	-0.29	-0.42	0.32
Cation exchange capacity	0.47	-0.027	0.049	-0.26	-0.096
Clay	0.25	0.21	-0.34	0.13	0.20
NDVI	-0.11	0.44	-0.024	-0.31	-0.19
Organic matter	0.39	-0.030	0.14	-0.38	-0.013
Phosphorus	0.34	-0.32	0.060	0.15	-0.065
pH	0.40	-0.037	0.077	-0.27	-0.22
Sand	0.37	-0.069	-0.13	0.23	0.047
Sept Vol. H_2O	0.18	0.16	-0.35	0.092	0.55
Sept aEC	0.22	0.43	-0.19	0.072	0.13
Eigenvalue	3.8	2.3	1.7	1.6	1.2
Percent	25%	16%	12%	10%	8.3%
Cumulative percent	25%	41%	53%	63%	71%

(aEC) Apparent EC
(%) Percent variance explained by the eigenvalue

Table 5.3. Principal component analysis results for October.

	Factor 1	Factor 2	Factor 3	Factor 4	Factor 5
Aspect	0.13	-0.28	-3.6×10^{-3}	0.12	-0.082
Elevation	-0.052	-0.53	0.096	0.086	-0.25
Profile Curvature	0.081	-0.18	-0.61	0.084	0.10
Plan Curvature	-0.053	0.21	0.53	-0.080	-0.40
Slope	0.11	-0.074	0.016	-0.58	-0.30
TWI	-0.14	0.22	0.37	0.29	0.45
Cation exchange capacity	0.46	0.074	0.045	0.26	-0.13
Clay	0.26	-0.16	0.30	-0.14	0.30
NDVI	-0.074	-0.45	0.23	0.22	-0.25
Oct aEC	0.29	-0.34	0.11	-0.11	0.28
Oct Vol. H2O	0.21	-0.21	0.18	-0.25	0.38
Organic matter	0.39	0.058	0.02	0.39	-0.014
pH	0.39	0.090	0.016	0.27	-0.26
Phosphorus	0.32	0.32	-0.10	-0.16	-0.10
Sand	0.36	0.076	6.3×10^{-3}	-0.28	0.018
Eigenvalue	3.8	2.3	1.7	1.6	1.1
Percent	26%	15%	11%	11%	7.0%
Cumulative percent	26%	41%	52%	63%	70%

(aEC) Apparent EC
(%) Percent variance explained by the eigenvalue

Basic statistics and outliers were tested using Quick and Exploratory Statistics in ISATIS®. Basic statistics for the selected soil-terrain attributes are illustrated in Table 5.4. Profile curvature exhibits a negative (left) skewness while all other attributes exhibit a positive (right) skewness. Elevation exhibited the smallest skewness value. Kurtosis, which was above 3.0 for all variables except elevation, indicated peakedness in the distribution. July volumetric water content and sand exhibited kurtosis values closest to 3.0. Outliers were detected for all attributes except clay and July volumetric water content. Normal distributions were tested by performing a Chi-squared significance test (0.05% significance) on the Q-Q plots between the experimental distribution and Gaussian distribution for each attribute (Figures 5.1 and 5.2). The Chi Squared test indicated that clay, slope, and profile curvature are the only normally distributed attributes. These findings justified performing variography and regression analyses on the Gaussian Anamorphosis (GA) transformed selected set of soil-terrain variables for each date. Gaussian Anamorphosis is described in detail in Chapter 4.

Table 5.4. Basic statistics for selected raw soil-terrain attributes.

	Minimum	Maximum	Mean	Variance	Skewness	Kurtosis
CEC	7.6	56	13	27	5.2	41
Clay (%)	17	38	25	9.3	0.77	5.1
Elevation (m)	2.7×10^2	2.9×10^2	2.8×10^2	66	0.10	1.8
July aEC	0.71	3.2	1.2	0.13	2.4	12
July H_20 (vol./vol.)	0.12	0.26	0.18	9.0×10^{-4}	0.59	3.3
Oct. aEC	1.1	5.3	2.2	0.67	1.8	6.1
Oct. H_20 (vol./vol.)	0.25	0.58	0.32	1.6×10^{-3}	2.6	16
Organic matter (%)	2.3	11	3.6	1.0	4.0	27
Profile Curvature (unitless)	-3.4	2.1	-0.03	0.45	-0.86	8.1
Sand (%)	6.1	18	11	5.3	0.91	3.6
Sep. (vol./vol.)	0.18	0.39	0.26	9.0×10^{-4}	1.0	5.0
Sep. aEC	1.0	4.2	1.8	0.36	1.8	6.8
Slope (unitless)	0.0	0.38	0.15	3.6×10^{-3}	0.61	4.6

(aEC) Apparent EC (mS/m)
(CEC) Cation exchange capacity (cmol/kg)
(OM) Organic matter (%)

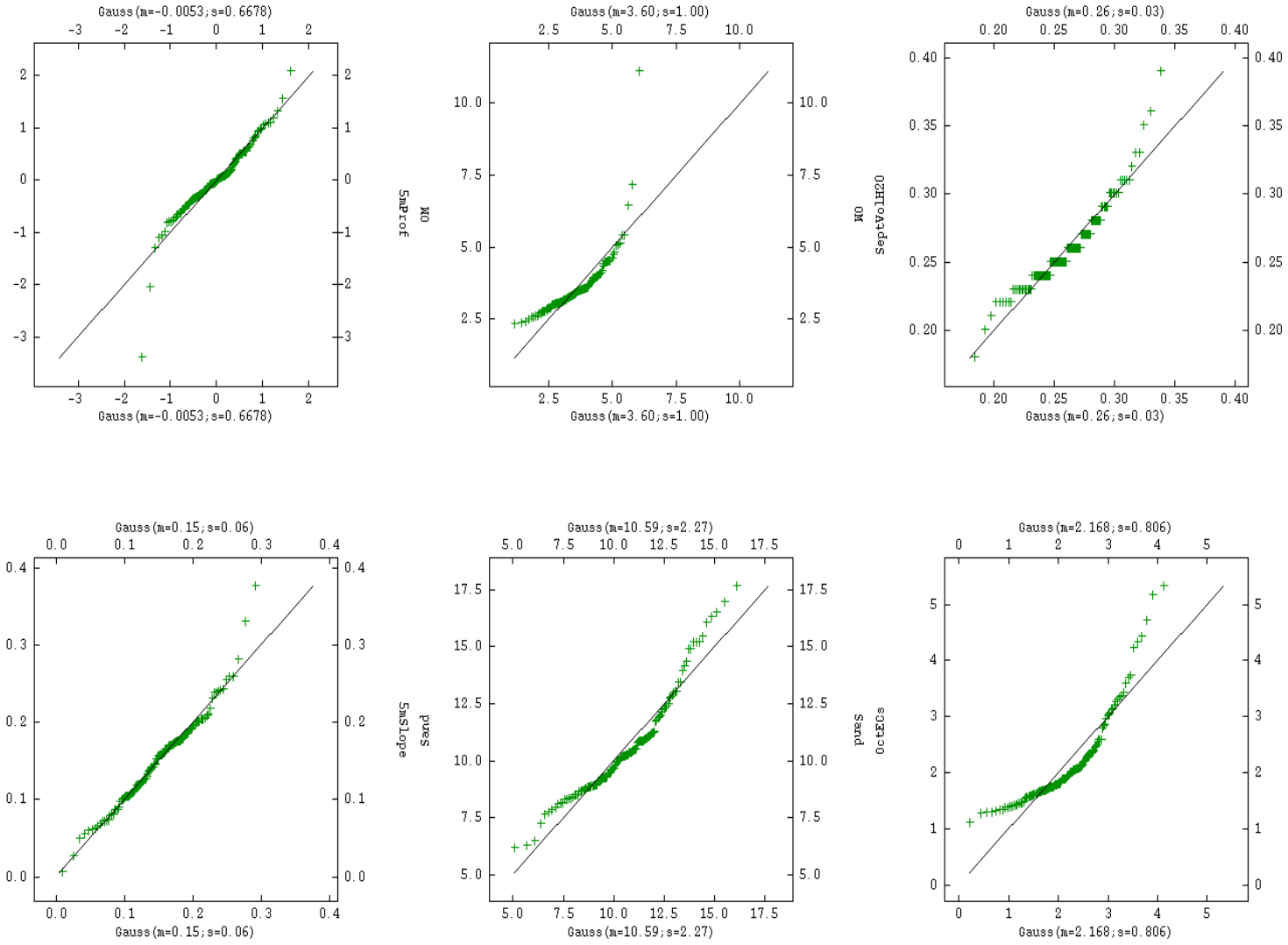

Figure 5.1. Q-Q plots for (from top left to bottom right) profile curvature, organic matter, September H_2O, slope, sand and October apparent EC.

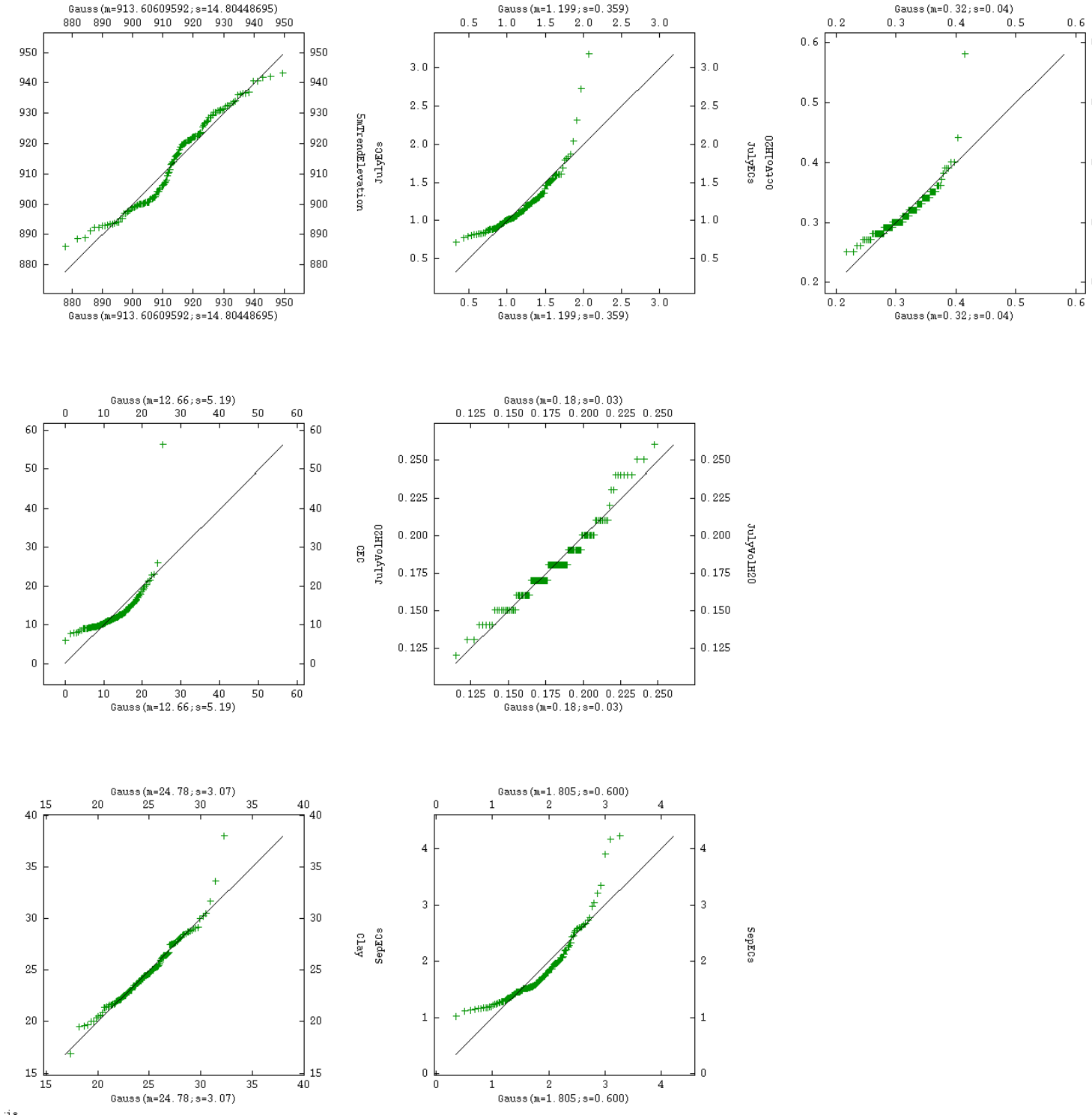

Figure 5.2. Q-Q plots for selected soil-terrain attributes (from top left to bottom right) elevation, July apparent EC, October H_2O, CEC, July H_2O, clay and September apparent EC.

July Multivariate Geostatistics and Spatial Regression

July volumetric soil moisture content was estimated around the plant wilting point (Saxton and Rawls 2006) with an average water content of 0.18 (vol./vol.). The LMC fitted to the set of direct and cross variograms for all three dates consisted of three basic structures: a nugget, a short-range (77 m) spherical model, and a long-range (203 m) spherical model. Cross validation statistics (Table 5.6) show estimates are unbiased and the variance of the standardized error fell within the tolerance threshold $\left(1 \pm 3\sqrt{\frac{2}{N}}\right)$ (Chilés and Delfiner 1999) where N is the number of samples for most variables. Organic matter and elevation fall beneath the tolerance threshold and slope fall above for July. Elevation persistently falls beneath the tolerance threshold for each date and this is credited to the strong autocorrelation within the data.

The total observed variation was partitioned according to each spatial function by applying PCA_{LMC} on the coregionalized variance-covariance (sill values) matrices. The nugget explained 18%, short-range 44%, and long-range 38%, of the total measured variation, respectively. Table 5.6 shows the correlation matrix for the short-range scale. Structural correlation coefficients between July volumetric water content and July apparent EC (0.71) and slope (0.56) are moderate for this range. Table 5.7 shows the correlation matrix for the long-range (203 m) scale. Structural correlation coefficients between volumetric water and soil physicochemical attributes including CEC, organic matter, sand, and clay, are much stronger at this scale than the short-range scale, indicating the strength of interaction between the variables is scale relevant. The first two regionalized factors are significant (eigenvalue > 1) for the short-range scale and explain 66% of the variation at this scale (Table 5.8). To interpret variables loading on

each regionalized factor, attention was focused on absolute values of loading values differing within 10% of the maximum loading value. CEC and slope explain most of the spatial variation at this scale. The first long-range regionalized factor (Table 5.9) is significant and explained 76% of the variation at this scale. Similar to findings established in Chapter 4, clay, volumetric water content, organic matter, and sand explained most of the variation at this scale. This result supports that soil moisture favors long-range variation during dry conditions.

Table 5.5. Cross validation for July LMC using Gaussian transformed variables.

	ME	MSE	VE	VSE
aEC	-9.0×10^{-2}	0.0	0.55	0.90
CEC	-4.1×10^{-2}	-4.2×10^{-2}	0.52	1.0
Clay	-2.6×10^{-2}	-2.3×10^{-2}	0.63	1.1
Elevation	-1.2×10^{-2}	-2.5×10^{-2}	0.13	0.22
Vol. H_2O	-9.0×10^{-3}	-1.7×10^{-2}	0.53	1.2
Organic matter	-4.9×10^{-3}	-3.0×10^{-2}	0.56	0.61
Profile	-3.0×10^{-2}	-2.8×10^{-2}	0.72	1.3
Sand	-1.4×10^{-2}	-2.0×10^{-2}	0.66	1.3
Slope	-1.1×10^{-2}	-2.3×10^{-2}	0.67	1.9

(aEC) Apparent EC
(CEC) Cation exchange capacity
(ME) Mean error
(MSE) Mean standardized error
(VE) Variance of the error
(VSE)Variance of the standardized error

Table 5.6. Short-range (77 m) structural correlation coefficients for Gaussian transformed July variables.

	CEC	aEC	Vol. H_2O	OM	Profile	Sand	Slope	Elevation	Clay
CEC	1.0								
aEC	0.55*	1.0							
Vol. H_2O	0.39*	0.72*	1.0						
OM	0.73*	0.32*	0.13	1.0					
Profile	0.48*	-0.12	0.10	0.60*	1.0				
Sand	0.10	0.10	0.23*	0.00	0.40*	1.0			
Slope	0.12	0.10	0.56*	-0.04	0.23*	0.50*	1.0		
Elevation	-0.67*	-0.01	-0.24*	-0.61*	-0.70*	-0.29*	-0.15	1.0	
Clay	0.54*	0.57*	0.45*	0.25*	-0.12	-0.13	0.38*	0.13	1.0

(aEC) Apparent EC
(CEC) Cation exchange capacity
*Significant ($p < 0.05$)

Table 5.7. Long-range (203 m) structural correlation coefficients for Gaussian transformed July variables.

	CEC	aEC	Vol. H_2O	OM	Profile	Sand	Slope	Elevation	Clay
CEC	1.0								
aEC	0.10	1.0							
Vol. H_2O	0.99*	0.19	1.0						
OM	0.86*	-0.18	0.82*	1.0					
Profile	-0.40*	-0.86*	-0.46*	-0.02	1.0				
Sand	0.99*	0.00	0.98*	0.90*	-0.30*	1.0			
Slope	-0.64*	0.26*	-0.64*	-0.58*	-0.30*	-0.67*	1.0		
Elevation	0.00	0.93*	0.10	-0.20	-0.70*	-0.10	0.27*	1.0	
Clay	0.94*	0.19	0.95*	0.76*	-0.34*	0.92*	-0.79*	0.13	1.0

(aEC) Apparent EC
(CEC) Cation exchange capacity
*Significant ($p < 0.05$)

Table 5.8. Regionalized factors for July at the short-range (77 m) scale.

	CEC	aEC	Vol. H_2O	OM	Profile	Sand	Slope	Elevation	Clay	Eigenvalue	%
F1	0.53	0.40	0.27	0.31	0.21	0.26	0.46	-0.030	0.27	1.5	39
F2	0.38	0.28	-0.10	0.34	-0.020	-0.44	-0.67	-0.010	0.10	1.1	27
F3	-0.19	0.47	0.25	-0.38	-0.55	-0.32	0.15	0.10	0.33	0.66	17
F4	0.10	-0.48	-0.10	0.16	0.10	-0.67	0.43	-0.010	0.30	0.37	10
F5	0.44	-0.25	-0.45	-0.37	-0.24	0.31	-0.13	0.020	0.48	0.14	3.6
F6	0.42	-0.10	0.38	-0.65	0.33	-0.22	-0.10	-0.10	-0.28	0.10	2.6
F7	0.38	-0.19	0.10	0.19	-0.68	0.00	0.17	-0.15	-0.52	0.10	1.3
F8	-0.10	-0.45	0.70	0.16	-0.14	0.20	-0.29	-0.10	0.36	0.00	0.45
F9	0.11	-0.10	0.12	0.03	-0.040	0.020	-0.010	0.98	-0.10	0.00	0.00

(aEC) Apparent EC
(CEC) Cation exchange capacity
(*)Significant ($p < 0.05$)
(%)Percent variance explained by regionalized factors (F)

Table 5.9. Regionalized factors for July at the long-range (203 m) scale.

	CEC	aEC	Vol. H_2O	OM	Profile	Sand	Slope	Elevation	Clay	Eigenvalue	%
F1	0.40	0.010	0.44	0.46	-0.030	0.41	-0.13	-0.010	0.51	2.6	76
F2	0.020	0.39	0.11	-0.27	-0.19	-0.06	0.10	0.82	0.19	0.57	17
F3	0.030	-0.10	0.10	-0.72	0.03	-0.03	-0.40	-0.28	0.47	0.14	4.0
F4	0.36	0.14	0.35	-0.36	-0.36	0.24	0.46	-0.28	-0.35	0.10	2.3
F5	-0.21	0.80	0.10	0.19	-0.17	-0.22	-0.26	-0.34	-0.030	0.010	0.17
F6	0.12	-0.11	0.59	-0.040	0.32	-0.18	-0.46	0.18	-0.50	0.00	0.00
F7	-0.17	-0.13	0.44	0.10	0.14	-0.61	0.50	-0.11	0.32	0.00	0.00
F8	-0.50	-0.36	0.25	0.10	-0.72	0.10	-0.20	0.10	-0.030	0.00	0.00
F9	-0.62	0.13	0.24	-0.12	0.42	0.56	0.19	-0.010	0.01	0.00	0.00

(aEC) Apparent EC
(CEC) Cation exchange capacity
(*)Significant ($p < 0.05$)
(%)Percent variance explained by regionalized factors (F)

Figures 5.3 and 5.4 illustrate the correlation plots for the short-range (77 m) and long-range (203 m) for July, respectively. For the short-range, there is close association between volumetric water content, clay, and profile curvature. At the long-range scale, clustering is better defined and clay maintains close association with volumetric water content, supporting the presence of intrinsic correlation. Intrinsic correlation is present when the spatial interaction between two or more variables is scale invariant. Other soil properties associating with volumetric soil moisture at the long-range scale include CEC, organic matter, and sand.

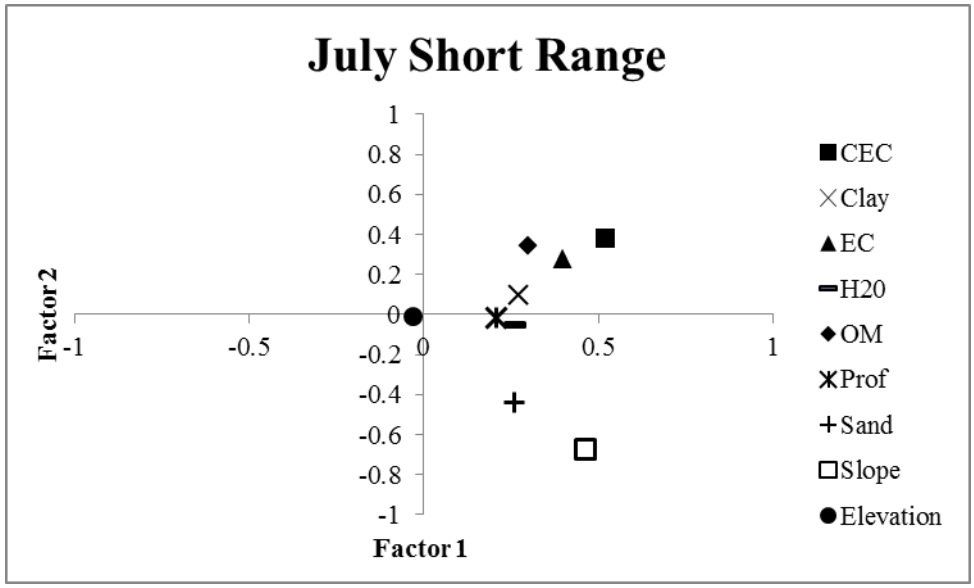

Figure 5.3. Correlation plot between the first and second short-range regionalized factors for July.

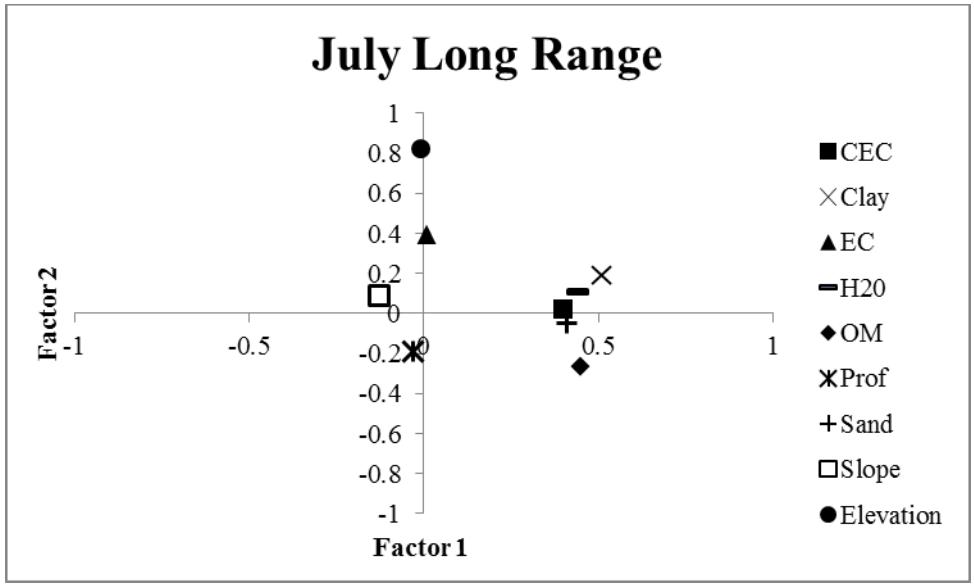

Figure 5.4. Correlation plot between the first and second long-range regionalized factors for July.

A total of 27 spatial filters were produced from SEVM analysis for July. Spatial filters can be considered as proxy variables representing the different spatial scales at which soil moisture exhibits variation. For ease of interpretation spatial filters were divided into three classes: microscale (spatial filters 19-27+), mesoscale (spatial filters 10 – 18), and macroscale (spatial filters 1-9). Stepwise regression selected 15 explanatory variables including CEC, apparent EC, OM, profile curvature, sand, clay, and spatial filters 2, 3, 6, 9, 12, 18, 20, 27, and 28. The multiple R-squared was 0.60 with an AIC of -84.62. The July date produced the largest number of explanatory variables. Out of the 15 variables selected for July, clay, sand, and spatial filters 2, 3, 9, 18, and 20 proved significant ($p < 0.05$) in explaining soil moisture variation (Table 5.10). The standardized coefficient for clay is greater than sand, indicating it is more important in explaining soil moisture variation between the two soil fractions. Significant spatial filters range from low frequency to high frequency suggesting soil moisture variation is significant over a range of spatial scales. Mapping significant spatial filters can help visualize the relative highs and lows in soil moisture across the landscape at different spatial scales (e.g. frequencies) (Figure 5-5). The standardized coefficients for spatial filters 3 and 9 are greater than other spatial filters indicating most of soil moisture spatial variation resides at the macroscale, which corresponds with the multivariate geostatistical findings. The total variation explained by the environmental variables and spatial proxy variables were 0.24 and 0.19, respectively (Table 5.11). The proportion of variation shared by both explanatory data sets was 0.17 (Table 5.11). Plotting the regression model residuals against the predicted values produced a null correlation value, indicating a linear model is a good fit for the data (Figure 5.6).

Table 5.10. Stepwise multivariate regression results for July.

	Estimate	Standardized Estimate	Standard Error	t value	Pr (>|t|)	Significance
(Intercept)	0.010	0.00	0.060	0.080	0.94	
CEC	0.19	0.19	0.12	1.6	0.11	
aEC	0.12	0.12	0.080	1.6	0.12	
OM	-0.14	-0.14	0.10	-1.4	0.16	
Profile	0.10	0.10	0.070	1.5	0.14	
Sand	0.18	0.18	0.080	2.3	0.020	*
Clay	0.28	0.28	0.080	3.5	0.00	***
Filter 2	1.6	0.15	0.70	2.3	0.020	*
Filter 3	3.1	0.28	0.78	4.0	0.00	***
Filter 6	1.3	0.12	0.69	1.9	0.060	
Filter 9	2.3	0.20	0.72	3.2	0.00	**
Filter 12	-1.1	-0.10	0.68	-1.6	0.13	
Filter 18	-1.6	-0.14	0.69	-2.3	0.020	*
Filter 20	-1.5	-0.13	0.70	-2.1	0.040	*
Filter 27	-1.0	-0.10	0.68	-1.5	0.14	
Filter 28	-1.3	-0.11	0.70	-1.8	0.080	

Explanatory variables include Gaussian transformed soil-terrain attributes in addition to SEVM spatial filters.
(aEC) Apparent EC
(CEC) Cation exchange capacity
(OM) Organic matter
(***) Significant at $p < 0.001$
(**) Significant at $p < 0.01$
(*) Significant at $p < 0.05$

Table 5.11. Partial regression results for July, September, and October.

	Environmental Predictor Set	Spatial Predictor Set	Shared	Unexplained
July Partitioned Variation	0.24	0.19	0.17	0.40
September Partitioned Variation	0.44	0.11	-0.018	0.47
October Partitioned Variation	0.15	0.16	0.031	0.66

Environmental predictor set constitutes the standardized soil-terrain variables and the spatial predictor set constitutes the standardized SEVM spatial filters.

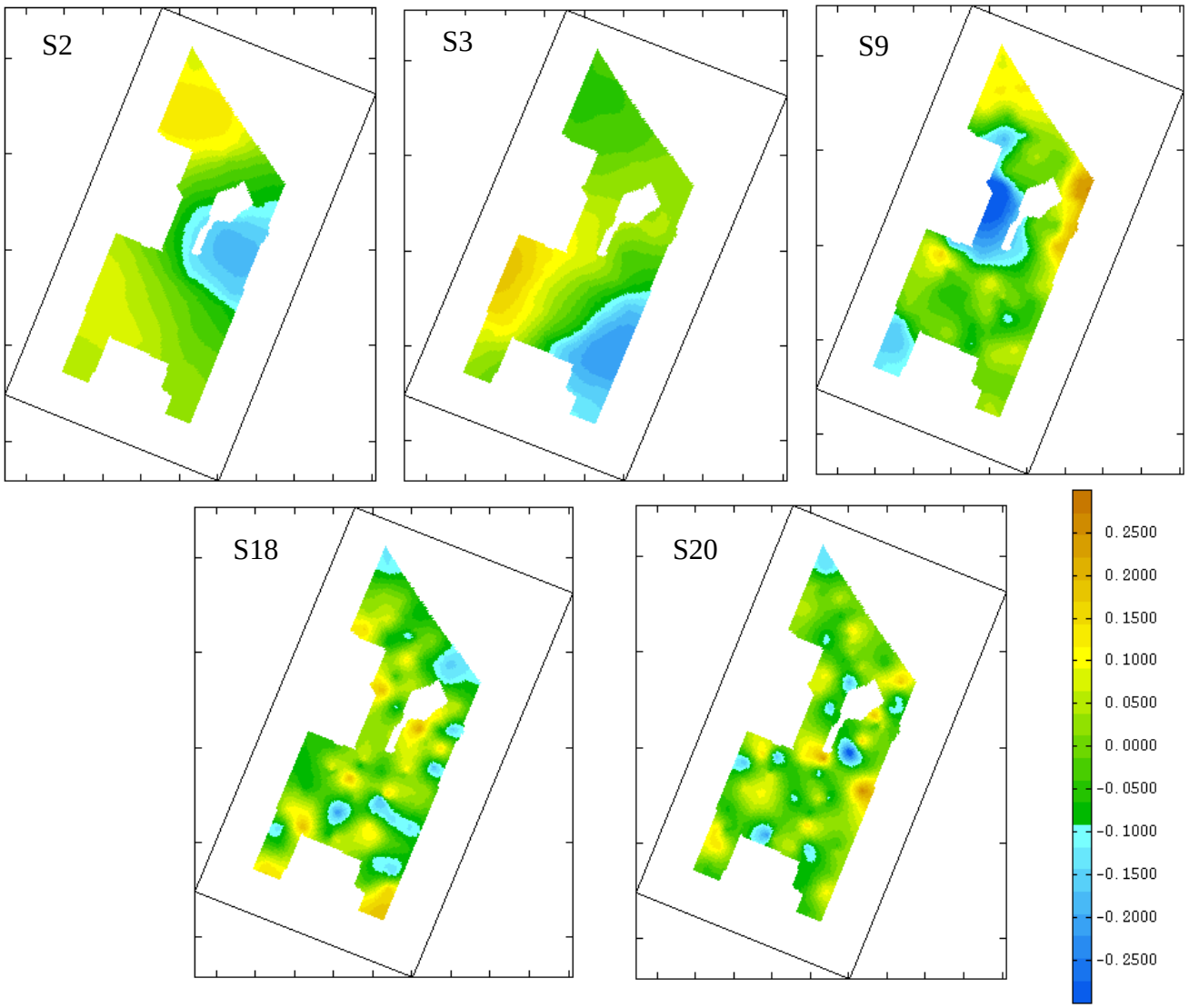

Figure 5.5. Significant spatial filters (S) for July interpolated on a 5 m grid.

The names for the spatial filters and corresponding regression coefficient in parentheses are: S2 – spatial filter 2 (1.6); S3 – spatial filter 3 (3.1); S9 – spatial filter 9 (2.3); S18 – spatial filter 18 (-1.6); and S20 – spatial filter 20 (-1.4). The maps can be interpreted the same as the mapped regionalized factors in Chapter 4. The color scheme represents relative highs and lows of soil moisture. If the coefficient is negative then the color scheme is inverted.

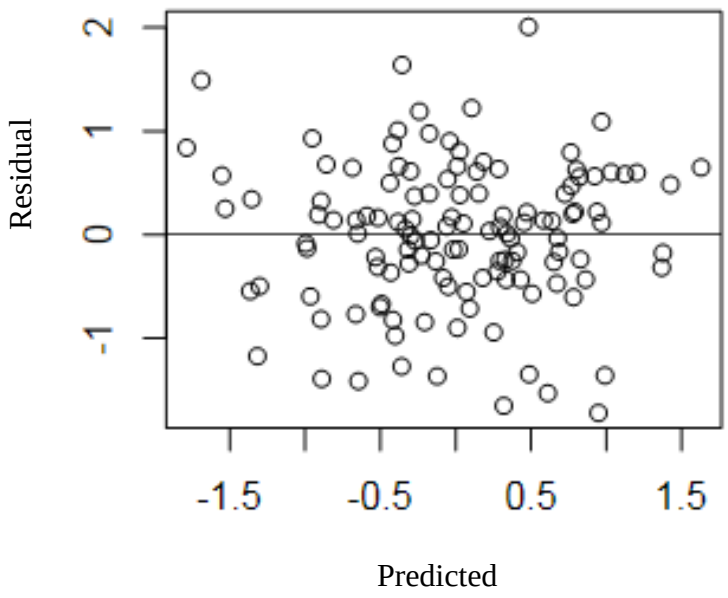

Figure 5.6. Plot of regression model residuals versus predicted values for July.

September Multivariate Geostatistics and Spatial Regression

The field average soil moisture content was 0.26 (vol./vol.) for September. This month represented the intermediate soil moisture content of the three observation dates. Cross validation statistics (Table 5.12) show estimates are unbiased and the variance of the standardized error are significant (Chilés and Delfiner 1999) for all variables except elevation for the aforementioned reason. The nested spherical model fitted to the matrix of direct and cross variograms consisted of a short-range of 79 m and a long-range of 201 m. The ranges established are similar to those in July showing the coregionalized spatial variation is the same regardless of the change in soil moisture content. The proportion of total variation explained by the nugget is relatively high (22%) by comparison to the short-range (41%) and long-range (36%) scales.

Overall, there is poor structural correlation between volumetric soil moisture content and other soil-terrain attributes at the short-range scale, albeit elevation shows a moderate (-0.40) inverse correlation (Table 5.13). The structural correlation coefficients (Table 5.14) at the long-range scale show soil moisture exhibits a strong correlation (correlation coefficients > ±0.90) with CEC, clay, and sand. These results hold true to the long-range results established for July and infers a time stable interaction (Chapter 4). Moderate structural correlation (correlation coefficients ±0.40 to ±0.70) was found between volumetric water content, profile curvature, slope, and organic matter (Table 5.14). To interpret variables loading on each regionalized factor, attention was focused on absolute values of loading values differing within 10% of the maximum loading value. The first and second regionalized factors were significant (eigenvalue greater than 1) at the short-range scale, explaining a cumulative 70% of the captured variation at this scale. Slope

and CEC explain most of the spatial variation at this scale (Table 5.15). The first long-range regionalized factor (Table 5.16) was significant for this date. Variables weighing on this coregionalized factor include clay, organic matter, sand and CEC. It is apparent soil moisture does not hold importance at either scale and might indicate a shift in relative importance between soil-terrain variables interacting with soil moisture.

Table 5.12. Cross validation statistics of LMC for September.

	ME	MSE	VE	VSE
aEC	-1.3×10^{-2}	-1.0×10^{-2}	0.55	0.87
CEC	-3.5×10^{-2}	-3.3×10^{-2}	0.47	0.88
Clay	3.6×10^{-2}	3.7×10^{-2}	0.57	1.1
Elevation	8.0×10^{-2}	1.2×10^{-2}	4.5×10^{-2}	0.28
Vol. H_2O	3.8×10^{-2}	3.8×10^{-2}	0.75	0.90
OM	-1.0×10^{-2}	-1.3×10^{-2}	0.51	1.1
Profile	1.0×10^{-2}	1.5×10^{-2}	0.96	1.1
Sand (%)	0.00	6.1×10^{-3}	0.62	1.1
Slope	-3.0×10^{-2}	-8.2×10^{-4}	0.60	0.98

(aEC) Apparent EC
(CEC) Cation exchange capacity
(OM) Organic matter
(ME) Mean error
(MSE) Mean standardized error
(VE) Variance of the error
(VSE) Variance of the standardized error

Table 5.13. Short-range (79 m) structural correlation coefficients of Gaussian transformed variables for September.

	CEC	Clay	OM	Profile	Sand	aEC	Vol. H_2O	Slope	Elevation
CEC	1.0								
Clay	0.40*	1.0							
OM	0.80*	0.21*	1.0						
Profile	0.57*	0.10	0.51*	1.0					
Sand	0.10	-0.10	0.00	0.48*	1.0				
aEC	0.74*	0.69*	0.74*	0.26*	0.20	1.0			
Vol. H_2O	-0.26*	0.00	0.13	-0.15	-0.32*	-0.10	1.0		
Slope	0.10	0.26*	0.00	0.19	0.48*	0.27*	0.10	1.0	
Elevation	-0.54*	0.13	-0.76*	-0.28*	-0.16	-0.47*	-0.40*	-0.13	1.0

(aEC) Apparent EC
(CEC) Cation exchange capacity
(OM) Organic matter
(*)Significant ($p < 0.05$)

Table 5.14. Long-range (201 m) structural correlation coefficients of Gaussian transformed variables for September.

	CEC	Clay	OM	Profile	Sand	aEC	Vol. H_2O	Slope	Elevation
CEC	1.0								
Clay	0.98*	1.0							
OM	0.82*	0.81*	1.0						
Profile	-0.46*	-0.55*	0.00	1.0					
Sand	0.99*	0.96*	0.86*	-0.36*	1.0				
aEC	-0.10	0.05	-0.48*	-0.83*	-0.20	1.0			
Vol. H_2O	0.94*	0.98*	0.68*	-0.69*	0.90*	0.24	1.0		
Slope	-0.71*	-0.72*	-0.87*	0.00	-0.75*	0.39*	-0.64*	1.0	
Elevation	0.00	0.14	-0.15	-0.61*	-0.10	0.76*	0.25	0.34*	1.0

(aEC) Apparent EC
(CEC) Cation exchange capacity
(OM) Organic matter
(*)Significant ($p < 0.05$)

Table 5.15. Regionalized factors at the short-range (79 m) scale for September.

	CEC	Clay	OM	Profile	Sand	aEC	Vol. H_2O	Slope	Elevation	Eigenvalue	%
F1	0.53	0.24	0.40	0.28	0.29	0.36	-0.040	0.45	-0.040	1.8	41
F2	0.39	0.10	0.37	0.00	-0.43	0.15	0.00	-0.71	-0.020	1.0	29
F3	0.10	-0.53	0.10	0.36	0.61	-0.18	-0.19	-0.37	-0.020	0.52	15
F4	0.010	0.59	-0.44	-0.10	0.34	0.21	-0.43	-0.32	0.11	0.26	7.2
F5	0.45	-0.10	-0.37	0.33	-0.38	-0.44	-0.40	0.20	0.10	0.17	4.7
F6	-0.27	0.40	-0.020	0.72	-0.030	-0.20	0.44	-0.10	0.040	0.14	3.9
F7	0.51	-0.00	-0.45	-0.20	0.22	-0.10	0.61	-0.11	-0.23	0.00	0.74
F8	0.14	0.00	0.10	-0.15	0.11	-0.14	0.19	-0.010	0.94	0.00	0.00
F9	-0.10	-0.38	-0.39	0.31	-0.20	0.72	0.10	0.010	0.21	0.00	0.00

(aEC) Apparent EC
(CEC) Cation exchange capacity
(OM) Organic matter
(%)Percent variance explained by regionalized factor (F).

Table 5.16. Regionalized factors at the long-range (201 m) scale for September.

	CEC	Clay	OM	Profile	Sand	aEC	Vol. H_2O	Slope	Elevation	Eigenvalue	%
F1	0.43	0.53	0.48	-0.10	0.43	-0.10	0.33	-0.13	0.00	2.3	71
F2	0.040	0.18	-0.29	-0.27	-0.040	0.56	0.22	0.10	0.66	0.72	23
F3	-0.20	-0.12	0.58	0.24	-0.18	-0.24	-0.17	-0.02	0.66	0.17	5.4
F4	0.38	-0.11	-0.28	-0.020	0.34	-0.45	-0.19	0.60	0.25	0.04	1.2
F5	0.11	-0.10	0.47	-0.17	-0.26	0.39	-0.10	0.66	-0.27	0.00	0.00
F6	0.020	0.40	0.00	-0.10	0.12	0.20	-0.87	-0.13	0.00	0.00	0.00
F7	-0.62	0.52	-0.10	0.36	0.15	-0.040	0.14	0.41	-0.10	0.00	0.00
F8	0.10	-0.40	0.10	0.54	0.55	0.48	-0.10	-0.030	0.00	0.00	0.00
F9	-0.49	-0.26	0.18	-0.63	0.51	-0.10	0.00	0.00	0.00	0.00	0.00

(aEC) Apparent EC
(CEC) Cation exchange capacity
(OM) Organic matter
(%)Percent variance explained by regionalized factor (F).

Unlike July, the correlation plot (Figure 5.7) for the short-range indicates no association between volumetric soil moisture content and the other soil-terrain variables, except elevation. Both soil moisture and elevation hold no importance on either regionalized short-range factors. For the long-range (Figure 5.8), soil moisture shows a slight departure from the soil physicochemical parameters it was more strongly associated with in July. The correlation plots reinforce the notion there is a shifting in relative importance between soil-terrain variables interacting with soil moisture for September.

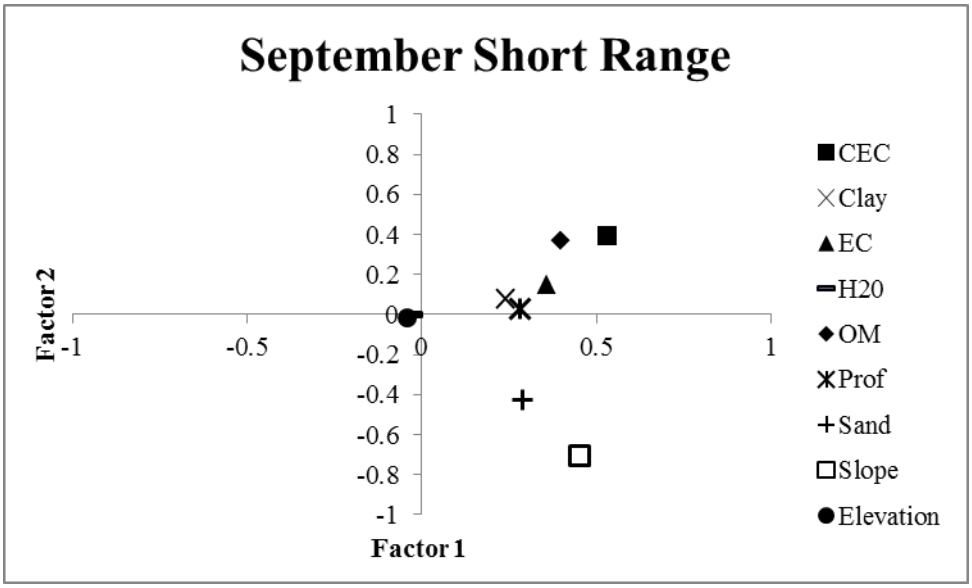

Figure 5.7. Correlation plot between the first and second short-range regionalized factors for September.

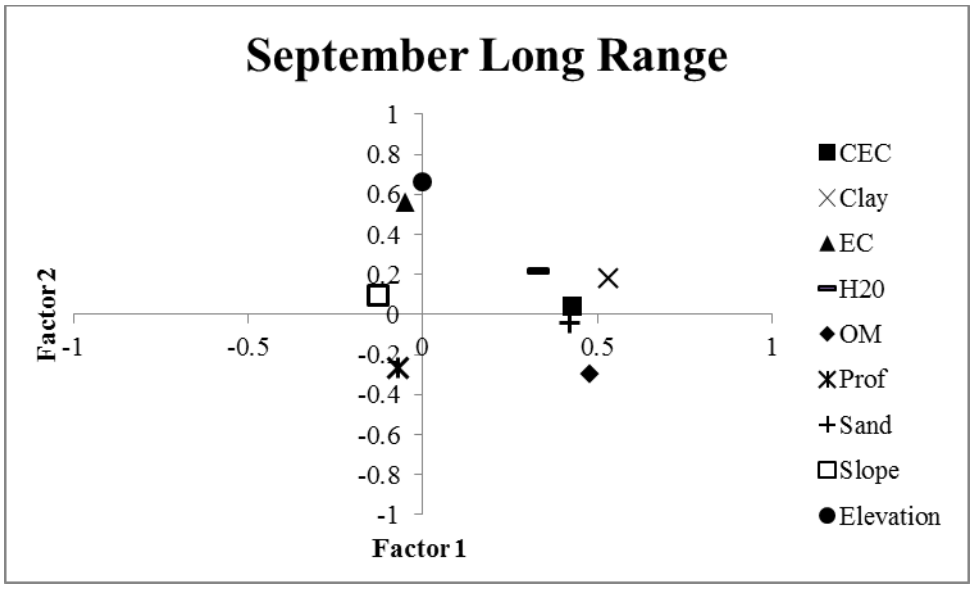

Figure 5.8. Correlation plot between first and second long-range regionalized factors for September.

SEVM analysis produced 29 spatial filters for September. Stepwise regression selected 11 explanatory variables for this date including: CEC, clay, OM, and apparent EC, in addition to spatial filters 1, 9, 13, 17, 20, 23, and 27 (Table 5.17). The multiple R-squares was 0.54 with and AIC of -73.8. Clay, OM, and apparent EC were significant ($p< 0.05$) . Spatial filters 9, 17, 23, and 27 were significant ($p < 0.05$) (Figure 5.9). The high frequency spatial filters 23 and 27 hold more importance in explaining soil moisture variation for this date, which implies an association with the relatively high nugget effect established via the fitted LMC. Clay and spatial filter 9 are the only two explanatory variables holding their relevance between consecutive time steps in explaining soil moisture variation. The majority (0.44) of total variation is explained by the environmental variables for this September by comparison to the spatial proxy variables that explain a smaller proportion (0.11) (Table 5.11). The shared variation between the two explanatory data sets was infinitesimal (-0.018) (Table 5.11). Like July, plotting the regression model residuals against the predicted values produced a null correlation value, indicating a linear model is a good fit for the data (Figure 5.10).

Based on the findings here September might be the "transition period" showing the shift in relative importance between soil-terrain parameters instead of October, as suggested in Chapter 4. The regionalized factors showed that soil moisture did not weigh at either spatial scale. Microscale spatial filters (23 and 27) explained most of the soil moisture variation, which is most likely related to the high nugget for this date. Because clay holds its relevance in explaining soil moisture variation, as shown by the spatial regression results and the long-range structural correlation coefficients, between time

steps is it is suspected that adsorption processes are still influencing soil moisture variation in September.

Table 5.17. Stepwise multivariate regression results for September.

	Estimate	Standardized Estimate	Standard Error	t value	Pr (>|t|)	Significance
(Intercept)	0.01	0.00	0.060	0.16	0.87	
CEC	-0.23	-0.23	0.13	-1.73	0.086	
Clay	0.38	0.37	0.083	4.5	0.00	***
OM	0.49	0.49	0.11	4.3	0.00	***
aEC	0.31	0.31	0.094	3.4	0.00	**
Filter 1	1.22	0.11	0.86	1.4	0.16	
Filter 9	1.59	0.14	0.74	2.1	0.034	*
Filter 13	1.11	0.10	0.71	1.6	0.12	
Filter 17	-1.5	-0.13	0.73	-2.0	0.050	*
Filter 20	-1.1	-0.10	0.73	-1.5	0.15	
Filter 23	2.0	0.18	0.72	2.7	7.0×10^{-3}	**
Filter 27	2.0	0.18	0.72	2.8	6.0×10^{-3}	**

Explanatory variables include Gaussian transformed soil-terrain attributes in addition to SEVM spatial filters.
(aEC) Apparent EC
(CEC) Cation exchange capacity
(OM) Organic matter
(***) Significant at $p < 0.001$
(**) Significant at $p < 0.01$
(*) Significant at $p < 0.05$

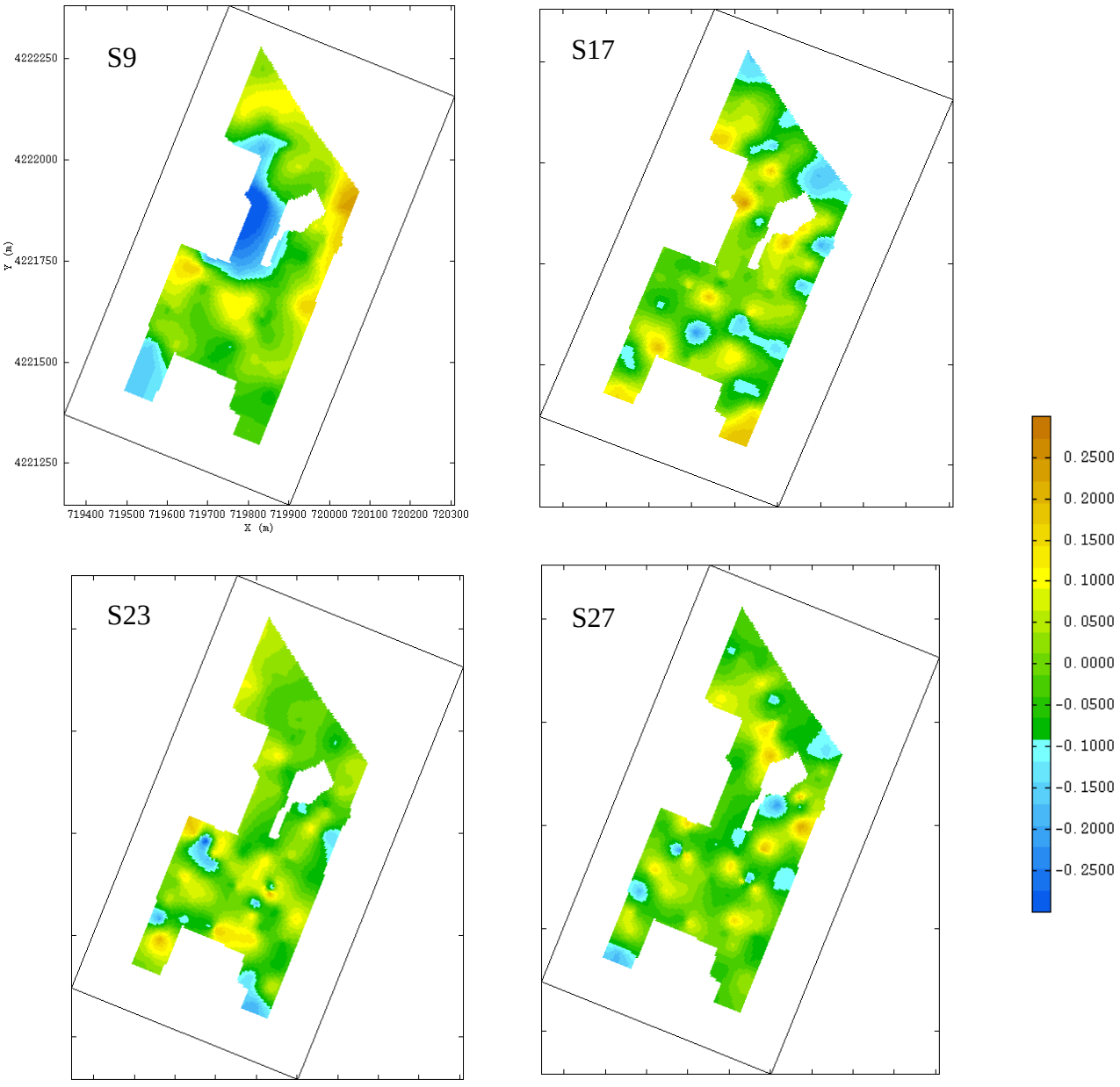

Figure 5.9. Interpolated significant spatial filters (S) for September.

The names for the spatial filters and corresponding regression coefficient in parentheses: S9 – spatial filter 9 (1.6); S17 – spatial filter 17 (-1.5); S23 – spatial filter 23 (2.0)); and S27 – spatial filter 27 (2.0). The maps can be interpreted the same as the mapped regionalized factors in Chapter 4. The color scheme represents relative highs and lows of soil moisture. If the coefficient is negative then the color scheme is inverted.

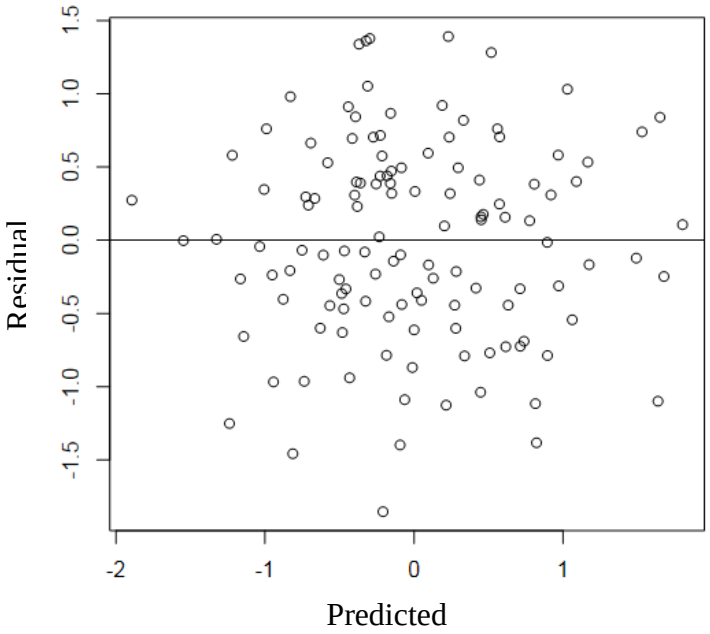

Figure 5.10. Plot of regression model residuals versus predicted values for September.

October Multivariate Geostatistics and Spatial Regression

October was the wettest (0.31 vol./vol.) observation date with the field average soil moisture content approaching field capacity for the silt loam soils investigated (Saxton and Rawls 2006). Cross validation statistics (Table 5.18) show estimates are unbiased and the variance of the standardized error fell within the tolerance threshold (Chilés and Delfiner 1999) for all variables except elevation. The fitted LMC model consists of a nugget, a short-range of 78 m, and a long-range of 206 m that explained 17%, 50%, and 33% of the total observed variation, respectively. Out of all three dates, October shows the greatest percentage of variation explained at the short-range scale. Elevation's structural correlation with soil moisture at the short-range (78 m) improved from -0.40 in September to -0.68 for October (Table 5.19). Variables exhibiting strong structural correlations with volumetric water content at the long-range include sand (0.91), clay (0.88), organic matter (0.94), and CEC (0.93) (Table 5.20). Structural correlation coefficients between volumetric water and soil physicochemical attributes are persistent at this scale for all three dates, indicating a time stable association between soil moisture and soil physicochemical attributes (Chapter 4). The first two regionalized factors were significant (eigenvalue > 1) at the short-range scale, explaining 63% of the total variation at this scale and ~32% of the total observed variation. Variables loading on the first short-range include CEC, apparent EC, volumetric water content, and slope (Table 5.21). Slope weighs on the significant second short-range factor. The first long-range regionalized factor was significant where clay and organic matter explained the majority of variation at this scale. This indicates soil moisture exhibits greater spatial variation at the short-range scale, rather than the long-range scale, as the soils become wetter (Table 5.22).

Table 5.18. Cross validation statistics for October LMC.

	ME	MSE	VE	VSE
aEC	-1.4×10^{-2}	-1.1×10^{-2}	0.48	0.84
CEC	-2.4×10^{-2}	-1.9×10^{-2}	0.45	1.0
Clay	-8.8×10^{-4}	-3.8×10^{-3}	0.58	1.1
Elevation	6.6×10^{-3}	7.6×10^{-3}	3.9×10^{-2}	0.27
OM	1.6×10^{-3}	-1.1×10^{-3}	0.44	1.0
Profile	1.9×10^{-2}	2.4×10^{-2}	0.98	1.1
Sand	-1.0×10^{-2}	0.00	0.64	1.2
Slope	-3.1×10^{-2}	-2.7×10^{-2}	0.53	0.96
Vol. H_2O	-2.8×10^{-3}	-1.2×10^{-2}	0.91	1.3

(aEC) Apparent EC
(CEC) Cation exchange capacity
(OM) Organic matter
(ME) Mean error
(MSE) Mean standardized error
(VE) Variance of the error
(VSE) Variance of the standardized error

Table 5.19. Short-range (78 m) structural correlation coefficients of Gaussian transformed variables for October.

	CEC	Clay	OM	aEC	Vol. H_2O	Profile	Sand	Slope	Elevation
CEC	1.0								
Clay	0.45*	1.0							
OM	0.78*	0.26*	1.0						
aEC	0.73*	0.74*	0.69*	1.0					
Vol. H_2O	0.21	0.10	0.19	0.23*	1.0				
Profile	0.44*	0.10	0.51*	0.22*	0.29*	1.0			
Sand	0.18	-0.00	0.16	0.10	0.36*	0.41*	1.0		
Slope	0.10	0.32*	0.00	0.37*	0.31*	0.13	0.44*	1.0	
Elevation	-0.53*	0.20	-0.67*	-0.32*	-0.69*	-0.44*	-0.36*	0.00	1.0

(aEC) Apparent EC
(CEC) Cation exchange capacity
(OM) Organic matter
(*)Significant ($p < 0.05$)

Table 5.20. Long-range (201 m) structural correlation coefficients Gaussian transformed variables for October.

	CEC	Clay	OM	aEC	Vol. H_2O	Profile	Sand	Slope	Elevation
CEC	1.0								
Clay	0.93*	1.0							
OM	0.83*	0.75*	1.0						
aEC	0.11	0.29*	-0.33*	1.0					
Vol. H_2O	0.93*	0.88*	0.94*	-0.17	1.0				
Profile	-0.43*	-0.53*	0.00	-0.94*	-0.13	1.0			
Sand	0.95*	0.94*	0.77*	0.21	0.91*	-0.50*	1.0		
Slope	-0.45*	-0.67*	-0.56*	0.10	-0.65*	-0.00	-0.53*	1.0	
Elevation	0.00	0.13	-0.15	0.73*	-0.25	-0.63*	-0.10	0.19	1.0

(aEC) Apparent EC
(CEC) Cation exchange capacity
(OM) Organic matter
(*)Significant ($p < 0.05$)

Table 5.21. Regionalized factors for October at the short-range (78 m) scale.

	CEC	Clay	OM	aEC	Vol. H_2O	Profile	Sand	Slope	Elevation	Eigen	%
F1	0.48	0.23	0.34	0.38	0.40	0.23	0.31	0.39	-0.10	1.8	40
F2	0.46	0.12	0.38	0.22	-0.34	0.10	-0.37	-0.58	-0.010	1.1	23
F3	0.00	0.38	-0.13	0.30	-0.56	-0.25	-0.24	0.55	0.10	0.66	15
F4	0.10	-0.25	0.14	-0.17	-0.63	0.29	0.63	0.10	0.010	0.49	11
F5	0.10	0.44	-0.28	0.09	0.03	-0.51	0.55	-0.38	0.04	0.20	4.3
F6	-0.22	0.59	-0.26	-0.10	-0.010	0.70	-0.020	-0.16	0.10	0.16	3.6
F7	-0.70	0.10	0.57	0.36	-0.010	-0.10	0.15	-0.12	-0.03	0.12	2.7
F8	-0.040	-0.40	-0.48	0.74	-0.030	0.19	0.10	-0.15	-0.10	0.00	0.61
F9	-0.020	0.11	-0.10	-0.10	-0.10	0.010	-0.010	0.020	-1.0	0.00	0.00

(aEC) Apparent EC
(CEC) Cation exchange capacity
(%) Percent explained by regionalized factor (F)

Table 5.22. Regionalized factors for October at the long-range (201 m) scale.

	CEC	Clay	OM	aEC	Vol. H_2O	Profile	Sand	Slope	Elevation	Eigen	%
F1	0.43	0.56	0.52	0.02	0.21	-0.05	0.41	-0.14	-0.01	2.0	67
F2	0.040	0.23	-0.31	0.55	-0.09	-0.23	0.10	0.10	0.69	0.66	22.
F3	-0.10	-0.21	0.59	-0.30	-0.01	0.14	-0.30	0.10	0.63	0.20	6.6
F4	-0.42	0.34	-0.10	-0.03	0.00	0.14	-0.22	-0.80	0.06	0.10	3.0
F5	-0.54	-0.36	0.33	0.31	0.00	-0.14	0.59	-0.10	0.040	0.020	0.58
F6	0.030	-0.10	-0.40	-0.62	-0.10	0.10	0.57	-0.10	0.32	0.00	0.00
F7	0.48	-0.37	0.10	0.10	-0.60	-0.22	0.01	-0.46	-0.030	0.00	0.00
F8	0.16	-0.32	-0.10	-0.10	0.69	-0.54	-0.12	-0.26	0.10	0.00	0.00
F9	-0.29	0.32	0.10	-0.33	-0.33	-0.73	-0.10	0.19	-0.10	0.00	0.00

(aEC) Apparent EC
(CEC) Cation exchange capacity
(%) Percent explained by regionalized factor (F)

The correlation plots for October show a clear shift in clustering between volumetric water content and soil-terrain attributes for the short-range (Figure 5.11). It is apparent volumetric water content migrates away from clay and profile curvature (as seen for July) toward slope and sand. At the long-range scale (Figure 5.12), the association between soil moisture and soil attributes (clay, CEC, OM, and sand) weakens as made evident by soil moisture shifting toward the centroid of the plot.

October is important because it shows there a shift in relative importance from the long-range scale to the short-range scale for soil moisture as the soils become wet with time. The coregionalized correlation matrices and regionalized factor loading values for October indicate that terrain parameters (elevation and slope) exhibit stronger interactions with soil moisture for October. The fact these interactions operate predominately at the short-range scale was unanticipated.

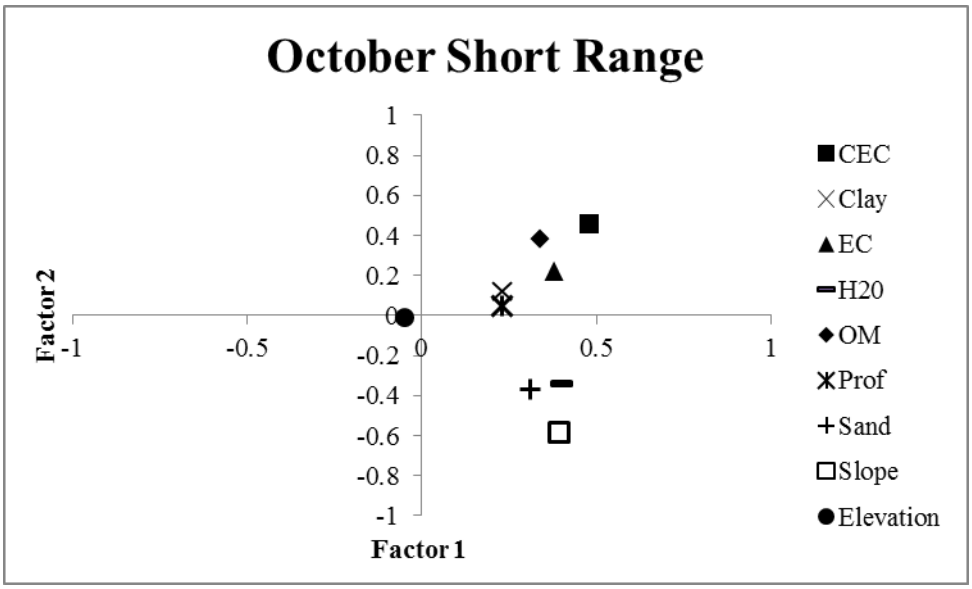

Figure 5.11. Correlation plot between the first and second short-range regionalized factor for October.

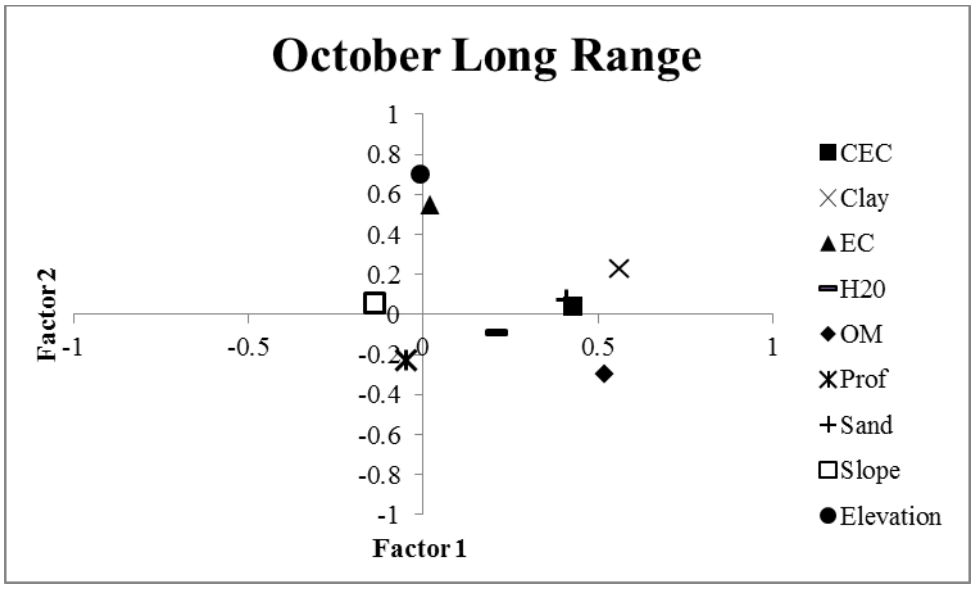

Figure 5.12. Correlation plot between the first and second short-range regionalized factor for October.

October produced 27 spatial filters via SEVM analysis. Stepwise regression selected 10 relevant explanatory variables (Table 5.23) with profile curvature, sand, spatial filter 1, and spatial filter 3 (Figure 5-11) being significant ($p < 0.05$). The multiple R-squares was 0.34 with an AIC of -30.8. Notably, sand and spatial filter 3 also proved significant for July.

Soil moisture variation favors macroscale spatial variation for October. This implies that soil moisture spatial variation attains a larger range of spatial autocorrelation with increasing soil moisture content. With time there is a general decrease in the number of significant spatial filters indicating greater homogeneity in soil moisture variation as the soils become wet. The soil-terrain variables and spatial proxy variables explained .15 and 0.16 of the total variation, respectively (Table 5.24). The amount of shared variation between the two explanatory data sets was minimal (0.031) (Table 5.11). Like the two previous dates, plotting the regression model residuals against the predicted values produced a null correlation value, indicating a linear model is a good fit for the data (Figure 5.14).

Table 5.23. Stepwise multivariate regression results for October.

	Estimate	Standardized Estimate	Standard Error	t value	Pr (>|t|)	Significance
(Intercept)	0.00	0.00	7.6×10^{-2}	-5.7×10^{-2}	0.96	
CEC	0.17	0.17	9.8×10^{-2}	1.7	0.10	
Profile curvature	0.19	0.19	8.0×10^{-2}	2.3	2.1×10^{-2}	*
Sand	0.20	0.20	9.7×10^{-2}	2.1	4.3×10^{-2}	*
Filter 1	-1.9	-0.17	0.85	-2.2	3.0×10^{-2}	*
Filter 3	2.4	0.22	0.91	2.6	1.0×10^{-2}	**
Filter 6	1.4	0.13	0.85	1.7	0.10	
Filter 9	1.7	0.15	0.88	1.9	6.0×10^{-2}	
Filter 23	-1.5	-0.14	0.85	-1.8	7.3×10^{-2}	
Filter 25	1.6	0.15	0.86	1.9	6.3×10^{-2}	
Filter 26	-1.3	-.012	0.85	-1.5	0.13	

Explanatory variables include Gaussian transformed soil-terrain attributes in addition to SEVM spatial filters.
(CEC) Cation exchange capacity
(**) Significant at $p < 0.01$
(*) Significant at $p < 0.05$

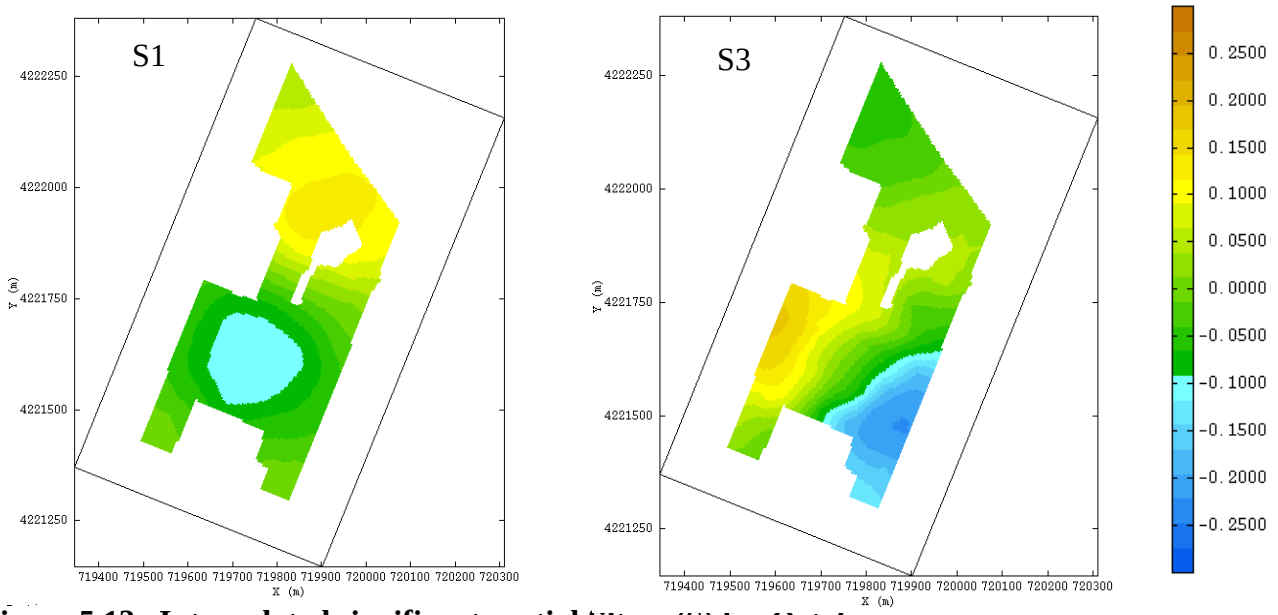

Figure 5.13. Interpolated significant spatial filters (S) for October.

The names for the spatial filters and corresponding regression coefficient in parentheses are as follows: S1 – spatial filter 1 (-1.9); S3 – spatial filter 3 (2.4). The maps can be interpreted the same as the mapped regionalized factors in Chapter 4. The color scheme represents relative highs and lows of soil moisture. If the coefficient is negative then the color scheme is inverted.

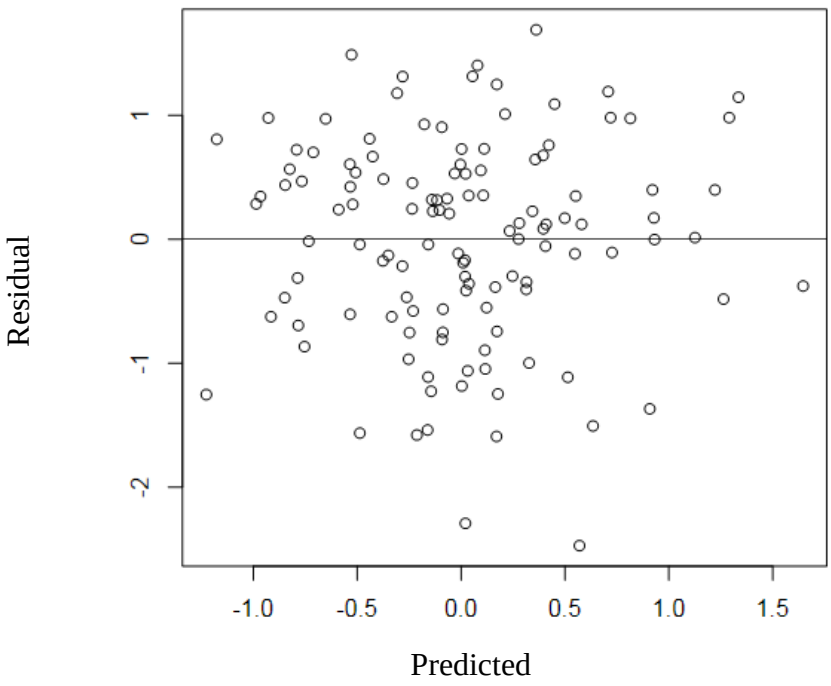

Figure 5.14. Plot of regression model residuals versus predicted values for October.

To capitalize the full value of these techniques it is beneficial to discuss the congruent and incongruent findings established between them. The multivariate geostatistical approach is holistic in that it characterizes soil moisture variation as part of an integrated system of spatial variables while spatial regression is considered a reductionist approach because it characterizes soil moisture with respect to several individual spatial frequencies and soil-terrain attributes.

Both analytical techniques show there is a relative importance between soil-terrain variables influencing soil moisture variation with time and according to spatial scale. For July, both approaches provided concurring evidence that most of the structured variation associated with soil moisture resides at the long-range scale in which texture is a driving factor explaining the variation observed, albeit clay more so than sand. This is expected because clay has a greater surface area to adsorb water than the sand fraction.

September represents an intermediate soil moisture content amid the three observation dates. Although the structural correlation coefficients for the long-range hold their strength between dates the regionalized factors indicate the sources of variation are changing. Moreover, the high frequency spatial filters (23 and 27) dominate in explaining soil moisture variation and their relevance is related to the relatively high nugget effect for this date.

The geostatistical and spatial regression outputs both show that sand and terrain attributes affect soil moisture variation approaching field capacity (October). However, stepwise regression analysis showed profile curvature was significant, whereas the short-range (78 m) structural correlation coefficients and regionalized factors indicate elevation

and slope are important. Albeit, stepwise regression analysis favored profile curvature in comparison to slope, these terrain parameters exhibit relations when parameterizing landscape hydrodynamics. In general, profile curvature represents the localized shape of the slope where upwardly convex shapes (negative profile curvature) increase flow velocity and tend to be associated with dryer upper sloping regions. Conversely, upwardly concave curvature (positive profile curvature) decreases flow velocity and tend to be associated with wetter lower sloping regions (McBratney et al. 2012). Both techniques show that sand holds its relevance as soil moisture increases. This is expected to be the case when drainage processes are prevalent because sand also relates to the soil's ability to drain quickly via gravitational forces (Jawson and Niemann 2007).

Both techniques are inherently opposite in their approaches and this produces nuanced findings between them. For example, elevation does show a temporal relevance with changes in soil moisture content made evident by the short-range structural correlation coefficients. With each consecutive time step elevation shows an improving inverse correlation with soil moisture from -0.24, -0.40, and -0.69, in July, September, and October, respectively. The spatial regression analyses did not recognize elevation as being influential.

Another example focuses on the October findings produced by the spatial regression technique. Stepwise egression (Table 5.23) analysis indicates that long-range soil moisture spatial variation dominates for the wettest date. Although this concurs with what was initially hypothesized, it contradicts findings established by the multivariate geostatistical technique in which there is a shift in dominance from the long-range to the short-range for the wettest date. Based on the geostatistical results, terrain attributes

operate at the short-range scale and are driving this shift. It is possible sand is operating at these spatial frequencies because it exhibits long-range variation in the geostatistical approach. However, partial regression results (Table 5.25) show that the shared variation between the environmental variables and spatial proxy variables is miniscule for this date. With this said, it is suspected some other variable(s) not defined within the scope of this study is (are) responsible for the long-range soil moisture variation indicated by spatial regression. It is noteworthy that the observation extent of the area studied does not fully capture the long-range spatial autocorrelation in elevation. Expanding the observation extent might reveal that long-range elevation is influencing soil moisture variation during wetter soil conditions.

Several variables selected via the stepwise procedure maintain their relevance and/or significance with time. For some variables, the magnitude and sign of the standardized coefficient changed with observation date. It is noticeable that variables maintaining their significance between dates held their sign but variables gaining or losing their statistical significance between dates were susceptible to a change in sign. The change in magnitude and sign is thought to arise from changing interactions between variables as they are added or subtracted from the multivariate regression equation. This phenomenon is explained by the Simpson's paradox, in which the magnitude and direction (e.g. sign) between variables is influenced by the addition or subtraction of other variables (Sheskin 2000).

To better understand how the magnitude and sign of standardized explanatory variables changed in the presence of other variables, the stepwise regression models were rebuilt with emphasis on the most important explanatory variables. To complete the rebuilding

approach a simple linear regression constituting soil moisture and the most important explanatory variable for that date was modeled. Next, the second most important variable for that date was added to the regression equation and modeled. This additive rebuilding sequence continued until the four most important variables were included in the regression model. Tables 5.24, 5.26 and 5.28 show the results for the rebuilt multivariate equations. There is no change in direction with the addition of variables, however, the magnitude of explanatory variables change slightly as the models grow in the number of explanatory variables. Particularly for October, profile curvature proves insignificant during the rebuilding process. The partial correlation coefficients were also calculated for the significant variables illustrated in Tables 5.10, 5.17, and 5.23 and are shown below in Tables 5.25, 5.27, and 5.329, respectively. Reviewing the partial correlation coefficients indicates that the stepwise regression models depreciate the magnitude of influence of significant variables, which is most likely due to the numerous insignificant variables included in the stepwise models (Tables 5.10, 5.17, and 5.23).

It is important to highlight that regression is simply interested in the form of the relationship between multiple variables and soil moisture - it does not reveal the causative agent behind this relationship. It is speculated that changes in soil moisture content drive different interactions between soil moisture and explanatory variables. Partially rebuilding the regression models and calculating the partial correlation coefficients suggests that interactions among explanatory variables induced different interactions (e.g. magnitude) between soil moisture and these variables with time. Although attempts were made to avoid multicollinearity during variable selection, this might be one possible explanation for the changes in magnitude and direction,

especially in models in which organic matter and CEC are present. The presence of confounding variables is another possible explanation.

Table 5.24. Rebuilt multivariate regression equation for July.

		Standardized Estimate	Standard Error	t statistic	Pr (>|t|)	Significance
Model 1	Intercept	0.00	0.08	0.00	1.00	
	Clay	0.54	0.08	7.09	0.00	***
Model 2	Intercept	0.00	0.07	0.00	1.00	
	Clay	0.43	0.08	5.58	0.00	***
	Filter 3	0.30	0.08	3.88	0.00	***
Model 3	Intercept	0.00	0.07	0.00	1.00	
	Clay	0.43	0.07	5.77	0.00	***
	Filter 3	0.30	0.07	3.96	0.00	***
	Filter 9	0.19	0.07	2.67	0.01	**
Model 4	Intercept	0.00	0.07	0.00	1.00	
	Clay	0.36	0.08	4.74	0.00	***
	Filter 3	0.27	0.07	3.69	0.00	***
	Filter 9	0.15	0.07	2.21	0.03	*
	Sand	0.24	0.07	3.21	0.00	**

(***) Significant at $p < 0.001$
(**) Significant at $p < 0.01$
(*) Significant at $p < 0.05$

Table 5.25. Partial correlations between July volumetric water and selected standardized explanatory variables.

Partial Correlation	Clay	Sand	Filter 2	Filter 3	Filter 9	Filter 18	Filter 20
July H_2O	0.41***	0.29***	0.21*	0.34***	0.21*	-0.23**	-0.14

Partial correlation coefficient of significant variables exhibited in Table 5.10.
(***) Significant at $p < 0.001$
(**) Significant at $p < 0.01$
(*) Significant at $p < 0.05$

Table 5.26. Rebuilt multivariate regression equation for September.

		Standardized Estimate	Standard Error	t statistic	Pr (>|t|)	Significance
Model 1	Intercept	0.00	0.08	0.00	1.00	
	Organic Matter	0.49	0.08	6.18	0.00	***
Model 2	Intercept	0.00	0.07	0.00	1.00	
	Organic Matter	0.31	0.08	4.12	0.00	***
	Clay	0.43	0.08	5.62	0.00	***
Model 3	Intercept	0.00	0.07	0.00	1.00	
	Organic Matter	0.32	0.08	4.28	0.00	***
	Clay	0.34	0.08	4.16	0.00	***
	Apparent EC	0.18	0.08	2.37	0.02	*
Model 4	Intercept	0.00	0.07	0.00	1.00	
	Organic Matter	0.32	0.07	4.41	0.00	***
	Clay	0.34	0.08	4.13	0.00	***
	Apparent EC	0.19	0.08	2.52	0.01	*
	Filter 23	0.16	0.07	2.33	0.02	*

(***) Significant at $p < 0.001$
(**) Significant at $p < 0.01$
(*) Significant at $p < 0.05$

Table 5.27. Partial correlations between September volumetric water and selected standardized explanatory variables.

Partial Correlation	Clay	Organic Matter	Apparent EC	Filter 9	Filter 23	Filter 27
Sept. H_2O	0.39***	0.38***	0.25**	0.17	0.22*	0.24**

Partial correlation coefficient of significant variables exhibited in Table 5.17.

(***) Significant at $p < 0.001$

(**) Significant at $p < 0.01$

(*) Significant at $p < 0.05$

Table 5.28. Rebuilt multivariate regression equation for October.

		Standardized Estimate	Standard Error	t stat	P value	Significance
Model 1	Intercept	0.00	0.09	0.00	1.00	
	Filter 3	0.29	0.09	3.37	0.00	***
Model 2	Intercept	0.00	0.08	0.00	1.00	
	Filter 3	0.22	0.08	2.61	0.01	*
	Sand	0.32	0.08	3.75	0.00	***
Model 3	Intercept	0.00	0.08	0.00	1.00	
	Filter 3	0.24	0.08	2.84	0.01	**
	Sand	0.29	0.08	3.46	0.00	***
	Profile Curvature	0.14	0.08	1.68	0.10	
Model 4	Intercept	0.00	0.08	0.00	1.00	
	Filter 3	0.24	0.08	2.88	0.00	**
	Sand	0.30	0.08	3.59	0.00	***
	Profile Curvature	0.15	0.08	1.78	0.08	
	Filter 1	-0.18	0.08	-2.18	0.03	*

(***) Significant at $p < 0.001$
(**) Significant at $p < 0.01$
(*) Significant at $p < 0.05$

Table 5.29. Partial correlations between October volumetric water and selected standardized explanatory variables.

Partial Correlation	Profile Curvature	Sand	Filter 3	Filter 1
Oct. H_2O	0.16	0.32***	0.26**	-0.20*

Partial correlation coefficient of significant variables exhibited in Table 5.24.

(***) Significant at $p < 0.001$
(**) Significant at $p < 0.01$
(*) Significant at $p < 0.05$

Discussion

The benefit to this research is it reveals the relative importance of various parameters affecting soil moisture variation according to time, space, and scale. The nested, irregular sampling scheme and modeling applications applied were able to capture and extract nested scales of soil moisture variation within the landscape according to the three soil moisture regimes studied. Overall, both analytical approaches (holistic and reductionist) confirm soil moisture variation exhibits scale relevance with time. At the plant wilting point, both techniques indicate short- and long-range spatial scales are relevant but the long-range scale, in which soil physicochemical properties dominated, is more significant. Dry conditions have been shown to exhibit greater spatial autocorrelation in soil moisture elsewhere (Western et al. 1998). Terrain features become more relevant as soil moisture approaches field capacity, which is expected because gravitational forces become more significant for soil moisture distribution. For example, Brocca et al. (2007) found the best correlation between shallow surface soil moisture and upland contributing area, slope, and elevation when the soils were sufficiently wet to laterally redistribute water. Nonetheless, it was unexpected terrain interaction would dominate at the short-range (~70 m) scale and soil interactions at the long-range scale (~200m).

Shorter ranges have also been established characteristic to terrain attributes influencing soil moisture distribution. For example, Nyberg et al. (1996) showed that terrain attributes with a shorter range of influence (around 20 m) best represented topographically homogenous regions that were influential for soil moisture distribution. Jawson and Niemann (2007) also found elevation to exhibit short-range variation and soil

properties to exhibit long-range variation. Both of these studies were performed in topographically diverse areas characterized by rolling hills and steep slopes. Elevation, slope and, to a degree profile curvature (July), exhibited short-range spatial variation for this study. Because the area investigated overlies karst geology the undulating terrain is most likely responsible for the short-range behavior.

Chapter 4 indicated that October represented the beginning of a "transition period," alluding to an apparent shift in the sources of soil moisture variation. Analyzing each time step separately revealed that September, not October, marks the transition period from long-range soil physicochemical properties in July to short-range terrain attributes in October. Transition periods have been noted by higher soil moisture variation (Western et al. 2003, Kornelsen and Coulibaly 2013) and possibly explain why September exhibits the largest nugget effect.

Although terrain attributes become influential as the soils wet, soil physicochemical attributes still hold enough influence to maintain long-range time stability for the three dates, which reinforces the findings in Chapter 4. It is possible, however, that once the soils become saturated the short-range terrain attributes will gain dominance over the long-range soil attributes in explaining soil moisture variation. This shift in dominance would, therefore, likely cause time instability in the soil moisture patterns established in Chapter 4. If this is the case, then the time instability in soil moisture variation is suspected to be short lived (Kornelsen and Coulibaly 2013) considering the soils will drain and soil properties will once again play a more influential role in soil moisture distribution. It is also possible, however, that as soils reach saturation the shared dominance will once again revert back to the soil properties. This was found to be the

case for Perry et al. (2007) in which terrain attributes were relevant only during "intermediate conditions" between wet and dry states. More observations are needed over multiple wetting and drying seasons to add concreteness to these proposed hypotheses.

Wu and David (2002) stated that "Landscapes can be perceived as near-decomposable, nested spatial hierarchies in which hierarchical levels correspond to structural and functional units at distinct spatial and temporal scales (p. 11)." The landscape studied is near-decomposable according to the characteristic scales soil moisture and associated hydrologic parameters exhibit spatial variation. Near-decomposable means that the interactions between scales are, for the most part, independent. This research showed that different hydrologic parameters operate at independent (e.g. orthogonal) scales to influence soil moisture variation with time. Soil physicochemical properties dominated during relatively dry soil conditions (July and September) and operated at the long-range scale whereas terrain attributes dominated under relatively wet soil conditions (October) and operated at the short-range scale. Most likely, different mechanistic processes are driving soil moisture redistribution at these spatial scales based on fluctuations in soil moisture content with time. During dry conditions capillary suction is most likely driving the fate and residence of soil moisture, while drainage and throughflow begin to drive soil moisture redistribution as the soils become wetter.

The conceptual framework introduced by Vogel and Roth (2003), called the scaleway approach, operates on the principle of near-decomposability. The essence of this conceptual model is it emphasizes different hydrologic processes and properties operate independently at different hierarchical scales. Hence, each scale requires a discrete

hydrologic model entailing scale-specific water flow processes and associated physical parameters controlling these processes (Hopmans et al. 2002, Vogel and Roth 2003, Pachepsky et al. 2008). Findings established by this research suggest two prototype models would be prospective for modeling soil moisture variation within the observed karst landscape during drought conditions. During the driest soil conditions model development should focus on soil physicochemical attributes and unsaturated flow mechanisms over large observation scales. During wetter soil conditions model development should focus on terrain attributes and saturated flow mechanisms over smaller observation scales. The underlying motivation here is that each model will represent the respective "factors" and "functions" (Lin 2003) driving soil moisture variation at each observation scale that are relevant to time. To prospect model development under non-drought conditions for the landscape studied, more research is necessary over multiple wetting and drying cycles to pinpoint where exactly along soil moisture spectrum (from plant wilting point to saturation) associated hydrologic parameters, and their scale of spatial autocorrelation, operate.

There is a strong push within the soil science and hydrologic communities to reconceptualize, or rethink, current modeling approaches (Tetzlaff et al. 2008). Tying findings from this research to a conceptual framework is an effort to help the soil science community discuss and develop stronger hypotheses and methodologies that will hopefully result in more effective soil hydrologic models in terms of governing equations and relevant hydrologic parameters, especially in karst Kentucky landscapes during drought conditions. Ideally, discussing and developing such models will lead to more informed water management decisions specific to the investigator's scale of interest,

whether it be watershed planning, irrigation management, or contaminant fate and transport.

Scale invariance, or intrinsic correlation (Webster and Oliver 2001), is important for developing scaling relations to transfer information from one scale to the next with physical meaning. This is the foundational basis for pedotransfer functions. For example, Zeleke and Si (2005) found clay to be scale-invariant and used it as scaling index for hydraulic conductivity through means of an empirical multifractal scaling model. Scaling indices, in the most general sense, are conversion factors that relate the physical characteristics measured at one scale with the physical characteristics measured at another scale (Vereecken et al. 2007). The correlation plots for July showed the relationship between clay and soil moisture was scale invariant. What is important to emphasize here is that the intrinsic correlation between clay and soil moisture was, in fact, time relevant to dry soil conditions and did not hold any relevance when the soils breached the plant wilting point. Therefore, scaling relations should be considered relevant to time.

Conclusion

This research explored the future challenges and needs established within the literature to better understand soil moisture dynamics over multiple spatial scales (Corwin et al. 2006). Soil moisture exhibited a preferential interaction with scale-dependent parameters according to fluctuations in soil moisture with time. Soil parameters were influential at a longer range during dry conditions whereas terrain attributes became more influential at shorter ranges during wetter conditions.

Findings add to the evidence that a single physical model might be insufficient for predicting soil moisture spatial distribution with time for the topographically diverse central Kentucky landscape studied. The findings established by this research are a working contribution to the advances in hydropedology and highlight the ongoing need for multiscale research, especially over larger spatial extents such as landscapes (Sobieraj et al. 2006, Pachepsky et al. 2008). Future work should study the scale-dependent relevance of soil-terrain parameters during cyclic wetting and drying events to pinpoint the soil moisture ranges in which these parameters are most relevant under typical Kentucky weather patterns. The multivariate geostatistical and spatial regression tools can assist with this effort.

Chapter 6

Concluding Remarks and Future Directions

One of the major challenges facing field investigators is determining the optimal observation scale(s) to capture and manage soil moisture variation in space with time. This dissertation captured and characterized soil moisture spatiotemporal variation within a topographically diverse Inner Bluegrass Kentucky landscape. One of the motivations to this work (using various geostatistical and geospatial analytical techniques) was to determine at which scales soil-terrain parameters operate to influence soil moisture variation. The applied multivariate geostatistical approach distilled four main scales of variation within the Inner Bluegrass landscape at approximately: 40, 70, 200, and 250 m (with an effective range of 750 m).

In general, soil physicochemical properties exhibited variation at the long-range scales (200 and 250 m) whereas terrain attributes exhibited variation at the short-range scale (70 m). These findings contradict the general assumption that terrain attributes primarily operate at long ranges and soil attributes at short ranges. This research attributes this, in part, to the karst geology typical to Inner Bluegrass region. Other studies in similar landscape settings have exhibited analogous results (Nyberg 1997, Jawson and Niemann 2007). Nevertheless, these findings are most likely location specific and might not hold true in dissimilar geographic regions, such as the Central Plains.

Applying the geostatistics and geospatial techniques shown in Chapters 4 and 5 can help determine the optimal ranges over which soil properties and terrain attributes affect soil moisture variation and, by accordance, the optimal ranges to observe and manage soil moisture variation across a diverse set of geographic regions. Soil moisture management

can encompass irrigation input, monitoring, and controlling the fate and residence of soluble soil contaminants, and water resource conservation, for example. Specific to the Inner Bluegrass region, findings obtained from this research could help field investigators establish optimal sampling and monitoring intervals to best capture soil moisture variation across landscapes typical to central Kentucky, especially during dry soil conditions.

This research showed that selecting an optimal observation scale to assess and manage soil moisture variation is time relevant between the three observation dates. During July both spatial scales were relevant, with the long-range scale dominating due to the strong influence of soil physicochemical parameters. As the soils became wet in October there was a shift in dominance from the long-range to the short-range scale in which terrain attributes assumed a stronger influence on soil moisture variation. It is suggested that future modeling approaches take this information into account when trying to predict soil moisture variability across Inner Bluegrass Kentucky landscapes in drought conditions. It is anticipated that findings will help improve the precision and accuracy of modeling soil moisture variation in space with time by revealing explanatory variables most relevant to shifts in soil moisture content. However, these results are specific to three observation dates that fell during a drought period for central Kentucky. Future research should be dedicated to observing a diverse set of soil moisture dates to determine where along the soil moisture spectrum optimal observation scales show a relative dominance under typical soil moisture conditions.

Even though there was a shift in relative importance from the long-range to the short-range scale this was not enough to cause time instability for the three dates. Findings

from Chapter 4 showed soil moisture's interaction with soil physicochemical properties is a primary factor driving the observed time stable patterned variation for the three relatively dry dates. Agriculture is one of the most sensitive industries to drought. Modern climate trends are stressing agriculture production and are forecasted to persist in the future (FAO 2011). According to the United Stated Department of Agriculture, the 2012 drought alone was estimated to increase global crop import costs to $1.24 trillion as inventories of corn, wheat, soybean, and rice declined around the world. The world's population is expected to reach 9 billion by 2050 and 8 billion of these people will live in developing countries where food demand is expected to grow by at least 70 percent (FAO 2011). Advanced modern agricultural practices will be needed to produce more resourceful, effective, and economic site-specific management strategies to secure sufficient food production in the future.

To help secure water resources and food production well into the future it is necessary to optimize water use efficiency specific to irrigation input. Ideally, time stable soil moisture patterns generated during drier soil conditions can be used to direct irrigation input on a localized basis and, therefore, optimize water use efficiency. The time stable soil moisture patterns could also be used to guide more parsimonious soil moisture sampling and monitoring schemes that will lead to more informed irrigation management decisions. Chapter 4 introduced a diverse suite of analytical techniques that could be readily adapted to a sparse or comprehensive time series dataset to study soil moisture time stability.

Water appropriation is another important topic when water becomes scarce. Current surface and subsurface water withdrawal by domestic, petroleum, and agriculture sectors

is not regulated by Kentucky statutes. Water appropriation, especially during drought years, among public and private sectors is a foreseeable regulatory reality for Kentucky. Regulatory and municipal entities will ultimately strive to develop plans to reduce water use and dependency. Current government databases are rich with information that could be subjected to the analytical tools set forth in Chapter 4 and Chapter 5 to generate spatial and temporal information that could help develop water appropriation statutes for water withdrawal; strategize and launch credit incentives for water conservation in high risk locations for water scarcity and/or demand; and establish regulatory standards for water use across the Commonwealth of Kentucky.

The results obtained from this research showed apparent EC was a good surrogate to downscale sparse soil moisture measurements during drought conditions to produce soil moisture maps with greater spatial continuity and higher resolution. Proximal sensing becomes important when direct sampling efforts are limited, especially over large observation extents such as landscapes. Remote and proximal sensing technologies, specific to LiDAR and environmental geophysics, are becoming omnipresent field investigative techniques. Their use calls for more robust analytical platforms capable of fusing multiple datasets with unique sampling supports and units to make predictions. This research made a contribution to this effort by fusing LiDAR, apparent EC, and direct soil measurements to study the scale-dependent spatial tendencies of soil moisture in space with time (Landrum et al. in press). The geostatistical platform in this case was multicollocated factorial cokriging analysis (MFCA). To date, little literature is available on this topic and presents an avenue for future research (Taylor et al. 2008, De Benedetto et al. 2013).

Conceptual models are the foundation to any science. Basic sciences, such as chemistry and biology, exercise conceptual models to aid in the general analysis of complex interactions between properties and processes. Although conceptual models have been introduced to soil science, none have been widely accepted, especially to model soil hydrologic processes. Currently, studies entailing hydropedology encompass one of the largest ongoing research efforts to develop a conceptual framework for describing soil hydrologic processes and properties according to time, space, and scale (Lin 2003). This research made a working contribution to this scientific effort specific to an Inner Bluegrass Kentucky landscape under relatively dry soil conditions. Findings herein illustrated that spatial scales of soil moisture variation are independent from one another and that different soil-terrain parameters associate with soil moisture according to scale.

According to hiearchy theory, the structural relationship between discrete scales is thought to be organized in a ladder framework (i.e. hierarchy) in which scales exhibiting shorter-range variation reside below scales exhibiting longer-range variation (Wu and David 2002). Reasoning to this organization is that smaller scales are thought to serve as building blocks for larger scales and larger scales are thought to present constraints on smaller scales (Wu et al. 2000; Wu and David 2002). It was initially hypothesized that terrain attributes, or topography, would exhibit long-range variation and reside above soil physicochemical attributes that would exhibit short-range variation. This intuitive reasoning derived in part from the fact topography is one of the soil forming factors and thereby imposes constraints on soil formation. Conversely, soil properties, such as bulk density, texture, and chemistry, which indirectly influence water residence and transport, would serve as the building blocks that ultimately mold the geomorphology of a region

by regulating the physical and chemical weathering of bedrock and parent material. Findings herein did not support this hierarchical structure, in fact, it supported the inverse.

As alluded to in Chapter 5, it is possible that the observation extent for this research does not fully encompass the large-scale variability for topography and associated terrain attributes. Extending the observation extent (e.g. watershed scale) might reveal that in fact, topography and associated terrain attributes can exhibit large-scale variation in addition to small-scale variation. Nonetheless, this research shows that the archetype hierarchical organization is not universally applicable for all situations and needs reconsideration when trying to understand the interaction and organization between environmental components that makeup complex systems. These findings and suggested future directions can help develop a conceptual framework for understanding soil hydrologic processes and properties according to time, space, and scale specifically within the Inner Bluegrass region of Kentucky.

Appendix A

Basic statistics for soil attributes. Sample number = 100 for all attributes except July.

	Min	Max	Mean	Skewness	Kurtosis	Variance
Bulk Density (cm^3/cm^3)	1.1	1.5	1.3	0.28	-0.02	1.0×10^{-2}
Calcium (mg/L)	1.8×10^{3}	2.1×10^{4}	4.5×10^{3}	5.1	39	4.1×10^{6}
CEC (cmol/kg)	0.05	0.54	0.18	1.8	4.8	1.0×10^{-2}
Clay (%)	17	38	25	0.73	1.9	9.5
July H_20 (vol./vol.)	0.12	0.26	0.18	0.65	0.38	7.5×10^{-4}
July aEC (D) (mS/m)	0.51	14	4.9	1.2	5.7	2.4
July aEC (S) (mS/m)	0.20	3.6	1.2	1.5	6.8	0.13
Potassium (mg/L)	92	925	205	2.8	11	1.7×10^{4}
Magnesium (mg/L)	127	598	291	0.87	1.2	7.2×10^{3}
Nitrogen (mg/L)	0.12	0.37	0.22	1.1	0.83	2.4×10^{-3}
Oct aEC (D) (mS/m)	4.2	199	75	0.2	4.0	400
Oct aEC (S) (mS/m)	0.35	8.3	2.3	1.7	7.2	0.79
October H_20 (vol./vol.)	0.25	0.44	0.31	0.85	1.3	1.1×10^{-3}
OM (%)	2.3	11	3.6	3.9	24	1.0
Phosphorous (mg/L)	62	1.0×10^{3}	355	1.5	3.4	2.6×10^{4}
pH	5.2	7.7	5.7	2.4	9.3	0.12
Sand (%)	6.2	17.6	10.6	0.93	0.73	5.2
Sept aEC (D) (mS/m)	0.65	17.3	5.80	1.18	5.60	0.42
Sept aEC (S) (mS/m)	0.11	7.77	1.89	1.81	8.80	0.42
September H_20 (vol./vol.)	0.00	0.39	0.26	-1.68	14.8	1.6×10^{-3}
Silt (%)	50	72.0	64.6	-0.72	0.59	189
Zinc (mg/L)	47	271	63	5.0	35	828

(aEC) Apparent EC
(S) Shallow; (D) Deep
(CEC) Cation Exchange Capacity

Basic statistics for terrain features and NDVI. Sample number = 100.

	Min	Max	Mean	Skewness	Kurtosis	Variance
Aspect	1.1	3.5×10^{2}	1.1×10^{2}	1.34	0.94	9.2×10^{3}
Elevation (m)	8.9×10^{2}	9.4×10^{2}	9.1×10^{2}	0.10	-1.2	2.2×10^{2}
NDVI	0.11	0.44	0.30	-0.10	1.6	0.010
Plan Curvature	-0.10	6.0×10^{-2}	0.0	-0.60	0.58	1.0×10^{-3}
Profile Curvature	-0.10	7.0×10^{-2}	0.0	-0.12	8.0×10^{-2}	5.9×10^{-4}
Slope	1.0×10^{-2}	0.09	0.04	0.27	-0.28	2.7×10^{-4}
TWI	6.1	13.95	8.57	1.73	3.4	2.0
Upland Contributing Area	20	2.58×10^{4}	780	7.57	67	6.9×10^{6}

(NDVI) Normalized Difference Vegetation Index
(TWI) Topographic Wetness Index

Appendix B

Glossary

Annealing (Chapter 2) - Adapted from metallurgy describing the cooling of molten metal. Cooling allows for the reorganization of compositional elements to increase the overall strength of the metal.

Capacitance Monitoring (Chapter 1) – Capacitance monitoring is an *in situ*, indirect method to assess soil moisture. Capacitance measures the dielectric permittivity of a soil medium, or its ability to store electrical charge. Capacitance probes are sensitive to soil moisture because soil moisture exhibits a measurable difference in capacitance when compared to air, organic material, and minerals.

Complex Systems Theory (Chapter 1) – An integrated approach using both mathematical modeling and philosophy to solve problems. The notion behind Complex Systems Theory is to understand how interrelationships and environmental interactions of individual parts give rise to the system's overall behavior.

Confusion Matrix (Chapter 4) – Statistical metric commonly used to assess a model's performance by measuring the accordance (See **Spatial Accordance** below) between expected and predicted values. Output is presented in a classification matrix.

Digital Elevation Model (DEM) (Chapter 1, 3, 4, & 5) - Georeferenced 2D or 3D representation of the elevation of the Earth's surface constructed from terrain data. Elevation is typically referenced to mean sea level.

Digital Surface Model (DSM) - Similar to DEM but includes all features on the Earth's surface.

Ground Penetrating Radar (GPR) (Chapters 1 & 4) - Noninvasive geophysical technique that transmits electromagnetic pulses into the subsurface using antennas of specific frequencies. Pulses are reflected back to the surface at different velocities based on the physical and chemical subsurface properties the pulses pass through. Calculating the travel time of the electromagnetic pulses it is possible to determine the distance, or depth, of target features in the subsurface. The dielectric permittivity of the soil determines the extent to which the electromagnetic pulses are attenuated.

Hermite polynomial (Chapter 3) - Finite sum of an orthogonal polynomial sequence with fitted weighting functions.

Hierarchy Theory (Chapters 1 & 5) - Originates from **Complex Systems Theory**. Hierarchy Theory recognizes that environmental interactions and interrelationships of a system's individual parts are scale-dependent and attempts to organize these parts based

on their scale-dependent spatiotemporal variation. The structural relationship between scales is thought to be organized in a hierarchical framework in which scales exhibiting short range variation reside below, and give rise to, scales of long range variation. It is generally understood that the scaling relations between scales is not necessarily linear within this framework and the emergent scale-dependent interactions between variables are not necessarily the "sum of their parts." Hierarchies inherently derive from the user's scale(s) of observation.

Hydrogeophysics (Chapter 1) - An approach to study water in natural systems by integrating hydrology with geophysics. The American Geophysical Union alternatively defines Hydrogeophysics as "the use of geophysical methods to estimate parameters and monitor processes important to hydrological investigations, such as those associated with water resources, contaminant transport, ecological and climate investigations." (http://water.usgs.gov/ogw/bgas/research.html).

Hydropedology (Chapters 1, 4, & 5)– An emerging field in soil science that bridges theory and science nested in pedology, soil physics and hydrology to characterize soil-landscape-water interactions across spatial and temporal scales. Henry Lin, the proprietor of Hydropedology, provides an alternative definition "…an intertwined branch of soil science and hydrology that embraces interdisciplinary and multiscale approaches for the study of interactive pedologic and hydrologic processes and properties in the Earth's critical zone."(pg. 2). Lin, H. (2006) Hydropedology: Bridging Disciplines, Scales and Data. Vadose Zone Journal. 2**(1)**: 1-11.

Intrinsic Random Function of Order-k (IRF-k) (Chapters 1 & 3) - Nonstationary geostatistical technique that employs a generalized covariance function, instead of the semivariogram, for kriging. The idea is to decompose the total measured variation into a slowly varying drift component and rapidly varying spatially correlated stochastic component (with zero mean). The drift is calculated as a function of position (x,y) using a linear combination of spatial increments of a higher order-k. Spatial increments of a higher order are used to create stationary residuals that are then fitted to a generalized covariance model.

Inverse Distance Weighting (IDW) (Chapters 1, 3 & 4) - A deterministic calculation that operates on the notion that things closer together are more alike than things farther apart. Values closest to the target (predicted) value will influence the target estimation more than distant values.

LiDAR (Chapters 3, 4, and 5) - Light Detection and Ranging; laser pulses of light are transmitted and received by an airborne or terrestrial platform. The calculated travel distance of the light pulse determines the height of the Earth's surface and other objects that interfere with the light pulse's path.

Linear Model of Coregionalization (LMC) (Chapters 1, 4 & 5) – A linear combination of multiple variogram models. Each variogram model represents an independent scale of spatial variation. The LMC results in a scale-dependent (e.g. regionalized) variance-covariance matrix derived from fitting the direct and cross variograms of the multiple variables studied.

Mean Relative Difference (MRD)(Chapters 1 & 4) – First introduced by Vachaud in 1985 to assess time stability. The MRD measures how an individual observation compares to the mean, or average, of the observation domain. Certain observations will be persistently higher or lower relative the observation average through time. Observations exhibiting a small standard deviation of the relative differences are said to be time stable.

Metropolis Criterion (Chapter 2) – Used in context with spatial annealing. Accepts change based on the overall "cost" in terms of measured entropy. An increase in entropy is considered as an increase in cost whereas a decrease in entropy is considered as a decrease in cost. If a decrease in cost is encountered this is considered favorable for the stability of the energy system and will be accepted if it falls within a given statistical probability.

Multicollocated Factorial Cokriging Analysis (MFCA) (Chapters 1 & 4) - Multivariate kriging procedure that optimizes an estimation using the criteria of unbiasedness and minimizing the mean square estimation error. There are three main steps to complete MFCA: 1) model the scale-dependent spatial variation of the variables studied using the **Linear Model of Coregionalization** (LMC); 2) assess the scale-dependent intercorrelation between variables by applying **principal component analysis (PCA)**; and 3) krig the scale-dependent principal components produced in Step 2. Multicollocated cokriging is a cokriging technique that utilizes secondary information (auxiliary measures) only at nodes that are collocated with the target node (point to be estimated) primary nodes (direct measures). The benefit to multicollocated cokriging is it reduces computation time and adds stability to solving the kriging system.

Nonstationarity (Chapters 1 & 3) – The quality of a process by which its statistical parameters (e.g. mean) are not constant throughout the domain studied (i.e. space, time).

Polygon Kriging (Chapters 1 & 4) – Instead of estimating a value at a target node an average value is computed for an area bounded by a regularly or irregularly shaped polygon. This technique is akin to block kriging.

Principal Component Analysis (PCA) (Chapters 1, 4 & 5) - A nonparametric statistical assessment. PCA is commonly employed as a data mining tool to reduce data redundancy among multiple variables. PCA collapses redundant variables into representative homogeneous units called principal components. The first principal

component explains most of the total measured variation, and conversely, the last principal component explains the least. The number of principal components within a dataset matches that of the number of variables studied. All variables weigh on each principal component to explain their relative contribution. Each principal component is orthogonal to all other principle components.

Semivariogram (Chapters 1, 3, 4 & 5) – Measures the spatial autocorrelation of a variable as a function of direction and distance. It is calculated as half the average squared difference between points separated by a distance (**h**).

Spatial Accordance (Chapter 4) – A global measure included in the Confusion Matrix. Describes the general agreement of measurements at a given location through time.

Spatial Eigenfunction Analysis (Chapter 5) – Suite of methods used to study multiscale spatial variability in multivariate response data (e.g. regression). Geographic distance matrices are used to produce eigenvectors, or spatial filters of varying geographic spatial frequencies. "Geographic" refers to the spatial coordinates of the sampling grid. The more irregular the sampling grid the more eigenvectors produced. Eigenvectors are used as predictor variables in the regression model to deduce which spatial frequencies (e.g. scales) the response variable exhibits variation.

References

Abdu, H., D. Robinson, M. Seyfried, S. Jones (2008). "Geophysical Imaging of Watershed Subsurface Patterns and Prediction of Soil Texture and Water Holding Capacity." Water Resources Research **44**: W00D18, doi:10.1029/2008wr007043.

Ali, G., A. Roy, P. Legendre (2010). "Spatial Relationships between Soil Moisture Patterns and Topographic Variables at Multiple Scales in a Humid Temperate Forested Catchment." Water Resource Research **46**: 1-17.

Allen, T., P. Allen, D. Wixon (2009). "Hierarchy Theory in Hydropedology." Hydrology and Earth System Sciences Discussions **6**: 2931-2959.

Allred, B., J. Daniels, M. Ehsani (2008). Handbook of Agricultural Geophysics. Boca Raton, CRC Press.

Amidu, S. (2008). Electrical Resistivity Imaging for Characterizing Dynamic Hydrologic Systems. Department of Geology, Baylor University. **Dissertation:** 118.

Amidu, A., J. Dunbar (2007). "Geoelectric Studies of Seasonal Wetting and Drying of a Texas Vertisol." Vadose Zone Journal **6**(3): 511-523.

Amirun, W., M. Amin, D. Ahmad, M. Hanafi, C. Chan (2007). "Spatial Variability of Bulk Soil Electrical Conductivity in a Malaysian Paddy Field: Key to Soil Management." Paddy Water Environment **5**: 113-121.

Anderson, E., J. Thompson, R. Austin (2007). "LiDAR Density and Linear Interpolator Effects on Elevation Estimates." International Journal of Remote Sensing **26**(18): 3889-3900.

Anonymous. (2000). Soil Analysis Handbook of Reference Methods. I. Soil and Plant Analysis Council. Boca Raton, FL.

Atkinson, P., C. Joyd (2012). Geostatistics for Environmental Applications. New York, Springer.

Atkinson, P., N. Tate (2000). "Spatial Scale Problems and Geostatistical Solutions: A Review." Professional Geographer **52**(4): 607-623.

Besson, A., I. Cousin, H. Bourennane, B. Nicoullaud, C. Pasquier, G. Richard, A. Dorigny, D. King (2010). "The Spatial and Temporal Organization of Soil Water at the Field Scale as Described by Electrical Resistivity Measurements." European Journal of Soil Science **61**: 120-132.

Besson, A., I. Cousin, A. Dorigny, M. Dabas, D. King (2008). "The Temperature Correction for the Electrical Resistivity Measurements in Undisturbed Soil Samples: Analysis of Existing Conversion Models and Proposal of a New Model." Soil Science **173**(10): 707-720.

Besson, A., I. Cousin, A. Samouelian, H. Biozard, G. Richard (2004). "Structural Heterogeneity of the Soil Tilled Layer as Characterized by 2D Electrical Resistivity Surveying." Soil and Tillage Research **79**: 239-249.

Blanchet, F., P. Legendre, D. Borcard (2008). "Forward Selection of Explanatory Variables." Ecology **89**(9): 2623-2632.

Bleines, C., S. Perseval, F. Rambert, D. Renard, Y. Touffait (2012). Isatis Software Manual. Cedex, France, Geovariances.

Bogena, H., M. Herbst, J. Huisman, U. Rosenbaum, A. Weuthen, H. Vereecken (2010). "Potential of Wireless Sensor Networks for Measuring Soil Water Content Variability." Vadose Zone Journal **9**: 1002-1013.

Bourgault, G., D. Marcotte (1991). "Multivariable Variogram and Its Application to the Linear Model of Coregionalization." Mathematical Geology **23**(7): 11-19.

Brevik, E., T. Fenton, A. Lazari (2006). "Soil Electrical Conductivity as a Function of Soil Wate Content and Implications for Soil Mapping." Precision Agriculture **7**: 393-404.

Brocca, L., F. Melone, T. Moramarco, R. Morbidelli (2009). "Soil Moisture Temporal Stability Over Experimental Areas in Central Italy." Geoderma **148**: 364-374.

Brocca, L., F. Melone, T. Moramarco, R. Morbidelli (2010). "Spatio-temporal variability of Soil Moisture and Its Estimation Across Scales". Water Resources Research **(46):** WO2516 doi: 10.1029/2009WR008016. Brocca, L., R. Morbidelli, F. Melone, T. Moramarco (2007). "Soil Moisture Spatial Variability in Experimental Areas of Central Italy." Journal of Hydrology **(333)**: 356-373.

Brunet, P., R. Clement, C. Bouvier (2010). "Monitoring Soil Water Content and Deficit Using Electrical Resistivity Tomography (ERT) - A Case Study in the Cevennes Area, France." Journal of Hydrology **380**: 146-153.

Buttafuoco, G., A. Castrignanò (2005). "Study of the Spatio-Temporal Varition of Soil Moisture Under Forest Using Intrinsic Random Function of Order-k." Geoderma **128**: 208-220.

Buttafuoco, G., C. Tommaso, R. Coscarelli (2011). "Spatial and Temporal Patterns of the Mean Annual Precipitation at Decadal Time Scale in Southern Italy." Theoretical and Applied Climatology **105**: 431-444.

Cafarelli, B., A. Castrignanò (2011). "The Use of Geoadditive Models to Estimate the Spatial Distribution of Grain Weight in an Agronomic Field: A Comparison with Kriging with External Drift." Environmetrics **22**: 769-780.

Campbell, J. B. (2007). Introduction to Remote Sensing. New York, The Guilford Press.

Castrignanò, A., E. Costantini, R. Barbetti, D. Sollitto (2009). "Accounting for Extensive Topographic and Pedologic Secondary Information to Improve Soil Mapping." Catena **77**: 28-38.

Castrignanò, A., F. Fornaro, B. Basso, M. Tomaiuolo (2004). Assessing Non-Stationary Variability in Durum Wheat Yield Using Intrinsic Random Functions of Order K. 7th International Conference on Precision Agriculture, Minneapolis, MN, Precision Agriculture Center.

Castrignanò, A., L Giugliarini, R. Risaliti, N. Martinelli (2000). "Study of Spatial Relationships Among Some Soil Physio-Chemical Properties of a Field in Central Italy Using Multivariate Geostatistics." Geoderma **97**: 39-60.

Castrignanò A., M. Wong., M. Stelluti, D. De Benedetto, D. Sollitto (2012). "Use of EMI, gamma-ray emission and GPS height as multi-sensor data for soil characterisation." Geoderma **(175-176)**: 78–89.

Chen, Y. (2006) Letter to the Editor on "Rank Stability or Temporal Stability". Soil Science Society of America Journal **70**(1): 306.

Chilés, J., P. Delfiner (1999). Geostatistics: Modeling Spatial Uncertainty. New York, John Wiley & Sons, Inc.

Choi, M., J. Jacobs, M. Cosh (2007) "Scaled Spatial Variability of Soil Moisture Fields." Geophysical Research Letters **34**: L01401, doi: 10.1029/2006GL028247.

Ciotoli, G., F. Stigliano, F. Marconi, M. Moscatelli, M. Mancini, G. Cavinato (2011). Mapping the Anthropic Backfill of the Historical Center of Rome (Italy) by Using Intrinsic Random Functions of Order k (IRF-k). Computational Science and Its Applications - ICCSA 2011, Santander, Spain, Springer.

Coleman, M., J. Niemann (2013). "Controls on Topographic Dependence and Temporal Instability in Catchment-Scale Soil Moisture Patterns." Water Resources Research **49**: 1-18, doi: 10.1002/wrcr.20159.

Comegna, V., A. Basile (1994). "Temporal Stability of Spatial Patterns of Soil Water Storage in a Cultivated Vesuvian Soil." Geoderma **62**: 299-310.

Corwin, D., J. Hopmans,G. de Rooij (2006). "From Field- to Landscape-Scale Vadose Zone Processes: Scale Issues, Modeling, and Monitoring." Vadose Zone Journal **5**: 129-139.

Corwin, D., S. Lesch (2003). "Application of Soil Electrical Conductivity to Precision Agriculture: Theory, Principles, and Guidelines." Agronomy Journal **95**(3): 231-259.

Corwin, D., S. Lesch (2005a). "Characterizing Soil Spatial Variability with Apparent Soil Electrical Conductivity I. Survey Protocols." Computers and Electronics in Agriculture **46**: 103-133.

Corwin, D., S . Lesch (2005b). "Apparent Soil Electrical Conductivity Measurements in Agriculture." Computers and Electronics in Agriculture **46**: 11-43.

Cosh, M., T. Jackson, S. Moran, R. Bindlish (2008). "Temporal Persistence and Stability of Surface Soil Moisture in a Semi-Arid Watershed." Remote Sensing of Environment **112**: 304-313.

Cousin, I., A. Besson, H. Bourennane, H., C. Pasquier, B. Nicoullaud, D. King, G. Richard (2009). "From Spatial-Continuous Electrical Resistivity Measurements to the Soil Hydraulic Functioning at the Field Scale." Comptes Rendus Geoscience **341**: 859-867.

Da Silva, P., A. Nadler, B. Kay (2001). "Factors Contributing to Temporal Stability in Spatial Patterns of Water Content in the Tillage Zone." Soil and Tillage Research **58**: 207-218.

De Benedetto, D., A. Castrignanò, M. Rinaldi, S. Ruggieri, F. Santoro, B. Figorito, S. Gualano,
M. Diacono, R. Tamborrino, (2013). "An approach for delineating homogeneous zones by
using multi-sensor data." Geoderma **(199)** 117–127.

De Benedetto, D., A. Castrignanò, D. Sollitto, F. Modugno, G. Buttafuoco, G. lo Papa (2012). "Integrateing Geophysical and Geostatistical Techniques to map the Spatial Variation of Clay." Geoderma **171-172**: 53-63.

De Lannoy, G., N. Verhoest, P. Houser, T. Gish, M. Meirvenne (2006). "Spatial and Temporal Characteristics of Soil Moisture in An Intensively Monitored Agricultural Field (OPE^3)." Journal of Hydrology **331**: 719-730.

Diacono, M., A. Castrignanò, A. Troccoli, D. De Benedetto, B. Basso, P. Rubino (2012). "Spatial and Temporal Variability of Wheat Grain Yield and Quality in a Mediterranean Environment: A Multivariate Geostatistical Approach." Field Crops Research **131**: 49-62.

Dormann, C., J. McPherson, M. Araujo, R. Bivand, J. Bolliger, G. Carl, R. Davies, A. Hirzel, W. Jetz, W. Kissling, I. Kuhn, R. Ohlmuller, P. Peres-Neto, B. Reineking, B. Schroder, F. Schurr, R. Wilson (2007). "Methods to Account for Spatial Autocorrelation in the Analysis of Species Distibutional Data: A Review." Ecography **30**: 609-628.

Dray, S., P. Legendre, P. Peres-Neto (2006). "Spatial Modeling: A Comprehensive Framework for Principal Coordinate Analysis of Neighbour Matrices (PCNM)." Ecological Modeling **196**: 483-493.

Edlefsen, N., A. Anderson (1941). "The Four-Electrode Resistance Method for Measuring Soil-Moisture Content Under Field Conditions." Soil Science **51**: 367-376.

Famiglietti, J., J. Rudnicki, M. Rodell (1998). "Variability in Surface Soil Moisture Content Along a Hillslope Transect: Rattlesnake Hill, Texas." Journal of Hydrology **210**: 259-281.

FAO (2011). Save and Grow. A policymaker's guide to the sustainable intensification of smallholder crop production. Food and Agriculture Organization of the United Nations (FAO). ISBN 978-92-5-106871-7.

Farahani, H., G. Buchleiter, M. Brodahl (2005). "Characterization of Apparent Soil Electrical Conductivity Variability in Irrigated Sandy and Non-Saline Fields in Colorado." American Society of Agricultural Engineers **48**(4): 155-168.

Florinsky, I. (2012). Digital Terrain Analysis in Soil Science and Geology, Academic Press**:** 432.

Florinsky, I., R. Eilers, G. Manning, L. Fuller (2002). "Prediction of Soil Properties by Digital Terrain Modelling." Environmental Modelling and Software **17**: 295-311.

Friedman, S. (2005). "Soil Properties Influencing Apparent Electrical Conductivity: A Review." Computers and Electronics in Agriculture **46**: 45-70.

Gallant, J., J.Wilson (1996). "TAPES-G: A Grid-Based Terrain Analysis Program for the Enivronmental Sciences." Computers and Geoscience **22**(7): 713-722.

Gao, X., P. Wu, X. Zhao, Y. Shi, J. Wang, B. Zhang (2011). "Soil Moisture Variability Along Transects Over a Well-Developed Gully in the Loess Plateau, China." Catena **87**: 357-367.

Garambois, S., P. Senechal, H. Perroud (2002). "On the Use of Combined Geophysical Methods to Assess Water Content and Water Conductivity of Near-Surface Formations." Journal of Hydrology **259**: 32-48.

Garre, S., M. Javaux, J. Vanderborght, L. Pages, H. Vereecken (2011). "Three-Dimensional Electrical Resistivity Tomography to Monitor Root Zone Water Dynamics." Vadose Zone Journal **10**: 412-424.

Gee, G., J. Bauder. (1986). Methods of Soil Analysis, Part I: Physical and Mineralogical Methods. Madison, WI, American Society of Agronomy Inc.

Geovariances (2012). "Isatis Software." France. http://www.geovariances.com/en.

Gómez-Plaza, A., J. Alvarez-Rogel, J. Albaladejo, V. Castillo (2000). "Spatial Patterns and Temporal Stability of Soil Moisture Across a Range of Scales in a Semi-Arid Environment." Hydrological Processes **14**: 1261-1277.

Gómez-Plaza, A., M. Martínez-Mena, J. Albaladejo, V. Castillo (2001). "Factors Regulating Spatial Distribution of Soil Water Content in Small Semiarid Catchmenets." Journal of Hydrology **253**: 211-226.

Goovaerts, P. (1992). "Factorial Kriging Analysis: A Useful Tool for Exploring the Structure of Multivariate Spatial Information." Journal of Soil Science **43**: 597-619.

Goovaerts, P. (1994). "Study of Spatial Relationships Between Two Sets of Variables Using Mutivariate Geostatistics." Geoderma **62**: 93-107.

Goovaerts, P. (1997). Geostatistics for Natural Resource Evaluation. Athens, Oxford University Press.

Goovaerts, P. (1998). "Geostatistical Tools for Characterizing the Spatial Variability of Microbiological and Physio-Chemical Soil Properties." Biology and Fertility of Soils **27**: 315-334.

Goovaerts, P., R. Webster (1994). "Scale-Dependent Correlation Between Topsoil Copper and Cobalt Concentrations in Scotland." European Journal of Soil Science **45**: 79-95.

Goyal, V., P. Gupta, S. Seth, V. Singh (1996). "Estimation of Temporal Changes in Soil Moisture Using Resistivity Method." Hydrological Processes **10**: 1147-1154.

Grayson, R., A. Western (1998). "Toward Areal Estimation of Soil Water Content from Point Measurements: Time and Space Stability of Mean Response." Journal of Hydrology **207**: 68-82.

Grayson, R., G. Bloschl, A. Western, T. McMahon (2002). "Advances in the Use of Observed Spatial Patterns of Catchment Hydrological Response." Advances in Water Resources **25**: 1313-1334.

Grayson, R., A. Western (2001). "Terrain and the Distribution of Soil Moisture." Hydrological Processes **15**(13): 2689-2690.

Grayson, R., A. Western, F. Chiew, G. Bloschl (1997). "Preferred States in Spatial Soil Moisture Patterns: Local and Nonlocal Controls." Water Resource Research **33**(12): 2897-2908.

Griffith, D., P. Peres-Neto (2006). "Spatial Modeling in Ecology: The Flexibility of Eigenfunction Spatial Analyses." Ecology **87**(10): 2603-2613.

Guagliardi, I., G. Buttafuoco, D. Cicchella, R. De Rosa (2012). A Multivariate Appraoch for Anomaly Separation of Potentially Toxic Trace Elements in Urban and Peri-Urban Soils: An Application in a Southern Italy Area. Journal of Soil Sediment (13): 117-128.

Guber, A., T. Gish, Y. Pachepsky, M. van Genuchten, C. Daughtry, T. Nicholson, R. Cady (2008). "Temporal Stability in Soil Water Content Patterns Across Agricultural Fields." Catena **73**: 125-133.

Guo, Q., W. Li, H. Yu, O. Alvarez (2010). "Effects of Topographic Variability and LiDAR Sampling Density on Several DEM Interpolation Methods." Photogrammetric Engineering & Remote Sensing **76**(6): 1-12.

Haas, J. (2010). Soil Moisture Modelling using TWI and Satellite Imagery in the Stockholm Region. School of Archtecture and the Built Environment. Stockholm, Sweden, Royal Institute of Technology (KTH). **Masters**.

Haining, R., R. Kerry, M. Oliver (2009). "Geography, Spatial Data Analysis, and Geostatistics: An Overview." Geographical Analysis **42**: 7-31.

Hall, O., G. Hay, A. Bouchard, D. Marceau (2004). "Detecting Dominant Landscape Objects through Multiple Scales: An Integration of Object-Specific Methods and Watershed Segmentation." Landscape Ecology **19**: 59-76.

Hartsock, N. (2001). In Situ Soil Electrical Conductivity Variability in Several Kentucky Agricultural Fields. Plant and Soil Sciences. Lexington, University of Kentucky. **Thesis**.

Haws, N., B. Liu, C. Boast, P. Rao, E. Kladivko,D. Franzmeier (2004). "Spatial Variabiltiy and Measurement Scale of Infiltration Rate on an Agricultural Landscape." Soil Science Society of America Journal **68**: 1818-1826.

Hay, G., P. Dube, A. Bouchard, D. Marceau (2002). "A Scale-Space Primer for Exploring and Quantifying Complex Landscapes." Ecological Modeling **153**(2002): 27-49.

Hopmans, J., D. Nielson, K. Bristow (2002). "How Useful are Small-Scale Soil Hydraulic Property Measurements for Large-Scale Vadose Zone Modeling?" Geophysical Monograph **129**: 247-258.

Hopmans, J., G. Schoups (2006). Soil Water Flow at Different Spatial Scales. Encyclolpedia of Hydrological Sciences, John Wiley & Sons, Ltd.

Hu, W., M. Shao, F. Han, K. Reichardt (2009). "Time Stability of Soil Water Storage Measured by Neutron Probe and the Effects of Calibration Procedures in a Small Watershed." Catena **79**: 72-82.

Huang, H., T. Link, A. Smith, C. Chen (2011). Accuracy of the LiDAR-Derived DEM In Dense Shrub Areas in Mountainous NW US. Spatial Data Mining and Geographical Knowledge Services (ICSDM), Fuzhou.

Inman, D., R. Freeland, R. Yoder, J. Ammons, L. Leonard (2001). "Evaluating GPR and EMI for Morphological Studies of Loessial Soils." Soil Science **166**(9): 622-630.

Jacobs, J. M., B. Mahontany, E. Hsu, D. Miller (2004). "SMEX02: Field Scale Variability, Time Stability and Similarity of Soil Moisture." Remote Sensing of Environment **92**: 436-446.

Jawson, S., J. Niemann (2007). "Spatial Patterns from EOF Analysis of Soil Moisture at a Large Scale and Their Dependence on Soil, Landuse, and Topographic Properties." Advances in Water Resources **30**: 366-381.

Jayawickereme, D., R. Van Dam, D. Hyndman (2010). "Hydrological Consequences of Land-Cover Change: Quantifying the Influence of Plants on Soil Moisture with Time-Lapse Electrical Resistivity." Geophysics **75**(4): WA43-WA50, doi: 10.1190/1.3464760.

Johnson, C., R. Eigenberg, J. Doran, B. Wienhold, B. Eghball, B. Woodbury (2003). "Status of Soil Electrical Conductivity Studies by Central State Researchers." American Society of Agricultural Engineers **48**(3): 979-989.

Jung, W., N. Kitchen, K. Sudduth, R. Kremer, P. Motavalli (2005). "Relationship of Apparent Soil Electrical Conductivity to Claypan Soil Properties." Soil Science Society of America Journal **69**: 883-892.

Kachanoski, R. (1988). "Scale Dependence and the Temporal Persistence of Spatial Patterns of Soil Water Storage." Water Resources Research **24**: 85-91.

Kienzle, S. (2004). "The Effect of DEM Raster Resolution on First Order, Second Order and Compound Terrain Derivatives." Transactions in GIS **8**(1): 83-111.

Kim, D. (in press). "Incorporation of Multi-Scale Spatial Autocorrelation in Soil Moisture-Landscape Modeling." Physical Geography **In press.**

Koch, K., J. Wenninger, S. Uhlenbrook, M. Bonell (2009). "Joint Interpretation of Hydrological and Geophysical Data: Electrical Resistivity Tomography Results from a Process Hydrological Research Site in the Black Forest Mountains, Germany." Hydrological Processes **23**: 1501-1513.

Kornelsen, K., P. Coulibaly (2013). "McMaster Mesonet Soil Moisture Dataset: Description and Spatio-Temporal Variability Analysis." Hydrological Earth System Science **17**: 1589-1606.

Korres, W., N. Koyama, P. Fiener, K. Schneider (2010). "Analysis of Surface Soil Moisture Patterns in Agricultural Landscapes Using Emperical Orthogonal Functions." Hydrology and Earth System Sciences **14**: 751-764.

Kühn, J., A. Brenning, M. Wehrhan, S. Koszinski, M. Sommer (2009). "Interpretation of Electrical Conductivity Patterns by Soil Properties and Geological Maps for Precision Agriculture." Precision Agriculture **10**: 490-507.

Kutilek, M., D. Nielson (2007). "Interdisciplinarity of Hydropedology." Geoderma **252-260**.

Landis, R., G. Koch (1977). "The Measurement of Observer Agreement for Categorical Data." Biometrics **33**(1): 159-174.

Landrum, C., A. Castrignanò, T. Mueller, D. Zourarakis, J. Zhu, D. De Benedetto (In press). "An Approach for Delineating Homogeneous Within-Field Zones Using Proximal Sensing and Multivariate Geostatistics" Agricultural Water Management.
Lark, M., R. Webster (2006). "Geostatistical Mapping of Geomorphic Variables in the Presence of Trend." Earth Surface Processes and Landforms **31**: 862-874.

Legendre, P., L. Legendre (2012). Numerical Ecology. Amsterdam, Elsevier.

Lesch, S., D. Corwin (2003). "Using the Dual-Pathway Parallel Conductance Model to Determine How Different Soil Properties Influence Conductivity Survey Data." Agronomy Journal **95**: 365-379.

Lin, H. (2003). "Hydropedology: Bridging Disciplines, Scales, and Data." Vadose Zone Journal **2**: 1-11.

Lin, H. (2006). "Temporal Stability of Soil Moisture Spatial Patterns and Subsurface Preferential Flow Pathways in the Shale Hills Catchment." Vadose Zone Journal **5**: 317-340.

Lin, H. (2010). "Repeated Electromagnetic Induction Surveys for Determining Subsurface Hydrologic Dynamics in an Agricultural Landscape." Soil and Water Management and Conservation **74**(5): 1750-1762.

Lin, H. (2012). Hydropedology: Synergistic Integration of Soil Science and Hydrology. Weltham, MA, Academic Press.

Lin, H., J. Bouma, Y. Pachepsky, A. Western, J. Thompson, R. van Genuchten, H. Vogel, A. Lilly (2006). "Hydropedology: Synergistic Integration of Pedology and Hydrology." Water Resource Research **42**(42): 1-13.

Lin, H., E. Brooks, P. McDaniel, J. Boll (2008a). Hydropedology and Surface/Subsurface Runoff Processes. Encylopedia of Hydrological Sciences. M. G. Anderson, John Wiley & Sons, Ltd.

Lin, Y., T. Chang, C. Shih, C. Tseng (2002). "Factorial and Indicator Kriging Methods Using a Geographic Information System to Delineate Spatial Variation and Pollution Sources of Soil Heavy Metals." Environmental Geology **42**: 900-909.

Lin, H., D. Wheeler, J. Bell, L. Wilding (2005). "Assessment of Soil Spatial Variability at Multiple Scales." Ecological Modeling **182**: 271-290.

Lin, H., X. Zhou (2008b). "Evidence of Subsurface Preferential Flow Using Soil Hydrologic Monitoring in hte Shale Hills Catchment." European Journal of Soil Science **59**: 34-49.

Liu, X. (2008) Airborne LiDAR for DEM Generation: Some Critical Issues. Progress in Physical Geography **32**: 31-49.

Lohr, U. (1998). "Digital Elevation Models by Laser Scanning." Photogrammetric Record **16**(91): 105-109.

Ma, R., A. McBratney, B. Whelan, B. Minasny and M. Short (2011). "Comparing Temperature Correction Models for Soil Electrical Conductivity Measurement." Precision Agriculture **12**: 55-66.

Manfreda, S., M. McCabe, M. Fiorentino, I. Rodriquez-Iturbe, E. Wood (2007). "Scaling Characteristics of Spatial Patterns of Soil Moisture from Distributed Modelling." Advances in Water Resources **30**: 2145-2150.

Martínez-Fernández, J., A. Ceballos (2003). "Temporal Stability of Soil Moisture in a Large-Field Experiment in Spain." Soil Science Society of America Journal **67**: 1647-1656.

McBratney, A. (1998). "Some Considerations on Methods for Spatilly Aggregating and Disaggregating Soil Information." Nutrient Cycling in Agroecosystems **50**: 51-62.

McBratney, A., B. Minasny, R. MacMillan, F. Carre (2012). Digital Soil Mapping. Handbook of Soil Sciences Properties and Processes. P. Huang, Y. Li, M. Summer, CRC Press**:** 37-31 - 37-38.

Meng, X., N. Currit, K. Zhao (2010). "Ground Filtering Algorithms for Airborne LiDAR Data: A Review of Critical Issues." Remote Sensing **2**(3): 833-860.

Mertens, F., S. Patzold, G. Welp (2008). "Spatial Heterogeniety of Soil Properties and its Mapping with Apparent Electrical Conductivity." Journal of Plant Nutrition and Soil Science **171**: 146-154.

Michot, D., Y. Benderitter, A. Dorigny, B. Nicoullaud, D. King, A. Tabbagh (2003) "Spatial and Temporal Monitoring of Soil Water Content with an Irrigated Corn Crop Cover Using Surface Electrical Resistivity Tomography." Water Resources Research **39**, DOI: 10.1029/2002WR001581

Minet, J., N. Verhoest, S. Lambot, M. Vanclooster (2013). "Temporal Stability of Soil Moisture Patterns Measured by Proximal Ground-Penentrating Radar." Hydrology and Earth System Sciences Discussions **10**: 4063-4097.

Mohanty, B., T. Skaggs (2001). "Spatio-temporal Evolution and Time-Stable Characteristics of Soil Moisturer within Remote Sensing Footprints with Varying Soil, Slope and Vegetation." Advances in Water Resources **24**: 1051-1067.

Moller, M., M. Volk, K. Friedrich, L. Lymburner (2008). "Placing Soil-Genesis and Transport Processes into a Landscape Context: A Multiscale Terrain-Analysis Approach." Journal of Plant Nutrition and Soil Science **171**: 419-430.

Morari, F., A. Castrignanó, C. Pagliarin (2009). "Application of Multivariate Geostatistics in Delineating Management Zones with a Gravelly Vineyard using Geo-Electrical Sensors." Computers and Electronics in Agriculture **68**: 97-107.

Mueller, T., N. Hartsock, T. Sombaugh, S. Shearer, P. Cornelius, R. Barnhisel (2003). "Soil Electrical Conductivity Map Variability in Limestone Soils Overlain by Loess." Agronomy Journal **95**: 496-507.

Nyberg, L. (1996). "Spatial Variability of Soil Water Content in the Covered Catchment at Gardsjon, Sweden." Hydrological Processes **10**: 89-103.

Oliver, M.A. 2010. Geostatisical Applications for Precision Agriculture. Springer.

Oliver, M., R. Webster (1986). "Combining Nested and Linear Sampling for Determining the Scale and Form of Spatial Variation of Regionalized Variables." Geographic Analysis **18**(3): 227-242.

Pachepsky, Y., D. Gimenez, A. Lilly, A. Nemes (2008). "Promises of Hydropedology." CAB Reviews: Perspectives in Agriculture, Veterinary Science, Nutrition and Natural Resources **3**(04): 1-19.

Pachepsky, Y., W. Rawls, H. Lin (2006). "Hydropedology and Pedotransfer Functions." Geoderma **131**: 308-316.

Pachepsky, Y., A. Guber, D. Jacques (2005). "Temporal Persistence in Vertical Distributins of Soil Moisture Contents." Soil Science Society of America Journal **69**: 347-352.

Park, S., N. van de Giesen (2004). "Soil-Landscape Delineation to Define Spatial Sampling Domains for Hillslope Hydrology." Journal of Hydrology **295**: 28-46.

Park, S., K. McSweeney, B. Lowery (2000). "Identification of the Spatial Distribution of Soils Using a Process-Based Terrain Characterization." Geoderma **103**: 249-272.

Penna, D., L. Brocca, M. Borga, G. Fontana (2013). "Soil Moisture Temporal Stabilility at Different Depths on Two Alpine Hillslopes During Wet and Dry Periods." Journal of Hydrology **477**: 55-71.

Perry, M., J. Niemann (2007). "Analysis and Estimation of Soil Moisture at the Catchment Scale using EOF's." Journal of Hydrology **334**: 388-404.

R Development Core Team (2008). R: A language and environment for statistical computing. R Foundation for Statistical Computing, Vienna, Austria. ISBN 3-900051-07-0, URL http://www.R-project.org.

Reutebuch, S., H. Anderson, R. McGaughey (2005). "Light Detection and Ranging (LiDAR): An Emerging Tool for Multiple Resource Inventory." Journal of Forestry **103**(6): 286-292.

Rhoades, J., F. Chanduvi, S. Lesch (1999) Soil Salinity Assessment: Methods and Interpretation of Electrical Conductivity Measurements. Food and Agriculture Organization of the United Nations.

Robinson, D., H. Abdu, S. Jones, M. Seyfried, I. Lebron, R. Knight (2008a). "Eco-Geophysical Imaging of Watershed-Scale Soil Patterns Links with Plant Community Spatial Patterns." Vadose Zone Journal **7**: 1132-1138.

Robinson, D., A. Binley, N. Crook, F. Day-Lewis, T. Ferre, V. Grauch, R. Knight, M. Knoll, V. Lakshmi, R. Miller, J. Nyquist, L. Pellerin, K. Singha, L. Slater (2008b). "Advancing Process-Based Watershed Hydrological Research Using Near-Surface Geophysics: A Vision for, and Review of, Electrical and Magnetic Geophysical Methods." Hydrological Processes **22**: 3604-3635.

Robinson, D. A., I. Lebron, B. Kocar, K. Phan, M. Sampson, N. Crook, S. Fendorf (2009) Time-Lapse Geophysical Imaging of Soil Moisture Dynamics in Tropical Deltaic Soils: An Aid to Ineterpreting Hydrological and Geochemical Processes. Water Resource Research **45**,

Robinson, D., H. Abdu, I. Lebron, S. Jones (2012). "Imaging of Hill-Slope Soil Moisture Wetting Patterns in a Semi-Arid Oak Savanna Catchment using Time-Lapse Electromagnetic Induction." Journal of Hydrology **416-417**: 39-49.

Rosso, P., S. Ustin, A. Hastings (2006). "Use of LiDAR to Study Changes Associated with Spartina Invasion in San Francisco Bay Marshes." Remote Sensing of Environment 1**00**(3): 295-306.

Rubin, Y., S. Hubbard (2005). Hydrogeophysics. New York, Springer.

Saey, T., D. Simpson, H. Vermeersch, L. Cockx, M. van Meirvenne (2009). "Comparing the EM38DD and DUALEM-21S Sensors for Depth-to-Clay Mapping." Soil Science Society of America Journal **73**(1): 7-12.

Samouelian, A., I. Cousin, A. Tabbagh, A. Bruand, G. Richard (2005). "Electrical Resistivity Surve in Soil Science: A Review." Soil and Tillage Research **83**: 173-193.

Saxton, K., J. Rawls. (2006). "Soil Water Characteristic Estimates by Texture and Organic Matter for Hydrologic Solutions." Soil Science Society of America Journal **70**: 1569-1578.

Schmid, K., B. Hadley, N. Wijekoon (2011). "Vertical Accuracy and Use of Topographic LiDAR Data in Coastal Marshes." Journal of Coastal Research **27**(6A): 116-132.

Schwartz, B., M. Schreiber, T. Yan (2008). "Quantifying Field-Scale Soil Moisture Using Electrical Resistivity Imaging." Journal of Hydrology **362**: 234-246.

Seger, M., I. Cousin, A. Frison, H. Boizard, G. Richard (2009). "Characterization of the Structural Heterogeneity of the Soil Tilled Layer by using In Situ 2D and 3D Electrical Resistivity Measurements." Soil and Tillage Research **103**: 387-398.

Sheskin, D. (2000). Handbook of Parametric and Nonparametric Statistical Procedures. Boca Raton, Chapman & Hall/CRC.

Sobieraj, J. A., H. Elsenbeer, and G. Cameron (2004). "Scale Dependency in Spatial Patterns of Saturated Hydraulic Conductivity." Catena **55**: 49-77.

Sollitto, D., M. Romic, A. Castrignanò, D. Romic, H. Bakic (2010). "Assessing Heavy Metal Contamination in Soils of the Zagreb Region (Northwest Croatia) using Multivariate Geostatisics." Catena **80**: 182-194.

Stein, A., J. Riley, N. Halberg (2001). "Issues of Scale for Environmental Indicators." Agriculture, Ecosystems and Environment **87**: 215-232.

Sudduth, K., N. Kitchen, G. Bollero, D. Bullock, W. Wiebold (2003). "Comparison of Electomagnetic Induction and Direct Sensing of Soil Electrical Conductivity." Agronomy Journal **95**: 472-482.

Syms, C. (2008) Principal components analysis. Encyclopedia of Ecology. Elsevier, Oxford, pp. 2940-2949.

Tabbagh, A., M. Dabas, A. Hesse, C. Panissod (2000). "Soil Resistivity: A Non-Invasive Tool to Map Soil Structure Horizonation." Geoderma **97**: 393-404.

Takagi, K., H. Lin (2012). "Changing Controls of Soil Moisture Spatial Organization in the Shale Hills Catchment." Geoderma **173-174**: 289-302

Tarboton, D., K. Schreuders, D. Watson, M. Baker (2009). "Generalized Terrain-Based Flow Analysis of Digital Elevation Models." 18th World IMACS/MODSIM Congress. Cairns, Australia**:** 2000-2006.

Taylor, J., M. Short, A. McBratney, J. Wilson (2008). "Comparison of the ability of multiple soil sensors to predict soil properties in a Scottish potato production system." Proceedings of 1st Global Workshop on high resolution digital soil sensing & mapping. Sydney, Australia.

Tetzlaff, D., S. Carey, H. Laudon, K. McGuire (2010). "Catchment Processes and Heterogeneity at Multiple Scales - Benchmarking Observartions, Conceptualization and Prediction." Hydrological Processes **24**: 2203-2208.

Tetzlaff, D., J. McDonnell, S. Uhlenbrook, K. McGuire, P. Bogaart, F. Naef, A. Baird, S. Dunn, C. Sousby (2008). "Conceptualizing Catchment Processes: Simply Too Complex?" Hydrological Processe **22**(11): 1727-1730.

Teuling, A., R. Uijlenhoet, F. Hupet, E. van Loon, P. Troch (2006). "Estimating Spatial Mean Root-Zone Soil Moisture from Point-Scale Observations." Hydrology and Earth System Sciences Discussions **3**: 1447-1485.

Thomas, G. (1982). Exchangeable Cations. Methods of Soil Analysis, Part 2. Chemical and Microbiological Properties. Madison, WI, American Society of Agronomy Inc.

Troch, P., G. Carrillo, I. Heidbuchel, S. Rajagopal, M. Switanek, T. Volkmann, M. Yaeger (2009). "Dealing with Landscape Heterogeneity in Watershed Hydrology: A

Review of Recent Progress toward New Hydrological Theory." Geography Compass **3**(1): 375-392.

Turner, M., V. Dale, R. Gardner (1989). "Predicting Across Scales: Theory Development and Testing." Landscape Ecology **3**(3/4): 245-252.

USDA-NRCS (2013). Official Soil Series Classification Database. <www.websoils urvey.nrcs.usda.gov/>.

Vachaud, G., A. De Silans, P. Balabanis, M. Vauclin (1985). "Temporal Stability of Spatially Measured Soil Water Probability Density Function." Soil Science Society of America Journal **49**: 822-828.

van Groenigen, J., W. Siderius, A. Stein (1999). "Constrained Optimisation of Soil Sampling for Minimization of the Kriging Variance." Geoderma **87**: 239-259.

van Meirvenne, M., P. Goovaerts (2002). "Accounting for Spatial Dependence in the Processing of Mutli-Temporal SAR Images using Factorial Kriging." International Journal of Remote Sensing **23**(2): 371-387.

Vanderlinden, K., H. Vereecken, H. Hardelauf, M. Herbst, G. Martinez, M. Cosh, Y. Pachepsky (2011) "Temporal Stability of Soil Water Contents: A Review of Data and Analyses." Vadose Zone Journal **11**(4): doi:10.21236/vaj2011.0178.

Vereecken, H., R. Kasteel, J. Vanderborght, T. Harter (2007). "Upscaling Hydraulic Properties and Soil Water Flow Processes in Heterogeneous Soils: A Review." Vadose Zone Journal **6**: 1-28.

Vogel, H., K. Roth (2003). "Moving Through Scales of Flow and Transport in Soils." Journal of Hydrology **272**: 95-106.

Wackernagel, H. (2003). Multivariate Geostatistics: An Introduction with Applications. Verlag Berlin Springer.

Wagener, T., M. Sivapalan, P. Troch, R. Woods (2007). "Catchment Classification and Hydrologic Similarity." Geography Compass **1**: 1-31.

Wagenet, T. (1998). "Scale Issues in Agroecological Research Chains." Nutrient Cycling in Agroecosystems **50**: 23-34.

Webster, R., M. Oliver (2001). Geostatistics for Environmental Scientists. New York, John Wiley & Sons, LTD.

Wechsler, N., T. Rockwell, Y. Ben-Zion, (2009). "Application of High Resolution DEM Data to Detect Rock Damage from Geomorphic Signals Along the Central San Jacinto Fault." Geomorphology **113**(1-2): 82-96.

Wehr, A., U. Lohr (1999). "Airborne Laser Scanning - An Introduction and Overview." ISPRS Journal of Photogrammetry & Remote Sensing **54**: 68-82.

Weitkamp, C. (2005). LiDAR: Range-Resolved Optical Remote Sensing of the Atmosphere. Singapore.

Weitz, A., D. Bunte, H. Hersemann (1993). "Application of Nested Sampling Technique to Determine the Scale of Variation in Soil Physical and Chemical Properties." Catena **20**: 207-214.

Western, A., G. Bloschl, R. Grayson (1998). "Geostatistical Characterization of Soil Moisture Patterns in the Tarrawarra Catchment." Journal of Hydrology **205**: 20-37.

Western, A., R. Grayson, G. Bloschl (2002). "Scaling of Soil Moisture: A Hydrologic Perspective." Annual Review of Earth Planet Science **30**: 149-180.

Western, A., R. Grayson, G. Bloschl, D. Wilson (2003). Spatial Variability of Soil Moisture and Its Implications for Scaling. Scaling Methods in Soil Physics. Y. Pachepsky, D. Radcliffe, H. Selim. Boca Raton, CRC Press**:** 119-142.

Western, A., R. Grayson, G. Blochl, G. Willgoose, T. McMahon (1999). "Observed Spatial Organization of Soil Moisture and its Relation to Terrain Indices." Water Resources Research **35**(3): 797-810.

Wiens, J. (1989). "Spatial Scaling in Ecology." Functional Ecology **3**(4): 385-397.

Wilding, L., H. Lin (2006). "Advancing the Frontiers of Soil Science towards a Geoscience." Geoderma **131**: 257-274.

Williams, C., J. McNamara, D. Chandler (2009). "Controls on the Temporal and Spatial Variability of Soil Moisture in a Mountainous Landscape: The Signature of Snow and Complex Terrain." Hydrological Earth System Science **13**: 1325-1336.

Wilson, D., A. Western, R. Grayson (2004) Identifying and Quantifying Sources of Variability in Temporal and Spatial Soil Moisture Observations. Water Resources Research **40**, DOI: 10.1029/2003WR002306.

Wu, J. (1999). "Hierarchy and Scaling: Extrapolating Information Along a Scaling Ladder." Canadain Journal of Remote Sensing **25**(4): 367-380.

Wu, J. (2004). "Effects of Changing Scale on Landscape Pattern Analysis: Scaling Relations." Landscape Ecology **19**: 125-138.

Wu, J., D. Jelinski, M. Luck, P. Tueller (2000). "Multiscale Analysis fo Landscape Heterogeneity: Scale Variance and Pattern Metrics." Geographic Information Sciences **6**(1): 6-19.

Wu, J., J. David (2002). "A Spatially Explicit Hierarchial Approach to Modeling Complex Ecological Systems: Theory and Applications." Ecological Modeling **153**: 7-26.

Yang, M., S. Liu, Z. Yang, T. Sun, R. Beazley (2009). "Multivariate and Geostatistical Analysis of Wetland Soil Salinity in Nested Areas of the Yellow River Delta." Australian Journal of Soil Research **47**: 486-497.

Wu, J., Y., Qi (2000). "Dealing with Scale in Landscape Analysis: An Overview." Geographic Information Sciences **6**(1): 1-5.

Yao, X., B. Fu, Y. Lu, R. Chang, S. Wang, Y. Wang, C. Su (2012). "The Multi-Scale Spatial Variance of Soil Moisture in the Semi-Arid Loess Plateau of China." Journal of Soils Sediments **12**: 694-703.

Zeleke, T., B. Si (2005). "Scaling Relationships between Saturated Hydraulic Conductivity and Soil Physical Properties." Soil Science Society of America Journal **69**: 1691-1702.

Zheng, S., J. Liu, G. Zhu (2007) Facet-Based Airborne Light Detection and Ranging Data Filtering Method. Optical Engineering **46**,

Zhao, Y., P. Hallet, X. Wang, M. Giese, Y. Gao, R. Horn (2011). "Factors Controlling the Spatial Patterns of Soil Moisture in a Grazed Semi-Arid Steppe Investigated by Multivariate Geostatistics." Ecohydrology **4**: 36-48.

Zhao, Y., S. Peth, X. Y. Wang, H. Lin and R. Horn (2010). "Controls of Surface Soil Moisture Spatial Patterns and Their Temporal Stability in a Semi-Arid Steppe." Hydrological Processes **24**: 2507-2519.

Zhou, X., H. Lin, Q. Zhu (2007). "Temporal Stability of Soil Moisture Spatial Variability at Two Scales and Its Implications for Optimal Field Monitoring." Hydrology and Earth System Sciences Discussions **4**: 1185-1214.

Zhu, Q. (2009). Hydropedological Processes and Their Implications for Precision Agriculture. Department of Crop and Soil Sciences. Ann Arbor, MI, Pennsylvania State University. **Dissertation:** 226.

Zhu, Q., K. Liao, Y. Xu, G. Yang, S. Wu, S. Zhou (2012). "Monitoring and Predition of Soil Moisture Spatio-Temporal Variation From a Hydrpedological Perspective: A Review." Soil Research **50**: 625-637.

Zhu, Q., H., Lin (2009). "Simulation and Validation of Concentrated Subsurface Lateral Flow Paths in an Agricultural Landscape." Hydrological Earth System Science **13**: 1503-1518.

Zhu, Q., H. Lin (2011). "Influences of Soil, Terrain, and Crop Growth on Soil Moisture Variation from Transect to Farm Scales " Geoderma **163**: 45-54.

Vitae

Education

The University of Tulsa – Tulsa, OK
Masters of Science in Biogeosciences, May 2010

The University of Tulsa – Tulsa, OK
Bachelor of Science in Biogeosciences, December 2007

Employment

- Kentucky Department for Environmental Protection (KDEP)
- Teaching Assistant, University of Kentucky, 2012
- PhD Research Assistantship, University of Kentucky, 2010 - 2012
- PhD Directorial Teaching Assistantship, University of Tulsa, 2009 - 2010
- PhD Teaching Assistantship, University of Tulsa, 2008-2009
- Graduate Summer Research Assistantship, University of Tulsa, 2008
- TURC Undergraduate Research Program, University of Tulsa, Summer 2006/2007
- Undergraduate Laboratory/Field Assistant, University of Tulsa, 2005-2007
- Geographic Information System (GIS) Consulting, Lithochimiea, 2006
- Environmental, Health and Safety Internship, Devon Energy, 2005
- Equine Management, 2004-2005
- Clothing Retail, 2000-2005

Scholarships and Honors

Kentucky Department for Environmental Protection PhD Scholar (2012-2013); PhD Chapman Distinguished Scholar (University of Tulsa; 2009 & 2010); Indu Meshri Scholar (University of Tulsa; 2008); Oklahoma Energy Resource Board Scholar (University of Tulsa; 2007 & 2008); Phillip Chenowith Scholar (University of Tulsa; 2006 & 2007); University of Tulsa Academic Scholar (University of Tulsa; 2006 & 2007); Mabel Hildreth Crook Scholar (University of Tulsa; 2007); P.J. and G.F. McMahon Scholar (University of Tulsa; 2007); State Rock and Mineral Society Scholar (University of Tulsa; 2006); J. Woncik Memorial Scholar (University of Tulsa; 2006 & 2007)

Publications

Carla Landrum, Annamaria Castrignanó, Tom Mueller, Demetrio Zourarakis, Junfeng Zhu, and Daniela De Benedetto. *An Approach for Delineating Homogeneous Within-Field Zones Using Proximal Sensing and Multivariate Geostatistics*. Agricultural Water Management. Submitted winter 2013.

Carla Landrum, Annamaria Castrignanó, Tom Mueller, Demetrio Zourarakis, and Junfeng Zhu. *An Approach for Delineating Homogeneous Within-Field Zones Using Proximal Sensing and Multivariate Geostatistics*. 1st CIGR Inter-Regional Conference on Land and Water Challenges, Bari, Italy. Extended abstract. 2013.

Eleanor M. Jennings, Dan Weber, Carla Landrum, Shoeb Munshi, Jennifer Bush-Harris, Kerry Sublette, William Redman, J. Berton Fisher, Bryan Tapp, and Kenneth Roberts. *Emerging Issues in the Remediation and Restoration of Terrestrial Brine Spills*. Published online. 2009.

Jennifer Busch-Harris, Kerry Sublette, Kenneth P. Roberts, Carla Landrum, Aaron D. Peacock, Greg Davis,Dora Ogles, William E. Holmes, David Harris, Christopher Ota, Xiaomin Yang, and Arati Kolhatkar. *Bio-Traps Coupled with Molecular Biological Methods and Stable Isotope Probing Demonstrate the In Situ Biodegradation Potential of MTBE and TBA in Gasoline-Contaminated Aquifers*. Groundwater Monitoring & Remediation. 2008.